Julie Janssen

Application of modelling and simulation to optimize anticancer treatment of special patient populations



Application of modelling and simulation to optimize anticancer treatment of special patient populations

Julie Michelle Janssen

Application of modelling and simulation to optimize anticancer treatment of special patient populations

© Julie M. Janssen, Utrecht 2020

ISBN: 978-94-6380-751-7

Cover design: Wendy Schoneveld, www.wenziD.nl
Book design & lay-out: Wendy Schoneveld, www.wenziD.nl
Print: ProefschriftMaken

The research in this thesis was performed at the Department of Pharmacy & Pharmacology of the Netherlands Cancer Institute-Antoni van Leeuwenhoek, Amsterdam, The Netherlands and in collaboration with other institutes.

Printing of this thesis was financially supported by: The Netherlands Cancer Institute
Pfizer

Application of modelling and simulation to optimize anticancer treatment of special patient populations

Optimalisatie van de behandeling van kanker in bijzondere patiëntenpopulaties door middel van modellering en simulatie

(met een Nederlandse samenvatting)

Proefschrift

ter verkrijging van de graad van doctor aan de Universiteit Utrecht
op gezag van de rector magnificus, prof. dr. H.R.B.M. Kummeling,
ingevolge het besluit van het college voor promoties
in het openbaar te verdedigen
op donderdag 23 april 2020 des middags te 2.30 uur

door

Julie Michelle Janssen

Geboren op 3 februari 1991 te Eindhoven

Promotoren Prof. dr. A.D.R. Huitema
Prof. dr. J.H. Beijnen

Copromotor dr. T.P.C. Dorlo

Contents

	Preface	9
Chapter 1	**Special patient populations: Paediatrics**	
1.1	Pharmacokinetic Targets for Therapeutic Drug Monitoring of Kinase Inhibitors in Pediatric Oncology *Clin Pharmacol Ther. 2020; Epub ahead of print*	15
1.2	Clinical trial simulations in paediatric oncology: a feasibility study from the Innovative Therapies for Children with Cancer Consortium *Eur J Cancer. 2017; 85 :78-85*	45
1.3	A Semi-Mechanistic Population Pharmacokinetic/ Pharmacodynamic Model of Bortezomib in Pediatric Patients with Relapsed/Refractory Acute Lymphoblastic Leukemia *Clin Pharmacokinet. 2019; 59: 207-216*	59
Chapter 2	**Special patient populations: Pregnant women**	
2.1	Population Pharmacokinetics of Docetaxel, Paclitaxel, Doxorubicin and Epirubicin in Pregnant Women with Cancer *Submitted*	77
2.2	Semi-physiological enriched population pharmacokinetic modelling to predict the effects of pregnancy on the pharmacokinetics of cytotoxic drugs *Manuscript in preparation*	99
Chapter 3	**Exposure – response relationships**	
3.1	Population pharmacokinetics of intracellular 5'-fluorouridine 5'-triphosphate and its relationship with Hand-and-Foot Syndrome in patients treated with Capecitabine *Manuscript in preparation*	119
3.2	Quantification of the pharmacokinetic-pharmacodynamic relationship of oral docetaxel co-administered with ritonavir *Submitted*	137

3.3 Longitudinal modelling of EGFR mutations in circulating tumor DNA as predictor of disease progression in non-small cell lung cancer patients treated with EGFR inhibitors 151
Manuscript in preparation

Chapter 4 Therapeutic drug monitoring

4.1 Development and validation of a liquid chromatography-tandem mass spectrometry assay for nine oral anticancer drugs in human plasma 171
J Pharm Biomed Anal. 2019; 174: 561-566

4.2 Evaluation of extrapolation methods to predict trough concentrations to guide therapeutic drug monitoring of oral anticancer drugs 185
Submitted

4.3 Tyrosine kinase inhibitor levels matter in treating chronic GVHD 209
Bone Marrow Transplantation. 2019; 54: 1141-1144

Chapter 5 Conclusions and Perspectives 217

Appendices

Summary 227
Samenvatting 233
Author Affiliations 239
List of publications 247
Dankwoord 249
Curriculum Vitae 252

Preface

In 2018, an estimated 18.1 million people across the world were diagnosed with cancer, of which 2% of cases was diagnosed in the first 20 years of life. Moreover, 9.6 million patients with cancer died that year.(1) Approximately one out of 1,000 pregnancies is complicated by cancer and in The Netherlands approximately 600 children are diagnosed with cancer annually.(2) The development of new drugs to treat patients with cancer is rapidly evolving and this (and other improvements in diagnosis and treatments) has resulted in a markedly improved survival.(3) New targeted anti-cancer drugs have been introduced enabling precision medicine in which treatment is selected based on the specific molecular defect of the tumour. However, precision medicine also includes precision dosing, in which the optimal dose for the particular patient should be selected.(4)

Special patient populations such as children and pregnant women suffering from cancer represent a particular unmet clinical need, as these patient populations are not regularly included in drug development programs. In both children and pregnant women, the effects of anticancer drugs may be altered as a result of changing physiology. Changes in total body weight, total body water and proportion of body fat may influence drug distribution. In addition, altered blood flow to the various organs, hepatic enzyme activity and glomerular filtration rate may result in changed clearance of the drug from the body. These physiological changes, which evolve over time, might lead to low or high drug exposure that can result in suboptimal efficacy or substantial toxicity, respectively. Additionally, co-administration of other drugs and patient characteristics such as pharmacogenetics and organ function might also lead to variability in both efficacy and tolerability of the treatment from one patient to another. All these factors underline the importance of precision dosing in the era of precision medicine.(4)

Modelling and simulation using a population approach provides a method to describe, to interpret and to predict the pharmacokinetics (PK) and pharmacodynamics (PD) of a drug. By linking the PK to the PD, the relationship between dose, drug exposure and response over time can be assessed.(5) Drug response can be measured by survival, tumour size, change in a biomarker or toxicity. In addition, variability between patients can be defined and explained by individual patient characteristics such as age, body weight and other intrinsic and extrinsic factors. Lastly, modelling and simulation enables the analysis of heterogeneous data, including studies in which a limited number of patients was included or sparse sampling was used. This is especially the case for clinical studies including special patient populations such as children and pregnant women. Once the PK and PD behavior of a drug is identified, the developed models can be used to assess the effects of different dosing strategies and study designs and can be used to extrapolate to different patient populations.(5) Individual

dosing regimens can be developed which may reduce the variability in response and hence optimize treatment. Furthermore, identified exposure-response and exposure-toxicity relationships can provide specific thresholds that can be used to monitor and to adjust the dose in an individual patient while on treatment.

Thesis outline

This thesis describes the application of PK/PD modelling and simulation to precision dosing in order to optimize anticancer treatment, with an emphasis on special patient populations.

The first two chapters focus on PK/PD in children and pregnant cancer patients. Chapter 1.1 provides practical recommendations for PK targets to guide dosing in paediatric patients with cancer. Chapter 1.2 describes the evaluation of an efficient trial design for dose finding in paediatric oncology. Given the low patient numbers, innovative designs for dose finding are urgently needed. Here a simulation method that can be used to predict and to optimize the power of paediatric clinical trial designs is provided. Chapter 1.3 discusses the PK and PD of bortezomib in paediatric patients with relapsed acute lymphoblastic leukaemia. The development of a semi-physiological PK/PD model that describes the saturable distribution of bortezomib within the central compartment and the direct effect of bortezomib concentrations on the inhibition of the proteasome activity is presented. Chapter 2.1 reports on the population PK of the four widely used cytotoxic drugs docetaxel, paclitaxel, doxorubicin and epirubicin in pregnant women with cancer. In particular, the differences in PK between pregnant and non-pregnant patients are shown. In order to predict the exposure of drugs in pregnant patients for which no *a priori* data is available, a model was developed that integrates the physiological changes during pregnancy with PK information from non-pregnant patients. The development and evaluation of this model are presented in chapter 2.2.

To optimize treatment, exposure-efficacy and exposure-toxicity analyses are of key importance. Chapters 3.1 and 3.2 describe the relationship between drug exposure and the development of toxicity in patients treated with oral docetaxel and capecitabine, respectively. A mechanistic model describing the change in circulating tumour DNA over time is presented in chapter 3.3. In addition, this chapter describes the relationship between circulating tumour DNA and disease progression in patients with non-small cell lung cancer who were treated with the targeted anticancer drugs erlotinib or gefitinib.

The ultimate goal of treatment individualization is to improve the treatment by increasing efficacy but at the same time protecting from toxicity. Precision dosing in oncology can be achieved by the application of therapeutic drug monitoring which is

addressed in chapter 4. In chapter 4.1 a bioanalytical method for the quantification of nine oral anticancer drugs in human plasma is described. These concentrations can be interpreted by using PK targets that are minimally required for efficacy. A practical PK target is most often the trough concentration in a dosing interval. A simulation study that assesses different methods for the extrapolation of the individual trough concentration was performed, which is described in chapter 4.2. Chapter 4.3 reports on the exposure-response relationship of the anticancer drug nilotinib in patients with chronic Graft versus Host disease.

References

1. Bray F, Ferlay J, Soerjomataram I, Siegel RL, Torre LA, Jemal A. Global cancer statistics 2018: GLOBOCAN estimates of incidence and mortality worldwide for 36 cancers in 185 countries. CA Cancer J Clin. 2018;68:394–424.
2. de Haan J, Verheecke M, Van Calsteren K, Calster B Van, Shmakov RG, Gziri MM, et al. Oncological management and obstetric and neonatal outcomes for women diagnosed with cancer during pregnancy : a 20-year international cohort study of 1170 patients. Lancet Oncol. 2018;19:337–46.
3. Arnold M, Rutherford MJ, Bardot A, Ferlay J, Andersson TM-L, Myklebust TÅ, et al. Progress in cancer survival, mortality, and incidence in seven high-income countries 1995-2014 (ICBP SURVMARK-2): a population-based study. Lancet Oncol. 2019;20:1493–505.
4. Peck RW. The right dose for every patient: a key step for precision medicine. Nat Rev Drug Discov. 2016;15:145–6.
5. Ette, E & Williams, P. Pharmacometrics: The Science of Quantitative Pharmacology. (Wiley-Interscience, 2007).

CHAPTER 1

Special patient populations: Paediatrics



Chapter 1.1

Pharmacokinetic Targets for Therapeutic Drug Monitoring of Small Molecule Kinase Inhibitors in Pediatric Oncology

Clin Pharmacol Ther. 2020; Epub ahead of print

J.M. Janssen
T.P.C. Dorlo
N. Steeghs
J.H. Beijnen
L.M. Hanff
N.K.A. van Eijkelenburg
J. van der Lugt
C.M. Zwaan
A.D.R. Huitema

Abstract

In recent years new targeted small molecule kinase inhibitors (KI) have become available for pediatric patients with cancer. Relationships between drug exposure and treatment response have been established for several of these drugs in adults. Following these exposure-response relationships, pharmacokinetic (PK) target C_{min} values to guide therapeutic drug monitoring (TDM) in adults have been proposed. Despite the fact that variability in PK may be even larger in pediatric patients, TDM is only sparsely applied in pediatric oncology. Based on knowledge of the PK, mechanism of action, molecular driver and pathophysiology of the disease, we bridge available data on the exposure-efficacy relationship from adults to children and propose target C_{min} values to guide TDM for the pediatric population. Dose adjustments in individual pediatric patients can be based on these targets. Nevertheless, further research should be performed to validate these targets.

Introduction

The number of targeted small molecule kinase inhibitors (KIs) approved for the treatment of cancer in adults is rapidly expanding, which has led to increased pediatric treatment options as well. Over the past two decades, efforts have been made by clinicians and regulatory agencies to increase the incorporation of pediatric research into the registration processes.(1) This includes the requirement to agree on a pediatric investigational plan before an adult marketing access can be obtained in Europe and several extrapolation approaches that use existing information in the adult population to accelerate pediatric development.(2,3) However, since the type of adult cancer for which a drug is approved often does not occur in children, waivers are frequently granted for pediatric development, and it has been argued that in fact a target based waiver system would be more appropriate.(4)

Up to 2016 only two KIs have been approved by the FDA for the treatment of childhood cancers: imatinib for Philadelphia chromosome-positive (Ph+) Chronic Myeloid Leukaemia (CML) and everolimus for subependymal giant-cell astrocytoma.(2,3) Only recently, also dasatinib, nilotinib and larotrectinib have been approved by the FDA for the treatment of pediatric cancers.(5,6) To incentivize the pediatric development of approved adult KIs in oncology, the EMA and FDA both provide guidance for pediatric study plans based on expression of molecular targets.

Large pharmacokinetic (PK) variability has been observed for almost all of the KIs approved in adults. A broad range of factors, such as genetics, food intake, drug formulation and use of concomitant medication may influence the absorption, distribution, metabolism and excretion of drugs.(7–9) As a result of changing body composition, body size, maturation of organ functions and treatment compliance, additional dimensions of variability in PK are present in pediatric patients.(10) Resulting variability in exposure may, especially in children, lead to suboptimal efficacy or substantial toxicity caused by low or high drug exposure, respectively. Hence, by using exposure-efficacy relationships, dose adaptation based on therapeutic drug monitoring (TDM) may optimize treatment of pediatric patients treated with anti-cancer KIs. In fact, TDM to improve pediatric treatment outcomes has proven its value in non-oncology diseases like post-transplantation and in infectious diseases.(11,12)

Practical recommendations for TDM of KIs in the adult setting have been proposed and proven beneficial for several anti-cancer drugs and indications.(13–15) Despite this existing knowledge, TDM is still only sparsely applied, particularly in pediatric oncology. The majority of KIs that are being investigated for the treatment of pediatric malignancies are currently still in early stages of development. Consequently, quantitative exposure-response and exposure-toxicity relationships have not yet been established for these drugs in relation to pediatric indications. Therefore, the aim of

this review is to elaborate on the current knowledge on exposure-response relationships of KIs in pediatric oncology, and if exposure-relationships are lacking to summarize the available clinical exposure and response data in pediatrics and adults. The ultimate goal is to evaluate the available information in order to propose empirical and practical targets, to guide TDM of KIs in pediatric oncology.

Determination of TDM targets in pediatric malignancies

The literature was searched for pediatric PK data on KIs for which adult thresholds have previously been proposed. PubMed searches were performed using the following search terms: ((((((pediatric[Title/Abstract]) OR pediatrics[Title/Abstract]) OR pediatric[Title/Abstract]) OR peadiatric[Title/Abstract]) OR pediatric patient*[Title/Abstract]) OR pediatric patient*[Title/Abstract]) OR child[Title/Abstract]) OR children[Title/Abstract])) AND (imatinib OR glivec) for afatinib, alectinib, axitinib, bosutinib, cabozantinib, ceritinib, cobimetinib, crizotinib, dabrafenib, dasatinib, erlotinib, everolimus, gefitinib, ibrutinib, idelalisib, imatinib, lapatinib, lenvatinib, nilotinib, nintedanib, osimertinib, palbociclib, pazopanib, ponatinib, regorafenib, sorafenib, sunitinib, trametinib, vandetanib and vemurafenib. Additionally, the US FDA Clinical Pharmacology and Biopharmaceutics Review and the Committee for Medicinal Products for Human Use European Public Assessment Report were reviewed for pediatric data.

Determination of a target was performed in a step-wise manner as described in Figure 1. A practical PK target was defined as the minimally required drug exposure for efficacy, which is feasible to measure or to extrapolate in clinical practice for the

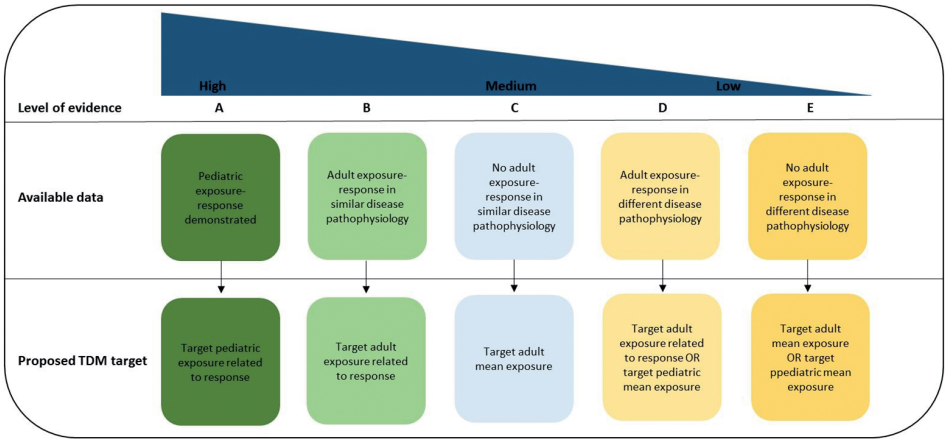

Figure 1. Framework to guide TDM in pediatric oncology.

pediatric population. When a PK-PD relationship in pediatrics has been described in literature, the corresponding cut-off C_{min} that was related to improved efficacy was proposed to guide pediatric TDM (level A in Figure 1). When such a relationship was not available but the target and the disease pathophysiology was deemed similar compared to adults, the adult target that was previously proposed was used (level B).(16) When an exposure-response relationship in adults was not available but the disease pathophysiology was considered similar in adult and pediatrics, the average exposure in adults that corresponds to the therapeutic dose was proposed as an exploratory target to guide pediatric dosing (level C). When the molecular target was similar in adults and pediatrics but the pathophysiology of the disease was different (level D), the proposed adult target (either derived from an exposure-response relationship or the average exposure at the approved dose) was used. Furthermore, if in this case pediatric PK data were available, the average exposure in pediatrics was proposed as an exploratory target (both level D and E).

Practical recommendations for TDM of KIs in pediatric malignancies

Based on the identified literature, recommendations for pediatric targets were defined. Table 1 provides an overview of the included drugs, the previously published targets in adults and the proposed targets in pediatrics.

Anaplastic lymphoma kinase (ALK) inhibitors

The ALK gene has initially been identified as the fusion gene in anaplastic large cell non-Hodgkin lymphoma (ALCL), which accounts for 10-15% of all childhood lymphomas. ALK fusions have also been identified in pediatric inflammatory myofibroblastic tumors (IMTs) and infant high grade gliomas. Activating kinase domain mutations or gene amplifications of the full-length ALK receptor have been identified in 8% of neuroblastoma patients.(17) In adult non-small cell lung cancer (NSCLC), translocations in ALK have been identified as a key driver in the malignant process. It has been shown that the inhibition of mutant ALK is more complex compared with translocated ALK in NSCLC. Based on the variability in underlying molecular changes in the ALK gene and based on the variability in response in NSCLC, the biology of ALK in pediatric cancer patients may differ from that in adults. Hence, sensitivity to treatment with ALK inhibitors may also differ between pediatric patients and adults.(17,18) We here describe ALK inhibitors for which target C_{min} values in adults have been proposed.

Crizotinib

In a study investigating crizotinib for the treatment of pediatric relapsed/refractory ALK-positive ALCL an ORR of 90% was observed (n = 26, age range 3.7 – 20.8 years old).(18) At the maximum tolerated dose (280 mg/m^2 BID), the mean C_{min} in pediatrics was 480 ng/mL, corresponding to a free drug concentration of 50 ng/mL.(19) The unbound

Table 1. Proposed TDM targets for KIs in pediatric oncology.

		Pediatric		Adult			References
Drug	**Molecular target**	**Proposed target (ng/mL)**	**Level of evidence[a]**	**Proposed target (ng/mL)[b]**	**Mean/median exposure (ng/mL)**	**Outcome parameter associated with TDM target**	
Alectinib	ALK	$C_{min} \geq 435$	D	$C_{min} \geq 435$	$C_{min} = 572$	Increased ORR	[13]
Ceritinib	ALK	$C_{min} \geq 871$	D	$C_{min} \geq 871$	$C_{min} = 871$	Observed exposure	[13]
Crizotinib	ALK	$C_{min} \geq 480$	E	$C_{min} \geq 235$	$C_{min} = 274$	Increased PFS	[18]
Bosutinib	Brc-Abl	$C_{min} \geq 147$	B	$C_{min} \geq 147$	$C_{min} = 147$	Observed exposure	[13]
Dasatinib	Bcr-Abl	$C_{min} \geq 2.61$	B	$C_{min} \geq 2.61$	$C_{min} = 2.61$	Observed exposure	[13]
Imatinib	Bcr-Abl	$C_{min} \geq 1000$ (CML) $C_{min} \geq 1100$ (GIST)	B	$C_{min} \geq 1000$ (CML) $C_{min} \geq 1100$ (GIST)	$C_{min} = 1170$ (CML) $C_{min} = 1193$ (GIST)	Improved MMR, CCYR	[13]
Nilotinib	Bcr-Abl	$C_{min} \geq 469$	B	$C_{min} \geq 469$	$C_{min} = 1165$	Prolonged TTP	[13]
Ponatinib	Bcr-Abl	$C_{min} \geq 22.8$	E	$C_{min} \geq 34.2$	$C_{min} = 34.2$	Observed exposure	[38,39]
Afatinib	EGFR	$C_{min} \geq 14.4$	D	$C_{min} \geq 14.4$	$C_{min} = 14.4$	Observed exposure	[13]
Erlotinib	EGFR	$C_{min} > 500$	D	$C_{min} > 500$	$C_{min} = 1010$	Observed exposure	[13]
Gefitinib	EGFR	$C_{min} \geq 200$	D	$C_{min} \geq 200$	$C_{min} = 291$	Increased OS	[13]
Lapatinib	EGFR	$C_{min} \geq 780$	E	$C_{min} \geq 780$	$C_{min} = 780$	Observed exposure	[13]
Osimertinib	EGFR	$C_{min} \geq 166$	E	$C_{min} \geq 166$	$C_{min} = 166$	Observed exposure	[13]
Axitinib	VEGFR	$C_{min} > 5$	D	$C_{min} > 5$	$C_{min} \geq 5$	Increased OS	[13]
Cabozantinib	VEGFR	$C_{min} \geq 1125$	C	$C_{min} \geq 1125$	$C_{min} = 1380$	Observed exposure	[13]
Lenvatinib	VEGFR	$C_{min} \geq 51.5$	C	$C_{min} \geq 51.5$	$C_{min} = 51.5$	Observed exposure	[13]
Nintedanib	VEGFR	$C_{min} \geq 13.1$	C	$C_{min} \geq 13.1$	$C_{min} = 13.1$	Observed exposure	[13]
Pazopanib	VEGFR	$C_{min} \geq 20000$	B	$C_{min} \geq 20000$	$C_{min} = 24000$	Increased PFS	[13]
Regorafenib	VEGFR	$C_{min} \geq 1400$	C	$C_{min} \geq 1400$	$C_{min} = 1400$	Observed exposure	[13]
Sorafenib	VEGFR	$C_{min} > 3890$	C	$C_{min} > 3750$	$C_{min} = 3750$	Observed exposure	[69]
Sunitinib[c]	VEGFR	$C_{min} \geq 50$ (4-2)	B	$C_{min} \geq 50$ (4-2)	$C_{min} = 51.6$	Increased OS	[13]

Vandetanib	VEGFR	C_{min} ≥ 730	C	C_{min} ≥ 795	C_{min} = 795	Observed exposure	[77,78]
Dabrafenib[d]	BRAF	C_{min} ≥ 99.6	E	C_{min} ≥ 99.6	C_{min} = 99.6	Observed exposure	[13]
Vemurafenib	BRAF	C_{min} > 42000	B	C_{min} > 42000	C_{min} = 39000	Increased PFS	[13]
Cobimetinib	BRAF	C_{min} ≥ 127	E	C_{min} ≥ 127	C_{min} = 127	Observed exposure	[13]
Trametinib	BRAF	C_{min} ≥ 10.6	D	C_{min} ≥ 10.6	C_{min} = 12.1	Increased PFS	[13]
Everolimus	mTOR	C_{min} ≥ 10.0	B	C_{min} ≥ 10.0	C_{min} = 13.2	Increased PFS	[13]
Ibrutinib	Btk	C_{min} ≥ 680	E	C_{min} ≥ 680	C_{min} = 680	Observed exposure	[13]
Idelalisib	PI3Kδ	C_{min} ≥ 318	E	C_{min} ≥ 318	C_{min} = 318	Observed exposure	[13]
Palbociclib	CDK4/6	C_{min} ≥ 61	E	C_{min} ≥ 61	C_{min} = 61	Observed exposure	[13]

Abbreviations: ALK, anaplastic lymphoma kinase; Bcr-Abl, breakpoint cluster region-abelson; EGFR, epidermal growth factor receptor; VEGFR, vascular endothelial growth factor receptor; BRAF, serine/threonine-protein kinase B-raf; mTOR, mammalian target of rapamycin; Btk, Bruton's tyrosine kinase; PI3Kδ, phosphatidylinositide 3-kinase; CDK4/6, cyclin-dependent kinases 4 and 6; CML, chronic myeloid leukemia; GIST, gastrointestinal stromal tumor; ORR, objective response rate; PFS, progression free survival; MMR, major molecular response; CCYR, complete cytogenetic response; TTP, time to progression; OS, overall survival. [a] (A) Pediatric exposure-response demonstrated; (B) Adult exposure-response in similar disease pathophysiology; (C) No adult exposure-response in similar disease pathophysiology; (D) Adult exposure-response in different disease pathophysiology; (E) No adult exposure-response in different disease pathophysiology. [b] [13] [c] Sum of sunitinib & N-desethylsunitinib. [d] Sum of dabrafenib & hydroxyl-dabrafenib.

drug concentration of 50 ng/mL exceeds the IC_{50} of 10 ng/mL of crizotinib in ALCL cell lines. No relationships between exposure and efficacy have been established for crizotinib in adults with NSCLC nor pediatric patients with ALCL.(13) Therefore, the best estimate for a minimum target for efficacy would be the mean pediatric C_{min} of 480 ng/mL. Further research is however needed to confirm this preliminary recommendation.

Ceritinib
A phase I study with ceritinib in pediatric patients with ALCL, IMT, rhabdomyosarcoma or neuroblastoma (n = 22, age range 2 – 17 years old) reported similar area under the concentration-time curve (AUC) and CL/F as in adults at the recommended dose for expansion (510 mg/m^2 QD). Detailed results on exposure (AUC) and clearance were not reported.(20) In adults with ALK positive NSCLC, only a trend towards higher objective response rate (ORR) with higher C_{min} could be identified.(21) Thus, the mean C_{min} ≥ 871 ng/mL that was reported in adults may provide preliminary guidance for individualized dosing in pediatric patients, until further information regarding the pediatric application is available.

Alectinib
There are no clinical studies available in which alectinib has been used in the treatment of pediatric malignancies. In adults with ALK positive NSCLC, a steady-state C_{min} ≥ 435 ng/mL has been proposed as a target to guide TDM of alectinib. Patients with a steady-state C_{min} above this target showed a larger reduction in tumor size compared to patients with a steady-state C_{min} below 435 ng/mL.(22) As described above, the biology of ALK may be different in pediatric malignancies. Extrapolation of exposure-response relationships from adults with NSCLC to children with other forms of malignancies may therefore not be appropriate. In addition, the C_{min} in pediatrics was unavailable. Thus, no specific threshold can be proposed at this time.

Break point cluster region - Abelson (Bcr-Abl) oncoprotein inhibitors
Chronic myeloid leukaemia (CML) represents 2-3% of pediatric leukemias, with increasing incidence with age. Philadelphia chromosome-positive (Ph+) CML patients are treated with Bcr-Abl inhibitors. Studies have shown that CML biology is slightly different in pediatric and adult disease.(23) A clear explanation for the difference in disease response has however not yet been found. Therefore, established exposure-response relationships for Bcr-Abl inhibitors in adults can be extrapolated to children with some caution.(24),Efforts should be made to identify exposure-response relationships in pediatric disease.

Imatinib
Several clinical studies in pediatrics with CML have shown that the PK of imatinib and its active metabolite (CGP74588) in children and adults are similar when children are treated with a BSA-based equivalent dose (260 mg/m^2 QD). Two population PK analyses

identified body weight as a significant covariate on imatinib clearance. The inclusion of age did not improve the model and was thus not included.(25,26) Additionally, steady-state plasma concentrations in children with solid tumors were similar to the steady-state plasma concentrations in children and adults with CML following body weight based dosing.(27) Nevertheless, information on the PK of imatinib during the first 2 years of age is lacking. Multiple trials in adults confirmed that the target C_{min} of ≥ 1000 ng/mL is associated with a better treatment outcome.(13) Until data on the pediatric exposure-response becomes available, we recommend the well-established exposure-response based adult target C_{min} ≥ 1000 ng/mL as a minimum target for dose individualization in children with CML.

Alongside its use in CML, imatinib has also been used to treat pediatric GIST. For this indication, imatinib is targeted against the stem cell receptor (KIT) and platelet-derived growth factor receptor (PDGFR).(28) It has been shown that pediatric GIST has a different pathophysiology and presentation than adult GIST. Genetic mutations in KIT or PDGFR are rare in pediatrics and tumors are more often located in the stomach.(29) Adult studies showed a significant increase in progression-free-survival (PFS) with increased $C_{min.}$(30) As it has been shown that the PK in pediatrics and adults was similar in patients CML and in patients with solid tumors, we propose the adult PK target of C_{min} ≥ 1100 ng/mL for dose individualization in pediatric GIST as an exploratory target.

Dasatinib

A large phase II trial with dasatinib in chronic phase CML showed similar to or higher efficacy of dasatinib in pediatric patients compared to historically observed efficacy in adults (n = 60, age range 1.5 – 27.6 years old). Children were treated with a BSA based dose (60 mg/m^2 QD) that was equivalent to the approved adult flat dose.(31) In a phase I study the dasatinib $AUC_{0\text{-last}}$ in pediatrics (n = 58, age range <2 years – 18 years old) treated with a BSA-based dose has been reported to be similar to the exposure that has been observed in adults, the AUC in adults was however not reported.(32) An exposure-response relationship in pediatrics has not been established as far as we know. In a population PK-PD analysis of the adult clinical trials with dasatinib, the weighted average steady-state concentration has been related to major cytogenetic response (2.11-fold increase of the odds of response for every doubling of the average steady-state concentration).(33) Given the clear exposure-efficacy relationship in adults and similarity in PK between adults and pediatrics, using the geometric mean C_{min} of 2.61 ng/mL that was observed in adults seems justified as a minimum TDM target for pediatric patients.

Nilotinib

The PK of nilotinib has been investigated in pediatric patients with Ph+ CML or ALL (n = 15). Here it has been shown that C_{min} achieved with BSA-based dosing (230 mg/m^2 BID) was slightly lower in both children aged 1 - < 10 years old (mean C_{min} 804.8 ng/mL)

and children aged 10 - <18 years old (mean C_{min} 1073 ng/mL) compared to adults (mean C_{min} 1165 ng/mL).(34) Several exposure-response relationships have been established by population PK-PD analyses of adult patient data, however, information on this relationship in pediatric patients is still lacking. Most importantly, a significantly longer time to complete cytogenetic response (CCyR) or major molecular response (MMR) and short time to progression have been identified for adult patients in the lowest C_{min} quartile comparted to the higher quartiles. The lowest quartile threshold C_{min} was 469 ng/mL for these analyses.(35) Considering the strong exposure-efficacy relationship in adults, a $C_{min} \geq 469$ ng/mL is recommended for TDM of nilotinib in pediatric patients.

Bosutinib

The first phase I/II study of bosutinib in pediatric patients with CML is currently ongoing (EudraCT no. 2015-002916-34). In adults with CML, associations between PK and CCyR, complete haematological response (CHR) and MMR have been shown. Additionally, in the pivotal adult CML trial the C_{min} was reported to be higher in responders than in nonresponders.(36) We recommend the median adult C_{min} of 147 ng/mL as a minimum threshold for TDM in pediatrics with CML, while awaiting the results of clinical trial in pediatrics.

Ponatinib

Preclinical studies have shown that a ponatinib concentration of 40 nM suppressed the emergence of any single mutation.(37) In adults, a statistically significant relationship between dose intensity and probability of major cytogenetic responses in patients with CML has been described. It has additionally been shown that toxicity was dose-dependent. The use of ponatinib in pediatric patients is still rare. Hence, pediatric PK and exposure-response data are not available.(38) Case-reports suggested that ponatinib treatment is effective in children with Ph+ acute lymphoblastic leukemia (ALL) or CML.(39,40) Based on the relationship between daily dose and toxicity that has been described in adults, the dose was lowered in the described pediatric cases. With this dose (15 mg OD), the serum concentration of ponatinib was 18.3 ng/mL at 9 h after dose at the last treatment day, which is slightly below the reported active concentration (40nM; 22.8 ng/mL). Given the very limited evidence available, no specific target can be proposed for ponatinib. We therefore recommend a $C_{min} \geq 22.8$ ng/mL as an exploratory target to guide dosing of individual pediatric patients.

Epidermal growth factor receptor (EGFR) inhibitors

The amplification of EGFR has been observed in 5-10% of pediatric high-grade gliomas (HGG) and overexpression of EGFR is seen in over 80% of pediatric malignant gliomas. Pediatric HGG are regarded as genetically different and more malignant tumors than adult brain tumors.(41–45) In adults, EGFR inhibitors are predominantly applied in EGFR mutated NSCLC. Analogy between NSCLC and brain tumors has not yet been demonstrated. Moreover, penetration of EGFR inhibitors in brain tumors may be limited

by the blood-brain barrier and, therefore, higher plasma concentrations may be needed for adequate target inhibition. It is therefore challenging to extrapolate the pediatric target C_{min} from adults to children with various brain tumors.

Gefitinib

The exposure of gefitinib in pediatric patients (n = 17, age range 1.8 – 21.2 years old) with solid tumors has been shown to be consistent with prior knowledge in adults.(46) Gefitinib apparent clearance was 13.7 ± 6.6 L/h/m^2 in children younger than 12 years (n = 10) and 14.4 ± 6.9 L/h/m^2 in children older than 12 years (n = 7). In addition, median steady-state $AUC_{0\text{-}24h}$ estimates were similar in pediatrics compared to adults. These findings have been confirmed in a PK analysis of 19 pediatric patients with newly diagnosed brainstem glioma (BSG). In an additional exploratory analysis, no evidence of a relationship between gefitinib PK and toxicity or efficacy has been identified. Moreover, the $AUC_{0\text{-}24h}$ achieved in children dosed 250 mg/m^2/d (11800 ng/mL*h, n = 6) were comparable with the $AUC_{0\text{-}24h}$ that was associated with antitumor activity in adults with solid tumors (8596 ng/mL*h, n = 7).(42,47) In a study with adult NSCLC patients, a C_{min} ≥ 200 ng/mL has been associated with a significantly higher overall survival (OS) (4.7 months vs. 14.6 months, P = 0.007).(13,48) Given the clear exposure-efficacy relationship in adults with NSCLC and absence of sufficient pediatric PK data and data on target inhibition in pediatric solid tumors and BSG, a preliminary C_{min} ≥ 200 ng/mL may provide guidance for dosing in pediatric patients.

Erlotinib

In population PK-PD analysis including adults with head and neck carcinoma (n = 42) and pediatric patients (n = 46, age range 2 – 19 years old) with malignant brain tumors a significantly higher elimination capacity in children was identified ($p < 0.0001$) compared to adults.(49,50) Typical clearance values of 0.146 L/h/kg and 0.095 L/h/kg have been found for children and adults, respectively, resulting in a higher recommended dose in children (125 mg/m^2 QD vs. 90 mg/m^2 QD in adults). As a result of heterogeneity in disease status between patients at time of enrolment, a relationship between exposure and response could not be established.(51) In the pediatric population, only AUC values have been reported but TDM based on AUC is difficult to implement. Until new data is available on the PK and brain penetration of erlotinib in pediatric patients with malignant brain tumors, the target that was proposed in adults, i.e. C_{min} > 500 ng/mL, could be used as a preliminary starting point for pediatric dose individualization.(13)

Lapatinib

Since the human epidermal growth factor receptor 2 (HER2) has been shown to play an important role in the pathophysiology of pediatric ependymomas, medulloblastomas and BSG, lapatinib has been investigated in children with these malignancies. In these clinical trials, lapatinib was administered in a twice-daily dose. It is therefore not

possible to compare PK data in children to those obtained in adults. The pediatric C_{min} (data not reported) was reported to be similar to the limited data that was obtained from adults treated with twice-daily lapatinib.(52,53) The proposed adult TDM target of $C_{min} \geq 780$ ng/mL has been based on the mean adult steady-state C_{min} at the standard dose (1500 mg QD), and is therefore not appropriate as a target for pediatric TDM. Future studies should focus on exposure-response and exposure-toxicity relationships in pediatric brain tumors, in order to establish a valid target for lapatinib TDM in pediatric diseases.

Afatinib

Afatinib is currently under investigation for the treatment of pediatrics with HGG, diffuse intrinsic pontine glioma (DIPG), low grade astrocytoma, medulloblastoma, ependymoma, neuroblastoma, rhabdomyosarcoma and tumors with known ErbB pathway deregulation (NCT-02372006).(54) A relationship between exposure and response has not yet been reported for afatinib in both pediatric and adult patients. However, it has been found that the C_{min} in adults experiencing Grade 3 diarrhea was higher than those experiencing Grade 1-2 diarrhea (35.8 ng/mL vs. 25.2-31.6 ng/mL).(55) Considering the very limited available data on the PK and brain penetration of afatinib in pediatric patients, extrapolation from data obtained from adults with NSCLC may be inappropriate. It could be considered to use the mean steady-state C_{min} found in adult patients, i.e. 14.4 ng/mL, as an exploratory minimum target for pediatric TDM.(13)

Osimertinib

To date osimertinib has not been investigated in pediatric malignancies. Nevertheless, osimertinib might be introduced in pediatric patients as it has been shown that EGFR mutations play a role in pediatric malignant brain tumors. An exposure-response analysis is lacking in the adult setting. In the absence of an exposure-response target, no appropriate target can be proposed. The geometric mean C_{min} of the approved 80 mg QD daily dose of 166 ng/mL could for now be used as a reference to guide future individual pediatric dosing.(13)

Vascular endothelial growth factor receptor (VEGFR)

VEGFR inhibitors are currently used in the treatment of adults with soft-tissue sarcomas (STS) and renal cell, hepatocellular and papillary thyroid carcinoma. Renal cell carcinoma (RCC) in children is rare and is different from adult RCC. Different genetic profiles and clinical behavior has been observed in pediatrics.(56) Hepatocellular and papillary thyroid carcinoma (PTC) are rare in the pediatric population, similarity in pathophysiology is therefore not clarified yet for these cancer types. However, it has been shown that VEGFR is overexpressed or plays a biological role in Wilms tumors, hepatocellular carcinoma, hepatoblastoma, (non-)rhabdomyosarcoma, STS, Ewing sarcoma, osteosarcoma and neuroblastoma.(57) Additionally, promising results have been reported from several small clinical trials treating pediatric patients with VEGFR inhibitors.

Axitinib

A phase I trial investigating axitinib in pediatrics with solid tumors has recently been published (n = 18, age range 5 – 17 years old). Pediatrics were treated with a BSA-based dose that was equivalent to the adult flat dose. Toxicity and exposure were found to be similar to adults with RCC. However, an association between steady-state C_{max} or $AUC_{0\text{-last}}$ and efficacy could not be established.(57) In adults, a practical target C_{min} of 5 ng/mL has been proposed based on a small study that found a relationship between axitinib C_{min} > 5 ng/mL and tumor response.(58) Considering the limited data in pediatrics, the adult cut-off is might serve as a preliminary starting point for pediatric dose individualization. The relationship between this target and efficacy in pediatric should however be assessed, given the differences in biology and pathophysiology of RCC in pediatrics and adults.

Cabozantinib

Cabozantinib has been investigated at various dose-levels in children with recurrent or refractory solid tumors in a phase I trial (n = 41, age range 4 – 18 years old). No biomarker changes were observed across dose-levels or among responding patients. The recommended phase 2 dose (RP2D) was 40 mg/m^2 QD, which is equivalent to the 60 mg QD adult dose that is registered for RCC. The PK and toxicity profiles at the RP2D (40 mg/m^2 QD) were similar to that observed in adults with RCC.(59) The apparent clearance in pediatrics was 1.1 – 1.8 L/hr/m^2 compared to 1.3 – 2 L/h/m^2 in healthy adults.(60) In a case-report, two children with clear cell RCC were treated with cabozantinib on the RP2D. Disease control was shown for over 15 months, which was twice the median progression free survival observed in an adult phase 2 trial of cabozantinib in RCC.(61) While no exposure-response relationship has been established for either adults or pediatrics, a specific minimum target cannot be proposed for cabozantinib. We recommend to use the mean C_{min} of 1125 ng/mL that was observed in adults with clear cell RCC as an exploratory guide to individualize dosing in pediatrics.(13)

Lenvatinib

Several phase I/II studies with lenvatinib in the pediatric setting are currently ongoing. A case-report described three patients with papillary thyroid carcinoma who were successfully treated with lenvatinib.(62) Two out of three patients remained stable for 11 months after start of lenvatinib. A model-based analysis of adult PK-PD data showed a correlation between lenvatinib $AUC_{0\text{-}24h}$ and reduction in tumor size, but a threshold to guide TDM was not reported.(63) Therefore, TDM in pediatric patients could be guided by the mean C_{min} of 51.5 ng/mL that was proposed a an exploratory minimum target in adults.(13)

Nintedanib

According to literature, nintedanib has not yet been applied in the pediatric setting. A decrease in soluble VEGFR levels with increasing C_{min} was observed in adults in a

small phase I study. Additionally, higher nintedanib concentrations have been associated with hepatotoxicity in an exploratory analysis.(64) Considering the very limited data on nintedanib exposure-response and exposure-toxicity relationships in both pediatrics and adults, the mean adult C_{min} of 13.1 ng/mL may be used as an exploratory minimum target in pediatric patients.(13)

Pazopanib

In a phase I study of pazopanib in children (n = 51, age range 3.8 – 23.9 years old) with soft tissue sarcoma (STS) and other refractory solid tumors, a MTD of 450 mg/m^2 QD has been determined, which is comparable to the adult recommended flat dose of 800 mg QD. At this dose-level the pediatric day 1 $AUC_{0\text{-}24h}$ was similar to adults (377.6 mg/L*h for children vs. 275.1 mg/L*h for adults). An exposure-response relationship could not be established.(65) Pazopanib $C_{ss} \geq 17.5$ mg/L has been suggested as target for optimal in vivo antitumor and antiangiogenic activity in preclinical models.(66) In a clinical study in adults, a prolonged PFS in patients with $C_{min} \geq 20.5$ mg/L compared to patients with a C_{min} below this target has been shown.(67) In a prospective clinical study in adults the safety and feasibility of C_{min} (≥ 20 mg/L) guided dosing in adults has successfully been demonstrated.(68) It has been shown that an equal number of patients discontinued treatment due to toxicity in the low C_{min} versus the high C_{min} group, and only one patient discontinued treatment after a dose escalation. Considering the exposure-efficacy and exposure-toxicity relationships in adults, a C_{min} of 20 mg/L seems justified as minimum target for TDM in pediatric patients.

Regorafenib

In an ongoing phase I trial of regorafenib in pediatric patients with solid tumors (n = 41, age range 3 – 17 years old), the toxicity profile was similar to adults, with the exception of hematologic events. Hematologic toxicity was seen at a higher rate in heavily pretreated pediatric patients than in adults.(69) Observed exposure of regorafenib and active metabolites was similar to the adult exposure in the therapeutic dose range, although details were not yet reported. Furthermore, using a physiology-based PK model, the RP2D of 72 mg/m^2 was predicted to result in 100% of adult exposure. An exposure-response relationship has not yet been determined in either adult or pediatric patients.(13) Based on the limited available data, the best estimate of a minimum target for regorafenib TDM in pediatric patients would be the steady-state mean C_{min} of 1.4 mg/L that was observed in adults.

Sorafenib

Sorafenib PK has been evaluated in phase I and II studies in pediatric patients. In a population pharmacokinetic analysis based on pooled data from several pediatric clinical trials, the median steady-state C_{min} for the RP2D (200 mg/m^2 BID) was 3.89 mg/L (range 1.39 – 10.3 mg/L, n = 37).(70) The pharmacokinetic findings from this analysis were consistent with the PK results from previous pediatric and adult phase I and phase

II studies.(13,71–73) No significant relationship could be identified between the change in VEGF or VEGFR2 and C_{min}. A solid exposure-response relationship has not yet been described. Considering the observed concentrations in pediatrics and lacking exposure-response analysis, a C_{min} of 3.89 mg/L seems justified to be the exploratory minimum target concentration in pediatrics.

Sunitinib

Sunitinib is metabolized into its active metabolite N-desethylsunitinib by cytochrome P450 3A4. For exposure-response analyses and TDM the sum of sunitinib and N-desethylsunitinib concentrations is generally used. Due to the development of myelosuppression and elevated transaminase levels, the RP2D for sunitinib in pediatrics was established at 15 mg/m^2 QD on a 4-weeks-on/2-weeks-off schedule, which is lower than the BSA-based adult equivalent (28 mg/m^2 QD). Hence, the exposure obtained in pediatrics was lower than adults. The total (sunitinib+N-desethylsunitinib) steady-state plasma C_{min} was 34.9 ng/mL (n = 11, range 15.6 – 90.5 ng/mL) in a phase I trial with pediatric patients with solid tumors and 55.4 ng/mL (n = 20, 22.9 – 109.7 ng/mL) in a phase II trial evaluating sunitinib for the treatment of pediatric high-grade glioma or ependymoma.(74,75) In a phase I/II study that investigated sunitinib in pediatric patients with advanced gastrointestinal stromal tumors (GIST), a longer median PFS in patients with higher C_{min} (median PFS 2.6 months in lower exposure group and PFS 9.0 months in higher exposure group, n = 6) was found.(29) In a case-series of pediatric patients with GIST, higher sunitinib doses were tolerated compared to the doses used in the clinical trials and toxicity profiles were similar to the ones observed in adult patients (treated with a 50 mg OD (4-weeks-on/2-weeks—off) flat dose).(76) This was attributed to the fact that the children included in clinical studies received more intensive therapy prior to entry in the clinical study compared to the children that were described in the case-series. Exposure-response and exposure-toxicity relationships have also extensively been studied in adult patients.(13,14) Additionally, a TDM feasibility trial in cancer patients confirmed that using a target of $C_{min} \geq 50$ ng/mL (sunitinib+N-desethylsunitinib) to guide dosing was successful and safe.(77) We therefore advise to guide individual dosing in pediatric patients based on the adult target of $C_{min} \geq 50$ ng/mL (sunitinib+N-desethylsunitinib) when sunitinib is administered in the 4 weeks on-2 weeks off schedule.

Vandetanib

In children with Multiple Endocrine Neoplasia Type 2B Associated Medullary Thyroid Carcinoma (MEN2B MTC), vandetanib was shown to be well tolerated and highly effective at a dose of 100 mg/m^2 QD (n = 16).(78,79) Exposure reached at this dose-level was similar to adults treated with the registered flat dose of 300 mg/day. Mean C_{ss} was 730 ng/mL in pediatrics and 795 ng/mL in adults. As a consequence of the small sample size and low frequency of progression of disease in the pediatric study, no exposure-response analyses could be performed. Also, in adults an exposure-response

relationship has not yet been published. Therefore, dose escalations could be considered for pediatric patients with an exposure below 730 ng/mL.

Serine/threonine-protein kinase B-raf (BRAF) and mitogen-activated protein kinase (MEK) inhibitors

It has extensively been shown that BRAF V600 mutations are important regulators of cell proliferation in adult patients with melanoma.(80) Similar mutations have been observed in adolescents and adults with melanoma. But similarity in disease pathophysiology could not be concluded as a result of very low enrolment.(81)⁸¹ Additionally, BRAF V600E mutations have been found in both high-grade and low-grade gliomas.(82) Given the differences in tumor location, extrapolations from adult melanoma patients to children with brain tumors should be performed carefully.

Vemurafenib

The pediatric PK of vemurafenib has only been studied in adolescents aged 12-17 years with BRAF mutation-positive melanoma (n = 6). All patients treated with the adult dose (960 mg BID) had a steady-state C_{min} above the adult target C_{min} of 42 mg/L. In the lower dose-level (720 mg BID), 2 out of 3 patients had a steady-state C_{min} below this target. Since this study was terminated due to extremely low enrolment, an exposure-response relationship could not be identified.(80) Considering the comparable exposure in adolescents compared to adults and presumably similar pathophysiology of melanoma, it seems reasonable to use the threshold of C_{min} > 42 mg/L for TDM of vemurafenib in pediatrics.(13)

Dabrafenib

A phase II trial with dabrafenib in combination with trametinib for pediatric V600-positive HGG and low-grade glioma (LGG) is currently ongoing. An interim analyses showed that the objective response rate in children was 38% (n = 31), including one complete response and 11 partial responses. Additionally, 14 patients had stable disease.(83) As no pediatric PK data was reported, no specific threshold can be proposed for dabrafenib. The adult target C_{min} can however serve to guide individual dosing in children. The proposed adult target C_{min} in melanoma was based on the median sum of parent dabrafenib and its active hydroxyl metabolite, which was C_{min} of 99.6 ng/mL.(84)

Trametinib

The MAPK/ERK pathway has been characterized as an important pathway in oncogenesis of pilocytic astrocytomas (PA). Only case series of patients (n=6) with PA that were treated with trametinib are available. Partial responses were seen with a good quality of life, only minor toxicities were observed.(82) A population analysis on data from adults with melanoma showed an increasing proportion of responders with increasing exposure to trametinib. This increase showed a plateau at a C_{min} of 10 ng/

mL.(85) Additionally, in an adult phase II study it was observed that patients with a C_{min} above 10.6 ng/mL had longer PFS than patients below this C_{min}. Nevertheless, this relationship was not confirmed in phase III trials. Given the absence of reported pediatric PK data, the adult target of C_{min} ≥ 10.6 ng/mL could be used as a preliminary target to individualize pediatric dosing.(13)

Cobimetinib

A phase I/II clinical trial investigating the safety and PK of cobimetinib in pediatrics with solid tumors is currently ongoing.(86) As this is the first clinical trial that investigates cobimetinib in pediatrics and exposure-response data is absent in adult patients, no specific target for the pediatric population can be proposed. The adult mean C_{min} ≥ 127 ng/mL might be used to guide TDM in pediatrics when treated with cobimetinib for melanoma, for the time being.(13)

Other kinase inhibitors used in oncology

Everolimus

Several in vitro and xenograft studies have shown that rhabdomysarcoma, neuroblastoma, medulloblastoma/primitive neuroectodermal tumors (PNET) and pediatric glioblastoma cell lines are sensitive to mTOR inhibition. TDM of everolimus has proven its value in children with non-oncology related diseases, but a target for TDM in oncology has not yet been reported.(11,87) In a phase I trial with everolimus in pediatric patients with solid tumors (n = 25, age range 3 – 21 years old) it has been shown that the BSA-adjusted dose resulted in an exposure (AUC_{0-inf}) similar to the exposure observed in adults treated with the registered flat dose of 10 mg QD.(88) In addition, it has been shown that the higher dose-levels of 3 to 5 mg/m^2 QD, corresponding to an AUC_{0-inf} of ≥ 200 ng/mL*h, were most effective at decreasing AKT phosphorylation. A meta-analysis of adult everolimus phase II oncology trials (n = 945) showed that a 2-fold increase in everolimus C_{min} was associated with improved tumor size reduction. Also, several analyses of adult RCC patients that were treated with everolimus found trends towards increased PFS for patients with higher C_{min} values.(89) Given the above, the adult threshold of C_{min} ≥ 10 ng/mL, which was based on an exposure-response analysis in adults with RCC and endocrine tumors of the pancreas, seems most appropriate to serve as exploratory target for pediatric TDM of everolimus.(13)

Ibrutinib

Ibrutinib, a Bruton's tyrosine kinase inhibitor, is currently being investigated for the treatment of pediatric relapsed or refractory mature B-cell non-Hodgkin lymphoma. Therefore, pediatric PK data is not yet available and a target for TDM should be based on knowledge from adult studies. The target that is used for adults is an AUC_{0-24h} of

953 ng/mL*h for mantle cell lymphoma and an $AUC_{0\text{-}24h}$ of 680 ng/mL*h for chronic lymphocytic leukemia (no C_{min} data reported). However, the implementation of an AUC target in clinical practice is practically challenging. Future clinical studies should therefore be performed in order to establish a well-defined and practical target to guide individual dosing of ibrutinib in pediatric patients.

Idelalisib
The use of idelalisib, a phosphatidylinositide 3-kinase (PI3Kδ) inhibitor, for the treatment of pediatric patients is very limited. A phase II study aimed to include both adults and pediatrics older than 12 years of age with Hodgkin Lymphoma, as it was expected that disease pathophysiology was similar in these two populations. However, no pediatric patients were included.(90) Only adult PK data are therefore available. Adult dose selection was supported by the finding that the EC_{90} of 125 ng/mL that was needed for *in vitro* PI3Kδ inhibition, was reached by the exposure on the approved dose.(91) The median C_{min} at the approved adult dose was 318 ng/mL, which could be used as exploratory minimum target for TDM in pediatric patients.(13)

Palbociclib
Palbociclib is a cycline-dependent kinase 4/6 inhibitor. To date, palbociclib has not yet been used for the treatment of pediatric cancers. Nevertheless, a NCI-COG Pediatric MATCH (Molecular Analysis for Therapy Choice) trial investigating palbociclib in pediatric patients with tumors harboring activating mutations in cell cycle genes is ongoing.(92) Also, a dose-escalation study with palbociclib in pediatric patients with recurrent/refractory solid tumors is ongoing. While data on the pediatric PK of palbociclib is lacking, individual concentrations could be compared to the adult target of $C_{min} \geq 61$ ng/mL in order to further guide individual dosing.(13)

Future perspectives

We explored and summarized the evidence for targets to guide dosing in the pediatric patient population and proposed TDM recommendations for each of the KIs for which a target has been proposed in adult oncology. For none of the KIs, statistical significant exposure-response or exposure-toxicity relationships that provide valid TDM targets for pediatrics have yet been published. This is due to the typically small clinical trial sample sizes, lack of phase II studies and inherent hurdles to collect PK data in children. Nevertheless, if no differences in disease pathophysiology or pharmacological target are expected between pediatrics and adults, established adult exposure-response relationships could be extrapolated to the pediatric context.

In this review we propose empirical and practical targets for KIs that can be used to individualize dosing in pediatric oncology. Targets are based on the minimally required

exposure for efficacy, following the methods of previously published reviews.(14,15,93) These values need to be validated; although the molecular target is the same in pediatrics and adults, additional factors may play a role in the successful treatment of the disease in pediatric patients. The role of the driving molecular target in tumor-cell survival may differ amongst different cancer types. Additionally, as the tumor site may be different, altered drug concentrations at the target site may occur, resulting in a changed exposure-response relationship. In adults, it has been shown that the TDM targets on average correspond to approximately 80% of the observed mean C_{min}. It has, therefore, been proposed, while awaiting exposure-response analyses, to use the mean population exposure as a reference target for individual exposure in individual patients when an exposure-response relationship has not yet been established.(13,14) Additionally, the algorithm presented here (Figure 1) provides also guidance for TDM of KIs in pediatric oncology when applied without prior knowledge on pediatric PK or PD. Several case-reports have reported the administration of body weight-based or BSA-based adult equivalent doses to pediatrics with good clinical results. We strongly urge to collect blood samples in all pediatric patients that are treated with molecular targeted KIs and determine drug concentrations, whenever feasible, in order to gain more insight in the exposure-response and exposure-toxicity relationships.

Exposure-response relationships are to be expected when taking the mechanisms of action and clinical pharmacological characteristics of KIs into account. The few KIs that are currently registered for treatment of children with cancer are administered in a fixed BSA-based dose. We do recognize the superiority of using a BSA-scaled dose over body weight-scaled dosing in pediatric. However, this dosing approach originates from the traditional toxicity based clinical trial designs that were used to guide dose-finding of conventional, mostly intravenous administered, cytotoxic agents. In the currently ongoing clinical trials with KIs for the treatment of pediatric cancer, this approach is still used. As this approach is based on finding the maximum tolerated dose rather than targeting a clinically effective concentration, a risk of overdosing might be introduced, which might hamper the determination of strong exposure-response relationships. However, pediatric clinical trials with innovative designs are emerging to accelerate the drug development in children and increase the availability of drugs for children. For instance, in a phase I study investigating bosutinib in children with CML, dose-finding is based on identifying a dose resulting in a mean exposure similar to the mean exposure that was found in adults.(94)

It is well-known that PK can differ between children and adults and may also vary among children of different ages. Drug distribution to various compartments of the body may differ in children since the proportion of body water and fat is age-dependent. In addition, the quantity of total plasma proteins is reduced in neonates and young children, which in turn may result in alterations in drug plasma concentrations. Moreover, the metabolism and elimination of drug is influenced by maturational

processes. Renal elimination is fully mature at around one year of age and the maturation of the activity of metabolic enzymes and drug transporters in the GI tract, liver and brains is complex and still not fully characterized.(10) Given these maturational changes and the high between-patient variability in exposure of KIs, individualization of dosing of KIs in pediatric oncology may be of great value in order to increase efficacy while regulating toxicity. In addition, administration issues in children, lack of adequate drug formulations or extemporaneously compounded formulations will influence exposure, supporting the need for TDM.

The tolerability of molecular targeted anti-cancer agents in pediatric patients is mostly similar to adults. In 75% of the investigated molecular targeted agents, the pediatric RP2D was 90-130% of the BSA-adjusted adult dose. Additionally, available PK parameters for these drugs were similar to adults.(95) This advocates for a treatment strategy in which the dose is increased on an individual basis until the adult target concentration is reached. It should however be noted that decreased plasma protein concentrations in pediatrics might theoretically result in an increase in free drug concentration and thus in a higher risk of developing toxicity. However, when dose reductions are required due to toxicity, TDM can be applied to explore whether this toxicity was related to high exposure. The dose could then be tapered while maintaining a plasma concentration above the target. Hence, this individual patient might still be successfully treated at a lower dose. A similar dose reduction strategy involving TDM could be considered when high exposure is related to long lasting side-effects in pediatrics. To date, such relationships have not yet been published. However, it should be noted that long-term toxicities are seen with molecular targeted agents, such as delayed growth and development.(96) In pediatric patients treated with VEGFR inhibitors growth plate toxicity has been observed. Future research in pediatrics is needed to evaluate the long-term impact of this toxicity on growth and developmental processes, as this information cannot be extrapolated from adult study results.(96)

In summary, we have described the available pediatric pharmacokinetics of targeted kinase inhibitors and propose pharmacokinetic targets in order to guide individualized dosing in pediatric cancer patients. For all KIs that were studied, pediatric exposure-response and exposure-toxicity targets are lacking. Therefore, most of the described targets are based on the exposures that are seen in adult patients. Dose adjustments in individual pediatric patients can be based on these targets. Nevertheless, these targets should be validated in prospective randomized clinical trials in order to show their value in increasing treatment efficacy and decreasing toxicity.

References

1. Moreno L, Pearson ADJ, Paoletti X, Jimenez I, Geoerger B, Kearns PR, et al. Early phase clinical trials of anticancer agents in children and adolescents — an ITCC perspective. Nat Rev Clin Oncol. 2017;14:497–507.

2. European Medicines Agency (EMA), Reflection paper on the use of extrapolation in the development of medicines for paediatrics. 2018.

3. FDA. General Clinical Pharmacology Considerations for Pediatric Studies for Drugs and Biological Products. 2014.

4. Pearson ADJ, Pfister SM, Baruchel A, Bourquin J-P, Casanova M, Chesler L, et al. From class waivers to precision medicine in paediatric oncology. Lancet Oncol. 2017;18:e394–404.

5. Vassal G, Zwaan CM, Ashley D, Le Deley MC, Hargrave D, Blanc P, et al. New drugs for children and adolescents with cancer: the need for novel development pathways. Lancet Oncol. 2013;14:117–24.

6. U.S. Food & Drug Administration. Hematology/Oncology (Cancer) Approvals & Safety Notifications. <https://www.fda.gov/drugs/informationondrugs/approveddrugs/ucm279174.htm>.

7. Terada T, Noda S, Inui K. Management of dose variability and side effects for individualized cancer pharmacotherapy with tyrosine kinase inhibitors. Pharmacol Ther. 2015;152:125–34.

8. Gao B, Yeap S, Clements A, Balakrishnar B, Wong M, Gurney H. Evidence for therapeutic drug monitoring of targeted anticancer therapies. J Clin Oncol. 2012;30:4017–25.

9. Widmer N, Bardin C, Chatelut E, Paci A, Beijnen J, Levêque D, et al. Review of therapeutic drug monitoring of anticancer drugs part two--targeted therapies. Eur J Cancer. 2014;50:2020–36.

10. Kearns GL, Abdel-Rahman SM, Alander SW, Blowey DL, Leeder JS, Kauffman RE. Developmental pharmacology--drug disposition, action, and therapy in infants and children. N Engl J Med. 2003;349:1157–67.

11. Shipkova M, Hesselink DA, Holt DW, Med D, Billaud EM, Gelder T Van, et al. Therapeutic Drug Monitoring of Everolimus: A Consensus Report. 2016;38:143–69.

12. van Luin M, Kuks PF, Burger DM. Use of therapeutic drug monitoring in HIV disease. Curr Opin HIV AIDS. 2008;3:266–71.

13. Verheijen RB, Yu H, Schellens JHM, Beijnen JH, Steeghs N, Huitema ADR. Practical Recommendations for Therapeutic Drug Monitoring of Kinase Inhibitors in Oncology. Clin Pharmacol Ther. 2017;102:765-776.

14. Yu H, Steeghs N, Nijenhuis CM, Schellens JHM, Beijnen JH, Huitema ADR. Practical guidelines for therapeutic drug monitoring of anticancer tyrosine kinase inhibitors: Focus on the pharmacokinetic targets. Clin Pharmacokinet. 2014;53:305–25.

15. Groenland SL, van Nuland M, Verheijen RB, Schellens JHM, Beijnen JH, Huitema ADR, et al. Therapeutic Drug Monitoring of Oral Anti-Hormonal Drugs in Oncology. Clin Pharmacokinet. 2018;58:299-308.

16. Verheijen RB, Yu H, Schellens JHM, Beijnen JH, Steeghs N, Huitema ADR. Practical Recommendations for Therapeutic Drug Monitoring of Kinase Inhibitors in Oncology. Clin Pharmacol Ther. 2017;102:765–76.

17. Carpenter EL, Yael P. Targeting ALK in neuroblastoma — preclinical and clinical advancements. Nat Rev Clin Oncol. 2012;9:391–9.

18. Mossé YP, Voss SD, Lim MS, Rolland D, Minard CG, Fox E, et al. Targeting ALK with crizotinib in pediatric anaplastic large cell lymphoma and inflammatory myofibroblastic tumor: A Children's Oncology Group study. J Clin Oncol. 2017;35:3215–21.

19. Balis FM, Thompson PA, Mosse YP, Blaney SM, Minard CG, Weigel BJ, et al. First-dose and steady-state pharmacokinetics of orally administered crizotinib in children with solid tumors: a report on ADVL0912 from the Children's Oncology Group Phase 1/Pilot Consortium. Cancer Chemother Pharmacol. 2016;79:181–187.

20. Geoerger B, Schulte J, Zwaan CM, Casanova M, Fischer M, Moreno L, et al. Phase I study of ceritinib in pediatric patients (Pts) with malignancies harboring a genetic alteration in ALK (ALK+): Safety, pharmacokinetic (PK), and efficacy results. J Clin Oncol. 2015;33(15_suppl):10005–10005.

21. Committee for Medicinal Products for Human Use (CHMP) European Medicines Agency Ceritinib European Public Assessment report. 44, (2015).

22. Food and Drug Administration. Center for Drug Evaluation and Research Alectinib Clinical Pharmacology and Biopharmaceutics Review. <http://www.accessdata.fda.gov/drugsatfda_docs/nda/2015/208434Orig1s000ClinPharmR.pdf> (2016).

23. Hijiya N, Schultz KR, Metzler M, Millot F, Suttorp M. Pediatric chronic myeloid leukemia is a unique disease that requires a different approach. Blood. 2014 Dec 11;124:3817–27.

24. Fuente J De, Baruchel A, Biondi A, de Bont ES, Dresse M-F, Suttorp M, et al. Managing children with chronic myeloid leukaemia (CML) Recommendations for the management of CML in children and young people up to the age of 18 years. Br J Haematol. 2014;167:33–47.

25. Petain A, Kattygnarath D, Azard J, Chatelut E, Delbaldo C, Geoerger B, et al. Population pharmacokinetics and pharmacogenetics of imatinib in children and adults. Clin Cancer Res. 2008;14:7102–9.

26. Menon-Andersen D, Mondick JT, Jayaraman B, Thompson PA, Blaney SM, Bernstein M, et al. Population pharmacokinetics of imatinib mesylate and its metabolite in children and young adults. Cancer Chemother Pharmacol. 2009;63:229–38.

27. Suttorp M, Bornhäuser M, Metzler M, Millot F, Schleyer E. Pharmacology and pharmacokinetics of imatinib in pediatric patients. Expert Rev Clin Pharmacol. 2018;11:219–31.

28. Geoerger B, Morland B, Ndiaye A, Doz F, Kalifa G, Geoffray A, et al. Target-driven exploratory study of imatinib mesylate in children with solid malignancies by the Innovative Therapies for Children with Cancer (ITCC) European Consortium. Eur J Cancer. 2009;45:2342–51.

29. Verschuur AC, Bajčiová V, Mascarenhas L, Khosravan R, Lin X, Ingrosso A, et al. Sunitinib in pediatric patients with advanced gastrointestinal stromal tumor: results from a phase I/II trial. Cancer Chemother Pharmacol. 2019;84:41-50.

30. Demetri GD, Wang Y, Wehrle E, Racine A, Nikolova Z, Blanke CD, et al. Imatinib plasma levels are correlated with clinical benefit in patients with unresectable/metastatic gastrointestinal stromal tumors. J Clin Oncol. 2009 Jul 1;27:3141–7.

31. Slayton WB, Schultz KR, Kairalla JA, Devidas M, Mi X, Pulsipher MA, et al. Dasatinib plus intensive chemotherapy in children, adolescents, and young adults with philadelphia chromosome–positive acute lymphoblastic leukemia: Results of children's oncology group trial AALL0622. J Clin Oncol. 2018;36:2306–13.

32. Zwaan CM, Rizzari C, Mechinaud F, Lancaster DL, Lehrnbecher T, van der Velden VHJ, et al. Dasatinib in children and adolescents with relapsed or refractory leukemia: results of the CA180-018 phase I dose-escalation study of the Innovative Therapies for Children with Cancer Consortium. J Clin Oncol. 2013;31:2460–8.

33. Ishida Y, Murai K, Yamaguchi K, Miyagishima T, Shindo M, Ogawa K, et al. Pharmacokinetics and pharmacodynamics of dasatinib in the chronic phase of newly diagnosed chronic myeloid leukemia. Eur J Clin Pharmacol. 2016;72:185–93.

34. ClinicalTrials.gov. A Pharmacokinetic (PK) Study of Nilotinib in Pediatric Patients With Philadelphia

Chromosome-positive (Ph+) Chronic Myelogenous Leukemia (CML) or Acute Lymphoblastic Leukemia (ALL). <https://clinicaltrials.gov/ct2/show/study/NCT0107754.

35. Giles FJ, Yin OQP, Sallas WM, le Coutre PD, Woodman RC, Ottmann OG, et al. Nilotinib population pharmacokinetics and exposure-response analysis in patients with imatinib-resistant or -intolerant chronic myeloid leukemia. Eur J Clin Pharmacol. 2013 Apr 5;69:813–23.

36. Committee for Medicinal Products for Human Use (CHMP) European Medicines Evaluation Agency Bosutinib European Public Assessment Report. <http://www.ema.europa.eu/docs/en_GB/ document_ library/EPAR_-_Public_assessment_report/human/ 002373/WC500141745.pdf> (.

37. Cortes JE, Kim D-W, Pinilla-Ibarz J, Le Coutre P, Paquette R, Chuah C, et al. A Phase 2 Trial of Ponatinib in Philadelphia Chromosome-Positive Leukemias. N Engl J Med. 2013;369:1783-96.

38. Food and Drug Administration. Center for Drug Evaluation and Research Ponatinib Clinical Pharmacology and Biopharmaceutics Review. <https://www.accessdata.fda.gov/drugsatfda_docs/nda/ 2012/203469Orig1s000ClinPharmR.pdf>.

39. Yamamoto M, Hori T, Igarashi K, Shimada H, Tsutsumi H. Response to ponatinib before hematopoietic stem cell transplantation in a child with relapsed Philadelphia chromosome-positive acute lymphoblastic leukemia. Pediatr Int. 2018;60:85–7.

40. Sheppard Nickel R, Daves M, Keller F. Treatment of an Adolescent With Chronic Myeloid Leukemia and the T315I Mutation With Ponatinib. Pediatr Blood Cancer. 2015;62:2050–1.

41. Geoerger B, Hargrave D, Thomas F, Ndiaye A, Frappaz D, Andreiuolo F, et al. Innovative therapies for children with cancer pediatric phase I study of erlotinib in brainstem glioma and relapsing/refractory brain tumors. Neuro Oncol. 2011;13:109–18.

42. Geyer JR, Stewart CF, Kocak M, Broniscer A, Phillips P, Douglas JG, et al. A phase i and biology study of gefitinib and radiation in children with newly diagnosed brain stem gliomas or supratentorial malignant gliomas. Eur J Cancer. 2010;46:3287–93.

43. Daw NC, Furman WL, Stewart CF, Iacono LC, Krailo M, Bernstein ML, et al. Phase I and Pharmacokinetic Study of Gefitinib in Children With Refractory Solid Tumors: A Children's Oncology Group Study. J Clin Oncol. 2005;23:6172-80.

44. Bredel M, Pollack IF, Hamilton RL, James CD. Epidermal Growth Factor Receptor Expression and Gene Amplification in High-Grade Non-Brainstem Gliomas. Clin Cancer Res. 1999;5:1786–92.

45. Paugh BS, Qu C, Jones C, Liu Z, Adamowicz-Brice M, Zhang J, et al. Integrated Molecular Genetic Profiling of Pediatric High-Grade Gliomas Reveals Key Differences With the Adult Disease. J Clin Oncol. 2010;28:3061–8.

46. Daw NC, Furman WL, Stewart CF, Iacono LC, Krailo M, Bernstein ML, et al. Phase I and pharmacokinetic study of gefitinib in children with refractory solid tumors: A children's oncology group study. J Clin Oncol. 2005;23:6172–80.

47. Ranson M, Hammond LA, Ferry D, Kris M, Tullo A, Murray PI, et al. ZD1839, a selective oral epidermal growth factor receptor-tyrosine kinase inhibitor, is well tolerated and active in patients with solid, malignant tumors: results of a phase I trial. J Clin Oncol. 2002;20:2240–50.

48. Zhao Y-Y, Li S, Zhang Y, Zhao H-Y, Liao H, Guo Y, et al. The relationship between drug exposure and clinical outcomes of non-small cell lung cancer patients treated with gefitinib. Med Oncol. 2011;28:697–702.

49. White-Koning M, Civade E, Geoerger B, Thomas F, Deley MC Le, Hennebelle I, et al. Population analysis of erlotinib in adults and children reveals pharmacokinetic characteristics as the main factor explaining tolerance particularities in children. Clin Cancer Res. 2011;17:4862–71.

50. Reddick SJ, Campagne O, Huang J, Onar A, Alberto T, Amar B. Pharmacokinetics and safety of erlotinib and

its metabolite OSI-420 in infants and children with primary brain tumors. Cancer Chemother Pharmacol. 2019;84:829-838.

51. White-Koning M, Civade E, Geoerger B, Thomas F, Le Deley M, Hennebelle I, et al. Population Analysis of Erlotinib and Children Reveals Pharmacokinetic Characteristics as the Main Factor Explaining Tolerance Particularities in Children. Clin Cancer Res. 2011 May 20;17:4862–71.

52. DeWire M, Fouladi M, Turner DC, Wetmore C, Hawkins C, Jacobs C, et al. An open-label, two-stage, phase II study of bevacizumab and lapatinib in children with recurrent or refractory ependymoma: a collaborative ependymoma research network study (CERN). J Neurooncol. 2015;123:85–91.

53. Fouladi M, Stewart CF, Blaney SM, Onar-Thomas A, Schaiquevich P, Packer RJ, et al. A molecular biology and phase II trial of lapatinib in children with refractory CNS malignancies: A pediatric brain tumor consortium study. J Neurooncol. 2013;114:173–9.

54. Food and Drug Administration. Center for Drug Evaluation and Research. Afatinib Clinical Pharmacology and Biopharmaceutics Review; 2012.

55. Wind S, Schmid M, Erhardt J, Goeldner R-G, Stopfer P. Pharmacokinetics of Afatinib, a Selective Irreversible ErbB Family Blocker, in Patients with Advanced Solid Tumours. Clin Pharmacokinet. 2013;52:1101–9.

56. Geller JI, Ehrlich PF, Cost NG, Khanna G, Mullen EA, Gratias EJ, et al. Characterization of Adolescent and Pediatric Renal Cell Carcinoma : A Report From the Children's Oncology Group Study AREN03B2. Cancer. 2015;121:2457–64.

57. Geller JI, Fox E, Turpin BK, Goldstein SL, Liu X, Minard CG, et al. A study of axitinib, a VEGF receptor tyrosine kinase inhibitor, in children and adolescents with recurrent or refractory solid tumors: A Children's Oncology Group Phase 1 and Pilot Consortium Trial (ADVL1315). Cancer. 2018;23:4548-4555.

58. Tsuchiya, N. et al. Association of pharmacokinetics of axitinib with treatment outcome and adverse events in advanced renal cell carcinoma patients. In Genitourinary Cancers Symposium. J Clin Oncol. 2015;33:suppl 7.

59. Chuk MK, Widemann BC, Minard CG, Liu X, Kim AR, Bernhardt MB, et al. A phase 1 study of cabozantinib in children and adolescents with recurrent or refractory solid tumors, including CNS tumors: Trial ADVL1211, a report from the Children's Oncology Group. Pediatr Blood Cancer. 2018;65:1–7.

60. Nguyen L, Benrimoh N, Xie Y, Offman E, Lacy S. Pharmacokinetics of cabozantinib tablet and capsule formulations in healthy adults. Anticancer Drugs. 2016 Aug 1;27:669–78.

61. Wedekind MF, Ranalli M, Shah N. Clinical efficacy of cabozantinib in two pediatric patients with recurrent renal cell carcinoma. Pediatr Blood Cancer. 2017;64:4–7.

62. Mahajan P, Dawrant J, Kheradpour A, Quintanilla NM, Lopez ME, Orth RC, et al. Response to Lenvatinib in Children with Papillary Thyroid Carcinoma. Thyroid. 2018;28:1450-1454.

63. Committee for Medicinal Products for Human Use (CHMP) European Medicines Agency Lenvatinib European Public Assessment report. <http://www.ema.europa.eu/docs/en_GB/document_library/EPAR_-_Public_assessment_report/human/003727/ WC500188676.pdf> (2015).

64. Okamoto I, Kaneda H, Satoh T, Okamoto W, Miyazaki M, Morinaga R, et al. Phase I safety, pharmacokinetic, and biomarker study of BIBF 1120, an oral triple tyrosine kinase inhibitor in patients with advanced solid tumors. Mol Cancer Ther. 2010;9:2825–33.

65. Glade Bender JL, Lee A, Reid JM, Baruchel S, Roberts T, Voss SD, et al. Phase I pharmacokinetic and pharmacodynamic study of pazopanib in children with soft tissue sarcoma and other refractory solid tumors: a children's oncology group phase I consortium report. J Clin Oncol. 2013;31:3034–43.

66. Kumar R, Knick VB, Rudolph SK, Johnson JH, Crosby RM, Crouthamel M-C, et al. Pharmacokinetic-pharmacodynamic correlation from mouse to human with pazopanib, a multikinase angiogenesis

inhibitor with potent antitumor and antiangiogenic activity. Mol Cancer Ther. 2007;6:2012–21.

67. Suttle AB, Ball HA, Molimard M, Hutson TE, Carpenter C, Rajagopalan D, et al. Relationships between pazopanib exposure and clinical safety and efficacy in patients with advanced renal cell carcinoma. Br J Cancer. 2014;111:1909–16.

68. Verheijen RB, Bins S, Mathijssen RHJ, Lolkema M, van Doorn L, Schellens JHM, et al. Individualized pazopanib dosing: a prospective feasibility study in cancer patients. Clin Cancer Res. 2016;22:5738-5746.

69. Geoerger B, Morland B, Jimenez I, Frappaz D, Pearson AD, Vassal G, et al. Phase I dose-escalation and pharmacokinetic (PK) study of regorafenib in pediatric patients with recurrent or refractory solid malignancies. J Clin Oncol. 2016;34(15_suppl):10542–10542.

70. Inaba H, Panetta JC, Pounds SB, Wang L, Li L, Navid F, et al. Sorafenib population pharmacokinetics and skin toxicities in children and adolescents with refractory/relapsed leukemia or solid tumor malignancies Hiroto. Clin Cancer Res. 2019;25:7320-7330.

71. Reed DR, Mascarenhas L, Manning K, Hale GA, Goldberg J, Gill J, et al. Pediatric phase I trial of oral sorafenib and topotecan in refractory or recurrent pediatric solid malignancies. Cancer Med. 2016;5:294–303.

72. Karajannis MA, Legault G, Fisher MJ, Milla SS, Cohen KJ, Wisoff JH, et al. Phase II study of sorafenib in children with recurrent or progressive low-grade astrocytomas. Neuro Oncol. 2014;16:1408–16.

73. Kim A, Widemann BC, Krailo M, Jayaprakash N, Fox E, Weigel B, et al. Phase 2 Trial of Sorafenib in Children and Young Adults With Refractory Solid Tumors: A Report From the Children's Oncology Group. Pediatr Blood Cancer. 2015;62:1562–6.

74. DuBois SG, Shusterman S, Ingle AM, Ahern CH, Reid JM, Wu B, et al. Phase I and pharmacokinetic study of sunitinib in pediatric patients with refractory solid tumors: A children's oncology group study. Clin Cancer Res. 2011;17:5113–22.

75. Wetmore C, Daryani VM, Billups CA, Boyett JM, Leary S, Tanos R, et al. Phase II evaluation of sunitinib in the treatment of recurrent or refractory high-grade glioma or ependymoma in children: a children's Oncology Group Study ACNS1021. Cancer Med. 2016;5:1416–24.

76. Janeway KA, Albritton KH, Van Den Abbeele AD, D'Amato GZ, Pedrazzoli P, Siena S, et al. Sunitinib Treatment in Pediatric Patients With Advanced GIST Following Failure of Imatinib Katherine. Adv Astronaut Sci. 2009;52:767–71.

77. Lankheet NAG, Kloth JSL, Gadellaa-van Hooijdonk CGM, Cirkel GA, Mathijssen RHJ, Lolkema MPJK, et al. Pharmacokinetically guided sunitinib dosing: a feasibility study in patients with advanced solid tumours. Br J Cancer. 2014;110:2441–9.

78. Fox E, Widemann BC, Chuk MK, Marcus L, Aikin A, Whitcomb PO, et al. Vandetanib in children and adolescents with multiple endocrine neoplasia type 2b associated medullary thyroid carcinoma. Clin Cancer Res. 2013;19:4239–48.

79. Fallahi P, Ferrari SM, Baldini E, Biricotti M, Ulisse S, Materazzi G, et al. The safety and efficacy of vandetanib in the treatment of progressive medullary thyroid cancer. Expert Rev Anticancer Ther. 2016;16:1109–18.

80. Chisholm JC, Suvada J, Dunkel IJ, Casanova M, Zhang W, Ritchie N, et al. BRIM-P: A phase I, open-label, multicenter, dose-escalation study of vemurafenib in pediatric patients with surgically incurable, BRAF mutation-positive melanoma. Pediatr Blood Cancer. 2018;65:1–9.

81. Bautista F, Paci A, Minard-Colin V, Dufour C, Grill J, Lacroix L, et al. Vemurafenib in Pediatric Patients With BRAFV600E Mutated High-Grade Gliomas Francisco. Pediatr Blood Cancer. 2014;61:1101–3.

82. Kondyli M, Larouche V, Saint-Martin C, Ellezam B, Pouliot L, Sinnett D, et al. Trametinib for progressive pediatric low-grade gliomas. J Neurooncol. 2018;140:435-444.

83. Hargrave DR, Moreno L, Broniscer A, Bouffet E, Aerts I, Andre N, et al. Dabrafenib in pediatric patients with *BRAF* V600–positive high-grade glioma (HGG). J Clin Oncol. 2018;36(15_suppl):10505–10505.

84. Food and Drug Administration. Center for Drug Evaluation and Research Dabrafenib Clinical Pharmacology and Biopharmaceutics Review. <http://www.accessdata.fda.gov/drugsatfda_docs/nda/2013/202806Orig1s000ClinPharmR.pdf> (2013).

85. Ouellet D, Kassir N, Chiu J, Mouksassi M-S, Leonowens C, Cox D, et al. Population pharmacokinetics and exposure–response of trametinib, a MEK inhibitor, in patients with BRAF V600 mutation-positive melanoma. Cancer Chemother Pharmacol. 2016 Apr 3;77:807–17.

86. ClinicalTrials.gov. Safety and Pharmacokinetics of Cobimetinib in Pediatric and Young Adult Participants With Previously Treated Solid Tumors (iMATRIXcobi). <https://clinicaltrials.gov/ct2/show/NCT02639546>.

87. Krueger DA, Care MM, Holland K, Agricola K, Tudor C, Mangeshkar P, et al. Everolimus for subependymal giant-cell astrocytomas in tuberous sclerosis. N Engl J Med. 2010;363:1801–11.

88. Fouladi M, Laningham F, Wu J, O'Shaughnessy MA, Molina K, Broniscer A, et al. Phase I study of everolimus in pediatric patients with refractory solid tumors. J Clin Oncol. 2007;25:4806–12.

89. Ravaud A, Urva SR, Grosch K, Cheung WK, Anak O, Sellami DB. Relationship between everolimus exposure and safety and efficacy: meta-analysis of clinical trials in oncology. Eur J Cancer. 2014;50:486–95.

90. Gopal AK, Fanale MA, Moskowitz CH, Shustov AR, Mitra S, Ye W, et al. Phase II study of idelalisib, a selective inhibitor of PI3Kδ, for relapsed/refractory classical Hodgkin lymphoma. Ann Oncol Off J Eur Soc Med Oncol. 2017;28:1057–63.

91. Ramanathan S, Jin F, Sharma S, Kearney BP. Clinical Pharmacokinetic and Pharmacodynamic Profile of Idelalisib. Clin Pharmacokinet. 2016;55:33–45.

92. ClinicalTrials.gov. Palbociclib in Treating Patients With Relapsed or Refractory Rb Positive Advanced Solid Tumors, Non-Hodgkin Lymphoma, or Histiocytic Disorders With Activating Alterations in Cell Cycle Genes (A Pediatric MATCH Treatment Trial).

93. A phase I/II study of Bosutinib in pediatric patients with Chronic Myeloid Leukemia who are resistant or intolerant to at least one prior Tyrosine Kinase Inhibitor therapy, ITCC-054/AAML1621 <https://www.clinicaltrialsregister.eu/ctr-search/trial/2015-002.

94. Paoletti X, Geoerger B, Doz F, Baruchel A, Lokiec F, Le Tourneau C. A comparative analysis of paediatric dose-finding trials of molecularly targeted agent with adults' trials. Eur J Cancer. 2013;49:2392–402.

95. Voss SD, Glade-Bender J, Spunt SL, DuBois SG, Widemann BC, Park JR, et al. Growth Plate Abnormalities in Pediatric Cancer Patients Undergoing Phase 1 Anti-Angiogenic Therapy: A Report From the Children's Oncology Group Phase I Consortium. Pediatr Blood Cancer. 2015;62:45–51.



Chapter 1.2

Clinical trial simulations in paediatric oncology: A feasibility study from the Innovative Therapies for Children with Cancer Consortium

Eur J Cancer. 2017; 85: 78-85

J.M. Janssen
C.M. Zwaan
J.H.M. Schellens
J.H. Beijnen
A.D.R. Huitema

Abstract

Introduction

Paediatric dose finding studies are challenging to perform due to ethical reasons, the limited number of available patients and restricted number of blood samples. In certain cases, the adult pharmacokinetic exposure can be used as target for dose finding in paediatrics. The aim of this study was to investigate the performance of a paediatric phase I dose finding clinical trial *in silico.*

Methods

Using an adult pharmacokinetic model, a clinical trial simulations were performed to determine the power of a proposed clinical trial design. Power was defined as the fraction of 1,000 trials with an area under the plasma concentration-time curve at steady-state ($AUC_{0\text{-}24,SS}$) within ±20% of the adult geometric mean $AUC_{0\text{-}24,SS}$. Different scenarios were compared to optimize the design of the trial. To show the potential of this framework for similar compounds, the current simulation method was also evaluated with adult and paediatric data from literature on sunitinib.

Results

At the starting dose of 300 mg/m^2, the power of the trial design was 66.9%. Power did not improve by dose-escalation to 350 mg/m^2 (65.3%). Power increased to 78.9% with inclusion of 10 patients per trial. Paediatric sunitinib PK data were adequately predicted from adult data with a mean prediction error of 1.80%.

Conclusion

The performance of PK based clinical trials in paediatrics can be predicted and optimized through PK modeling and simulation. Application of this approach enables clinical trials in paediatrics to be performed as efficient as possible while protecting the child from unnecessary harm.

Introduction

The development of new anticancer drugs that are safe and effective in the paediatric population is of great importance.(1) The main aim of phase I trials is to define the safe and appropriate dose for subsequent evaluation of efficacy in further clinical trials.(2) The most important variables in the design of a paediatric phase I and pharmacokinetic trial are the starting dose, the number of required blood samples and a convenient sampling schedule.(3)

It is widely accepted that pharmacokinetics (PK) as well as pharmacodynamics (PD) must play a more important role in early clinical trial design.(4,5) The International Conference on Harmonization guideline E11 and the European Medicines Agency guideline, describing the role of PK in the development of medicinal products in the paediatric population, both emphasize on the use of adult data for modeling and simulation to guide paediatric clinical trial designs.(6,7)Predictions regarding the optimal number of samples, sampling timepoints and patient numbers in order to perform an efficient and successful clinical trial can be obtained by a modeling and simulation approach.(8–10) One of the advantages of paediatric drug development is that clinical trials in general start with extensive existing knowledge on clinical pharmacology of the drug in adults. This also means that different scenarios can be explored before enrolling paediatric patients into a clinical trial. With previously developed PK models the expected exposure and associated variability can be simulated. However, no phase I clinical trial simulations have been reported regarding paediatric oncology hitherto.(11,12)

In paediatrics, chronic myelogenous leukemia (CML) is a rare disease, accounting for about 3% of all paediatric malignancies, with an approximate annual incidence of 1 per million children. CML is a hematopoietic stem cell disease and is characterized by a constitutive activation of the BCR-ABL fusion protein.(13) Bosutinib is a multi-targeting tyrosine kinase inhibitor (TKI), which is active against BCR-ABL mutations.(14). To date bosutinib has not been used in the treatment of paediatric CML. Since bosutinib may represent an additional therapeutic option for paediatric CML, a phase I/II study was designed to evaluate bosutinib in children and adolescents as part of a Paediatric Investigational Plan (EudraCT number 2015-002916-34). The aim of the current study was to evaluate the paediatric phase I trial design *in silico*, which may also serve as a proof of concept for other trials in paediatric oncology. Therefore, the developed simulation framework was applied to existing adult and paediatric data for another TKI (sunitinib) to show the potential applicability of this approach.

Methods

An ITCC paediatric phase I/II clinical trial has been designed for dose finding of bosutinib administered orally in paediatric patients with CML. The previously observed exposure in adult CML patients treated with the approved dose of 500 mg bosutinib OD served as a target for dose finding in children. The recommended phase II dose (RP2D) was defined in the protocol as the dose which results in an 24-hour area under the plasma concentration-time curve at steady-state ($AUC_{0\text{-}24,SS}$) within ± 20% of the geometric mean $AUC_{0\text{-}24,SS}$ that was found in adults (3640 h*ng/mL) and was considered safe (no dose limiting toxicities (DLT) in 6 patients or 1 DLT in 10 patients).(15)

The protocol stated six time points for blood withdrawal: pre-dose and 1, 3, 6, 8 and 24 hours post-dose at day 14 after start of treatment (i.e. steady-state). Furthermore, three dose levels (250 mg/m^2, 300 mg/m^2 and 350 mg/m^2) were predefined, with 300 mg/m^2 (max. 500 mg) as the starting dose based on BSA scaling from the 500 mg adult dose. The design of the simulation study to evaluate this study design is depicted in figure 1.

Paediatric PK simulations

A population PK model has previously been developed using a pooled PK dataset from three clinical trials of adult patients with Ph+ CP CML and solid tumors treated with bosutinib by Hsyu *et al.*(15) Paediatric bosutinib PK parameters ($CL_{paediatric}$, $Q_{paediatric}$, $V1_{paediatric}$ and $V2_{paediatric}$) were described using an allometric model, with power coefficients of 0.75 for clearance parameters and 1.0 for distribution parameters (equation 1-4).(16,17)

$$CL_{pediatric} = CL_{adult} \times (\frac{BW}{70})^{0.75} \times exp\,(\eta_{i,BSV,CL}) \quad (1)$$

$$Q_{pediatric} = Q_{adult} \times (\frac{BW}{70})^{0.75} \quad (2)$$

$$V1_{pediatric} = V1_{adult} \times (\frac{BW}{70})^{1} \times exp\,(\eta_{i,BSV,V1}) \quad (3)$$

$$V2_{pediatric} = V2_{adult} \times (\frac{BW}{70})^{1} \times exp\,(\eta_{i,BSV,V2}) \quad (4)$$

Where CL_{adult}, Q_{adult}, $V1_{adult}$ and $V2_{adult}$ are the parameter estimates in an adult with a body weight of 70 kg. BW is the simulated individual paediatric body weight and $\eta_{i,BSV}$ represents the between-subject-variability (BSV), distributed following N (0,ω^2) per parameter. To generate individual values for the BSV for every parameter, stochastic simulations with random sampling from a multivariate distribution were performed. (18) The covariance matrix from the developed PK model was used to perform these simulations.(15) This stochastic simulation method was also applied for the simulation of a realistic body weight and height distribution,as suggested in literature.(19)

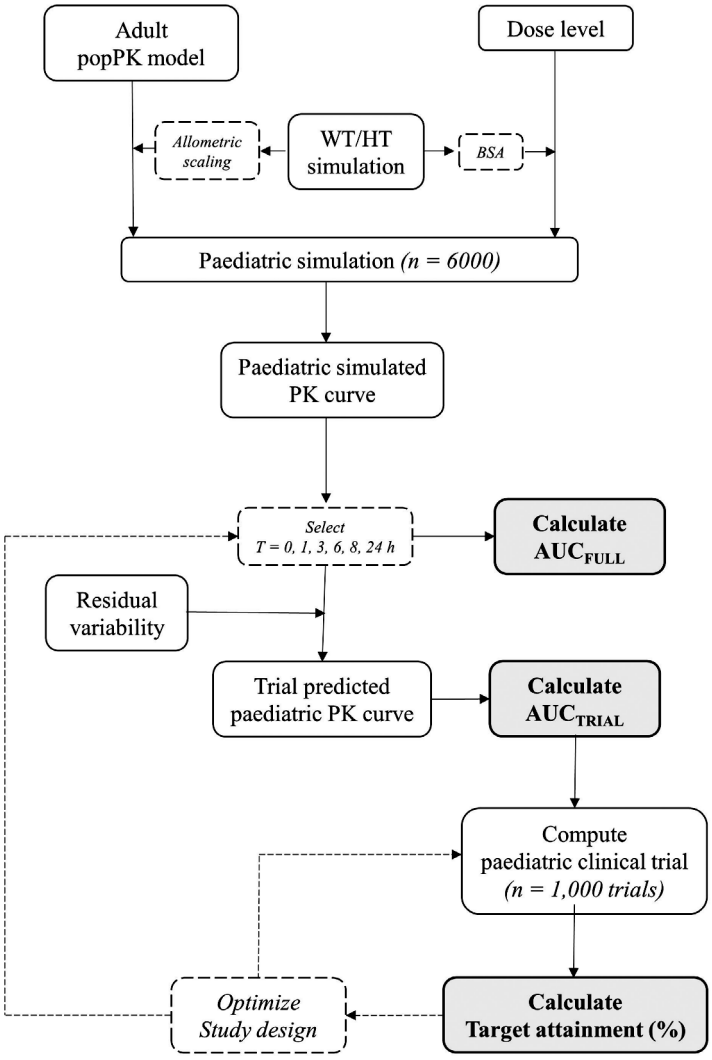

Figure 1. Flowchart representing the steps of the simulation method.

A dataset with matching body weights and heights from a clinical trial with paediatric patients with acute lymphoblastic leukemia (ALL) was available and used for this calculation (EudraCT number 2009-014037-25). With these simulated body weights and heights, the corresponding Body Surface Area (BSA) was calculated per individual by the Mosteller formula, as indicated in the clinical trial protocol.(20) Subsequently, BSA normalized doses were calculated. Doses that exceeded the maximum once-daily adult flat dose, i.e. 400 mg, 500 mg and 600 mg, respectively, were adjusted to the corresponding maximum adult dose.

Clinical trial simulations

A total dataset of 6,000 different paediatric patients was simulated in order to generate 1,000 virtual clinical trials, consisting of 6 paediatric patients per clinical trial. This was separately performed for the three dose levels. With the input parameters, the full plasma concentration-time curve was simulated per patient steady-state after repeated oral dosing. For this PK curve, bosutinib plasma concentrations were simulated every 30 minutes during a 24-hour dosing interval. Subsequently, the predicted trial PK curve was generated by selecting the concentrations at the proposed trial sample time points. These simulated concentrations were transformed to predicted observations at these time points taking the combined proportional and additive residual error model from the previously described bosutinib PK model into account, again by stochastic simulation from a multivariate normal distribution.(15) The $AUC_{0\text{-}24,SS}$ was calculated by non-compartmental analysis from each individual's simulated full PK profile and predicted trial PK profile, according to the clinical trial protocol. The maximum concentration at steady-state ($C_{max,SS}$) was determined as the highest concentration during the dose interval.

The power of the clinical trial design was defined as the fraction of 1,000 clinical trials, consisting of 6 paediatric patients each, with a geometric mean $AUC_{0\text{-}24,SS}$ within the target range of 2912 – 4368 h*ng/mL (± 20% of the adult geometric mean $AUC_{0\text{-}24,SS}$). Subsequently, simulations were performed to optimize the clinical trial design in order to improve the power of the clinical study design. Adjusted sampling schedules and a different number of patients per simulated trial were tested. For the simulation with 10 patients per clinical trial, a total of 10,000 paediatric patients was simulated.

External evaluation

The simulation framework was also evaluated using an adult PK model and paediatric PK data of the anticancer drug sunitinib derived from literature.(21,22) In this paediatric phase 1 trial, 8 patients were treated with 15 mg/m^2 sunitinib OD. Paediatric predicted AUCs from zero to 48 hours ($AUC_{0\text{-}48}$) were calculated and compared to the reported phase 1 results.

Bias was described by the mean prediction error (MPE%) which was calculated for the paediatric predicted trial sunitinib $AUC_{0\text{-}48}$ vs. sunitinib $AUC_{0\text{-}48}$ observed in the paediatric phase I trial, as depicted by equation 5.(23)

$$MPE\% = \left(\frac{(AUC_{est} - AUC_{obs})}{AUC_{obs}}\right) \times 100\% \quad (5)$$

Where AUC_{obs} is the observed sunitinib $AUC_{0\text{-}48}$ and AUC_{est} is the predicted trial sunitinib $AUC_{0\text{-}48.}$

Software

All PK simulations and calculations were performed with R (version 3.3.1), using the differential equation solving R-package deSolve.(24)

Results

Paediatric PK simulations

The simulated PK profiles for the three dose levels are depicted in figure 2. With increasing dose, the $C_{max,SS}$ and exposure increased as expected (table 1). Large variability in $C_{max,SS}$ and $AUC_{0\text{-}24,SS}$ between patients was observed, this variability was similar across the three dose levels. In addition, figure 3 shows the uniformity of the AUCs across the paediatric body weight ranges.

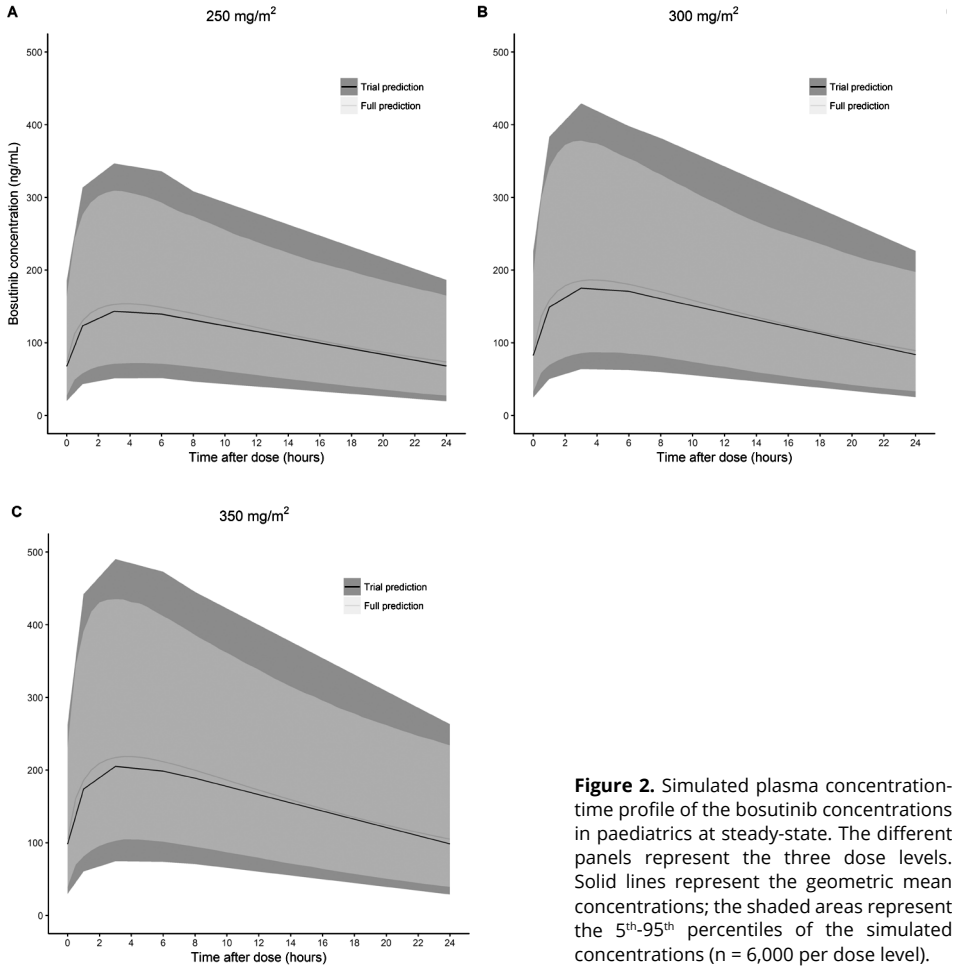

Figure 2. Simulated plasma concentration-time profile of the bosutinib concentrations in paediatrics at steady-state. The different panels represent the three dose levels. Solid lines represent the geometric mean concentrations; the shaded areas represent the 5th-95th percentiles of the simulated concentrations (n = 6,000 per dose level).

Table 1. $AUC_{0\text{-}24,SS}$, $C_{max,SS}$ and target attainment of bosutinib in paediatrics

	250 mg/m²	300 mg/m²	350 mg/m²
$C_{max,SS}$ (ng/mL)[a]			
Full prediction	159.7 (45.18)	193.7 (44.77)	227.4 (43.70)
Trial prediction	192.9 (48.33)	234.6 (49.11)	274.7 (47.01)
$AUC_{0\text{-}24,SS}$ (h*ng/mL)[a]			
Full prediction	2,838 (44.37)	3,442 (44.68)	4,045 (43.57)
Trial prediction	2,719 (48.65)	3,316 (48.92)	3,894 (46.99)
Power n=6 (%)[b]			
Successful trials	34.8	66.9	65.3
Below target	64.2	25.9	6.7
Above target	1.0	7.2	28.0
Power n=10 (%)[b]			
Successful trials	33.9	78.9	75.3
Below target	66.1	17.9	2.5
Above target	0	3.2	22.2

Abbreviations: $C_{max,SS}$, maximum concentration; $AUC_{0\text{-}24,SS}$, 24-hour area under the plasma concentration-time curve.
[a] Geometric mean and coefficient of variation (CV%) of n=6,000 simulated patients per dose. [b] Percentage successful trials out of 1,000 trials consisting of 6-10 patients based on the $AUC_{0\text{-}24,SS}$ target interval (± 20% of 3,640 h*ng/mL) by the different dose levels and percentage of trials with an $AUC_{0\text{-}24,SS}$ below or above the target range.

Clinical trial simulations

Table 1 summarizes the results of the clinical trial simulations. At the starting dose of 300 mg/m², the power to show target attainment was 66.9%, 25.9% of the trials showed an exposure below and 7.2% above the target range (table 1). The mean exposure on this dose level was predicted to be slightly lower than the mean exposure in adults (3,442 h*ng/mL vs 3,640 h*ng/mL). However, the next higher protocol defined dose level showed a slightly higher exposure than with the adult standard dose (4,045 h*ng/mL vs 3,640 h*ng/mL) and, consequently, the power of this dose level was similar (65.3% with 28.0% of trials below and 6.7% above the target range). As expected, the protocol defined dose level of 250 mg/m² OD shows a considerably lower power (34.8%), due to underexposure.

Study design optimization

Based on these simulation results the dose that best approached the target $AUC_{0\text{-}24,SS}$ with the proposed clinical trial design was calculated as 325 mg/m². The power with this intermediate dose level was 70.4%. Subsequently, different sampling designs with more or less samples and different time points were tested at this intermediate dose level (table 2). The sampling schedules with more sample points during 24 hours showed similar power compared to each other and to the original trial design (schedule

Table 2. Predicted trial $AUC_{0\text{-}24,SS}$ and target attainment for alternative sampling scenarios

	I[c]	II[d]	III[e]	IV[f]	V[g]	VI[h]	VII[i]
325 mg/m²							
Predicted trial $AUC_{0\text{-}24,SS}$[a]	3,605	3,540	3,551	3,621	3,641	3,384	3,610
Power (%)[b]	70.4	72.0	69.4	72.3	71.2	67.1	81.1
300 mg/m²							
Predicted trial $AUC_{0\text{-}24,SS}$[a]	3,316	3,220	3,250	3,312	3,337	3,107	3,340
Power (%)[b]	66.9	61.2	64.8	67.5	67.7	57.9	78.9

Abbreviations: $AUC_{0\text{-}24,SS}$, 24-hour area under the plasma concentration-time curve (h*ng/mL).
[a] Geometric mean. [b] Percentage successful trials based on the $AUC_{0\text{-}24,SS}$ target interval (± 20% of 3,640 h*ng/mL). [c] Sample at T=0, T=1, T=3, T=6, T=8, T=24 hours after dose (original sample schedule). [d] Sample at T=0, T=1, T=2, T=5, T=24 hours after dose. [e] Sample at T=0, T=1, T=3, T=6, T=24 hours after dose. [f] Sample at T=0, T=1, T=2, T=3, T=6, T=8, T=24 hours after dose. [g] Sample at T=0, T=1, T=3, T=6, T=8, T=12, T=24 hours after dose. [h] Sample at T=0, T=1, T=3, T=12, T=24 hours after dose. [i] 10 patients per trial with original sample schedule.

I versus IV and V). With the addition of one sample point in the absorption phase the power was 72.3%, addition of a sample point in the elimination phase resulted in a power of 71.2%. Likewise, fewer samples and samples collected at different time points only marginally reduced power (70.4% versus 72.0% and 67.1%, schedule I versus II and VI). Removal of the blood sample at 8 hours post-dose resulted in similar power compared to the original sample schedule (70.4% versus 69.4%, schedule I versus III). The different sample schedules were also applied to the proposed clinical trial starting dose (i.e. 300 mg/m²) with similar results. Increasing the number of patients to 10 patients per trial resulted in an increased power of 81.1% with the intermediate dose and a power of 78.9% with the proposed starting dose.

External evaluation

Simulation of the paediatric $AUC_{0\text{-}48}$ of sunitinib showed that the predictions were in good agreement with the observed values in the paediatric phase 1 trial (figure 5). The median predicted trial $AUC_{0\text{-}48}$ was 500.8 h*ng/mL (range 210.5 – 671.2 h*ng/mL) and the corresponding observed median $AUC_{0\text{-}48}$ in the paediatric clinical trial was 492.0 (range 247 – 1111).(22) The bias between the predicted trial $AUC_{0\text{-}48}$ and observed $AUC_{0\text{-}48}$ (MPE%) was 1.80%.

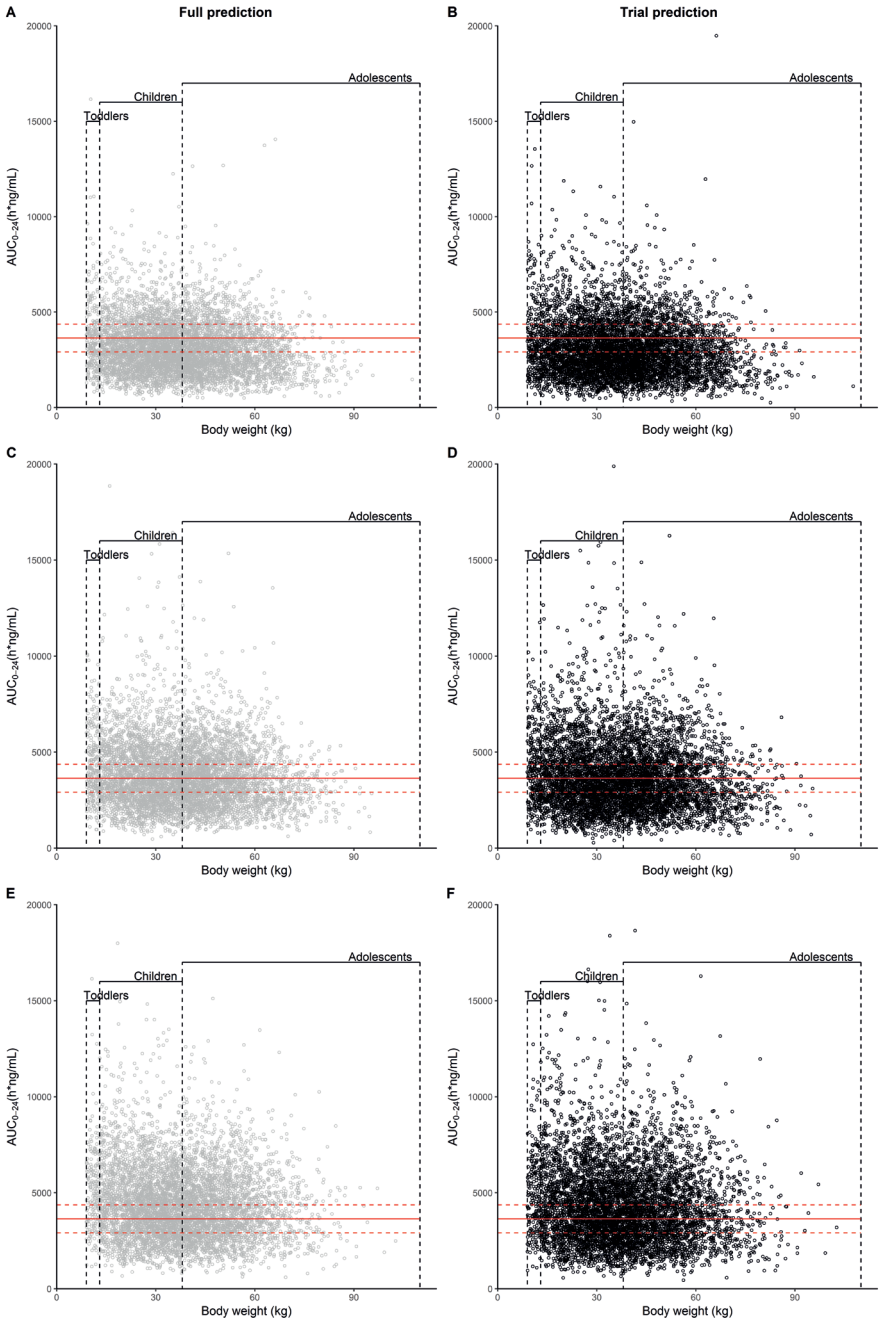

Figure 3. Distribution of the simulated paediatric $AUC_{0\text{-}24,SS}$ versus body weight for the three different dose levels (n = 6,000 per dose level). Panel A and B represent dose level 250 mg/m^2, panel C and D represent dose level 300 mg/m^2 and panel E and F represent dose level 350 mg/m^2. Expected body weight ranges for infants, preschool children, children and adolescents are indicated. The red dashed lines represent the $AUC_{0\text{-}24,SS}$ target area and the red solid line represents the adult geometric mean $AUC_{0\text{-}24,SS}$ in patients with CML.

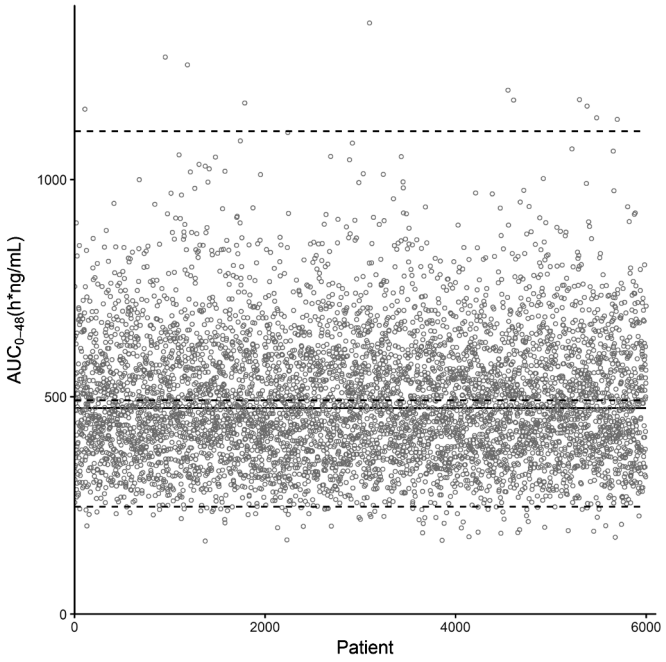

Figure 4. Distribution of the predicted trial sunitinib paediatric AUC_{0-48}. The dashed lines represent the range and median AUC_{0-48} observed in paediatric patients and the solid line represents the paediatric median predicted trial AUC_{0-48} (n = 6,000).

Discussion

Paediatric dose finding studies of targeted agents are very difficult to perform. First, for ethical reasons, the number of patients treated at low doses should be minimal to prevent under treatment. Secondly, the number of patients fulfilling the in- and exclusion criteria is usually low because of the rarity of malignancies in paediatrics. Thirdly, the number of blood samples to be collected should be as low as reasonably possible.(4,25,26) A thorough *a priori* evaluation of a proposed trial design could aid in the optimization of the design. We successfully performed an *in silico* evaluation of a proposed trial design for a dose finding study of bosutinib in paediatric patients with CML.

It has been extensively advocated in literature that PK should be better integrated in paediatric drug development.(6,7,27) Paoletti *et al.* found that the paediatric RP2D ranged between 90% and 130% of the BSA-adjusted approved dose in adults for 70% of 25 paediatric phase I trials that investigated molecularly targeted agents.(5) In addition, 63% of the patients did not receive an optimal dose. Suggesting early-phase clinical trials validating PK, PD and efficacy findings from adults while controlling for

toxicity appears to be an alternative to accelerate drug development in paediatric oncology. However, PK characteristics of a drug may differ between age groups due to the heterogeneity of many anatomical and physiological maturation processes, in particular in young children.(28) It is essential that these changes are considered to ensure appropriate trial rationales and dosing schedules among all age ranges.

Population pharmacokinetic model-based simulations were performed to determine an optimal clinical trial design based on the likelihood of achieving an *a priori* established PK target. Since this paediatric phase I trial is the first paediatric trial for bosutinib, no information regarding the exposure-efficacy relationship in paediatric patients with CML was available. Thus, the geometric mean $AUC_{0\text{-}24,SS}$ observed in adult patients was chosen as paediatric PK target for the clinical trial in this simulation study. The simulated full $AUC_{0\text{-}24,SS}$ values were higher than the predicted trial $AUC_{0\text{-}24,SS}$ at the three dose levels, which means that the true exposure is underestimated by the proposed sampling schedule. This can be explained by the use of non-compartmental method for calculation of the AUC. The power increased with increasing dose, with exception of the highest dose level. The power did not improve substantially with less, more samples or adapted sampling times. With carefully chosen sampling times, the power remained the same when only five sample time points were included instead of the original 6 time points. The clinical trial simulation consisting of 10 paediatric patients per trial showed an increased power of 81.1%. This is a plausible scenario since the trial will be extended to 10 patients if one DLT is observed in the first 6 patients. To assess whether the clinical trial simulation produces meaningful results, we also performed this simulation on a published dataset of sunitinib in adults and children. Results of this simulation showed that the PK of sunitinib in children could be adequately predicted on a population level from a PK model based on adult data only.

To date, only few studies have been published in the setting of paediatric clinical trial simulation that included PK. Mouksassi *et al.* presented a clinical trial simulation method in paediatric patients using an adult population PK model.(29) The scaled adult model included a maturation function of the glomerular filtration rate in addition to allometric scaling. Bosutinib is mainly metabolized by CYP3A isoenzymes into inactive metabolites.(14) The maturation of CYP3A4 is assumed to be complete at one year of age.(30,31) A maturation factor for CYP3A was not considered for this simulation because the clinical trial only includes patients older than one year of age. Moreover, CML is extremely rare in younger children and it is expected that the majority of included children will be even >10 years. Stockmann *et al.* and Reif *et al.* provide a usable method to design a paediatric clinical trial in a large group of paediatric patients based on adequate statistical power.(32,33) Translation of this clinical trial simulation method to paediatric oncology is not applicable because of the rarity of malignancies in paediatrics.

In conclusion, a simulation method has been developed for the prediction of bosutinib PK in paediatrics. Simulations revealed that the power of a clinical trial design can be predicted and optimized for various clinical trial designs. The developed simulation method will be further validated as part of the pharmacometric analysis of the bosutinib paediatric clinical trial.

References

1. Vassal G, Zwaan CM, Ashley D, Le Deley MC, Hargrave D, Blanc P, et al. New drugs for children and adolescents with cancer: the need for novel development pathways. Lancet Oncol. 2013;14(3):117–24.

2. Smith BM, Bernstein M, Bleyer WA, Borsi JD, Ho P, Lewis J, et al. Conduct of Phase I Trials in Children With Cancer. J Clin Oncol. 2016;16:966–78.

3. Panetta JC, Iacono LC, Adamson PC, Stewart CF. The Importance of Pharmacokinetic Limited Sampling Models for Childhood Cancer Drug Development. Clin Cancer Res. 2003;9:5068–77.

4. Doussau A, Geoerger B, Jimenez I, Paoletti X. Innovations for phase I dose-finding designs in pediatric oncology clinical trials. Contemp Clin Trials. 2016;47:217–27.

5. Paoletti X, Geoerger B, Doz F, Baruchel A, Lokiec F, Le Tourneau C. A comparative analysis of paediatric dose-finding trials of molecularly targeted agent with adults' trials. Eur J Cancer. 2013;49:2392–402.

6. European Medicines Agency. Guideline on the role of pharmacokinetics in the development of medicinal products in the paediatric population. 2008.

7. International Conference on Harmonisation (ICH). Clinical Investigation of Medicinal Products in the Pediatric Population (E11). 2000.

8. Holford N, Ma SC, Ploeger BA. Clinical Trial Simulation: A Review. Clin Pharmacol Ther. 2010;88:166–82.

9. De Cock RFW, Piana C, Krekels EHJ, Danhof M, Allegaert K, Knibbe CAJ. The role of population PK-PD modelling in paediatric clinical research. Eur J Clin Pharmacol. 2011;67(SUPPL. 1).

10. Läer S, Barrett JS, Meibohm B. The in silico child: using simulation to guide pediatric drug development and manage pediatric pharmacotherapy. J Clin Pharmacol. 2009;49:889–904.

11. Tod M, Jullien V, Pons G. Facilitation of drug evaluation in children by population methods and modelling. Clin Pharmacokinet. 2008;47:231–43.

12. Bellanti F, Della Pasqua O. Modelling and simulation as research tools in paediatric drug development. Eur J Clin Pharmacol. 2011;67(SUPPL. 1).

13. Hijiya N, Schultz KR, Metzler M, Millot F, Suttorp M. Pediatric chronic myeloid leukemia is a unique disease that requires a different approach. Blood. 2014 Dec 11;124:3817–27.

14. Abbas R, Hsyu P-H. Clinical Pharmacokinetics and Pharmacodynamics of Bosutinib. Clin Pharmacokinet. 2016 Oct 25;55:1191–204.

15. Hsyu P, Mould DR, Abbas R, Amantea M. Population Pharmacokinetic and Pharmacodynamic Analysis of Bosutinib. Drug Metab Pharmacokinet. 2014;29:441–8.

16. West GB, Brown JH, Enquist BJ. A General Model for the Origin of Allometric Scaling Laws in Biology. Science. 1997;276:122–6.

17. Anderson BJ, Holford NHG. Mechanistic basis of using body size and maturation to predict clearance in humans. Drug Metab Pharmacokinet. 2009;24:25–36.

18. Tannenbaum SJ, Holford NHG, Lee H, Peck CC, Mould DR. Simulation of correlated continuous and categorical variables using a single multivariate distribution. J Pharmacokinet Pharmacodyn. 2006;33:773–94.

19. Burton A, Altman DG, Royston P, Holder RL. The design of simulation studies in medical statistics. Stat Med. 2008;27:4817–34.

20. Mosteller RD. Simplified calculation of body-surface area. N Engl J Med. 1987 Oct 22;317:1098.

21. Yu H, Steeghs N, Kloth JSL, De Wit D, Van Hasselt JGC, Van Erp NP, et al. Integrated semi-physiological pharmacokinetic model for both sunitinib and its active metabolite SU12662. Br J Clin Pharmacol. 2015;79:809–19.

22. DuBois SG, Shusterman S, Ingle AM, Ahern CH, Reid JM, Wu B, et al. Phase I and pharmacokinetic study of sunitinib in pediatric patients with refractory solid tumors: A children's oncology group study. Clin Cancer Res. 2011;17:5113–22.

23. Sheiner LB, Beal SL. Some suggestions for measuring predictive performance. J Pharmacokinet Biopharm. 1981;9:503–12.

24. Soetaert K, Petzoldt T SR. Solving Differential Equations in R: Package deSolve. J Stat Softw. 2010;33:1–25.

25. Smith M, Bernstein M, Bleyer WA, Borsi JD, Ho P, Lewis J, et al. Conduct of Phase I Trials in Children With Cancer. J Clin Oncol. 2016;16:966–78.

26. Altavilla A. Ethical key issues and fundamental rights in paediatric research. Eur J Clin Pharmacol. 2011;67:117–23.

27. Peigné S, Bouzom F, Brendel K, Gesson C, Fouliard S, Chenel M. Model-based approaches for ivabradine development in paediatric population, part I: study preparation assessment. J Pharmacokinet Pharmacodyn. 2016 Feb 12;43:13–27.

28. Batchelor HK, Marriott JF. Paediatric pharmacokinetics: Key considerations. Br J Clin Pharmacol. 2015;79:395–404.

29. Mouksassi MS, Marier JF, Cyran J, Vinks AA. Clinical Trial Simulations in Pediatric Patients Using Realistic Covariates: Application to Teduglutide, a Glucagon-Like Peptide-2 Analog in Neonates and Infants With Short-Bowel Syndrome. Clin Pharmacol Ther. 2009;86:667–71.

30. Hines RN. Ontogeny of human hepatic cytochromes P450. J Biochem Mol Toxicol. 2007;21:169–75.

31. Stevens JC, Hines RN, Gu C, Koukouritaki SB, Manro JR, Tandler PJ, et al. Developmental expression of the major human hepatic CYP3A enzymes. J Pharmacol Exp Ther. 2003 Nov;307:573–82.

32. Stockmann C, Barrett JS, Roberts JK, Sherwin C. Use of Modeling and Simulation in the Design and Conduct of Pediatric Clinical Trials and the Optimization of Individualized Dosing Regimens. CPT pharmacometrics Syst Pharmacol. 2015;4:630–40.

33. Reif S, Schultze-mosgau M, Sutter G. From Adults to Children Simulation-Based Choice of an Appropriate Sparse-Sampling Schedule. Pediatr Drugs. 2012;14:189–200.



Chapter 1.3

A Semi-Mechanistic Population Pharmacokinetic/ Pharmacodynamic Model of Bortezomib in Pediatric Patients with Relapsed/Refractory Acute Lymphoblastic Leukemia

Clin Pharmacokinet. 2019; 59: 207-216.

J.M. Janssen
T.P.C. Dorlo
D. Niewerth
A.J. Wilhelm
C.M. Zwaan
J.H. Beijnen
A. Attarbaschi
A. Baruchel
F. Fagioli
T. Klingebiel
B. De Moerloose
G. Palumbo
A. von Stackelberg
G.J.L. Kaspers
A.D.R. Huitema

Abstract

Introduction

The pharmacokinetics (PK) of the 20S proteasome inhibitor bortezomib are characterized by a large volume of distribution and a rapid decline in plasma concentrations within the first hour after administration. An increase in exposure was observed in the second week of treatment, which has previously been explained by extensive binding of bortezomib to proteasome in erythrocytes and peripheral tissues. We characterized the nonlinear population PK and pharmacodynamics (PD) of bortezomib in children with Acute Lymphoblastic (ALL).

Methods

323 samples from 28 patients were available from a pediatric clinical study investigating bortezomib at an intravenous dose of 1.3 mg/m^2 at a twice-weekly schedule (Dutch Trial Registry number 1881/ITCC021). A semi-physiological PK model for bortezomib was first developed. The PK was linked to the decrease in 20S proteasome activity in the final PK-PD model.

Results

The plasma PK data was adequately described by a two-compartment model with linear elimination. Increased concentrations were observed in week 2 compared to week 1, which was described by a Langmuir binding model. The decrease in 20S proteasome activity was best described by a direct effect model with a sigmoidal inhibitory E_{max} effect representing the relationship between plasma concentrations and effect. The maximal inhibitory effect was 0.696 pmol AMC/sec/mg protein (95% CI 0.664–0.728 pmol AMC/sec/mg protein) after administration.

Conclusion

The semi-physiological model adequately described the nonlinear PK and PD of bortezomib in plasma. This model can be used to further optimize dosing of bortezomib.

Introduction

The 5-year overall survival of children with acute lymphoblastic leukemia (ALL) exceeds 85% after primary treatment. However, relapse occurs in about 15-20% of patients and only 40% of relapsing patients can be cured, mainly caused by emerging resistance to conventional chemotherapy.(1) To improve the treatment options for pediatric malignancies, the development of new anticancer drugs is essential. Novel anticancer agents inhibiting specific molecular targets have promise to overcome resistance to previously administered therapy and enhance survival rates.(2)

Bortezomib is a small dipeptidyl boronic acid exhibiting reversible inhibitory effects on the chymotrypsin-like proteolytic activity of the 20S proteasome. By binding the 20S proteasome bortezomib interferes with the ubiquitin-proteasome pathway which plays a pivotal role in the degradation of proteins involved in tumor cell proliferation and cell survival.(3,4) Bortezomib is registered for the treatment of adults with multiple myeloma (MM) in a two-weekly schedule of 1.3 mg/m^2 intravenously on days 1, 4, 8 and 11.(3) Results from preclinical and in vivo studies showed high antileukemic activity of bortezomib towards ALL cell lines.(5)

Bortezomib pharmacokinetics (PK) have been studied in adults with relapsed MM and is characterized by large volume of distribution and rapid decline in plasma concentrations within the first hour after administration. In addition, a marked increase in bortezomib exposure associated with a decrease in clearance was observed in the second week of treatment.(4,6) The pharmacodynamic (PD) effect of bortezomib can be measured by 20S proteasome activity in whole blood. In adults, a rapid inhibition of 20S proteasome activity directly after drug administration was observed. Inhibition levels followed systemic exposure and declined with decreasing plasma concentrations. In accordance with the PK observations, the maximum 20S proteasome inhibition was higher in the second week of treatment.(4,6) In several pediatric studies with limited number of patients, bortezomib PK and PD were shown to be similar to that observed in adults.(7–9) A recently developed population pharmacokinetic model confirmed these results in a larger group of pediatric patients.(10) However, a semi-mechanistic characterization of the nonlinear PK behavior in children has not been published yet.

We previously conducted a phase II clinical trial investigating bortezomib in pediatric patients with ALL, where bortezomib was administered in a twice-weekly 1.3 mg/m^2 dosing schedule. Clinical results of this study have been presented earlier.(11) The primary goal of the population PK analysis that we present here was to characterize the time-dependent PK-PD profile of bortezomib in pediatric patients in a semi-physiological approach to better understand the processes driving observed non-linearities.

Methods

Patients, sampling and analytical methodology

An open label randomized feasibility and phase II study combining bortezomib with conventional chemotherapy for the treatment of pediatric patients with relapsed or refractory ALL (rALL) was performed by the Innovative Therapies for Children with Cancer (ITCC) consortium (Dutch National Trial Registry number 1881/ITCC021).(11) The primairy aim of this clinical study was to assess the antileukemic activity of bortezomib in combination with conventional chemotherapy in pediatric rALL. All patients were repeatedly treated with bortezomib in an intravenous dose of 1.3 mg/m^2 in a two-weeks cycle. Patients were randomized to receive bortezomib on day 1, 4, 8 and 11 in arm A, or on day 8, 11, 15 and 18 in arm B. Patients were additionally treated with standard reinduction chemotherapy consisting of 2 weeks of dexamethasone combined with 2 injections of vincristine given once-weekly, and with intrathecal administration of methotrexate. Samples for PK and PD assessment were collected after the first and third administration days of the first cycle after start of treatment at time-points pre-dose and 15 minutes, 3, 8, 24, 48 and 72 hours after dose. An additional sample was taken 30 minutes after dose on the second administration day. Demographic characteristics such as age, gender, total body weight and height were recorded at start of treatment. Informed consent was obtained from all individual participants or their legal guardians

After collection, peripheral blood samples for PK analysis were centrifuged at 4°C for 10 minutes at 1,000 g and plasma was stored at -70°C until analysis. Separation between metabolites and interfering endogenous compounds and detection was achieved by LC-MS/MS using a Waters Xbridge Shield RP18/50x2.1 mm 3.5 µm column at 40°C and using a ternary gradient of 0.1% formic acid in water as mobile phase A, acetonitrile as mobile phase B and 2-propanol:acetonitrile:water:ammonia (30:30:40:2, v/v/v/v) as mobile phase C. The initial flow rate was 0.40 mL/min. An Sciex 4000 quadrupole mass spectrometer equipped with a turbo ion spray source was used for detection in positive ion model. Quantification was based on multiple reaction monitoring of the transitions of m/z 367.2-226.2 for bortezomib and 376.3-234.2 for its internal standard. A linear calibration curve with a $1/x^2$ weighing factor ranging from 0.1 to 25.0 ng/mL was used.

The 20S proteasome activity was determined by measuring the rate of proteolytic hydrolysis of a fluorescent tagged peptide substrate Suc-Leu-Leu-Val-Tyr-AMC, in a lysate prepared from peripheral whole blood samples. The activity was normalized to the amount of protein present in the sample lysate. Protein concentrations were determined using a Pierce BCA protein assay kit ($R2>0.99$). The specific activity of each sample was determined against an AMC standard curve.

Structural model development

For the description of the PK of bortezomib one-to three-compartment models were evaluated using the bortezomib concentrations that were measured in plasma (C_{plasma}). Previously, binding of bortezomib to erythrocytes was suggested.(12) A semi-physiological approach was tested to describe this distribution, using the Langmuir equation for saturable binding equilibriums (eq. 1).

$$C_{bound} = \frac{B_{max} \cdot C_{plasma}}{C_{plasma} + K_D} \quad \text{(Eq. 1)}$$

where B_{max} (ng/mL) corresponds to the maximal binding capacity, and K_D (ng/mL) is the equilibrium dissociation constant. Meaning, if the plasma concentration is equal to K_D, the bound concentration (C_{bound}) is half maximal. It was assumed that distribution of bortezomib within the central compartment occurred instantaneously. Hence, the fractions erythrocyte bound and unbound bortezomib in whole blood and plasma, respectively, were assumed to be in equilibrium at any moment.

Total body weight (WT) was included in the PK model *a priori* using allometric scaling. All clearance and volume parameters were scaled to the median body weight in the dataset (i.e. 32 kg). The allometric exponents were fixed to 0.75 for clearance parameters and 1 for volumes of distribution according to allometric principles (eq. 2 and 3).(13)

$$P_{CL} = P0_{CL} \cdot \left(\frac{WT}{32}\right)^{0.75} \quad \text{(Eq. 2)}$$

$$P_V = P0_V \cdot \left(\frac{WT}{32}\right) \quad \text{(Eq. 3)}$$

where P represents the WT-adjusted population parameter and P0 represents the baseline population parameter estimate for parameter P. For all patients, WT at baseline was available.

An additional effect of maturation on clearance was also explored by extending equation 1 to equation 4.(14,15)

$$P_{CL} = P0_{CL} \cdot \left(\frac{WT}{32}\right)^{0.75} \cdot \frac{PMA^{Hill}}{PMA_{50}^{Hill} + PMA^{Hill}} \quad \text{(Eq. 4)}$$

were PMA_{50} is the postmenstrual age (PMA) (gestational plus postnatal age) at which CL reached 50% maturity, and *Hill* is the shape parameter.

Sequential modelling of PK and PD was used to determine the PK-PD model. The PD model was developed using the typical parameters from the final PK model as input, simulating individual bortezomib concentrations.(16) Models using either simulated

C_{plasma} or C_{bound} as PK drivers were explored. Exploratory plots were used to determine the relationship between the PK and the decreases in 20S proteasome activity after bortezomib administration. Linear, E_{max} and sigmoidal inhibitory E_{max} relationships between PK and 20S proteasome activity were investigated. Weight, gender and treatment arm were assessed as covariates for clinical and statistical significance.

Stochastic model

Between subject variability (BSV) and within subject variability (WSV) were evaluated for all parameters using an exponential error model (eq. 5):

$$P_i = P_{pop} \cdot \exp(\eta_{i,BSV} + \eta_{i,WSV}) \quad \text{(Eq. 5)}$$

where P_i represents the individual parameter estimate for individual *i*, P_{pop} represents the typical population parameter estimate, η_i either BSV or WSV effect for subject individual *i* where η_i was assumed to be normally distributed following $N(0, \sigma^2)$. Occasions were defined as individual treatment weeks, in which week 1 consists of the first and second bortezomib administration and week 2 was the third and fourth administration.

Residual unexplained variability was described by a proportional error model (eq. 6):

$$C_{obs,ij} = C_{pred,ij} \cdot (1 + \varepsilon_{p,ij}) \quad \text{(Eq. 6)}$$

where $C_{obs,ij}$ represents the observed concentration for individual *i* and observation *j*, $C_{pred,ij}$ respresents the individual predicted concentration and $\varepsilon_{p,ij}$ represents the proportional error distributed following $N(0, \sigma^2)$.

Model selection and evaluation

The model selection criteria were the same for the PK and PD analysis. Discrimination between models was guided by physiological plausibility, goodness-of-fit (GOF) plots, precision of parameter estimates and change in objective function value (OFV). A drop of ≥ 6.63, corresponding to a $P < 0.01$ (χ^2-distribution with 1 degree of freedom), was considered a significant improvement of the fit for hierarchical models. The adequacy of the models was assessed by GOF plots and prediction-corrected visual predictive checks (pcVPC).(17) Parameter precision was obtained by Sampling Importance Resampling (SIR).(18)

External evaluation

Nonlinear mixed-effects modeling was performed using NONMEM® v.7.3(ICON Development Solutions, Ellicott City, MD, USA) and Perl-speaks-NONMEM (PsN, version 4.4.8) with First-Order Conditional Estimation with interaction (FOCE-I) as estimation method. Piraña (version 2.9.7) was used as graphical user interface for NONMEM. (19–21) R (version 3.4.3) was used for processing of the data, graphical diagnostics and simulation purposes.(22)

Results

Patients and data

A total of 323 PK plasma samples and 356 PD whole blood samples from 28 patients were included in the final analysis data set. The median number of bortezomib plasma concentrations available per patient was 13 (range 4.0 – 14.0) and the median number of 20S proteasome activity samples was 15 (range 5.0 – 16.0). The patient characteristics are depicted in Table 1. The overall mean age at baseline was 9.94 years (range 1.0 – 17.6 years) and the mean weight at baseline was 34.4 kg (range 7.8 – 69.7 kg). The clinical results have been described in detail by Kaspers *et al.*(11)

Table 1. Patient characteristics

Age categories (years)	1 - < 6	6 - < 12	12 - < 18	All patients
Total number of patients, n	6	10	12	28
PK samples, n	68	113	142	323
PK samples/patient [mean±SD]	11.3 ± 3.77	11.3 ± 3.16	11.8 ± 2.17	11.7 ± 2.72
PD samples	82	132	142	356
PD samples/patient [mean±SD]	13.7 ± 4.27	13.2 ± 3.29	14.2 ± 2.66	13.7 ± 3.21
Age (years)[a] [mean±SD]	1.89 ± 0.93	8.59 ± 1.54	15.1 ± 1.58	9.94 ± 5.37
Height (m) [mean±SD]	82.3 ± 7.63	129 ± 8.15	155 ± 10.8	130 ± 29.4
Weight (kg) [mean±SD]	10.1 ± 1.88	27.7 ± 5.46	52.2 ± 9.83	34.4 ± 18.4
BSA (m^2) [mean±SD]	0.47 ± 0.05	0.99 ± 0.12	1.49 ± 0.16	1.09 ± 0.42
Sex [n(%)]				
Male	4 (66.7)	8 (80.0)	4 (33.3)	16 (57.1)
Female	2 (33.3)	2 (20.0)	8 (66.7)	12 (42.9)

Abbreviations: BSA, Body Surface Area; PK, pharmacokinetic; PD, pharmacodynamics; SD, standard deviation
[a] Age at baseline

Population PK analysis

A quick decrease in bortezomib plasma concentrations was observed within one hour after administration. The observed concentration-time profiles were well described by a two-compartment model with first-order elimination. Total body weight was included *a priori* as an allometric function for body size effect on all parameters. An additional maturation effect could not be identified. In addition, gender could not be identified as covariate that affected the PK in our population.

To explore the marked difference in plasma concentrations between the first and the second treatment week, an empirical approach was used first. Clearance and volumes of distribution parameters were separately estimated for both treatment weeks. This showed that the central and peripheral volumes of distribution were notably larger

in the first week of treatment. No difference in clearance was found between the two weeks. Saturable nonspecific binding of bortezomib in the central compartment was introduced in the model and resulted in a strong improvement in model fit (dOFV = -80). Furthermore, with the introduction of saturable binding, the decrease in volume of distribution during treatment disappeared. The parameter estimates for the final model are summarized in Table 2. The clearance of bortezomib from the central compartment was estimated at 6.32 L/h (95% CI 3.76 – 9.83 L/h). Volumes of distribution were large, 68.8 L (95% CI 44.7 – 104 L) and 622 L (95% CI 388 – 1102 L) for central and peripheral volume of distribution respectively. Figure 1 shows a schematic representation of the semi-physiological model. The relationship between C_{bound} and C_{plasma} within the central compartment was well described by the Langmuir equation. B_{max} was estimated at 60.4 ng/mL (95% CI 34.4-105 ng/mL) and K_D at 60.6 ng/mL (95% CI 33.4-113 ng/mL). The model included BSV on B_{max}, which was estimated as 51.8% (95% CI 39.2–70.7%). Introduction of BSV on the remaining structural parameters resulted in over-parameterization of the model. In addition, the incorporation of WSV did not result in a significant improvement of the model. Residual unexplained variability was characterized by a proportional error (%CV) of 68.1% (95% CI 63.1 – 74.1%).

Table 2. Parameter estimates of bortezomib in the final pharmacokinetic model

	Units	Estimate	95% CI[a]	Shrinkage (%)
Population Parameter				
Clearance (CL)[b]	L/h	6.32	3.76–9.83	
Central volume of distribution (V_c)[b]	L	68.8	44.7–104	
Inter-compartmental clearance (Q)[b]	L/h	34.5	21.8–53.0	
Peripheral volume of distribution (V_p)[b]	L	622	388–1102	
Equilibrium dissociation constant (K_d)	ng/mL	60.6	33.4–113	
Maximal binding capacity (B_{max})	ng/mL	60.4	34.4–105	
Between-subject variability				
Maximal binding capacity (B_{max})	CV%	51.8	39.2–70.7	3
Residual unexplained variability				
Proportional residual error	CV%	68.1	63.1–74.1	4

Abbreviations: CI, confidence interval; CV%, coefficient of variation
[a] 95% CI values were obtained by SIR. [b] Typical parameters provided for the median weight (i.e. 32 kg).

Population PD analysis

A quick decrease in 20S proteasome activity directly after administration of bortezomib with recovery to baseline before administration of the following dose was observed. The decrease of the 20S proteasome activity following administration of bortezomib was adequately described using a direct effect inhibitory sigmoidal E_{max} model with

proportional error. The relationship between drug exposure and 20S proteasome activity (PI) was described by the simulated C_{plasma}:

$$PI = PI_0 \times (1 - \left(\frac{E_{max} \times {C_{plasma}}^{Hill}}{{EC_{50}}^{Hill} + {C_{plasma}}^{Hill}}\right)) \quad \text{(Eq. 7)}$$

where PI_0 is the 20S proteasome activity at baseline, E_{max} and EC_{50} are the maximal decrease in 20S proteasome activity and the bortezomib C_{plasma} at which the effect is half maximal, respectively and *Hill* is the shape parameter.

Linear and E_{max} models were also investigated. Introduction of the Hill parameter resulted in a significantly improved fit and was thus retained in the final model. Exploration of an effect compartment model resulted in a large effect compartment rate estimate and no further improvement in model fit. Which confirmed the adequateness of the direct effect model. Univariate inclusion of covariates on the structural parameters did not improve the model fit. The final parameter estimates are summarized in table 3. The maximal decrease in 20S proteasome activity was 0.696 pmol AMC/sec/mg protein (95% CI 0.664 – 0.728 pmol AMC/sec/mg/protein) and 20S proteasome activity baseline was 0.104 pmol AMC/sec/mg protein (95% CI 0.087 – 0.124 pmol AMC/sec/mg/protein) with 40.7% (95% CI 32.3 – 49.3%) BSV.

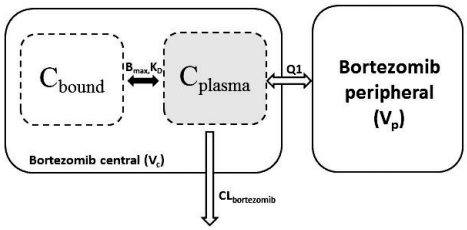

Figure 1. Schematic representation of the semi-mechanistic PK model for bortezomib. Instantaneous equilibriums are depicted by solid arrows. Open arrows represent kinetic processes. Bortezomib concentrations are measured in the plasma compartment.

Model evaluation

The GOF plots and pcVPC showed that the final models adequately described the PK and variability of the observed bortezomib plasma concentrations for each treatment week (figure 2 and figure 3). This indicates that the incorporation of saturable binding of bortezomib in the central compartment adequately explained the non-linearity in the observed PK profiles. A trend towards higher CWRES values for higher concentrations was observed. Nevertheless, the 95% CIs that were obtained by SIR were reasonably narrow, except for K_D and B_{max} which can be explained by the fact that detailed information on target binding was not available.

The pcVPC of the PD-model (figure 3) showed an over-prediction of the 20S proteasome activity at 8 hours post-dose. In addition, the CWRES vs. time plot shows a slight trend towards negative CWRES values after the third administration. Nevertheless, the GOF

Table 3. Parameter estimates of 20S proteasome activity in the final pharmacodynamic model

	Units	Estimate	95% CI[a]	Shrinkage (%)
Population Parameter				
20S proteasome activity baseline (E_{base})	pmol AMC/sec/mg protein	0.104	0.087–0.124	
Maximal inhibitory effect (E_{max})	pmol AMC/sec/mg protein	0.696	0.664–0.728	
Sensitivity (EC_{50})	ng/mL	2.03	1.75–2.33	
Shape parameter (Hill)	-	1.96	1.56–2.47	
Between-subject variability				
20S proteasome activity baseline (E_{base})	CV%	40.7	32.3–49.3	12
Residual unexplained variability				
Proportional residual error	CV%	20.7	19.2–22.6	4

Abbreviations: CI, confidence interval; CV%, coefficient of variation; AMC, 7-amino-4-methycoumarin.
[a] 95% CI values were obtained by SIR.

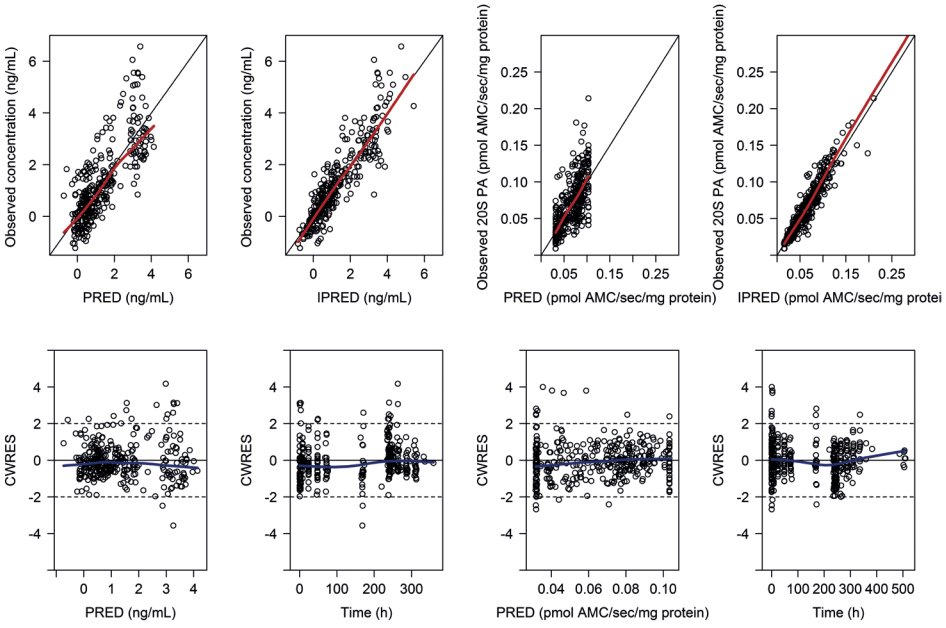

Figure 2. Goodness-of-fit plots of the final PK and PD model. Model predicted log-transformed bortezomib concentrations (ng/mL) and 20S proteasome activity (PA), including individual (IPRED) and population predictions (PRED) vs. observed values and conditional weighted residuals (CWRES) vs. time after first dose and PRED.

plots (figure 2) and pcVPC showed an adequate description of the 20S proteasome activity measured immediately after dose administration until 8 hours post-dose by the final PD model.

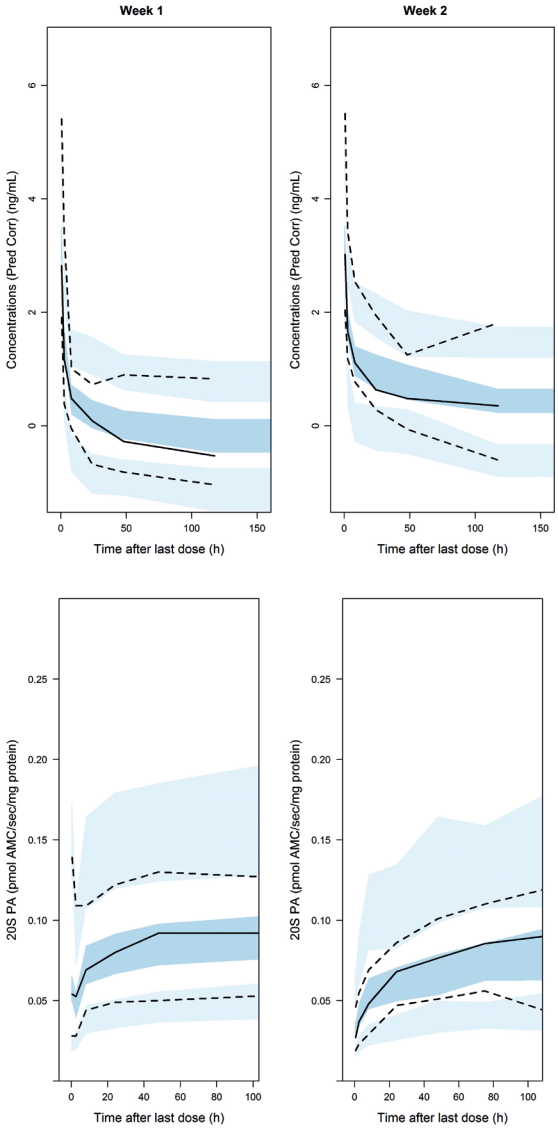

Figure 3. Prediction-corrected visual predictive check of the final PK (upper panels) and PD (lower panels) models stratified by treatment week. Solid lines and darker blue areas represent the median observed values and simulated 80% confidence intervals. Dashed lines and light blue areas represent the 10% and 90% percentiles of the observed values and 80% CIs of the simulated percentiles (n=1000).

Discussion

The complex pharmacokinetics of bortezomib were adequately described by a two-compartment model with linear elimination. Incorporation of non-linear binding in the central compartment significantly improved the model fit and explained the higher plasma concentrations in the second week of treatment. The distribution in whole blood was previously investigated in multiple myeloma patients. (23) The bortezomib concentration in whole blood was found to be approximately 3-fold higher than that in plasma. In addition, whole blood concentrations increased during treatment, suggesting a limited accumulation of bortezomib in red blood cells. Furthermore, Zhang *et al.* developed a physiologically-based pharmacokinetic model incorporating saturable target binding to capture the nonlinear bortezomib tissue distribution in mice. Bortezomib showed reversible high affinity for binding to the proteasome. As a result of high abundance of the proteasome in erythrocytes and slow dissociation kinetics, bortezomib is expected to rapidly bind but slowly dissociate from proteasome in erythrocytes and thus accumulate in red blood cells.(12) Notwithstanding, it could be hypothesized that bortezomib may bind to other proteins present in human plasma. Our semi-physiological model is the first description of the non-linearity in bortezomib PK in both children and adults. Although the current data was obtained from a trial in children, our modelling approach could be used for other drugs that are used in the treatment of both adults and pediatrics that show distribution to erythrocytes.

In the final PK model, large residual unexplained variability was observed. This may be due to inconsistencies in sample collection and registration of dosing and sampling records. Given the fast decline in concentrations within the first hour after administration, small deviations between the actual and registered administration and sampling times may easily lead to high residual variability. Nevertheless, the registered administration times were used in the analysis. Additionally, we were unable to include BSV or covariate effects on structural parameters other than BSV on B_{max} and body weight on all volumes of distribution and clearance parameters. Despite this limitation, the diagnostic plots and pcVPC show that the observed concentrations are well captured by the model.

The 20S proteasome activity versus time profile following bortezomib administration was well described by an inhibitory sigmoidal E_{max} model indicating that 20S proteasome activity in peripheral whole blood samples is directly related to bortezomib C_{plasma}. Large variability in baseline 20S proteasome activity was observed, which is demonstrated by the 40.6% BSV on baseline effect in our model. The covariates that were available were unable to explain this variability.

The overprediction of the 20S proteasome activity at 8 hours post-dose can be explained by the use of the direct effect model with simulated C_{plasma} as input. Some patients did not recover to baseline before the next dose was administered. At this

time, the concentrations in plasma are low while there is still drug bound to the proteasome. Direct effect models using estimated C_{bound} were explored but could not be estimated with adequate precision.

Our results are in line with the structural results from the previously published pediatric population PK analysis of bortezomib in the pediatric population. (10) A population clearance of 9.59 L/h hour and large volumes of distribution of 10.0 L, 32.5 L and 975 L for respectively V1, V2 and V3 were reported there. We were not able to identify BSV on other parameters than $B_{max,}$ as has been done by Hanley *et al.* This is most likely a result of the limited data that was available for our analysis and the complexity of our structural model. Despite our relatively small sample size, our model is superior to this previously published model in incorporating data from both treatment weeks into a semi-physiological approach, thereby explaining the observed non-linearity in PK. In the previously published empirical model, only data from the first week of treatment was included. Hanley *et al.* identified a covariate effect of BSA on CL and the intercompartmental clearance between the first and third compartment. We used total body weight for allometric scaling of all volumes of distribution and clearance parameters to account for changes in body size. Given the limited number of subjects and consequently limited weight range in our cohort, fixed allometric exponents were used.(14) An additional maturation effect using PMA could not be identified when weight was accounted for. This is most likely due to the lack of patients aged younger than two years in our cohort. Nevertheless, to our knowledge, this is the first model for bortezomib combining pharmacokinetics and pharmacodynamics.

A comparison of the results from our PD model to previous reports cannot be made as these analyses used relative 20S proteasome inhibition to describe the PD effect. (6,24) Our data showed that baseline 20S proteasome activity varied widely between patients. Hence, it was not rational to use relative 20S proteasome inhibition instead of 20 proteasome activity.

In conclusion, we successfully developed a model that describes the population PK-PD of bortezomib in pediatric patients with rALL. The observed nonlinearity could be explained by saturable distribution of bortezomib within the central compartment. Which is presumably caused by saturable binding to erythrocytes.

References

1. Pui C-H, Yang JJ, Hunger SP, Pieters R, Schrappe M, Biondi A, et al. Childhood Acute Lymphoblastic Leukemia: Progress Through Collaboration. J Clin Oncol. 2015;33:2938–48.

2. Moreno L, Pearson ADJ, Paoletti X, Jimenez I, Geoerger B, Kearns PR, et al. Early phase clinical trials of anticancer agents in children and adolescents — an ITCC perspective. Nat Rev Clin Oncol. 2017;14:497–507.

3. Bross PF, Kane R, Farrell AT, Abraham S, Benson K, Brower ME, et al. Approval Summary for Bortezomib for Injection in the Treatment of Multiple Myeloma. Clin Cancer Res. 2004;10:3954-64.

4. Tan CRC, Abdul-Majeed S, Cael B, Barta SK. Clinical pharmacokinetics and pharmacodynamics of Bortezomib. Clin Pharmacokinet. 2019;58:157-168.

5. Houghton PJ, Morton CL, Kolb EA, Lock R, Carol H, Reynolds CP, et al. Initial testing (stage 1) of the proteasome inhibitor bortezomib by the pediatric preclinical testing program. Pediatr Blood Cancer. 2008;50:37–45.

6. Reece DE, Sullivan D, Lonial S, Mohrbacher AF, Chatta G, Shustik C, et al. Pharmacokinetic and pharmacodynamic study of two doses of bortezomib in patients with relapsed multiple myeloma. Cancer Chemother Pharmacol. 2011;67:57–67.

7. Horton TM, Pati D, Plon SE, Thompson P a, Bomgaars LR, Adamson PC, et al. A phase 1 study of the proteasome inhibitor bortezomib in pediatric patients with refractory leukemia: a Children's Oncology Group study. Clin Cancer Res. 2007;13:1516–22.

8. Muscal JA, Thompson PA, Horton TM, Ingle AM, Ahern CH, McGovern RM, et al. A Phase I Trial of Vorinostat and Bortezomib in Children with Refractory or Recurrent Solid Tumors: A Children's Oncology Group Phase I Consortium Study (ADVL0916). Pediatr Blood Cancer. 2013;60:390–5.

9. Blaney SM, Bernstein M, Neville K, Ginsberg J, Kitchen B, Horton T, et al. Phase I Study of the Proteasome Inhibitor Bortezomib in Pediatric Patients With Refractory Solid Tumors: A Children's Oncology Group Study (ADVL0015). J Clin Oncol. 2004;22:4804–6.

10. Hanley MJ, Mould DR, Taylor TJ, Gupta N, Suryanarayan K, Neuwirth R, et al. Population Pharmacokinetic Analysis of Bortezomib in Pediatric Leukemia Patients: Model-Based Support for Body Surface Area-Based Dosing Over the 2- to 16-Year Age Range. J Clin Pharmacol. 2017;57:1183-1193

11. Kaspers GJL, Niewerth D, Wilhelm BAJ, Scholte-van Houtem P, Lopez-Yurda M, Berkhof J, et al. An effective modestly intensive re-induction regimen with bortezomib in relapsed or refractory paediatric acute lymphoblastic leukaemia. Br J Haematol. 2018;181:523-527.

12. Zhang L, Mager DE. Physiologically-based pharmacokinetic modeling of target-mediated drug disposition of bortezomib in mice. J Pharmacokinet Pharmacodyn. 2015;42:541–52.

13. West GB, Brown JH, Enquist BJ. A General Model for the Origin of Allometric Scaling Laws in Biology. Science. 1997;276:122–6.

14. Anderson BJ, Holford NHG. Mechanism-based concepts of size and maturity in pharmacokinetics. Annu Rev Pharmacol Toxicol. 2008;48:303–32.

15. Germovsek E, Barker C, Sharland M, Standing JF. Scaling Clearance in Paediatric Pharmacokinetics: all models are wrong, which are useful? Br J Clin Pharmacol. 2016;83:777–90.

16. Upton RN, Mould DR. Basic concepts in population modeling, simulation, and model-based drug development: part 3-introduction to pharmacodynamic modeling methods. CPT pharmacometrics Syst Pharmacol. 2014;3:e88.

17. Nguyen T, Mouksassi M-S, Holford N, Al-Huniti N, Freedman I, Hooker A, et al. Model Evaluation of Continuous Data Pharmacometric Models: Metrics and Graphics. CPT Pharmacometrics Syst Pharmacol. 2017;6:87–109.

18. Dosne A-G, Bergstrand M, Karlsson MO. An automated sampling importance resampling procedure for estimating parameter uncertainty. J Pharmacokinet Pharmacodyn. 2017;44:509–20.

19. Lindbom L, Ribbing J, Jonsson EN. Perl-speaks-NONMEM (PsN)—a Perl module for NONMEM related programming. Comput Methods Programs Biomed. 2004;75:85–94.

20. Keizer RJ, van Benten M, Beijnen JH, Schellens JHM, Huitema ADR. Pirana and PCluster: A modeling environment and cluster infrastructure for NONMEM. Comput Methods Programs Biomed. 2011;101:72–9.

21. Beal S, Boeckmann A, Sheiner L (1988). NONMEM user guides. University of California, San Francisco.

22. RC Team (2009) R: a language and environment for statistical computing. R Foundation for Statistical Computing, Vienna.

23. Osawa T, Naito T, Kaneko T, Mino Y, Ohnishi K, Yamada H, et al. Blood distribution of bortezomib and its kinetics in multiple myeloma patients. Clin Biochem. 2014;47:54–9.

24. Moreau P, Karamanesht II, Domnikova N, Kyselyova MY, Vilchevska K V., Doronin VA, et al. Pharmacokinetic, pharmacodynamic and covariate analysis of subcutaneous versus intravenous administration of bortezomib in patients with relapsed multiple myeloma. Clin Pharmacokinet. 2012;51:823–9.

CHAPTER 2

Special patient populations: Pregnant women

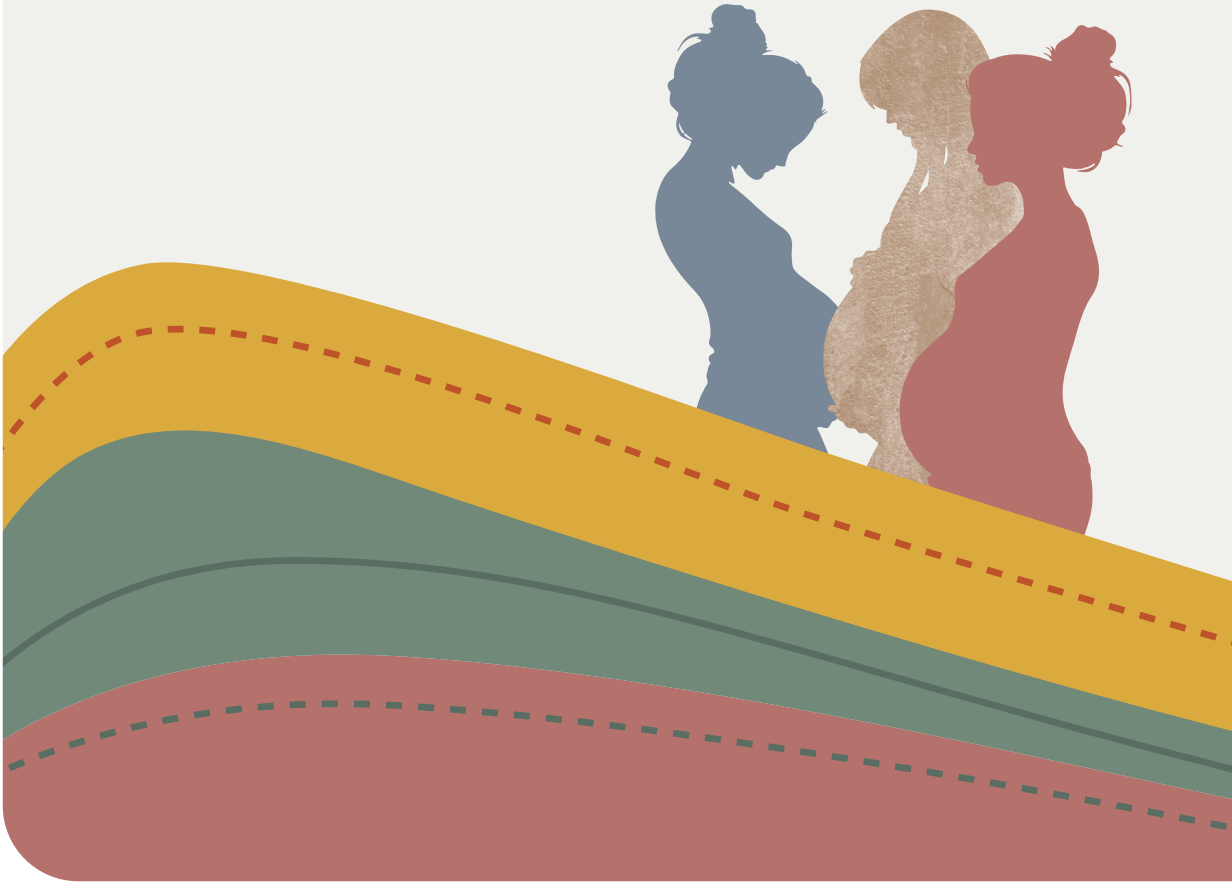

Chapter 2.1

Population Pharmacokinetics of Docetaxel, Paclitaxel, Doxorubicin and Epirubicin in Pregnant Women with Cancer. A study from the International Network of Cancer, Infertility and Pregnancy (INCIP)

Submitted

J.M. Janssen
K. Van Calsteren
T.P.C. Dorlo
M.J. Halaska
R. Fruscio
P. Ottevanger
C.P. Schröder
I. Boere
P.O. Witteveen
R.C. Painter
R. Bekkers
V. Drochytek
J.H. Beijnen
A.D.R. Huitema
F.C.H. Amant

Abstract

Background

Based on reassuring short term fetal and maternal safety data, there is an increasing trend to administer chemotherapy during the second and third trimester of pregnancy. The pharmacokinetics (PK) of drugs might change as a result of several physiological changes that occur during pregnancy, which may affect the efficacy and safety of chemotherapy. With this analysis we aim to quantitatively describe the changes in the PK of docetaxel, paclitaxel, doxorubicin and epirubicin in pregnant women compared to non-pregnant women.

Methods

PK data from 9, 20, 22 and 16 pregnant cancer patients from the International Network of Cancer, Infertility and Pregnancy (INCIP) were available for docetaxel, paclitaxel, doxorubicin and epirubicin, respectively. These samples were combined with available PK datasets of these drugs in non-pregnant patients. Empirical nonlinear mixed-effects models were developed evaluating fixed pregnancy effects and gestational age as covariates.

Findings

82, 189, 271, 227 plasma samples were collected from pregnant patients treated with docetaxel, paclitaxel, doxorubicin and epirubicin, respectively. The plasma PK data were adequately described by the respective models for all cytotoxic drugs. Typical increases in central and peripheral volumes of distribution of pregnant were identified for docetaxel, paclitaxel, doxorubicin and epirubicin, respectively. Additionally, docetaxel, doxorubicin and paclitaxel clearance were increased in pregnant patients.

Conclusion

Plasma concentrations of four widely used cytotoxic drugs docetaxel, paclitaxel, doxorubicin and epirubicin were lower in pregnant women compared to non-pregnant patients. The pregnancy effects on the PK of these four drugs were quantified. In light of the overall interpatient variability, the identified pregnancy-induced changes in PK do not directly warrant dose adjustments for any of the studied drugs. Nevertheless, these results underscore the need to investigate the efficacy of chemotherapy, when administered during pregnancy.

Introduction

Given that the pharmacology of drugs is typically unknown in the pregnant population, dosing in pregnancy is based on research in non-pregnant patients. Little research is being performed in order to investigate the effects of pharmacological treatment on the pregnant patient and the fetus. The US Food and Drug and Drug Administration and European Medicines Agency have released guidelines on how to cope with this highly vulnerable patient population.(1–3) It is advised to make use of the population pharmacokinetics (PK) approach. This method can quantify and explain the PK characteristics and variability in drug concentrations among individuals. In addition, this method enables optimal use of data from a very limited population and may limit the number of required PK assessments. The population PK approach can assess the effects of pregnancy on the PK and hence provide recommendations for dosing adjustments.(1,3)

Cancer complicates one out of 1000-2000 pregnancies.(4) In the treatment of pregnant cancer patients, clinicians were initially reluctant to use chemotherapy as the short- and long-term effects of exposure of cytotoxic drugs on the fetus were unknown but feared. Recently, treatment of pregnant women with cytotoxic drugs during pregnancy was shown to be safe in the short and middle long term for both the mother and the fetus, when considering both cancer prognosis and perinatal and selected childhood outcomes. Safety for the fetus has been demonstrated when chemotherapy has been administered after the 1st trimester.(5) The increased use of chemotherapy has resulted in an increase in livebirths and decrease in prematurity among pregnant cancer patients.(4,5)

With the empirical dosing approach based on non-pregnant patient data, potential gestational effects on the human physiology are ignored. Anecdotal reports suggest less chemotherapy related toxicity among pregnant women compared to non-pregnant women. Several physiological changes have been described during pregnancy, which may in theory have an effect on the PK of drugs. The most pronounced changes include an increase in body fluids such as plasma volume, extracellular water and total body water. Additionally, a decrease in plasma protein concentrations, increased glomerular filtration and changes in metabolizing enzyme activity have been reported.(6) It follows that these PK changes might thus result in over- or under exposure which might have a substantial influence on the efficacy and the development of toxicity of the treatment.

We previously reported that the PK of cytotoxic drugs is altered during pregnancy.(7,8) For all of the drugs that were studied, lower drug concentrations were observed in pregnant patients in the second and third trimester compared to non-pregnant patients.(8) A decrease in the area under the plasma concentration-time curve (AUC) was observed for docetaxel, paclitaxel, doxorubicin and epirubicin, respectively.

However, this preliminary analysis was limited by the very small number of pregnant patients that could be included at the time, in particular for patients treated with docetaxel or paclitaxel. This small sample size and large inter-individual variability hampered the determination of a continuous gestational effect on the PK of all four studied drugs. Despite the fact that the magnitude of the effect of pregnancy on PK is anticipated to be the largest in the third trimester, a continuous relationship with gestational age is expected given the time-dependent change and interplay of the various physiological parameters. Considering the limitations of the previous preliminary analysis, inclusion of patients in this patient cohort was continued and here we report the updated results.

Methods

Patients and sampling

PK datasets from previously reported analyses were extended with PK data from newly included pregnant patients for docetaxel, doxorubicin and epirubicin. Patients were recruited from the International Network of Cancer, Infertility and Pregnancy (INCIP) registry (NCT00330447). This study was approved by institutional review boards and independent ethics committees at participating institutions, and was carried out in accordance with the ethical principles of the Declaration of Helsinki.

PK samples were centrifuged and stored at -80°C after withdrawal. Subsequently, PK samples were transported to a central facility where drug concentrations were measured using validated bioanalytical methods.(9,10) Previously published PK data from non-pregnant patients were included from clinical trials and served as control data (table 1).(8) For paclitaxel, the dataset from a recently published PK model was used and enriched with our PK data from pregnant patients.(11) Due to the limited data, PK data collected post-partum was considered as non-pregnant in the current analysis.

Structural model development

The structural model was developed using the concentration-time data collected from both pregnant and non-pregnant patients. For the description of docetaxel, doxorubucin and epirubicin concentrations, one- to three-compartment models with linear elimination were first evaluated. For paclitaxel a linear three-compartment model was first tested. However, a recently published PK model for paclitaxel performed better in terms of parameter precision and goodness-of-fit plots (GOF).(11) This model consists of a three-compartment model with first-order distribution to the first peripheral compartment, saturable distribution to the second peripheral compartment and saturable elimination from the central compartment.

Stochastic model development

Between-subject variability (BSV) was evaluated for all parameters using an exponential error model (eq. 1):

$$P_i = P_{pop} \cdot exp\,(\eta_i) \quad \text{(Eq. 1)}$$

where P_i represents the individual parameter estimate for individual *i*, P_{pop} represents the typical population parameter estimate as defined by the structural model, η_i the BSV effect for subject individual *i*, which was assumed to be normally distributed following $N\,(0, \omega^2)$. Residual unexplained variability was described by a proportional error model for all four drugs (eq. 2):

$$C_{obs,ij} = C_{pred,ij} \cdot (1 + \varepsilon_{p,ij}) \quad \text{(Eq. 2)}$$

where $C_{obs,ij}$ represents the observed concentration for individual *i* and observation *j*, $C_{pred,ij}$ represents the individual predicted concentration and $\varepsilon_{p,ij}$ represents the proportional error distributed following $N\,(0, \sigma^2)$. Separate residual variabilities were estimated for the data from pregnant and non-pregnant patients as data was available from different clinical studies and different bioanalytical methods were used.

Covariate analysis

In order to identify relationships between covariates and the structural model parameters, plots of -values of the parameter of interest versus the covariate were visually assessed for trends. First, total body weight (WT) at time of PK sampling was tested in the PK model that included non-pregnant patients only (eq. 3).

$$P = P_{pop} \cdot \left(\frac{WT}{median\ WT}\right)^{COV} \quad \text{(Eq. 3)}$$

where *P* represents the WT-adjusted population parameter. All clearance (CL) and volume parameters (i.e. central compartment (V1), first peripheral compartment (V2) and second peripheral compartment (V3)) were scaled to the median WT in the dataset. The exponents (COV) were fixed to 0.75 for clearance parameters and 1 for volumes of distribution according to allometric principles.(12) WT at time of PK sampling was available for all patients.

Next, relationships between gestational age (GA) and CL and volume parameters were univariately tested in the model. Following visual inspection of the covariate plots, continuous models using GA or discrete gestational effects were considered. Covariate effects that were already present in the original paclitaxel PK model were retained in our model with the exception of bilirubin since this covariate was not prospectively collected for all pregnant patients.

Table 1. Characteristics of the patients included in the final model

	Docetaxel	Paclitaxel	Epirubicin	Doxorubicin
Pregnant patients (n)	9	20	22	16
Cycles (n)	10	25	27	22
GA 13 – 28.9 weeks	1	11	14	13
GA 29 – 40 weeks	9	14	13	9
GA (weeks) [median, range]	31.8 [26.1–35.0]	31.0 [13.7-35.7]	28.7 [15.0–36.3]	26.8 [19.0–34.0]
Post-partum (n)				
Cycles (n)	1	2	5	3
Days post-partum [weeks, range][a]	61	43 [30–56]	46.5 [28.0–61.0]	49.0 [49.0–56.0]
Non-pregnant patients (n)	35[b]	689[c]	66[d]	66[e]
Cycles (n)	35	3046	67	68

Abbreviations: GA, gestational age.
[a] Median and range provided for datasets with more than one post-partum cycle. [b] (30). [c] (11). [d] (8). [e] (20).

Model selection and evaluation

Discrimination between models was guided by physiological plausibility, GOF plots, precision of parameter estimates and change in objective function value (dOFV). A drop of ≥ 3.84 points, corresponding to a $P < 0.05$ (χ^2-distribution with 1 degree of freedom (df)), was considered a significant improvement of the fit for hierarchical nested models. The adequacy of the models was assessed by GOF plots and visual predictive checks (VPC).(13) Parameter precision was assessed by the sampling importance resampling (SIR) procedure.(14)

Simulations

Stochastic simulations using the final PK models were performed to evaluate the effect of pregnancy on the exposure of the respective drugs. Individual concentration-time curves were simulated for a typical patient with a body surface area (BSA) of 1.8 m^2 treated at the standard dose regimen. Inter-individual variability was taken into account in these simulations by using random sampling from covariance matrix from the final PK model. For each simulation dataset, 2000 patients were simulated (1000 pregnant patients and 1000 non-pregnant patients). The $AUC_{0\text{-}48h}$ and maximum plasma concentration (C_{max}) of each drug were assessed and compared between pregnant and non-pregnant patients.

Software

Nonlinear mixed-effects modeling was performed using NONMEM® (version 7.3, ICON Development Solutions, Ellicott City, MD, USA) and Perl-speaks-NONMEM (PsN, version 4.4.8) with First-Order Conditional Estimation with interaction (FOCE-I) as estimation method. Piraña (version 2.9.7) was used as graphical user interface for NONMEM. (15–17) R (version 3.4.3) was used for data management and graphical diagnostics.(18)

Results

Docetaxel

A total of 533 plasma samples from 44 patients (9 pregnant and 35 non-pregnant) were available for docetaxel. In addition, PK samples were collected post-partum from one patient (table 1). With the exception of one treatment cycle, all cycles in which PK samples were collected in pregnant patients took place during the third trimester. Median GA was 31.8 weeks (range 26.1 – 35.0 weeks).

The data was best described by a linear three-compartment model with first-order elimination. WT was not available for the control patients and was therefore not tested as a covariate. After graphical exploration it could be concluded that a continuous gestational effect could not be identified. A discrete pregnancy effect was, however, estimated for CL, V1 and V2 and an over-prediction of the higher concentration was observed in pregnant patients (supplementary material figure S1 and S3). Fold changes of 1.08 (95% confidence interval (CI) 0.92 – 1.24), 1.19 (95% CI 0.90 – 1.50), 1.12 (95% CI 0.82 – 1.50) were estimated for pregnant patients for CL, V1 and V2, respectively. After inclusion of the pregnancy effect, GOF plots and the VPC showed an improved fit (figure 1 and 2) but OFV did not decrease significantly (dOFV = -1.6 points, $P = 0.665$, df = 4). Final model parameters are depicted in table 2. Simulations showed that the docetaxel exposure in pregnant patients was lower by terms of both $AUC_{0\text{-}48}$ (mean±SD 3648±892.3 ng*h/mL vs. 3916±950.7 ng*h/mL) and C_{max} (mean±SD 2759±518.5 ng/mL vs. 2938±548.9 ng/mL) compared to non-pregnant patients. Relative change in pregnant patients compared to non-pregnant patients is depicted in figure 2.

Paclitaxel

A total of 6145 plasma samples from 708 patients (20 pregnant and 688 non-pregnant) were available for paclitaxel. PK samples from pregnant patients were obtained in the second (n = 11) as well as the third trimester (n = 14), median GA was 31.0 weeks (range 13.7 – 35.7 weeks).

A previously reported PK model was used as a starting point.(11) In this model, BSA, gender, bilirubin and age were included as covariates on the parameter describing the maximal elimination rate (VM_{EL}). Since bilirubin levels were not measured for all pregnant patients at time of PK sampling, we removed bilirubin as a covariate from the base model. This model was updated with the concentration-time curves of the pregnant patients. Continuous covariate relationships between GA and structural PK parameters could not be identified (see supplementary material figure S1). Inclusion of discrete covariate effects on V1, V3 and KM_{EL} resulted in a decrease in OFV of 30 points (model without pregnancy effect versus base model, $P < 0.00001$, df = 3). Additionally, GOF (figure 1), covariate plots (supplemental figure S1) and VPC (figure 1) indicated an improved model fit. The typical fold change in V1, V3 and KM_{EL} of pregnant

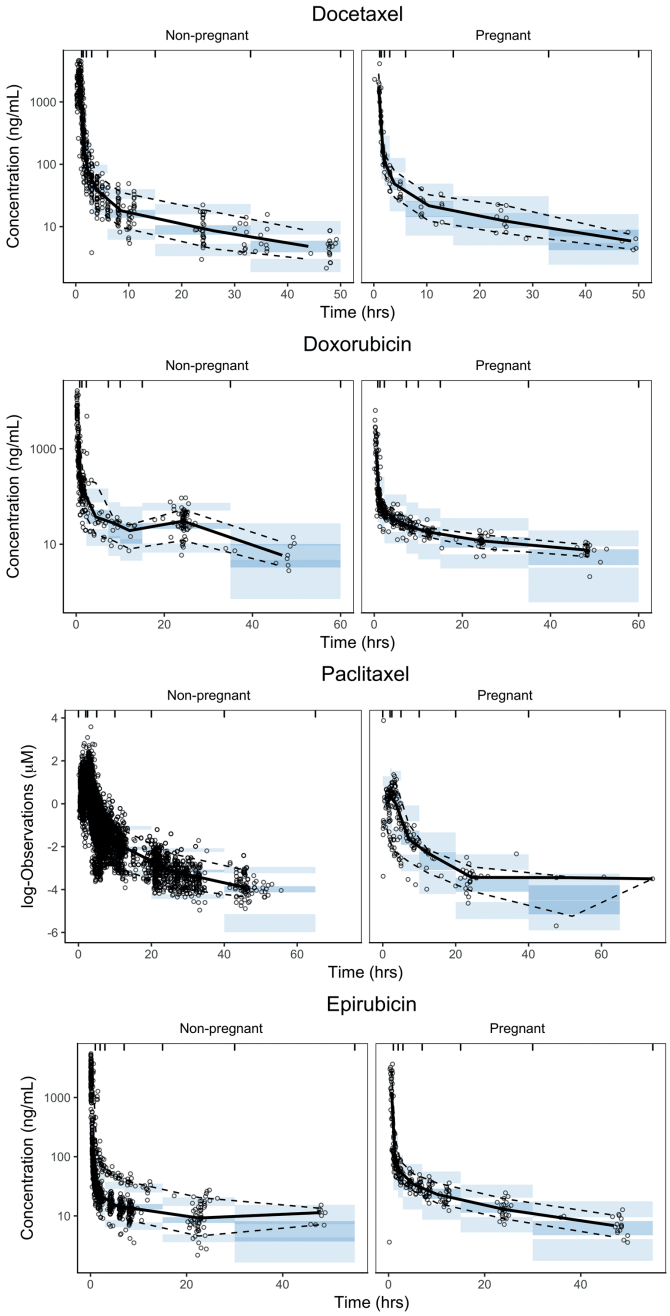

Figure 1. Visual predictive checks of the final PK models for docetaxel, paclitaxel, doxorubicin and epirubicin stratified by population. Solid lines and darker grey areas represent the median observed values and simulated 80% CI around the median. Dashed lines and light grey areas represent the 10% and 90% percentiles of the observed values and 80% prediction intervals of the simulated percentiles (n = 1000).

patients was 2.27 (95% CI 1.57 – 3.10), 2.28 (95% CI 1.54 – 3.63) and 1.32 (95% CI 1.03 – 1.69), respectively. Simulations showed lower $AUC_{0\text{-}48}$ (mean±SD 14.8±3.48 µmol*h/L vs. 16.9±4.40 µmol*h/L) and C_{max} (mean±SD 3.69±0.906 µmol/L vs. 4.85±1.50 µmol/L) in pregnant patients compared to non-pregnant patients.

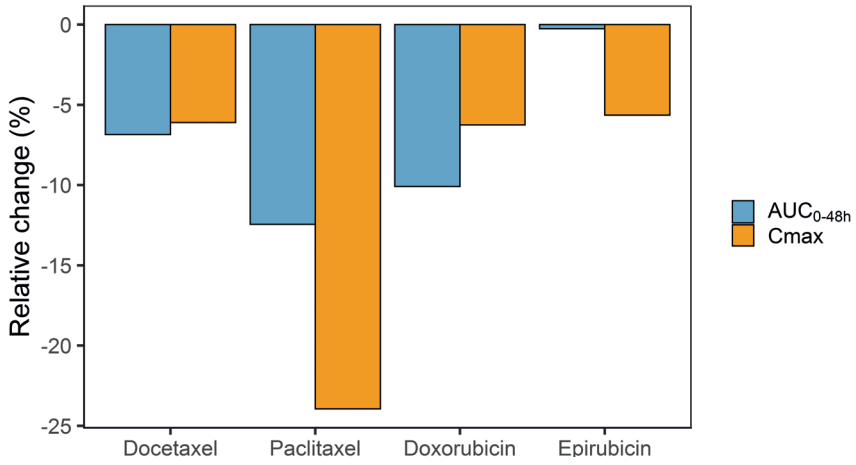

Figure 2. Relative change in $AUC_{0\text{-}48h}$ and C_{max} for docetaxel, paclitaxel, doxorubicin and epirubicin in pregnant patients compared to non-pregnant patients using the final PK models (n = 1000, relative change(%) = ((Pregnant – Non-pregnant)/Non-pregnant) * 100%).

Doxorubicin

A total of 580 samples from 87 patients (26 pregnant and 61 non-pregnant) were available for doxorubicin. Data from 4 pregnant patients was excluded because of sampling errors. For these patients, infusion and sample withdrawal times were unavailable. PK samples from pregnant patients were collected during the second (n = 14) and third trimester (n = 13), median GA was 28.7 weeks (range 15.0 – 36.3 weeks).

A linear three-compartment model with first-order elimination best described the doxorubicin data. The inclusion of WT as a covariate resulted in an improved fit of the non-pregnant data (dOFV = -65.3 points, $P < 0.00001$, df = 4). All CL and volume parameters were scaled to a standard WT of 70 kg. Graphical exploration indicated higher CL and V1 in pregnant patients compared to non-pregnant patients, however, there was no clear trend of a continuous gestational effect (supplementary material figure S1). Moreover, the GOF plots showed an overprediction of the concentrations for the pregnant patients (supplementary figure S3). Fold changes of 1.13 (95% CI 1.00 – 1.28) and 1.08 (95% CI 0.85 – 1.35) were estimated for pregnant patients for CL and V1. Addition of these pregnancy effects resulted in improvements in GOF (supplementary figure S2) and the VPC indicated that BSV was lower in pregnant versus

non-pregnant patients (figure 1). Inclusion of discrete covariate effects on CL and V1 resulted in a decrease in OFV of 5.7 points (model without pregnancy effect versus base model, *P* = 0.059, df = 2). Simulations showed that the doxorubicin exposure in pregnant patients was lower by terms of both $AUC_{0\text{-}48}$ (mean±SD 2090±736.1 ng*h/mL vs. 2324±812.4 ng*h/mL) and C_{max} (mean±SD 2223±393.5 ng/mL vs. 2371±396.1 ng/mL) compared to non-pregnant patients.

Table 2. Parameter estimates of the final models for docetaxel, paclitaxel, doxorubicin and epirubicin

	Estimate (95% CI[a])			
	Docetaxel	**Paclitaxel**	**Doxorubicin**	**Epirubicin**
Structural parameters				
CL (L/h)	44.6 (41.0 – 48.1)	-	41.7 (37.1 – 46.5)	84.5 (78.6 – 90.30
VM_{EL} (µmol/h)	-	31.8 (29.5 – 34.6)	-	-
KM_{EL} (µmol/L)	-	0.459 (0.404 – 0.527)	-	-
V1 (L)	9.19 (7.94 – 10.5)	12.1 (11.3 – 12.9)	10.1 (8.80 – 11.8)	12.2 (11.4 – 13.1)
Q1 (L/h)	5.96 (5.33 – 6.64)	-	11.4 (9.61 – 14.0)	14.5 (12.8 – 16.1)
VM_{TR} (µmol/h)	-	175 (165 – 186)	-	-
KM_{TR} (µmol/L)	-	1.63 (1.49 – 1.79)	-	-
K_{21} (h^{-1})	-	1.19 (1.12 – 1.27)	-	-
V2 (L)	7.35 (6.33 – 8.62)	-	25.4 (17.8 – 36.1)	9.90 (8.70 – 11.4)
Q2 (L/h)	14.2 (12.8 – 15.8)	16.9 (16.0 – 17.7)	38.2 (34.4 – 42.6)	69.6 (63.8 – 75.4)
V3 (L)	381 (338 – 437)	267 (246 – 289)	756 (606 – 987)	1100 (988.7-1227)
Gestational effect (proportional)[b]				
CL	1.08 (0.92 – 1.24)	-	1.14 (1.00 – 1.28)	-
KM_{EL}	-	1.32 (1.03 – 1.69)	-	-
V1	1.19 (0.90 – 1.50)	2.27 (1.57 – 3.10)	1.08 (0.85 – 1.35)	1.79 (1.49 – 2.12)
V2	1.12 (0.82 – 1.50)	-	-	2.94 (1.91 – 4.29)
V3	-	2.28 (1.54 – 3.63)	-	-
Inter-individual variability (CV%)				
CL	26.1 (21.1 – 32.2)	-	38.2 (31.7 – 49.1)	29.2 (24.8 – 34.9)
VM_{EL}	-	18.9 (16.4 – 21.8)	-	-
V1	33.5 (24.8 – 43.2)	-	35.6 (28.4 – 46.6)	20.1 (15.4 – 25.8)
Q1	-	-	-	34.8 (26.8 – 43.2)
VM_{TR}	-	26.3 (23.8 – 28.9)	-	-
KM_{TR}	-	60.1 (52.4 – 68.2)	-	-
Q2	20.0 (13.5 – 27.4)	47.3 (43.6 – 51.4)	-	29.0 (23.8 – 35.1)
V3	-	33.8 (29.5 – 39.0)	71.0 (56.9 – 89.8)	29.2 (22.6 – 36.1)
Inter-occasion variability (CV%)				
V1	-	47.1 (42.6 – 52.0)	-	-
VM_{EL}	-	16.4 (14.7 – 18.2)	-	-

Table 2. Continued

	Estimate (95% CI[a])			
	Docetaxel	**Paclitaxel**	**Doxorubicin**	**Epirubicin**
RUV (proportional, CV%)				
Pregnant patients	24.9 (21.5 – 29.7)	48.8 (44.6 – 54.1)	32.1 (29.5 – 35.1)	28.3 (25.9 – 31.3)
Non-pregnant patients				
Retrospective cohort 1		14.1 (13.6 – 14.5)		
Retrospective cohort 2	23 (21.3 – 24.9)	45.7 (39.0 – 53.9)	38.3 (33.6 – 43.1)	16.4 (15.1 – 17.8)
Prospective cohort		29.0 (27.1 – 31.1)		

Abbreviations: CL, clearance; VM_{EL}, maximal elimination rate; KM_{EL}, plasma concentration at half VM_{EL}; V1, central volume of distribution; Q1, intercompartmental clearance between central and first volume of distribution; VM_{TR}, maximal transport rate from the central to the first peripheral volume of distribution for paclitaxel; KM_{TR}, plasma concentration at half VM_{TR}, K_{21}, rate constant of the distribution from the first peripheral to the central volume of distribution for paclitaxel; V2, first peripheral volume of distribution; Q2, intercompartmental clearance from the central to second peripheral volume of distribution; V3, second peripheral volume of distribution; CI, confidence interval; CV%, coefficient of variation, RUV, residual unexplained variability.
[a]95% CI values were obtained from SIR. [b] Factor change, e.g. the docetaxel clearance for a typical pregnant patient can be calculated by: $CL_{pregnant}$ = 44.6 L * 1.08 = 48.2 L.

Epirubicin

A total of 976 plasma samples from 80 patients (16 pregnant and 64 non-pregnant) were available for epirubicin. PK curves from pregnant patients were obtained both in the second (n = 13) as well as the third trimester (n = 9), median GA was 26.8 weeks (range 19.0 – 34.0 weeks).

The data were best described by a linear three-compartment model with first-order elimination. Inclusion of WT did not improve the model and was thus not included in the model. Continuous covariate relationships between GA and structural PK parameters could not be identified (see supplementary material figure S1). However, inclusion of discrete covariate effects on V1, V2 resulted in a decrease in OFV of 60 points ($P < 0.0001$, df = 2) and GOF, VPC and covariate plots (supplementary figure S1 and figure 1) showed an improved model fit. Similar to doxorubicin, the variability was overpredicted for the pregnant population. The typical fold change in V1 and V2 of pregnant patients was 1.79 (95% CI 1.49 – 2.12) and 2.94 (95% CI 1.91 – 4.29). Simulations showed slightly lower $AUC_{0\text{-}48}$ (mean±SD 1992±508.5 ng*h/mL vs. 1997±512.3 ng*h/mL) and C_{max} (mean±SD 2108±355.4 ng/mL vs. 2233±411.5 ng/mL) in pregnant patients compared to non-pregnant patients.

Discussion

With this analysis we report on the updated population analysis of the effect of pregnancy on the PK of docetaxel, paclitaxel, doxorubicin and epirubicin. Previously reported models were extended with newly collected data. With this addition, the datasets changed substantially. The PK models were therefore re-estimated and covariate effects were re-assessed. Additionally, we successfully determined the pregnancy effect on the saturable pharmacokinetics of paclitaxel.

For all four drugs, typical increases in central volume of distribution of pregnant patients were identified. Increases were successfully estimated for docetaxel and epirubicin V2 and paclitaxel V3 in pregnant patients. Additionally, increases in CL were observed for docetaxel and doxorubicin and in KM_{EL} for paclitaxel. For docetaxel, only modest increases in typical parameters were observed. Meaning that the PK model for non-pregnant patients, which is characterized by large between-subject variability, also accounts for the small changes in docetaxel PK during pregnancy. GOF plots and VPCs showed an adequate description of both the pregnant and non-pregnant data. The VPCs for doxorubicin and epirubicin did, however, show a slight overprediction of the variability in the pregnant population. This might be explained by the large between-subject variability within the included non-pregnant population while this variability may be lower in pregnant patients since this is a much more homogeneous population (all relatively young non-pretreated females without much co-morbidity).

All drugs in this analysis are mainly eliminated by hepatic clearance. Docetaxel, paclitaxel, doxorubicin and epirubicin are all metabolized by CYP3A4, whereas paclitaxel is also metabolized by CYP2C8 and epirubicin is also metabolized by UGTB7. A modest increase in CYP3A4 activity during pregnancy has been described, a change in the CL of drugs metabolized by CYP3A4 is therefore expected. For CYP2C8 and UGTB7 gestational changes have not yet been described.(6) Despite the known pregnancy related increase in CYP3A4 activity, an effect of pregnancy could not be identified for the CL of epirubicin. Docetaxel and paclitaxel are largely distributed to the peripheral tissues and are highly protein bound. Doxorubicin and epirubicin are both distributed to the peripheral tissues and show moderate protein binding to albumin. As the albumin and alpha-1-glycoportein concentrations decline during pregnancy and body fluids increase, an increase in central and peripheral volumes of distribution was expected.

We were not able to identify continuous gestational effects on the PK of either docetaxel, paclitaxel, doxorubicin or epirubicin. Quantitative analyses have shown that the largest changes in GFR, body fluids, metabolizing enzyme activity and plasma protein concentrations occur gradually in the first 12 weeks following conception. Thereafter changes remain relatively small until the end of the third trimester.(6)

Contradictory results have been reported regarding the fetal safety of chemotherapy during the first weeks after conception. The extent of distribution of cytotoxic drugs across the placenta varies per drug and the safety of administration of cytotoxic drugs during organogenesis is still not fully unravelled.(19) For this reason, patients were treated with chemotherapy only in the second and third trimester. The absence of PK data obtained during the first trimester can most likely explain the unidentifiability of a continuous gestational effect in our analysis. The effect of WT on doxorubicin PK and the effect of BSA, gender and age on the paclitaxel PK were included in the respective PK models. Although several covariates have been reported to have an influence on the PK of the investigated cytotoxic drugs, no additional covariates could be investigated due to a lack of available data.(20–23) Additionally, the effect of bilirubin on the PK of paclitaxel was removed from the PK model because bilirubin levels were not measured at time of PK sampling in the pregnant population. Several methods for handling of missing covariates have been proposed in the past.(24,25) As the change in bilirubin levels during pregnancy has not been described quantitatively, using such method could potentially lead to the introduction of bias in the bilirubin covariate effect.(6,26) Nevertheless, as covariates could have explained part of the inter-individual variability in PK and differences between pregnant and non-pregnant patients, our results from non-pregnant patients are similar to the previously reported PK models.

By using a population PK approach we were able to specify the gestational effects on the PK of aforementioned drugs, despite the limited number of patients available. In addition, the population PK approach enabled to use all available data from non-pregnant patients as control data. Previously identified covariates such as gender, WT and age were included in the models thereby accounting for potential differences between the pregnant and non-pregnant patient population. To our knowledge, this PK analysis included the largest number of pregnant patients receiving chemotherapy thus far. PK data from non-pregnant and pregnant patients were combined allowing for an adequate estimation of structural models, and most importantly, the gestational effects.

The results of our analysis provide a good approximation of the pregnancy related changes in the PK of docetaxel, paclitaxel, doxorubicin and epirubicin in the patients that will potentially be treated with these drugs. For all four drugs, decreased systemic drug exposures were observed in pregnant patients although the effects were relatively small compared to the observed interpatient variability. The decrease in exposure suggests that potentially a higher dose might be administered to pregnant patients. However, An exposure-response relationship has not been described for the four cytotoxic drugs that we describe here, neither in non-pregnant, nor in pregnant patients. The current dataset, despite being the largest dataset with PK in pregnant cancer patients, is too small to assess the effect of the lower exposure on toxicity and efficacy. Therefore, the magnitude of impact of the typical underexposure in pregnant

patients on the efficacy of these drugs remains unknown. In breast cancer patients and patients with Hodgkin Lymphoma, no significant differences in long-term overall survival was observed between pregnant and non-pregnant patients, however, significant numbers of patients would be needed to find an effect on long-term survival, if possible at all.(27–29) Long-term efficacy results from pregnant patients derived from the INCIP registry (www.cancerinpregnancy.org) continue to be collected to address this question. As the effects found on PK are relatively small compared to the overall interpatient variability, it is advised to dose paclitaxel, docetaxel, epirubicin and doxorubicin similarly in pregnant patients as in non-pregnant patients.

Conclusion

From this analysis it can be concluded that the plasma concentrations of four widely used cytotoxic drugs docetaxel, paclitaxel, doxorubicin and epirubicin are decreased in pregnant women. The population PK models adequately described the pregnancy effect on the PK of these four drugs, despite the limited number of pregnant patients. These data underscore the need to further investigate maternal prognosis when chemotherapy is used during pregnancy. Only when this maternal outcome is affected, alternative drugs (characterised by less gestational changes) or dose adjustments based on efficacy and toxicity of these drugs in pregnant patients need to be considered. The here developed PK models can be used in future to guide any dose adjustments.

References

1. FDA Guidance for Industry – Pharmaockinetics in Pregnancy – Study Design, Data Analysis, and Impact on Dosing and Labeling. FDA Guidance (2004).

2. FDA Guidance for Industry – Establishing Pregnancy Exposure Registries. FDA Guidance (2002).

3. European Medicines Agency (EMA). Guideline on the exposure to medicinal products during pregnancy: need for post-authorization data (2006).

4. de Haan J, Verheecke M, Van Calsteren K, Calster B Van, Shmakov RG, Gziri MM, et al. Oncological management and obstetric and neonatal outcomes for women diagnosed with cancer during pregnancy : a 20-year international cohort study of 1170 patients. Lancet Oncol. 2018;19:337–46.

5. Amant F, Vandenbroucke T, Verheecke M, Fumagalli M, Halaska MJ, Boere I, et al. Pediatric Outcome after Maternal Cancer Diagnosed during Pregnancy. N Engl J Med. 2015;373:1824–34.

6. Abduljalil K, Furness P, Johnson TN, Rostami-Hodjegan A, Soltani H. Anatomical, Physiological and Metabolic Changes with Gestational Age during Normal Pregnancy. Clin Pharmacokinet. 2012;51:365–96.

7. Van Calsteren K, Verbesselt R, Ottevanger N, Halaska M, Heyns L, Van Bree R, et al. Pharmacokinetics of chemotherapeutic agents in pregnancy: a preclinical and clinical study. Acta Obstet Gynecol Scand. 2010;89:1338–45.

8. van Hasselt JGC, Van Calsteren K, Heyns L, Han S, Mhallem Gziri M, Schellens JHM, et al. Optimizing anticancer drug treatment in pregnant cancer patients: pharmacokinetic analysis of gestation-induced changes for doxorubicin, epirubicin, docetaxel and paclitaxel. Ann Oncol. 2014;25:2059–65.

9. Hendrikx JJMA, Hillebrand MJX, Thijssen B, Rosing H, Schinkel AH, Schellens JHM, et al. A sensitive combined assay for the quantification of paclitaxel, docetaxel and ritonavir in human plasma using liquid chromatography coupled with tandem mass spectrometry. J Chromatogr B. 2011;879:2984–90.

10. Beijnen JH, Meenhorst PL, Van Gijn R, Fromme M, Rosing H, Underberg WJM. HPLC determination of doxorubicin, doxorubicinol and four aglycone metabolites in plasma of AIDS patients. J Pharm Biomed Anal. 1991;9:995–1002.

11. Crombag M-RBS, de Vries Schultink AHM, Koolen SLW, Wijngaard S, Joerger M, Schellens JHM, et al. Impact of Older Age on the Exposure of Paclitaxel: a Population Pharmacokinetic Study. Pharm Res. 2019;36:33.

12. West GB, Brown JH, Enquist BJ. A General Model for the Origin of Allometric Scaling Laws in Biology. Science. 1997;276:122–6.

13. Nguyen T, Mouksassi M-S, Holford N, Al-Huniti N, Freedman I, Hooker A, et al. Model Evaluation of Continuous Data Pharmacometric Models: Metrics and Graphics. CPT Pharmacometrics Syst Pharmacol. 2017;6:87–109.

14. Dosne A-G, Bergstrand M, Karlsson MO. An automated sampling importance resampling procedure for estimating parameter uncertainty. J Pharmacokinet Pharmacodyn [Internet]. 2017;44:509–20.

15. Lindbom L, Ribbing J, Jonsson EN. Perl-speaks-NONMEM (PsN)—a Perl module for NONMEM related programming. Comput Methods Programs Biomed. 2004;75:85–94.

16. Keizer RJ, van Benten M, Beijnen JH, Schellens JHM, Huitema ADR. Pirana and PCluster: A modeling environment and cluster infrastructure for NONMEM. Comput Methods Programs Biomed. 2011;101:72–9.

17. Beal S, Boeckmann A, Sheiner L (1988). NONMEM user guides. University of California, San Francisco.

18. RC Team (2009) R: a language and environment for statistical computing. R Foundation for Statistical Computing, Vienna.

19. Vandenbroucke T, Verheecke M, Fumagalli M, Lok C, Amant F. Effects of cancer treatment during pregnancy on fetal and child development. Lancet Child Adolesc Heal. 2017;1:302–10.

20. Joerger M, Huitema ADR, Richel DJ, Dittrich C, Pavlidis N, Briasoulis E, et al. Population pharmacokinetics and pharmacodynamics of doxorubicin and cyclophosphamide in breast cancer patients: a study by the EORTC-PAMM-NDDG. Clin Pharmacokinet. 2007;46:1051–68.

21. Kontny NE, Würthwein G, Joachim B, Boddy A V., Krischke M, Fuhr U, et al. Population pharmacokinetics of doxorubicin: establishment of a NONMEM model for adults and children older than 3 years. Cancer Chemother Pharmacol. 2013;71:749–63.

22. Bruno R, Vivier N, Veyrat-Follet C, Montay G, Rhodes GR. Population pharmacokinetics and pharmacokinetic-pharmacodynamic relationships for docetaxel. Invest New Drugs. 2001;19:163–9.

23. Sandstrom M, Lindman H, Nygren P, Johansson M, Bergh J, Karlsson M. Population analysis of the pharmacokinetics and the haematological toxicity of the fluorouracil-epirubicin-cyclophosphamide regimen in breast cancer patients. Cancer Chemother Pharmacol. 2006;58:143–56.

24. Graham JW. Missing Data Analysis: Making It Work in the Real World. Annu Rev Psychol. 2009;60:549–76.

25. Schafer JL, Graham JW. Missing data: Our view of the state of the art. Psychol Methods. 2002;7:147–77.

26. Ince DI, Eissing T, Hempel G. Gestation-Specific Changes in the Anatomy and Physiology of Healthy Pregnant Women : An Extended Repository of Model Parameters for Physiologically Based Pharmacokinetic Modeling in Pregnancy. Clin Pharmacokinet. 2017;56:1303–30.

27. Amant F, Von Minckwitz G, Han SN, Bontenbal M, Ring AE, Giermek J, et al. Prognosis of women with primary breast cancer diagnosed during pregnancy: Results from an international collaborative study. J Clin Oncol. 2013;31:2532–9.

28. Ploquin A, Pistilli B, Tresch E, Frenel JS, Lerebours F, Lesur A, et al. 5-year overall survival after early breast cancer diagnosed during pregnancy: A retrospective case-control multicentre French study. Eur J Cancer. 2018;95:30–7.

29. Maggen C, Dierickx D, Lugtenburg P, Laenen A, Cardonick E, Smakov R, et al. Obstetric and maternal outcomes in patients diagnosed with Hodgkin lymphoma during pregnancy: a multicentre, retrospective, cohort study. Lancet Haematol. 2019;11:e551-561.

30. Koolen SLW, Oostendorp RL, Beijnen JH, Schellens JHM, Huitema ADR. Population pharmacokinetics of intravenously and orally administered docetaxel with or without co-administration of ritonavir in patients with advanced cancer. Br J Clin Pharmacol. 2010;69:465–74.

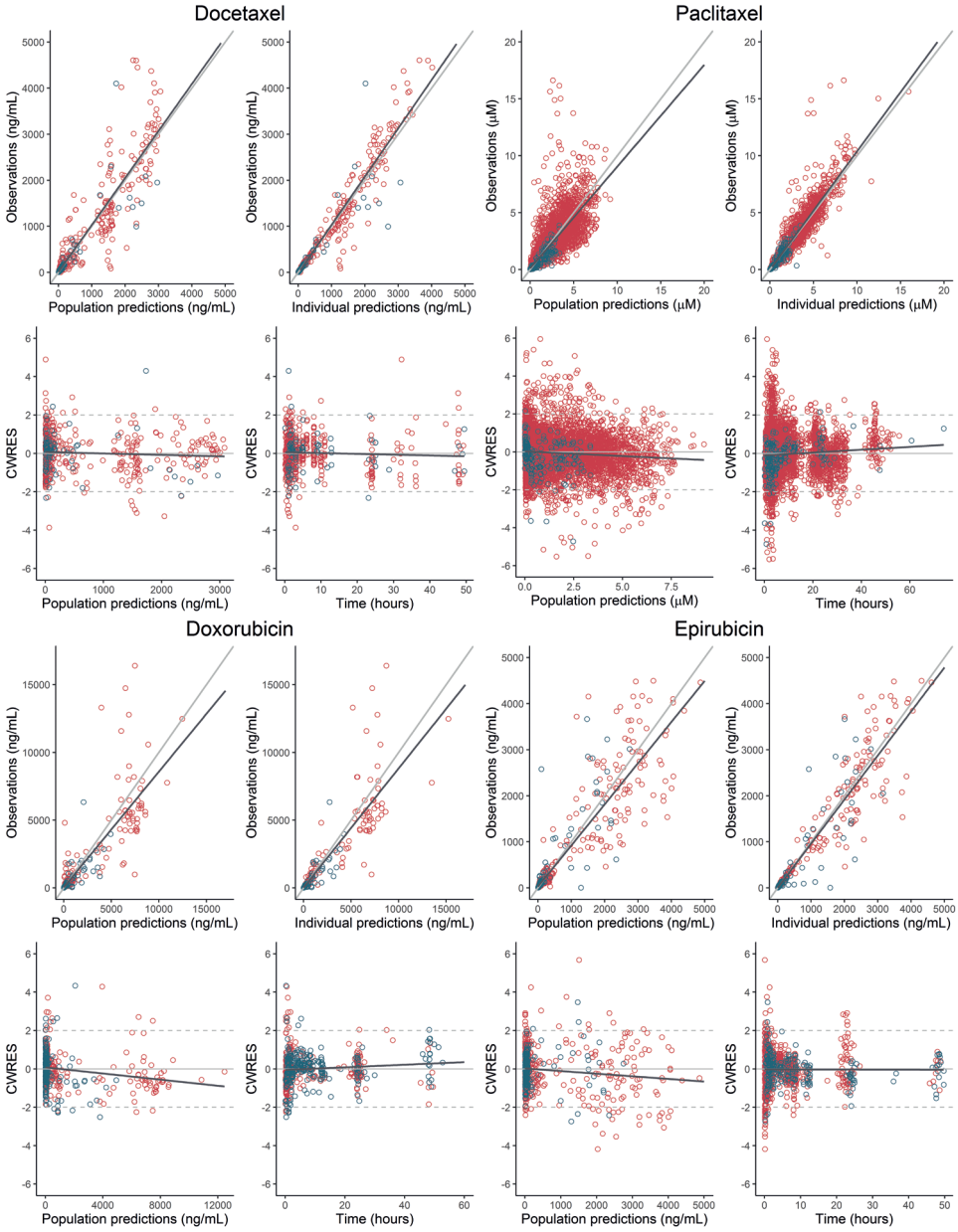

Figure S1. Goodness-of-fit plots of the base models for docetaxel, paclitaxel, doxorubicin and epirubicin without pregnancy effects included. Including individual (IPRED) and population predictions (PRED) *vs.* observed values and conditional weighted residuals (CWRES) *vs.* time after dose and PRED. Open dots represent the non-pregnant population and closed dots are the pregnant population.

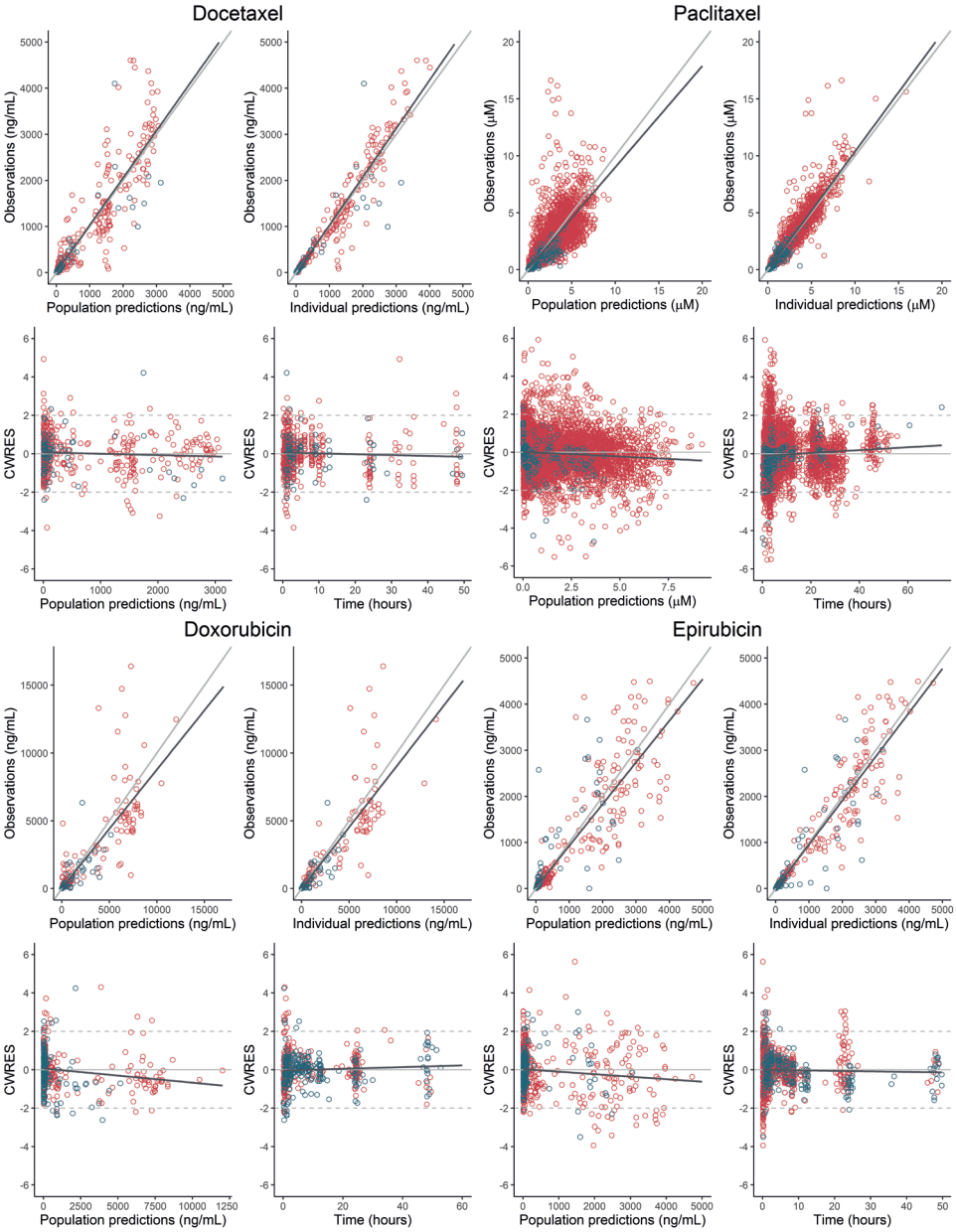

Figure S2. Goodness-of-fit plots of the final PK models for docetaxel, paclitaxel, doxorubicin and epirubicin. Including individual (IPRED) and population predictions (PRED) *vs.* observed values and conditional weighted residuals (CWRES) *vs.* time after dose and PRED. Open dots represent the non-pregnant population and closed dots are the pregnant population.

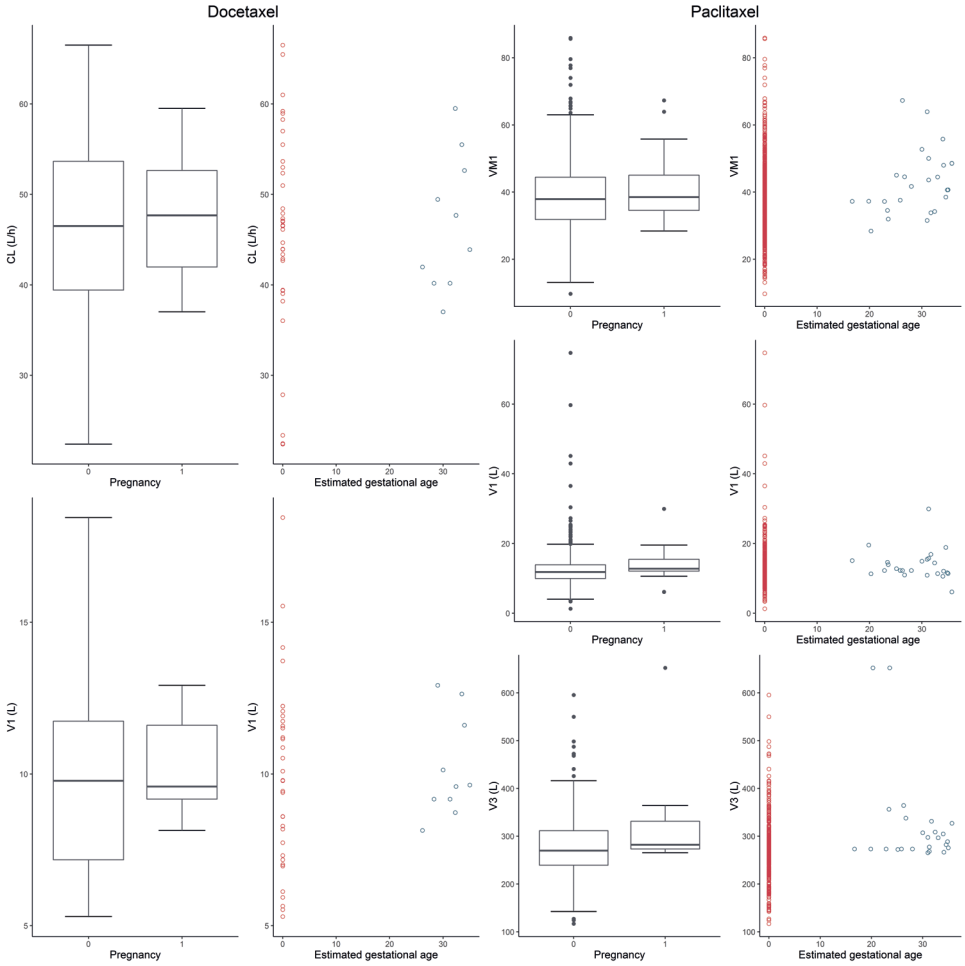

Figure S3. Covariate plots for the base models for docetaxel, paclitaxel, without pregnancy effects included. Gestational age is depicted in weeks. Open dots represent the non-pregnant population and closed dots are the pregnant population.

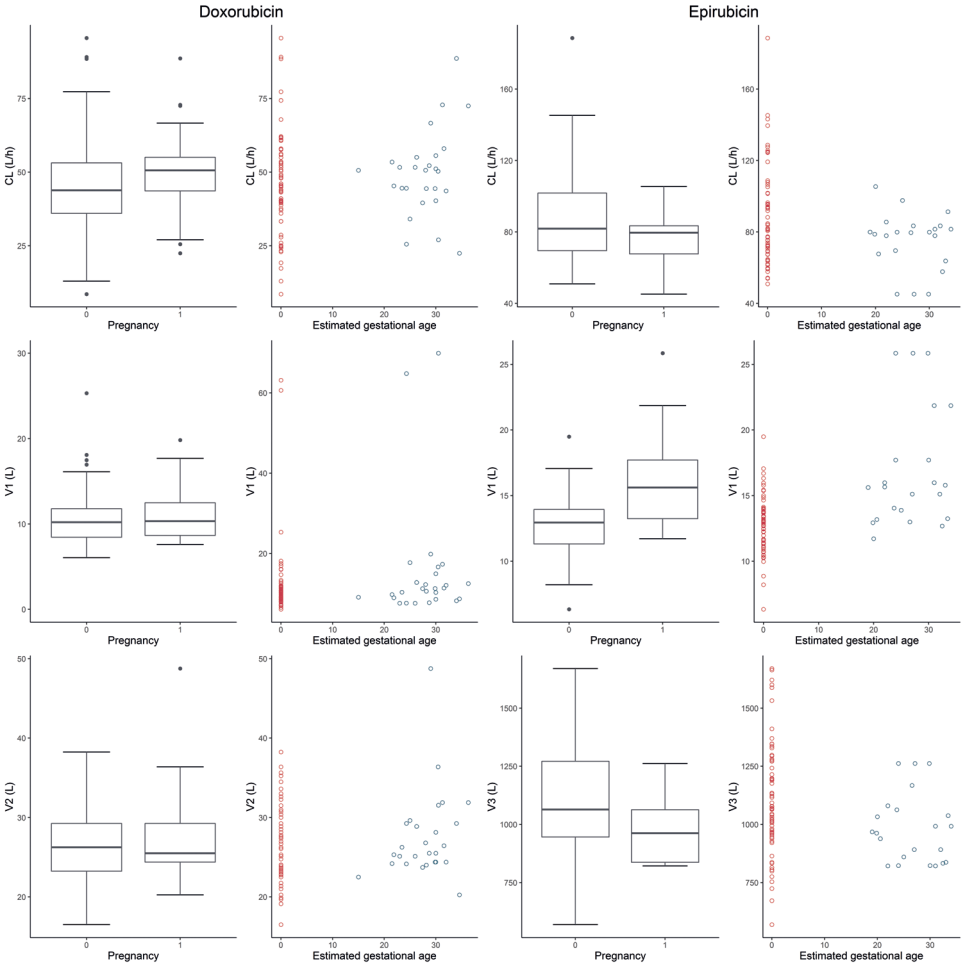

Figure S4. Covariate plots for the base models for doxorubicin and epirubicin, without pregnancy effects included. Gestational age is depicted in weeks. Open dots represent the non-pregnant population and closed dots are the pregnant population.

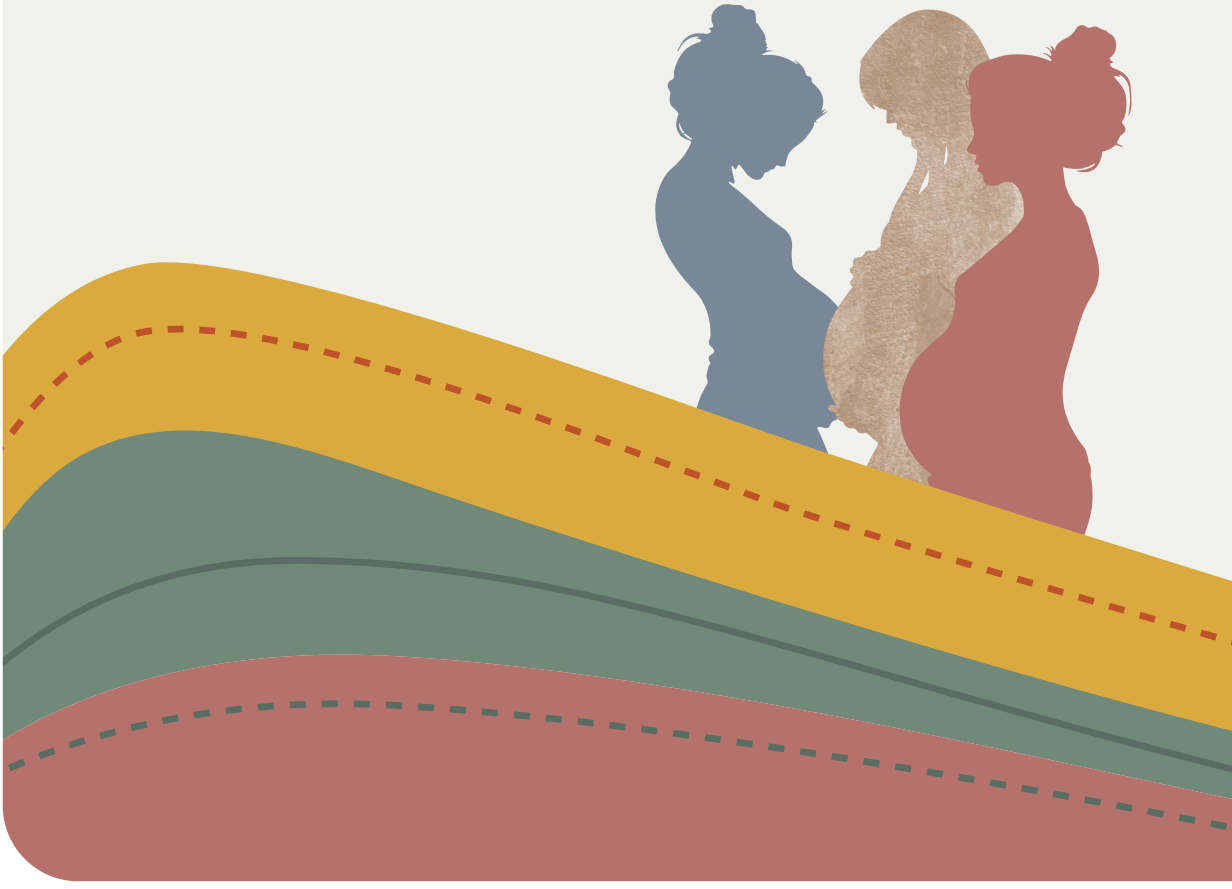

Chapter 2.2

Semi-physiological enriched population pharmacokinetic modelling to predict the effects of pregnancy on the pharmacokinetics of cytotoxic drugs

Manuscript in preparation

J.M. Janssen
J.G.C. van Hasselt
F.C.H. Amant
K. Van Calsteren
J.H. Beijnen
A.D.R. Huitema
T.P.C. Dorlo

Abstract

Introduction

As a result of changes in physiological processes in pregnant patients, the pharmacokinetics (PK) of drugs can be altered. It is unclear whether under- or overexposure occurs in pregnant cancer patients and thus also whether dosing regimens require adjustments in this population. Given the severity of the malignant disease but at the same time the potentially high impact on both the mother and child, there is a high unmet medical need for adequate and tolerable treatment of this patient population. We aimed to develop and evaluate a semi-physiological enriched model that incorporates physiological changes during pregnancy into available population PK models developed from non-pregnant patient data.

Methods

Gestational changes in plasma protein levels, renal function, hepatic function, plasma volume, extracellular water and total body water were implemented in existing empirical PK models for docetaxel, paclitaxel, epirubicin and doxorubicin. Subsequently, these models were used to predict concentration-time curves for pregnant patients, which were compared to observed data obtained from pregnant patients.

Results

The observed concentration-time profiles were well described by the semi-physiological enriched model. For docetaxel, paclitaxel and doxorubicin an overprediction of the lower concentrations was observed, most likely as a result of a lack of data on the variable gestational changes in metabolizing enzymes. For docetaxel, epirubicin and doxorubicin the semi-physiological enriched model performed better in predicting PK in pregnant patients compared to a model that was not adjusted for pregnancy induced changes.

Conclusion

By incorporating gestational changes into existing population pharmacokinetic models it is possible to adequately predict plasma concentrations of drugs in pregnant patients which may inform dose adjustments in pregnant patients.

Introduction

Cancer is manifested in one out of 1,000 pregnancies. Recently, it has been shown that oncological treatment during pregnancy, under strict guidelines and precautions, is safe and thus recommended. An increased use of chemotherapy during pregnancy has been associated with an increased number of livebirths.(1) Nevertheless, as pregnant patients are typically excluded from clinical trials and post-marketing studies in pregnant patients are rarely performed, information on the appropriateness of dosing strategies during pregnancy is missing.(2)

During pregnancy, pharmacokinetics (PK) of drugs can be altered as a result of various changes in several physiological processes. Over the past years, efforts have been made to quantify these physiological alterations during pregnancy.(3,4) Firstly, a gradual decrease in plasma levels for both albumin and α1-Acid-Glycoprotein over the course of pregnancy has been reported. Furthermore, it has been shown that the glomerular filtration rate (GFR) increases until the 3rd trimester but then slightly decreases again during late pregnancy. A 1.5-fold increase in total body water during pregnancy has additionally been shown, even as an increase in body fat, which may result in alterations in distribution volumes. Nevertheless, for other parameters, such as drug metabolizing enzymes, limited and on occasion conflicting data exists. These changes may result in increased or decreased drug concentrations compared to non-pregnant women and this may change over the course of pregnancy.(3)

Given the small therapeutic window of most cytotoxic drugs, small changes in concentrations of cytotoxic agents may influence the therapeutic effect. A major concern is that lower drug plasma concentrations in pregnant women might result in a negative effect on survival. Results from small cohorts with pregnant patients with breast cancer, cervical cancer and Hodgkin Lymphoma did however show that cancer prognosis is similar to that of non-pregnant patients.(5–7)

An empirical PK analysis of four cytotoxic agents obtained from pregnant cancer patients indeed showed alterations in PK parameter estimates compared to non-pregnant patients.(8) Given the complexity of the physiological changes during pregnancy, the magnitude and relevance of these alterations on the PK of anti-cancer drugs is not straightforward. Ideally, PK studies should be performed to quantify these changes. However, clinical studies in pregnant women are difficult to perform as a result of the low incidence of malignancies in women of child-bearing potential, and the many variables that should be taken into account (gestational age, cancer (sub) type, treatment regimen, co-medication).(9) Nevertheless, there is a high unmet medical need for adequate and tolerable treatment of this neglected patient population.
Whole body physiologically-based PK models can be used to predict pregnancy induced changes in PK.(10) However, for most cytotoxic agents, extensive knowledge on the PK

of the drug in non-pregnant patients is available mostly in the form of empirical population PK models. With this work we aimed to develop a methodology in which the advantages of physiologically based PK models are combined with relevant existing knowledge of the PK in non-pregnant patients enabling the prediction of individual PK profiles of a range of cytotoxic drugs in pregnant patients. To this end, we implemented a semi-physiological enriched pregnancy model including changes over the gestational time that allows the prediction of the PK of cytotoxic drugs in pregnant women using only available empirical compartmental models based on non-pregnant patient PK data. To evaluate the physiologically enriched model, we used PK data from pregnant women who were treated with either doxorubicin, epirubicin, docetaxel or paclitaxel, collected internationally over the course of 10 years.

Methods

Development of semi-physiological enriched model

Physiological changes over time during the course of pregnancy have extensively been described in literature.(3,11) In order to describe the typical change in PK parameters during pregnancy, a selection of relevant empirical equations for physiological changes from Abduljalil *et al.* were implemented in our semi-physiological predictions.(12) This work includes all relevant physiological parameters that might have an influence on the PK of either doxorubicin, epirubicin, docetaxel and paclitaxel.

Plasma proteins

Plasma protein levels, such as albumin and alpha1-acid glycoprotein (AAG), decrease during pregnancy, which may affect the unbound concentration of drugs that are highly protein bound. The unbound plasma concentration affects the pharmacological effect of the drug and it is mostly the unbound drug fraction that is renally or hepatically eliminated.(3) The following empirical equations describe the serum albumin concentration (C_{alb}) (eq. 1) and serum AAG concentration (C_{AAG}) (eq. 2) as a function of estimated gestational age (EGA):

$$C_{alb}(EGA)[g/L] = 45.8 - 0.177EGA - 0.0033EGA^2 \quad \text{(Eq. 1)}$$

$$C_{AAG}(EGA)\ [g/L] = 0.74 - 0.0088EGA + 0.0001EGA^2 \quad \text{(Eq. 2)}$$

In order to determine the change in unbound drug concentration (f_u) over time during pregnancy, the dissociation constant (k_D) was calculated by equation 3 and assumed to remain constant during the complete pregnancy period. Subsequently, equation 4 was used to determine the expected change in free unbound drug fraction during pregnancy, for which it was assumed that the free drug concentrations are much lower than k_D and that the maximal binding capacity per protein molecule is 1. This would

imply linear protein binding and thus an f_u independent of the free drug concentration.

$$k_D = \left(\frac{C_{protein}\,(EGA=0) \times f_u(EGA=0)}{1 - f_u(EGA=0)}\right) \quad \text{(Eq. 3)}$$

$$f_u = \frac{1}{\left(1+\frac{C_{protein}\,(EGA)}{k_D}\right)} \quad \text{(Eq. 4)}$$

where $C_{protein}$ is either C_{alb} or C_{AAG} as derived from equation 1 or 2. Previously established drug-specific non-pregnant (i.e. EGA = 0 weeks) percentage of protein binding was used for f_u(EGA=0) (Table 2).

Clearance

Clearance can be subdivided into renal (CL_R) and hepatic (CL_H) clearance as follows:

$$CL(EGA) = CL_R(EGA) + CL_H(EGA) \quad \text{(Eq. 5)}$$

Many changes occur in the urinary and hepatic system during pregnancy, including an increase in GFR, enhanced creatinine clearance (CL_{CR}) and hepatic blood flow (Q_H). Also, variable changes in activities of drug-metabolizing enzymes have been reported. Since all four studied drugs are eliminated by glomerular filtration and only the unbound drug fraction is eliminated, the change in renal clearance during pregnancy was defined by equation 6. In which GFR was described by equation 7 and CL_R(EGA=0) is the reported renal clearance in non-pregnant patients.

$$CL_R(EGA) = CL_R(EGA = 0) \times \frac{GFR(EGA)}{GFR(EGA=0)} \times \frac{f_u(EGA)}{f_u(EGA=0)} \quad \text{(Eq. 6)}$$

$$GFR(EGA)\ [mL/min] = 114 + 3.236EGA - 0.0572EGA^2 \quad \text{(Eq. 7)}$$

In order to describe the relationship between CL_H, hepatic blood flow (Q_H) and intrinsic clearance (CL_{int}), the following equation was used:

$$CL_H(EGA) = \left(\frac{Q_H\,(EGA=0) \times CL_{int}(EGA)}{Q_H\,(EGA=0) + CL_{int}(EGA)}\right) \quad \text{(Eq. 8)}$$

Limited and contradictory data is reported on the change in Q_H during pregnancy, we therefore assumed that the hepatic blood flow remained unchanged over pregnancy and was thus fixed to a typical non-pregnant value of 109 L/h.(13) Equation 8 was rearranged to determine the CL_{int} in non-pregnant patients, using previously estimated drug-specific values of CL_H (equation 11).

$$CL_{int}(EGA = 0)[L/h] = -\left(\frac{CL_H\,(EGA=0) \times Q_H}{CL_H\,(EGA=0) - Q_H}\right) \quad \text{(Eq. 11)}$$

To account for the changes in activities of enzymatic pathways during pregnancy, CL_{int} was corrected for the change in enzyme activity (E):

$$CL_{int}(EGA)[L/h] = CL_{int}(EGA = 0) \times \frac{E(EGA)}{E(EGA=0)} \quad \text{(Eq. 12)}$$

Where E(EGA) represents the enzyme activities of relevant enzymes during pregnancy, and EGA = 0 is the enzyme activity in the non-pregnant state (i.e. 100%). The change in drug-metabolizing enzyme activity of CYP3A4 was described as follows:

$$CYP3A4\ activity\ (EGA)[\%] = 100 + 2.9826EGA - 0.0741EGA^2 \quad \text{(Eq. 13)}$$

Although the activity of CYP2C8 and UGTB7 might be increased during pregnancy, little is known about the magnitude of this increase.(12) We therefore assumed that the activity of these enzymes remained unchanged over pregnancy.

Volume of distribution

We used the relationship between distribution volume (V_d), plasma volume (V_{plasma}) and a drug-specific metric for total body fluids (V_E) minus V_{plasma}, as previously proposed by Gibaldi and McNamara (14):

$$V_d(EGA)[L] = V_{plasma}(EGA) + [V_E(EGA) - V_{plasma}(EGA)]\ \frac{f_u}{f_t} \quad \text{(Eq. 14)}$$

where f_u is the fraction of unbound drug in plasma as described in equation 4, f_t is the unbound drug fraction in tissue and f_u/f_t represents the tissue partition coefficient. f_u/f_t was assumed to remain constant during pregnancy since it is expected that the change in plasma proteins affects f_u and f_t to a similar extent. An increase in V_{plasma} is observed during pregnancy, which is described by equation 15:

$$V_{plasma}(EGA)\ [L] = 2.5 - 0.0223EGA + 0.0042EGA^2 - 0.00007EGA^3 \quad \text{(Eq. 15)}$$

Apparent volumes of distribution were expected to change during pregnancy. Reported non-pregnant volumes of distribution were scaled to the pregnant state using equation 14-16. Where V_d is the volume of distribution of interest and V_E is represented by either total body water (TBW) or extracellular water (ECW), depending on the extent of the volumes of distribution:

$$TBW(EGA)\ [L] = 31.67 + 0.275EGA + 0.0024EGA^2 \quad \text{(Eq. 16)}$$

$$ECW(EGA)\ [L] = 11.86 + 0.0187EGA + 0.0016EGA^2 \quad \text{(Eq. 17)}$$

Prediction

Pharmacokinetic data for doxorubicin, epirubicin, docetaxel and paclitaxel was available from a prospective multinational and multicentre clinical study investigating the effects of the administration of chemotherapy during pregnancy. Pharmacokinetic and clinical results from this trial were reported previously.(1) Concentration-time curves from 26, 16, 9 and 19 pregnant patients were available for doxorubicin, epirubicin, docetaxel and paclitaxel, respectively.

We searched the literature to obtain nonlinear mixed effects population PK models that adequately described the PK of the four cytotoxic drugs in non-pregnant patients. These models were extended with the above described semi-physiological gestational changes in order to provide PK predictions for pregnant individuals. Covariates were excluded from the predictions in order to predict the typical change in PK parameters during pregnancy. Drug specific PK characteristics that were taken into account, such as protein binding and routes of metabolism, are depicted in Table 2. With these PK parameters, typical concentration-time profiles were predicted for EGA's that matched the observed dataset. In order to provide a valid comparison to the observed concentration-time profiles, the dosing regimens from the clinical data were used. Since dosing of doxorubicin, epirubicin, docetaxel and paclitaxel is based on a patients' body surface area (BSA), the median BSA found in the studied patients was used (Table 1).

Table 1. Patient characteristics PK study

	Docetaxel	Paclitaxel	Epirubicin	Doxorubicin
Total number of patients, n	9	20	16	22
Total number of cycles, n	10	25	22	27
EGA (weeks) [median (range)]	31.8 (26.1-35.0)	31.0 (16.7-35.7)	26.8 (19.0-34.0)	28.7 (15.0-36.3)
BSA (m^2) [median (range)]	1.91 (1.66-2.06)	1.92 (1.74-2.27)	1.89 (1.58-2.48)	1.78 (1.56-2.49)
Dosing schedule	100 mg/m^2	60 mg/m^2 80 mg/m^2 175 mg/m^2	100 mg/m^2	25 mg/m^2 50 mg/m^2 60 mg/m^2

Abbreviations: EGA, estimated gestational age; BSA, Body Surface Area.
[a](1,8)

Evaluation

The observed concentration-time profiles available from the clinical study were used to visually evaluate the performance of the semi-physiological enriched models. Secondly, individual model fits and predictions were obtained for the observed pharmacokinetic data from pregnant women based on individual Bayesian estimates which were obtained by using non-linear mixed effects modelling, more specifically by

using the MAXEVAL=0 and POSTHOC options in NONMEM®.(15) The fit of the semi-physiological model during pregnancy was compared to the fit of the model parameters for the non-pregnant state (EGA=0). Subsequently, changes in Objective Function Value (ΔOFV, corresponding to minus twice the log-likelihood) were evaluated to compare and assess both models.

Table 2. PK characteristics of the included drugs and non-pregnant population PK models

	Docetaxel[a]	**Paclitaxel[b]**	**Epirubicin[c]**	**Doxorubicin[d]**
Protein binding (%)	94	95	77	75
Metabolism	CYP3A4	CYP3A4 CYP2C8	CYP3A4 UGTB7	CYP3A4
CL_R (%)	6	6	10	5
Non-pregnant PK model[e]	CL = 44.1 L/h (29.4%) V1 = 8.9 L (37.8%) Q1 = 6.1 L/h V2 = 7.3 L Q2 = 14.4 L/h (20.3%) V3 = 388 L	V1 = 12 L V3 = 268 L (36.2%) VM_{EL} = 33.8 µmol/h (27.0%) KM_{EL} = 0.44 µmol/h VM_{TR} = 177 µmol/h (27.0%) KM_{TR} = 1.61 µmol/h (66.0%) K_{21} = 1.21 h^{-1} Q2 = 16.8 L/h (49.5%)	CL = 71.7 L/h (15%) V1 = 13.1 L Q1 = 70.6 L/h V2 = 776 L Q2 = 17.8 L/h V3 = 14.6 L	CL = 47.6 L/h (24.6%) V1 = 12.3 L (11.8%) Q1 = 60.3 L/h (20.7%) V2 = 421 L (25.0%)

Abbreviations: CL_R, renal clearance; V1, volume of central compartment; V2, volume of first peripheral compartment; V3, volume of second peripheral compartment; CL, clearance; Q1, inter-compartmental clearance between central and first peripheral compartment; Q2, inter-compartmental clearance between central and second peripheral compartment; VM_{EL}, maximal elimination rate; KM_{EL}, plasma concentration at half VM_{EL}; VM_{TR}, maximal transport rate from the central to the first peripheral compartment; KM_{TR}, plasma concentration at half VM_{TR}; K_{21}, rate constant from the first peripheral compartment to the central compartment.
[a] (17). [b] (18). [c] (20). [d] (19). [e] Parameter estimates from base models (inter-individual variability, expressed as percentage coefficient of variation (CV%)).

Software

Predictions were performed using a differential equation system in R (version 3.4.3) together with the R package deSolve.(16) NONMEM® v.7.3 (ICON Development Solutions, Ellicott City, MD, USA) was used to evaluate the developed model.(15)

Results

Docetaxel

The PK of intravenously administered docetaxel has adequately been described by a linear three-compartment model with linear elimination.(17) Docetaxel is mainly metabolized by CYP3A4 and thereafter eliminated as inactive metabolites in the faeces. Hence, the change in CYP3A4 enzyme activity during pregnancy was incorporated in

the predictions. As docetaxel is mainly bound to AAG in the plasma, equation 2 was incorporated in order to account for protein binding. Table 3 shows the typical change in the docetaxel PK parameters during pregnancy. The largest increase was observed for V3. Additionally, clearance increased during the first two trimesters, but decreased again during the third trimester. Typical concentration-time curves were predicted for the median GA, which was 32 weeks for the patients treated with docetaxel. Although trough concentrations were slightly overpredicted, the typical observed pregnant concentrations were well described by the semi-physiological enriched model (Figure 1). Additionally, the predictions clearly demonstrated that the use of non-pregnant parameter estimates resulted in an overprediction of the observed concentrations (Figure 1). Comparison of the model fit for the individual predictions based on the semi-physiological pregnant parameter estimates versus non-pregnant parameter estimates resulted in a decrease in OFV of 4.66 points.

Table 3. Typical gestational changes in PK parameters by trimester

	Docetaxel	Paclitaxel	Epirubicin	Doxorubicin
EGA 12 weeks				
CL (L/h)	+ 15.9%	-	+ 14.3%	+ 11.3%
VM_{EL} (µmol/h)	-	+ 17.8%	-	-
V1 (L)	+ 4.27%	+ 4.17%	+ 3.25%	+ 3.82%
V2 (L)	+ 4.67%	-	+ 11.6%	+ 3.42%
V3 (L)	+ 15.7%	+ 15.7%	-	+ 16.0%
EGA 28 weeks				
CL (L/h)	+ 18.1%	-	+ 15.8%	+ 14.2%
VM_{EL} (µmol/h)	-	+ 19.8%	-	-
V1 (L)	+ 18.0%	+ 15.0%	+ 14.6%	+ 14.5%
V2 (L)	+ 20.0%	-	+ 29.0%	+ 13.7%
V3 (L)	+ 38.7%	+ 38.4%	-	+ 39.0%
EGA 40 weeks				
CL (L/h)	+ 4.99%	-	+ 3.57%	+ 7.11%
VM_{EL} (µmol/h)	-	+ 5.33%	-	-
V1 (L)	+ 30.3%	+ 27.5%	+ 27.6%	+ 27.5%
V2 (L)	+ 32.2%	-	+ 46.1%	+ 26.7%
V3 (L)	+ 57.2%	+ 56.7%	-	+ 57.7%

Abbreviations: EGA, estimated gestational age; V1, volume of central compartment; V2, volume of first peripheral compartment; V3, volume of second peripheral compartment; CL, clearance; VM_{EL}, maximal elimination rate.

Paclitaxel

For paclitaxel, a population PK model that consists of a three compartment model with saturable distribution to the first peripheral compartment and saturable clearance for

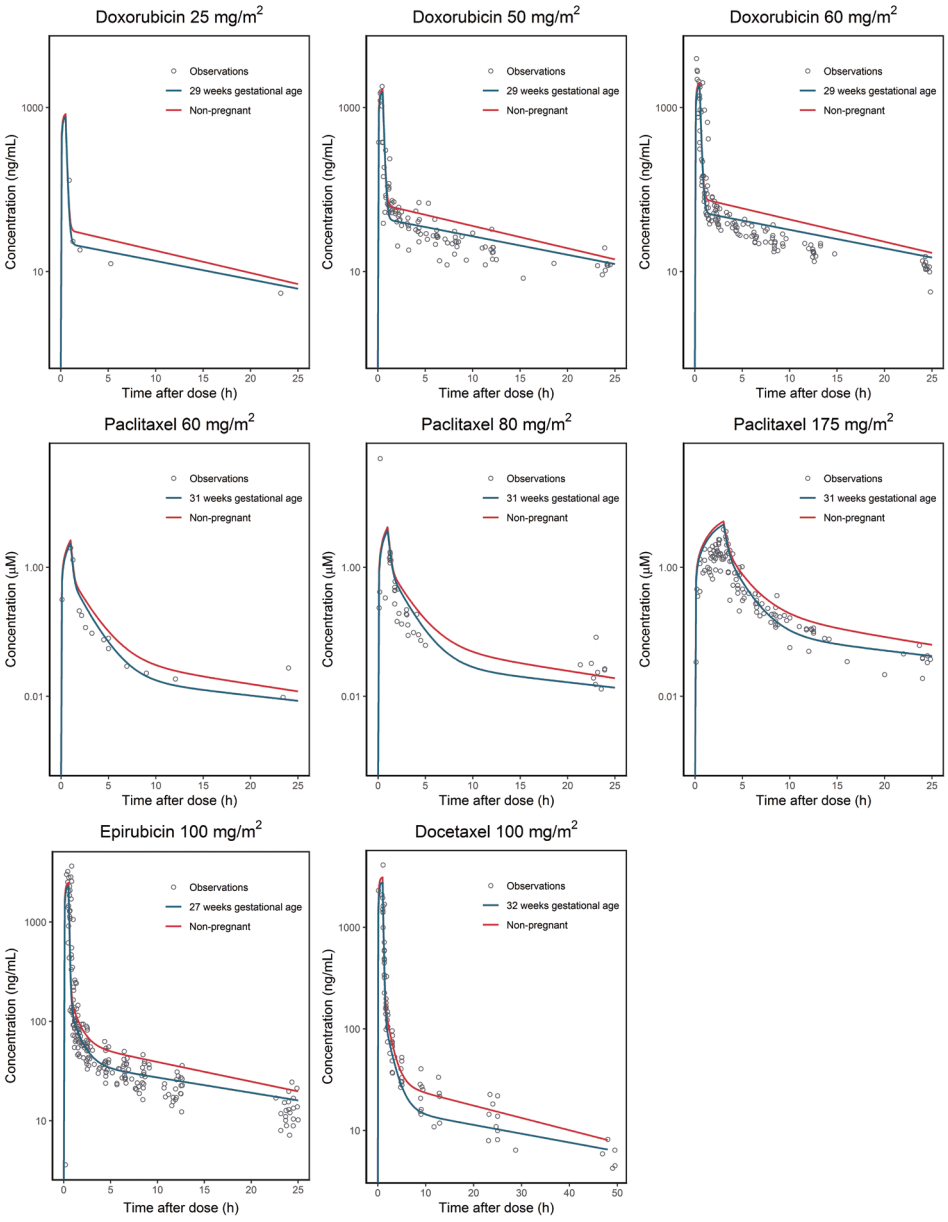

Figure 1. Predicted and observed concentration-time profiles of docetaxel, paclitaxel, doxorubicin and epirubicin for non-pregnant and pregnant patients.

the central compartment has been published.(18) Paclitaxel is mainly bound to albumin in plasma, metabolized by both CYP3A4 and CYP2C8 and partly eliminated by the faeces. Hence, the change in albumin plasma levels and CYP3A4 enzyme activity were used. Data on the gestational change in CYP2C8 activity is still lacking and could therefore not be included. To account for the change in clearance of paclitaxel during pregnancy, the maximal elimination rate (VM_{EL}) was scaled according to equations 8-13. Typical parameter changes were similar to the changes that were observed for docetaxel. All volumes of distribution increased during pregnancy, with a maximum increase of approximately 60% for V3. VM_{EL} initially increased, but decreased again towards baseline during the third trimester. Concentration-time curves were predicted for the median GA of 31 weeks that was observed in the evaluation dataset (Figure 1). The semi-physiological predictions adequately described the observed paclitaxel concentrations. A minor overprediction of the observed concentrations between pre-dose and 5 hours after administration was observed. Notwithstanding, an overprediction of the observations was evident when non-pregnant estimates were used, especially in the elimination phase of the concentration-time curve. The model fit for the individual predictions based on the semi-physiological pregnant parameter estimates showed decrease of the OFV of 18.4 compared to non-pregnant parameter estimates.

Doxorubicin

The PK of doxorubicin has previously been described by a two-compartment model with linear clearance and extensive distribution (Table 2).(19) Doxorubicin is metabolized by CYP3A4 and into both active and inactive metabolites, which are mainly excreted by the faeces. Small initial increases ranging from 0 – 15% were observed for CL and V1. The largest increase was observed for V2, which increased by 46.1% in the third trimester. Typical concentration-time curves were predicted for the median GA, which was 29 weeks for the patients treated with doxorubicin. Although doxorubicin concentrations were still slightly overpredicted in the terminal elimination phase, this overprediction was smaller than for the non-pregnant model-based predictions and concentrations were well described in the initial part of the elimination phase until about 5 hours after administration. Figure 1 clearly demonstrates that predictions using model parameters based on the non-pregnant state resulted in an overprediction of the observed doxorubicin concentrations. In addition, the model fit for the individual predictions based on the semi-physiological pregnant parameter estimates showed a decrease of the OFV of 50.4 compared to non-pregnant parameter estimates.

Epirubicin

For epirubicin, a three-compartment model with linear clearance and extensive tissue distribution has been published.(20) Epirubicin is metabolized by CYP3A4, glucuronidized and thereafter excreted by the faeces. For epirubicin, typical parameter increases in CL and V1 were comparable with the observed increases in doxorubicin

CL and V1. However, V2 and V3 showed a larger increase then was observed for doxorubicin V2. Concentration-time curves were predicted for the median observed GA of 27 weeks. The semi-physiological enriched model adequately predicted the epirubicin concentration-time curves that were observed during pregnancy. Additionally, the predictions using non-pregnant estimates showed an overprediction of the observed concentration-time curve. Comparison of the model fit for the individual predictions based on the non-pregnant versus the semi-physiological pregnant parameter estimates showed a significantly improved fit for the latter: a decrease in OFV of 148 points was observed for epirubicin.

Discussion

With this work we demonstrated the feasibility and relevance of a semi-physiological prediction approach in which prior knowledge of both the human population PK of a cytotoxic drug and physiological changes during pregnancy are combined to predict changes in PK in pregnant patients. To this end, we used the physiological alterations during pregnancy that have been described in a quantitative manner by Abduljalil *et al*.(12)

The US Food and Drug Administration (FDA) and European Medicines Agency (EMA) provided guidance on the use of medicinal products during pregnancy.(2,21,22) In these guidelines, it is stated that post-marketing studies should be performed and exposure registries should be established for drugs that are used in women of child-bearing age. With these studies, data on the outcomes of pregnancies exposed to these drugs is collected. The EMA additionally advises to use a population PK approach to identify potential gestational effects and hence simulate doses that achieve PK exposure in pregnant patients similar to non-pregnant patients.

An alternative widely used approach is the development of a full physiologically-based pharmacokinetic model. These models are constructed from known anatomical and physiological characteristics (system-related parameters) combined with physicochemical and clinical pharmacological drug characteristics (drug-related parameters). With these models extrapolation to unstudied conditions can be made e.g. for drug-drug interactions, use of drugs in children or in pregnant patients. However, when drugs are introduced for the treatment of pregnant patients, clinical information on the drug's disposition and elimination in non-pregnant patients is generally already available in the form of empirical population PK models and can be of great value to inform the extrapolation to pregnant patients. The here presented semi-physiological enriched model implements a hybrid methodology that integrates actual patient data with the quantitative and longitudinal physiological changes during pregnancy. This latter aspect is comparable to the use of system-related parameters

in physiologically-based pharmacokinetic models. This provides a first prediction of the PK profile in pregnant women based on their GA, taking into account established non-pregnant empirical PK models. This is particularly relevant for cytotoxic agents as their application in pregnant cancer patients is rare and difficult due to their mutagenic and teratogenic potential, but nevertheless optimal treatment is sometimes required for maternal survival.(1)

For docetaxel the semi-physiological approach did not perform significantly better than the non-pregnant PK model parameters and only modest changes in typical parameters were observed. This shows that pregnancy has a limited effect on the PK of docetaxel and predictions using the parameters based on non-pregnant data perform well for the pregnant population. In an empirical population PK analysis, we found small changes in docetaxel PK during pregnancy as well. For the paclitaxel 80 mg/m^2 dose regimen, the predictions showed an overprediction of the concentrations. This could be explained by the very small sample size and wide gestational age range in the pregnancy dataset that was available for evaluation. In addition to CYP3A4, paclitaxel is metabolized by CYP2C8 for which no relationship with gestational age is available, due to a lack of data on the dynamics of this enzyme. An underestimation of the CYP2C8 activity during pregnancy could in theory be a potential cause for the observed overprediction. Furthermore, the PK of taxanes is characterized by large inter-individual variability which complicates the identifiability of an effect of gestation in a small sample size. The predicted epirubicin concentrations were in good agreement with the observations, although some overprediction of the trough concentrations was observed. Epirubicin is metabolized by both CYP3A4 and UGTB7. For UGTB7 increased activity during pregnancy has been reported but this has not been quantified.(3) The assumption of unchanged UGTB7 activity during pregnancy could fairly result in an underprediction of the clearance of epirubicin. For doxorubicin we used a previously described two-compartment model that was developed using sparsely collected PK data. Predictions with this non-pregnant model for the pregnant population resulted in an overprediction of the observed concentrations in the terminal elimination phase. The observed, rich sampled, data indicates that a three-compartment model might be better suitable to describe the doxorubicin PK. Nevertheless, the semi-physiological approach performed significantly better than the model based predictions based on non-pregnant parameter estimates. Overall, our semi-physiological enriched model provided a reasonable prediction of the PK in women at any stage of gestation for various cytotoxic drugs. In line with previous findings, lower drug concentrations were predicted during pregnancy compared to the non-pregnant state.(8) Moreover, the semi-physiological model resulted in a significant better fit of the PK data from pregnant patients than the literature-based models for paclitaxel, epirubicin and doxorubicin.

This semi-physiological enriched model is depending on assumptions and simplifications which might all pose limitations. Firstly, we only accounted for changes in maternal PK

and did not include changes related to the fetal compartment. It has been shown that the placenta is a good protector for taxanes and anthracyclines. In animal studies, fetal paclitaxel plasma concentrations were approximately 1% of the maternal concentrations while fetal plasma docetaxel levels were not detectable. In addition, placental passage was 4% for epirubicin and 8% for doxorubicin.(9) This suggests very limited distribution to the fetal compartment of the here investigated chemotherapeutics. However, the semi-physiological based model could easily be extended with a fetal compartment for drugs that cross the placenta. Consequently, fetal exposure can be predicted, based on the predicted maternal PK. Secondly, we assumed unchanged partition coefficients that account for the distribution between body compartments. As the proportion of body fat shows a typical increase in addition to alterations in body fluids, this assumption might lead to an underprediction of the pregnant volumes of distribution. The hepatic blood flow was also assumed to remain constant during pregnancy. Contradictory results have been published regarding the change in hepatic blood flow during pregnancy. In these studies, different measurement methods were applied resulting in highly variable and inconsistent results. In addition, the relationship between the gestational induced change in other cardiovascular parameters such as cardiac output or haematocrit and the hepatic blood flow remains unclear.(3) Hence, the change in hepatic clearance during pregnancy was driven by the change in metabolizing enzyme activity. A maternal increase in CYP3A4 activity has been shown in several studies and was, therefore, included in our semi-physiological enriched model. The activity of UGTB7 has been suggested to increase over pregnancy as well, but the magnitude of this increase is still not quantitatively described.(12) Changes in CYP2C8 could not be incorporated because no relationships with gestation have been established. Consequently, non-pregnant metabolizing activity was assumed for these enzymes over pregnancy. Also, it should be noted that the developed semi-physiological model relies on the validity and accuracy of the estimates from the non-pregnant PK studies. In addition, we assumed similar variability in PK parameters between pregnant versus non-pregnant patients and used the typical parameter estimates for predictions. High variability and bias in these estimates could potentially result in inadequate predictions of the pregnant PK. It should be noted, however, that when relevant changes in these parameters are described, they can be implemented in this model similarly to the other implemented changes. In this respect, the semi-physiological enriched model developed here incorporates similar processes as full physiologically-based pharmacokinetic models.

Conclusion

The semi-physiological enriched model provided an adequate prediction of the PK for four cytotoxic agents of two distinct drug classes in women over varying stages of gestation. It can be concluded that this semi-physiological enriched model is applicable

to cytotoxic drugs with different pharmacological characteristics. This method may therefore be used for extrapolation purposes to adjust dosing regimens in pregnant women for drugs for which PK data from pregnant women are unavailable.

References

1. de Haan J, Verheecke M, Van Calsteren K, Calster B Van, Shmakov RG, Gziri MM, et al. Oncological management and obstetric and neonatal outcomes for women diagnosed with cancer during pregnancy : a 20-year international cohort study of 1170 patients. Lancet Oncol. 2018;19:337–46.

2. European Medicines Agency (EMA). Guideline on the exposure to medicinal products during pregnancy: need for post-authorization data (2006).

3. Abduljalil K, Furness P, Johnson TN, Rostami-Hodjegan A, Soltani H. Anatomical, Physiological and Metabolic Changes with Gestational Age during Normal Pregnancy A Database for Parameters Required in Physiologically Based Pharmacokinetic Modelling. 2012;51:365-96.

4. Dallmann A, Ince I, Meyer M, Willmann S, Eissing T, Hempel G. Gestation-Specific Changes in the Anatomy and Physiology of Healthy Pregnant Women: An Extended Repository of Model Parameters for Physiologically Based Pharmacokinetic Modeling in Pregnancy. Clin Pharmacokinet. 2017;56:1303-30.

5. Amant F, Vandenbroucke T, Verheecke M, Fumagalli M, Halaska MJ, Boere I, et al. Pediatric Outcome after Maternal Cancer Diagnosed during Pregnancy. N Engl J Med. 2015;373:1824–34.

6. Halaska MJ, Uzan C, Han SN, Fruscio R, Dahl Steffensen K, Van Calster B, et al. Characteristics of patients with cervical cancer during pregnancy: a multicenter matched cohort study. An initiative from the International Network on Cancer, Infertility and Pregnancy. Int J Gynecol Cancer. 2019;29:676–82.

7. Maggen C, Dierickx D, Lugtenburg P, Laenen A, Cardonick E, Smakov R, et al. Obstetric and maternal outcomes in patients diagnosed with Hodgkin lymphoma during pregnancy: a multicentre, retrospective, cohort study. Lancet Haematol. 2019;6:e551-e561.

8. van Hasselt JGC, Van Calsteren K, Heyns L, Han S, Mhallem Gziri M, Schellens JHM, et al. Optimizing anticancer drug treatment in pregnant cancer patients: pharmacokinetic analysis of gestation-induced changes for doxorubicin, epirubicin, docetaxel and paclitaxel. Ann Oncol. 2014;25:2059–65.

9. Vandenbroucke T, Verheecke M, Fumagalli M, Lok C, Amant F. Effects of cancer treatment during pregnancy on fetal and child development. Lancet Child Adolesc Heal. 2017;1:302–10.

10. Dallmann A, Mian P, den Anker J Van, Allegaert K. Clinical Pharmacokinetic Studies in Pregnant Women and the Relevance of Pharmacometric Tools. Curr Pharm Des. 2019;25:483-495.

11. Ince DI, Eissing T, Hempel G. Gestation-Specific Changes in the Anatomy and Physiology of Healthy Pregnant Women : An Extended Repository of Model Parameters for Physiologically Based Pharmacokinetic Modeling in Pregnancy. Clin Pharmacokinet. 2017;56:1303–30.

12. Abduljalil K, Furness P, Johnson TN, Rostami-Hodjegan A, Soltani H. Anatomical, Physiological and Metabolic Changes with Gestational Age during Normal Pregnancy. Clin Pharmacokinet. 2012;51:365–96.

13. Nakai A, Sekiya I, Oya A, Koshino T, Araki T. Assessment of the hepatic arterial and portal venous blood flows during pregnancy with Doppler ultrasonography. Arch Gynecol Obstet. 2006;266:25–9.

14. Gibaldi M, McNamara PJ. Apparent volumes of distribution and drug binding to plasma proteins and tissues. Eur J Clin Pharmacol. 1978;13:373–8.

15. Bauer RJ. NONMEM USERS GUIDE INTRODUCTION TO NONMEM 7.3.0. ICON Development Solutions, 2014.

16. RC Team (2009) R: a language and environment for statistical computing. R Foundation for Statistical Computing, Vienna.

17. Koolen SLW, Oostendorp RL, Beijnen JH, Schellens JHM, Huitema ADR. Population pharmacokinetics of intravenously and orally administered docetaxel with or without co-administration of ritonavir in patients with advanced cancer. Br J Clin Pharmacol. 2010;69:465–74.

18. Crombag M-RBS, de Vries Schultink AHM, Koolen SLW, Wijngaard S, Joerger M, Schellens JHM, et al. Impact of Older Age on the Exposure of Paclitaxel: a Population Pharmacokinetic Study. Pharm Res. 2019;36:33.

19. Joerger M, Huitema ADR, Richel DJ, Dittrich C, Pavlidis N, Briasoulis E, et al. Population Pharmacokinetics and Pharmacodynamics of Doxorubicin and Cyclophosphamide in Breast Cancer Patients A Study by the EORTC-PAMM-NDDG. 2007;46:1051–68.

20. Sandstrom M, Lindman H, Nygren P, Johansson M, Bergh J, Karlsson M. Population analysis of the pharmacokinetics and the haematological toxicity of the fluorouracil-epirubicin-cyclophosphamide regimen in breast cancer patients. Cancer Chemother Pharmacol. 2006;58:143–56.

21. FDA Guidance for Industry – Pharmaockinetics in Pregnancy – Study Design, Data Analysis, and Impact on Dosing and Labeling. FDA Guidance (2004).

22. FDA Guidance for Industry – Establishing Pregnancy Exposure Registries. FDA Guidance (2002).

CHAPTER 3

Exposure – response relationships



Chapter 3.1

Population pharmacokinetics of intracellular 5-fluorouridine 5'triphosphate and its relationship with hand-and-foot syndrome in patients treated with capecitabine

Manuscript in preparation

J.M. Janssen
B.A.W. Jacobs
J. Roosendaal
E.J.B. Derissen
S. Marchetti
J.H. Beijnen
A.D.R. Huitema
T.P.C. Dorlo

Abstract

Introduction

Capecitabine is an oral pro-drug of 5-fluorouracil (5-FU). Patients with solid tumors who are treated with capecitabine may develop hand-and-foot syndrome (HFS) as side effect. It is hypothesized that this might be a result of accumulation of intracellular 5-FU metabolites. We characterized the pharmacokinetics (PK) of 5-fluorouridine 5'-triphosphate (FUTP) in peripheral blood mononuclear cells (PBMCs) and assessed the relationship between exposure to capecitabine and/or its metabolites and the development of HFS.

Methods

PK data was available from three clinical studies that investigated plasma and intracellular capecitabine PK. A previously developed model describing the PK of capecitabine and four metabolites in plasma was extended with an intracellular compartment describing intracellular FUTP concentrations. Ordered categorical HFS data (scored using the CTCAE criteria) was available from one of the clinical trials. Based on these observations, a continuous-time Markov model (CTMM) was developed to describe the development of HFS during treatment with capecitabine. The influences of capecitabine and metabolite concentrations on the development of HFS were evaluated.

Results

The PK of intracellular FUTP was best described by a one-compartment model with first-order elimination ($k_{e,FUTP}$ was 0.028 h^{-1} (95% confidence interval 0.002-0.039)) where the rate of influx of FUTP was proportional to the 5-FU plasma concentrations. The predicted individual intracellular FUTP concentration was identified as a significant predictor for the development and severity of HFS. Simulations demonstrated a clear exposure-response relationship. The percentage of patients experiencing clinically relevant HFS (grade 2 and 3) increases with dose and time on capecitabine treatment.

Conclusion

The final PK model successfully describes the cumulative intracellular FUTP concentrations. In addition, a significant relationship between these intracellular FUTP concentrations and the development and severity of HFS was identified. This model can be used to simulate future dosing regimens and thereby optimize treatment with capecitabine.

Introduction

Capecitabine is an oral pro-drug of the anti-cancer drug 5-fluorouracil (5-FU) which is frequently used for the treatment of patients with breast, gastric and colorectal cancer. Following oral administration, capecitabine is rapidly and completely absorbed from the gastro-intestinal tract. Capecitabine is enzymatically converted into 5'-deoxy-5-fluorocytidine (dFCR). dFCR is then converted into 5'-deoxy-5-fluorouridine (dFUR) which is further metabolized into the pharmacologically active metabolite 5-FU by thymidine phosphorylase (TP).(1) Approximately 3-5% of 5-FU is intracellularly converted to the cytotoxic metabolites 5-fluoro-2'-deoxyuridine 5'-monophosphate (FdUMP), 5-fluoro-2'-deoxyuridine 5'-triphosphate (FdUTP) and 5-fluorouridine 5'-triphosphate (FUTP).(2) However, 80% of 5-FU is catabolized into the inactive metabolite dihydro-5-FU by dihydropyrimidine dehydrogenase (DPD) and subsequently into the final inactive metabolite fluoro-β-alanine (FBAL), which is renally excreted. By binding to the nucleotide-binding site of the nucleotide synthetic enzyme thymidylate synthase (TS), FdUMP disrupts DNA synthesis, which results in DNA damage. In addition, FdUTP can be misincorporated into DNA which leads to DNA strand breaks and cell death. By incorporation into RNA, the 5-FU metabolite FUTP interferes with RNA functionalities.(3)

The most commonly observed severe adverse event associated with capecitabine treatment is hand-and-foot syndrome (HFS). The development of HFS may require dose modifications (reduction, interruptions) and/or discontinuation of treatment with capecitabine. In most cases, treatment interruptions followed by dose reductions result in recovery of the symptoms.(4) Although several mechanisms for the development of HFS in patients treated with capecitabine have been proposed, the pathophysiology is not yet fully unfolded.(4,5) Pressure from walking or use of the hands has been related to the release of capecitabine or its metabolites into surrounding tissue as a result of rupture of the tiny capillaries in the dermis. A previous study showed a decrease in the incidence of HFS during treatment with capecitabine in patients treated with celecoxib compared to patients treated with capecitabine alone, which suggests an inflammatory reaction caused by COX-2 expression in the palms and soles of the hand and the feet, respectively.(6–8) Another possible mechanism could be an increased local activation and accumulation of 5-FU and metabolites in the keratinocytes in the skin of the palms and soles as a result of higher TP concentrations in this tissue, as shown by Milano and colleagues.(4) As HFS typically develops after several weeks on capecitabine treatment, it is hypothesized that a cumulative drug effect is causing this toxicity. Previous population-based analyses have shown that the development of HFS seems to be associated with cumulative capecitabine dose administration. A significant relationship between capecitabine or metabolite concentrations and severity of HFS has however not been shown.(9,10) These studies investigated the predictive value of plasma capecitabine and metabolite concentrations, but did not investigate exposure to intracellular active metabolites.

With this analysis, we aimed to describe the population pharmacokinetics (PK) of the intracellular metabolite FUTP by integration into a previously developed population PK model of capecitabine and the metabolites dFCR, dFUR, 5-FU and FBAL.(11) The ultimate goal was to identify whether the intracellular metabolite FUTP is predictive for the development and severity of HFS in patients treated with capecitabine.

Methods

Patients, study design and data

Capecitabine, dFCR, dFUR, 5-FU, FBAL and FUTP PK data were available from patients with solid tumours who participated in two clinical phase I dose-escalation studies and one phase 0 clinical study.(12,13) In all three studies, the intracellular FUTP concentrations were determined in peripheral blood mononuclear cells (PBMCs). All studies were approved by the Medical Ethics Committee of the Netherlands Cancer Institute and were performed in compliance with the WHO declaration of Helsinki. In study 1, patients received oral capecitabine twice-daily (BID) in a chronomodulated treatment regimen on days 1-21 of a 21-day cycle. Dose-levels ranged from 375 mg/m^2 in the morning and 625 mg/m^2 in the evening to 950 mg/m^2 in the morning and 1600 mg/m^2 in the evening. Plasma samples were collected at pre-dose, 0.5, 1, 1.5, 2, 3, 5, 11, 15 h after the capecitabine morning dose on day 7 and during the following night (day 8), 0.5, 1, 1.5, 2, 3, 5 and 9 h after the evening capecitabine intake. PBMCs were obtained at pre-dose, 1.5 and 3 h after the capecitabine intake in the morning on day 7 of treatment. In study 2, patients received capecitabine on day 1-14 of a 21-day cycle. Capecitabine doses ranged from 500 to 1000 mg/m^2 BID. Plasma samples were collected at pre-dose, 1, 2, 3, 4, 6 and 8 hours after administration on day 1. PBMCs were obtained on day 1 and 14 of the first cycle at pre-dose, 2, 4, 8 and 12 hours after administration.(12) In study 3, patients received a single dose of 1000 mg oral capecitabine in the morning. PBMC samples were obtained at pre-dose, 1, 2, 3, 4, 6 and 24 h after administration.(13)

Capecitabine, dFCR, dFUR, 5-FU and FBAL concentrations were quantified in plasma using a validated liquid chromatography-tandem mass spectrometry (LC-MS/MS) assay as previously described.(14) In all three studies, FUTP concentrations were determined in PBMCs. PBMCs were isolated from peripheral heparinized blood using Ficoll-plaque density gradient and counted using previously described methods.(15) The concentrations in PBMCs were calculated based on the amount of the analyte and the number of PBMCs in the obtained lysate.

HFS data was available from study 1 and was assessed weekly during the first treatment cycle and at the end (day 21) of each subsequent cycle. The severity of HFS was graded between 0 and 3, according to the Common Terminology Criteria for Adverse Events (CTCAE) version 4.03.

Intracellular pharmacokinetic model

Structural model

Sequential PK modelling was applied using a previously published population PK model describing capecitabine, dFCR, dFUR, 5-FU and FBAL.(11) The PK parameters from this model were fixed and used to predict individual capecitabine and metabolite concentrations while retaining the PK data in the database.(16) Effect compartment models and indirect response models were explored for the description of the intracellular FUTP concentrations.(17) The intermediate metabolites 5-fluorouridine 5'-monophosphate (FUMP) and 5-fluorouridine 5'-diphosphate (FUDP) were not detectable in the PBMC samples. Therefore, the predicted 5-FU concentrations in plasma were used to stimulate the production of intracellular FUTP concentrations. Linear, E_{max} and sigmoid E_{max} models were explored to describe the relationship between 5-FU and intracellular FUTP concentrations.

Stochastic model

Inter-individual variability (IIV) was evaluated for all parameters using an exponential model (equation 1):

$$P_i = P_{pop} \cdot exp\,(\eta_i) \qquad \text{(Eq. 1)}$$

where the typical population parameter estimate and the individual parameter estimate for individual *i* are represented by P_{pop} and P_i, respectively.

The IIV for subject individual *i* is represented by η_i, which was assumed to be normally distributed following $N\,(0,\ \omega^2)$. Residual unexplained variability in intracellular FUTP concentrations was described by a proportional error (equation 2):

$$C_{obs,ij} = C_{pred,ij} \cdot (1 + \varepsilon_{p,ij}) \qquad \text{(Eq. 2)}$$

where $C_{obs,ij}$ represents the observed concentration for individual *i* and observation *j*, $C_{pred,ij}$ represents the individual predicted concentration and $\varepsilon_{p,ij}$ represents the proportional error distributed following $N\,(0,\ \sigma^2)$.

HFS model

To model the ordered categorical HFS data, a continuous-time Markov transition model (CTMM) was applied.(18) CTCAE grade 0 and 1 were grouped into a single category as a result of the low frequency of grade 1 observed and the fact that dose adaptation are indicated from grade 2. This resulted in three different HFS grades (0/1, 2, 3). All patients started with HFS grade 0. Consequently, the initial probability for HFS grade 0/1 was set to 1 for all patients. Thereafter, the model was updated after each observation. To simplify the model, only transitions between neighbouring grades were considered in the analysis. Sequential modelling was used to relate the PK to HFS.(16)

The individual empirical Bayesian parameter estimates of plasma capecitabine, plasma metabolites and intracellular FUTP PK were fixed and used to derive model-based individual plasma and intracellular concentrations. A common drug effect was tested on each increasing transition rate (k_{01}, k_{12}, k_{23}). The drug effect was firstly introduced as a proportional direct effect by relating predicted concentration (C_p) to the transition rates. Secondly, an indirect effect was tested by using cumulative exposure (area under the concentration-time curve (AUC) instead of C_p as explanatory factors. Lastly, an effect compartment model including a first-order recovery rate (k_{rec}) was considered. Linear (i.e. proportional) and nonlinear (E_{max}) models were explored to describe the relation between plasma capecitabine, plasma 5-FU and intracellular FUTP concentrations and HFS.

To further assess the clinical impact of the established FUTP-HFS relationship, the final model for HFS was used to simulate the HFS grades for patients treated with the dose-levels that were investigated in study 1 (375/625 mg/m^2, 475/800 mg/m^2, 600/1000 mg/m^2, 750/1250 mg/m^2 and 950/1600 mg/m^2) continuously during 42 days. Doses were administered twice-daily at 09:00h in the morning and 24:00h in the evening. For each dose-level, individual FUTP concentrations and HFS grades were simulated for 1000 patients with a standardized body surface area of 1.75 m^2.

Model selection and evaluation

Discrimination between PK models was guided by physiological and scientific plausibility, general goodness-of-fit (GOF) plots, visual predictive checks (VPCs), precision of parameter estimates and change in objective function value (dOFV). A drop of ≥3.84, corresponding to a $P < 0.05$ (χ^2-distribution with 1 degree of freedom (df)), was considered a significant improvement of the fit for hierarchical nested models. The HFS models were evaluated by visual predictive checks (VPCs) by simulating 500 datasets and generating the 95% prediction intervals from these simulations. The observed proportion of patients with a certain HFS grade were compared with the simulated HFS grade over time. Additionally, predictive checks were performed by comparing the simulated and observed transitions between different HFS grade. Parameter precision was assessed by the sampling importance resampling (SIR) procedure.(19)

Software

Nonlinear mixed-effects modelling was performed using NONMEM® (version 7.3, ICON Development Solutions, Ellicott City, MD, USA) and Perl-speaks-NONMEM (PsN, version 4.4.8) with First-Order Conditional Estimation with interaction (FOCE-I) as estimation method for the PK model. For the HFS model, the Laplacian method was used. Pirana (version 2.9.7) was used for model interpretation and comparison.(20–22) R (version 3.4.3) was used for data management and graphical diagnostics.(23)

Results

Intracellular pharmacokinetic model

A total of 175 PBMC samples were obtained from 45 patients and included in the analysis. Graphical inspection of the intracellular FUTP concentration-time data showed higher concentrations at day 7 compared to the first week after start of treatment. The model that best described these data was found to be a one-compartment model with first-order elimination ($k_{e,FUTP}$) where the rate of influx into PBMCs was directly proportional to the 5-FU plasma concentration. (equation 3):

$$\frac{dC_{IC}}{dt} = k_{5-FU/FUTP} \cdot C_{5-FU} - k_{e,FUTP} \cdot C_{IC} \quad \text{(Eq. 3)}$$

Where C_{IC} represents the concentration in the intracellular FUTP compartment and $C_{5\text{-}FU}$ represents the 5-FU plasma concentration. The 5-FU plasma concentration was related to the intracellular FUTP concentration using a proportional model ($k_{5\text{-}FU/FUTP}$). Final parameter estimates are presented in Table 1. $K_{5\text{-}FU/FUTP}$ was 0.029 h^{-1}*fmol/million PBMCs/nM (95% confidence interval (CI) 0.028-0.149 h^{-1}*fmol/million PBMCs/nM) and $k_{e,FUTP}$ was 0.028 h^{-1} (95% CI 0.002-0.039 h^{-1}) which corresponds to a FUTP elimination half-life of 24 hours. IIV was identified for $k_{5\text{-}FU/FUTP}$ (66.0% (95% CI 53.1%-84.8%)) and could not be estimated for $k_{e,FUTP}$. The final model adequately predicted the FUTP concentrations over time, as shown by the GOF plots (Figure 1) and VPC (Figure 2). Figure 2 also shows that the increased concentrations in the second week of treatment are well predicted by the model.

Table 1. Population estimates for the final intracellular FUTP model

	Units	Estimate (95% CI[a])	IIV[b] (95% CI[a]) [Shr%]
Parameter			
$k_{5\text{-}FU/FUTP}$	h^{-1}*fmol/million PBMCs/nM	0.029 (0.028 – 0.149)	66.0 (53.1 – 84.8) [2%]
$k_{e,FUTP}$	h^{-1}	0.028 (0.022 – 0.039)	-
Residual variability			
Proportional	CV%	38.6 (34.6 – 44.9)	-

Abbreviations: CI, confidence interval; CV%, coefficient of variation; IIV, inter-individual variability
[a] 95% CI values were obtained from SIR. [b] IIV expressed as CV%.

HFS

HFS data were available only for the 24 patients that were included in study 1. In order to estimate the probability of observing each HFS grade at every observation, the HFS grades were modelled as differential equations including transition rates to- and from neighbouring grades (k_{01}, k_{10}, k_{12}, k_{21}).(18)

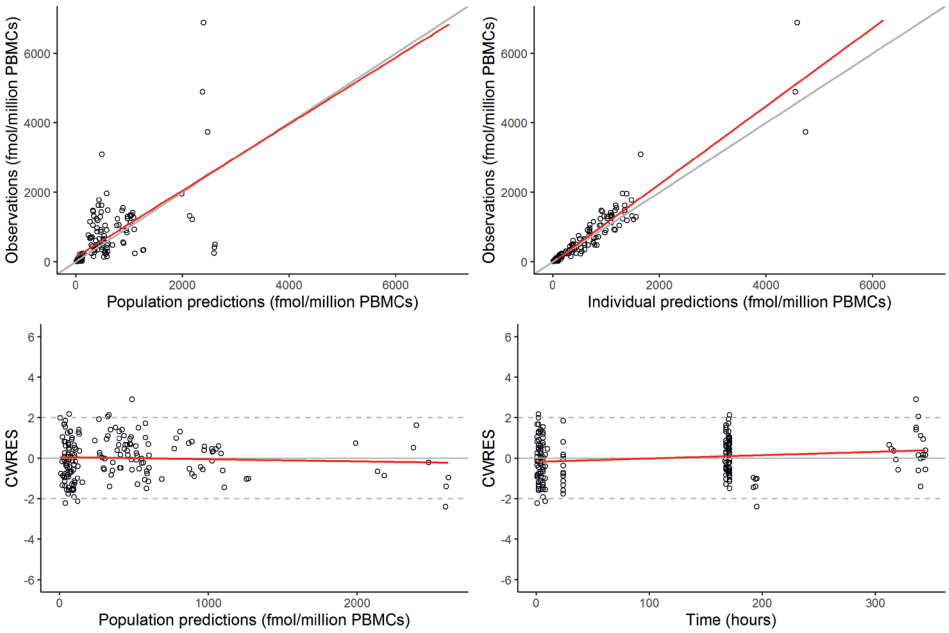

Figure 1. Goodness-of-fit plots of the final PK model for intracellular FUTP concentrations. Including individual and population predictions vs. observed values and conditional weighted residuals (CWRES) vs. time after dose and PRED.

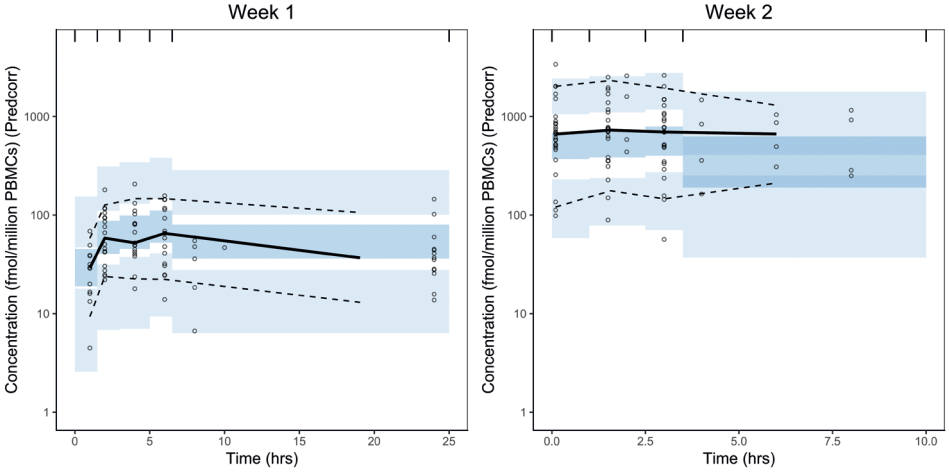

Figure 2. Prediction-corrected visual predictive check of the final pharmacokinetic model for FUTP stratified by week. Solid lines and darker blue areas represent the median observed values and simulated 95% CIs. Dashed lines and light blue areas represent the 5% and 95% percentiles of the observed values and the 95% CIs of the simulated percentiles (n = 500). *CIs, confidence intervals.*

When included univariately on the increasing transition rates, concentrations of capecitabine, 5-FU and FUTP all showed an improved fit of the model for HFS compared to the model without an effect of capecitabine administration included (dOFV = -8.30 for capecitabine, dOFV = -8.44 for 5-FU and dOFV = -13.4 for FUTP). The data was best described by a model including a direct effect of predicted FUTP concentrations. Representative individual model fits are depicted in Figure 3. An indirect effect using the AUC or by using an effect compartment did not significantly improve the model. Adequate parameter precision could be obtained as depicted in Table 2. The VPC for the final Markov model for HFS (Figure 4) showed that the percentage of patients experiencing HFS grades over time was well predicted by the model.

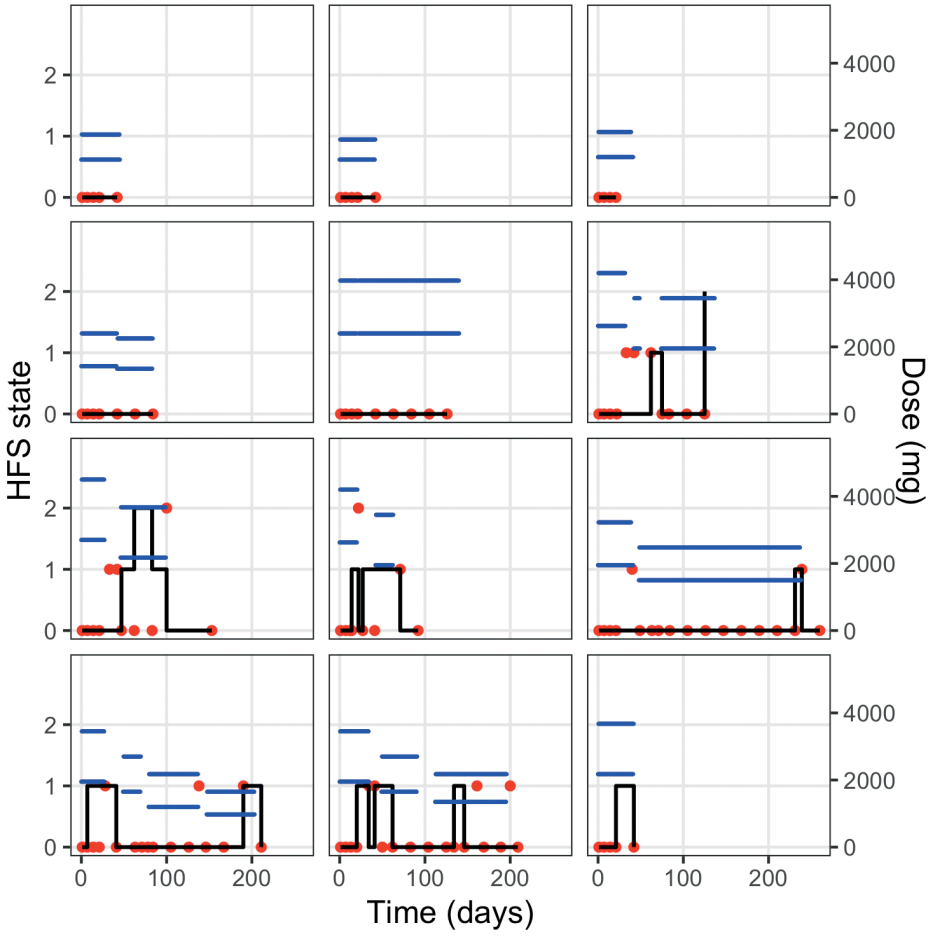

Figure 3. Hand-and-foot syndrome (HFS) grade versus time profiles for 12 representative individual patients. State 0 is HFS grade 0/1, state 1 is grade 2 and state 2 is grade 3. Red dots are the observed HFS grades, solid black lines are the simulations from the continuous-time Markov model and blue horizontal lines represent the administered capecitabine doses.

Table 2. Estimates for the final Markov model for HFS

	Units	Estimate (95% CI[a])
Parameter		
Transition rate from grade 0/1 to 2 (k_{01})	week^{-1}	$2.38x10^{-6}$ ($4.56x10^{-7}$ – $9.14x10^{-6}$)
Transition rate from grade 2 to 0/1 (k_{10})	week^{-1}	$4.08x10^{-5}$ ($2.10x10^{-5}$ – $8.03x10^{-5}$)
Transition rate from grade 2 to 3 (k_{12})	week^{-1}	$7.14x10^{-6}$ ($1.20x10^{-6}$ – $2.81x10^{-5}$)
Transition rate from grade 3 to 2 (k_{21})	week^{-1}	$1.11x10^{-4}$ ($2.71x10^{-5}$ – $3.70x10^{-4}$)
Direct effect FUTP (E_{FUTP})[b]	fmol/million PBMCs	0.0023 ($1.79 x10^{-4}$ – $1.33x10^{-2}$)

[a] 95% CI values were obtained from SIR. [b] Slope of the linear effect of predicted FUTP concentrations.

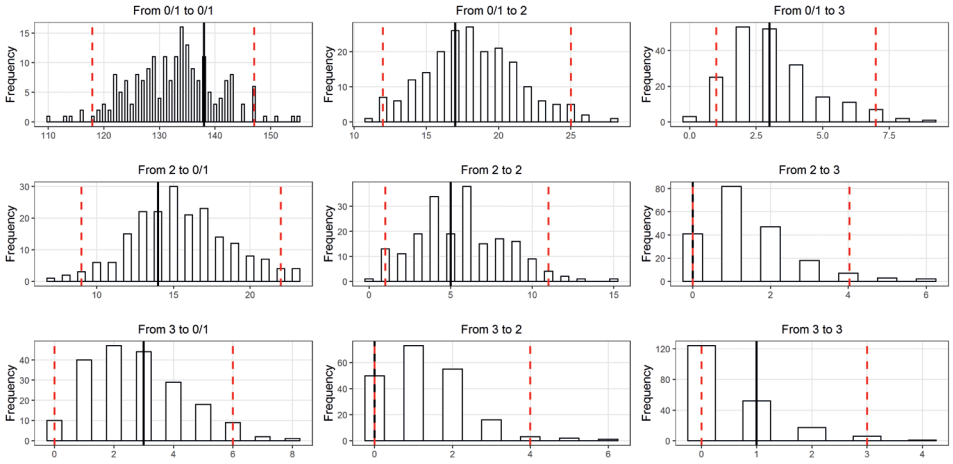

Figure 4. Visual predictive check of the Markov model for capecitabine-induced hand-and-foot syndrome (HFS) grades stratified by grade. The grey areas represent the 95% prediction intervals for the proportion of patients developing HFS and the solid lines represent the observed proportion of patients developing HFS (n=500).

Figure 5 shows the simulated and observed transitions for the final model. The 95% prediction intervals calculated from the simulated transitions adequately captured the observed number of transitions. Figure 6 shows the simulated proportions of clinically most relevant HFS grades (grade 2 and 3) on day 21 after start of continuous treatment with capecitabine for five different dosing regimens, without taking into account clinically indicated treatment interruptions or dose adjustments. The percentage of patients experiencing grade 2 or grade 3 increased with higher dose regimens. The percentage of patients increased by 70% from 8.8% to 12.8% for grade 2 and from 2% to 3.5% for grade 3 when comparing the 375/625 mg/m^2 and 950/1600 mg/m^2 dosing regimens. Nevertheless, grade 3 HFS was simulated for a small number of patients. This is roughly in line with the HFS observations from study 1, were grade 3 HFS was

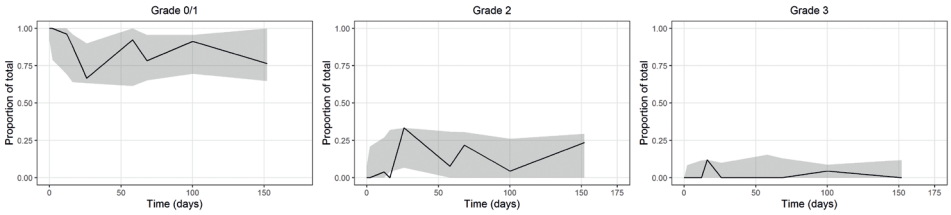

Figure 5. Predictive check of the grade transitions for the Markov model for capecitabine-induced hand-and-foot syndrome including the intracellular FUTP effect. The histograms show the distribution frequency of the transitions simulated by the model (n = 500), the dashed lines represent the 5th and 95th percentiles of the simulations and the solid line represents the observed number of transitions.

only observed at the highest dose-level (n=3, dose-level 950/1600 mg/m^2). The simulations additionally showed the delayed effect of FUTP on the development of HFS (supplemental Figure S1). The percentage of patients experiencing grade 2 or 3 HFS increased with time and seems to be on a plateau after day 21, in the absence of treatment interruptions or dose adjustments.

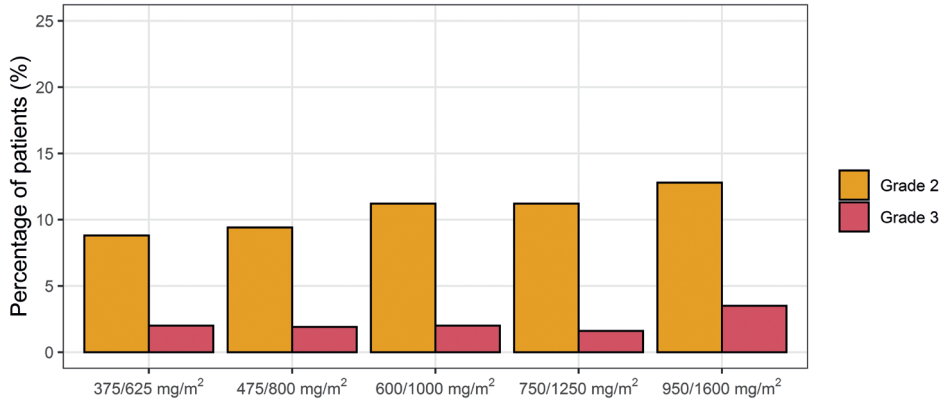

Figure 6. Simulated percentage of patients experiencing HFS grade 2 and 3 on day 21 after start of treatment with capecitabine for the dose-levels that were evaluated in study 1 (n=1000).

Discussion

A PK model that represents the FUTP concentrations in PBMCs of patients treated with capecitabine was successfully developed. The production of intracellular FUTP concentrations was described by a model where the plasma 5-FU concentrations drive the intracellular FUTP concentrations. FUTP elimination was characterized by a half-life of 24 hours.

In addition, a CTMM characterized the onset and grade of HFS. The collection of toxicity data in our study had a non-uniform frequency, with weekly observations during the first cycle followed by 3-weekly observations until the patient stopped treatment with capecitabine. The CTMM was thus used to describe the dynamics of HFS during treatment with capecitabine. The model-derived individual intracellular FUTP concentration was identified as best predictor of the development and grade of HFS in this patient population. Models describing HFS by including capecitabine and 5-FU plasma concentrations as predictor did not result in an improvement of the model fit compared to a model with intracellular FUTP concentrations as predictor. Simulations showed an increased percentage of patients experiencing clinically relevant HFS with higher dosing regimens (Grade 2 in 12.8% of patients dosed 950/1600 mg/m^2 compared to 8.8% of patients dosed 375/625 mg/m^2 and grade 3 in 3.5% of patients versus 2% of patients). Additionally, the cumulative effect of FUTP concentrations on the development of HFS was shown in the simulations. It should however be noted that a dose reduction or interruption would be applied when a patient experiences HFS in clinical practice, which was not included in our simulations. Previously, a model that describes the risk of developing HFS driven by plasma exposure to capecitabine has been developed.(9) However, this model was only informed by dosing history without actual PK data and did not investigate the effects of intracellular metabolites. HFS is most often observed after patients have been on capecitabine therapy for several days or weeks emphasizing the delayed nature of HFS. It has therefore been hypothesized that HFS is a result of accumulation of capecitabine metabolites. Our analysis supports this latter hypothesis as intracellular FUTP concentrations related strongly to HFS. Due to the long half-life of intracellular FUTP this metabolite shows accumulation during treatment, which also is in agreement with the observed cumulative nature of HFS.

The current analysis does harbour some limitations. Firstly, the intracellular concentrations that we used were measured in PBMCs and not in actual target tissue cells. Direct measurement of capecitabine and metabolite concentrations in skin samples might gain additional information for the here proposed model. However, this is impractical, highly invasive, and therefore very difficult to perform in patients experiencing HFS. In addition, intracellular concentrations of the intermediate metabolites FUMP and FUDP were not detectable and therefore not included in the model. However, given the extremely low concentrations of these metabolites compared to FUTP, the role of these metabolites in HFS is questionable.(2) Secondly, as a result of limited data we decided to combine grade 0 and grade 1 into one category. This was considered reasonable since dose reductions and delays are only clinically indicated at grade 2 or higher. Lastly, we could not identify additional covariates in either the PK or the Markov model because they were unavailable for the PK dataset. Hypothetically, covariates such as genetic predispositions, renal function and baseline characteristics could influence the development of HFS and therefore improve the here presented models.

Conclusion

The here proposed integrated PK-PD model shows that, during capecitabine treatment, intracellular FUTP concentrations accumulate over time and are associated with the development and severity of HFS, which strengthens the hypothesis that HFS is a result of intracellular FUTP accumulation. In addition, this is the first analysis that demonstrates a clinically relevant relationship between intracellular FUTP concentrations following clinically relevant capecitabine dose regimens and HFS. The developed model can be used for simulation purposes such as the evaluation of the effect of alternative capecitabine dosing strategies on the development of HFS and overall optimization of capecitabine treatment.

References

1. Reigner B, Blesch K, Weidekamm E. Clinical Pharmacokinetics of Capecitabine. Clin Pharmacokinet. 2001;40:85–104.

2. Derissen EJB, Jacobs BAW, Huitema ADR, Rosing H, Schellens JHM, Beijnen JH. Exploring the intracellular pharmacokinetics of the 5-fluorouracil nucleotides during capecitabine treatment. Br J Clin Pharmacol. 2016;81:949–57.

3. Longley DB, Harkin DP, Johnston PG. 5-Flourouracil: mechanisms of action and clinical strategies. Nat Rev Cancer. 2003;3:330–8.

4. Milano G, Mari M, Lassalle S, Formento J, Francoual M, Lacour J, et al. Candidate mechanisms for capecitabine-related hand-foot syndrome. Br J Clin Pharmacol. 2008;66:88–95.

5. Wilkes GM, Doyle D. Palmar-plantar erythrodysesthesia. Clin J Oncol Nurs. 2005;9:103–6.

6. Lin E, Morris JS, Ayers GD. Effect of celecoxib on capecitabine-induced hand-foot syndrome and antitumor activity. Oncology. 2002;16(12 Suppl No 14):31–7.

7. Kara IO, Sahin B, Erkisi M. Palmar-plantar erythrodysesthesia due to docetaxel-capecitabine therapy is treated with vitamin E without dose reduction. Breast. 2006;15:414–24.

8. Zhang RX, Wu XJ, Wan DS, Lu ZH, Kong LH, Pan ZZ, et al. Celecoxib can prevent capecitabine-related hand-foot syndrome in stage II and III colorectal cancer patients: Result of a single-center, prospective randomized phase III trial. Ann Oncol. 2012;23:1348–53.

9. Hénin E, You B, VanCutsem E, Hoff P, Cassidy J, Twelves C, et al. A Dynamic Model of Hand-and-Foot Syndrome in Patients Receiving Capecitabine. Clin Pharmacol Ther. 2009;85:418–25.

10. Gieschke R, Burger H, Reigner B, Blesch KS, Steimer J. Population pharmacokinetics and concentration – effect relationships of capecitabine metabolites in colorectal cancer patients. Br J Clin Pharmacol. 2002;55:252–63.

11. Jacobs BAW, Deenen MJ, Joerger M, Rosing H, de Vries N, Meulendijks D, et al. Pharmacokinetics of capecitabine and four metabolites in a heterogeneous population of cancer patients: a comprehensive analysis. CPT Pharmacometrics Syst Pharmacol. 2019; Epub ahead of print.

12. Deenen MJ, Meulendijks D, Boot H, Legdeur M-CJC, Beijnen JH, Schellens JHM, et al. Phase 1a/1b and pharmacogenetic study of docetaxel, oxaliplatin and capecitabine in patients with advanced cancer of the stomach or the gastroesophageal junction. Cancer Chemother Pharmacol. 2015;76:1285–95.

13. Jacobs BAW, Meulenaar J, Rosing H, Pluim D, Tibben MM, de Vries N, et al. A phase 0 clinical trial of novel candidate extended-release formulations of capecitabine. Cancer Chemother Pharmacol. 2016;77:1201–7.

14. Deenen MJ, Rosing H, Hillebrand MJ, Schellens JHM, Beijnen JH. Quantitative determination of capecitabine and its six metabolites in human plasma using liquid chromatography coupled to electrospray tandem mass spectrometry. J Chromatogr B Anal Technol Biomed Life Sci. 2013;913–914:30–40.

15. Derissen EJB, Hillebrand MJX, Rosing H, Schellens JHM, Beijnen JH. Development of an LC–MS/MS assay for the quantitative determination of the intracellular 5-fluorouracil nucleotides responsible for the anticancer effect of 5-fluorouracil. J Pharm Biomed Anal. 2015;110:58–66.

16. Zhang L, Beal SL, Sheiner LB. Simultaneous vs. Sequential Analysis for Population PK/PD Data I: Best-case Performance. J Pharmacokinet Pharmacodyn. 2003;30:387–404.

17. Upton RN, Mould DR. Basic concepts in population modeling, simulation, and model-based drug development: part 3-introduction to pharmacodynamic modeling methods. CPT pharmacometrics Syst Pharmacol. 2014;3:e88.

18. Schindler E, Karlsson MO. A Minimal Continuous-Time Markov Pharmacometric Model. AAPS J. 2017;19:1424–35.

19. Dosne A-G, Bergstrand M, Karlsson MO. An automated sampling importance resampling procedure for estimating parameter uncertainty. J Pharmacokinet Pharmacodyn. 2017;44:509–20.

20. Lindbom L, Ribbing J, Jonsson EN. Perl-speaks-NONMEM (PsN)—a Perl module for NONMEM related programming. Comput Methods Programs Biomed. 2004;75:85–94.

21. Boeckmann AJ, Beal SL, Sheiner LB. NONMEM User's Guide, Part V. Introductory Guide. NONMEM Proj Gr. 1998.

22. Keizer RJ, van Benten M, Beijnen JH, Schellens JHM, Huitema ADR. Pirana and PCluster: A modeling environment and cluster infrastructure for NONMEM. Comput Methods Programs Biomed. 2011;101:72–9.

23. RC Team (2009) R: a language and environment for statistical computing. R Foundation for Statistical Computing, Vienna.

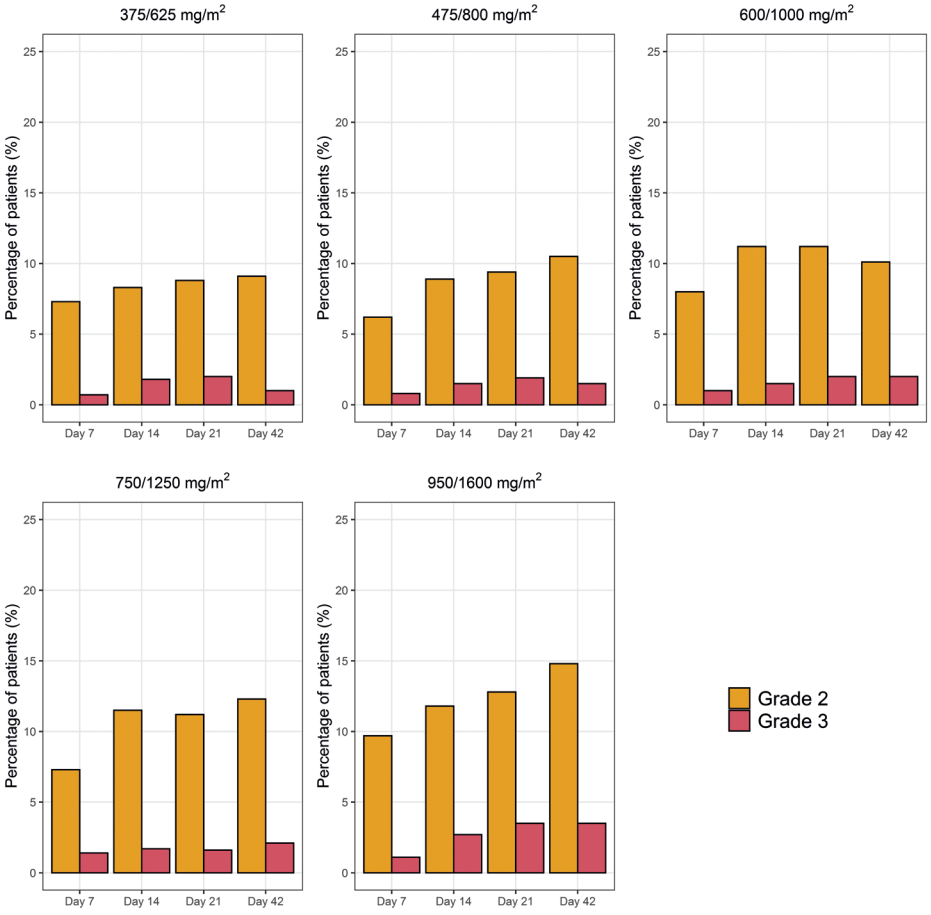

Figure S1. Simulated percentage of patients experiencing HFS grade 2 and 3 during the first 42 days of treatment with capecitabine for the dose-levels that were evaluated in study 1.



Chapter 3.2

Quantification of the pharmacokinetic-toxicodynamic relationship of oral docetaxel co-administered with ritonavir

Submitted

H. Yu
J.M. Janssen
V.A. de Weger
B. Nuijen
R.E. Stuurman
S. Marchetti
J.H.M. Schellens
J.H. Beijnen
T.P.C. Dorlo
A.D.R. Huitema

Abstract

Aims

Oral formulations of docetaxel have been successfully developed as an alternative for intravenous administration. By co-administration of oral docetaxel with the strong Cytochrome P450 3A4 enzyme inhibitor ritonavir the plasma exposure of docetaxel is boosted. In dose-escalation trials, the maximum tolerated doses for two different dosing regimens were established and dose-limiting toxicities (DLTs) were recorded. The aim of this study was to establish a pharmacokinetic (PK)-toxicodynamic (TOX) model to quantify the relationship between docetaxel exposure and DLT and to optimise the dose regimen of this combination treatment.

Methods

In total 85 patients were included in the current analysis, among which 18 patients showed a DLT in a four-week observation period. A PK-TOX model was developed and a simulation based on the PK-TOX model was performed.

Results

The final PK-TOX model consisted of an effect compartment representing harmful effect caused by docetaxel, which was linked to the probability of a DLT. The amount of docetaxel in the effect compartment was a significant predictor for DLT. Simulations of once-daily 60 mg and twice-daily 30 mg followed by 20 mg of oral docetaxel suggested that 14% and 34% of patients, respectively, would have a probability of > 25% to develop a DLT in a four-week period.

Conclusion

In conclusion, a PK-TOX model was successfully developed and this model can be used to evaluate the toxicity of different dose regimens of the combination of docetaxel and ritonavir and to predict tolerability of alternative dose regimens.

Introduction

Oral administration of docetaxel is currently in clinical development as a convenient alternative for intravenous administration.(1) A solid dispersion capsule formulation with improved dissolution characteristics compared to crystalline docetaxel, ModraDoc001 capsule, was initially developed followed by a further improved solid dispersion tablet formulation, ModraDoc006.(2–4) A major limitation for oral administration of docetaxel is its low bioavailability due to transport by P-glycoprotein (Pgp) and metabolism by Cytochrome P450 3A4 (CYP3A4).(5–7) In order to boost docetaxel exposure after oral administration, ritonavir is co-administered, which strongly boosts oral bioavailability of docetaxel by inhibiting CYP3A4.(8,9)

The ModraDoc capsules and tablets were studied in two dose-escalation trials with co-administration of ritonavir.(10,11) The maximum tolerated doses (MTDs) of ModraDoc006/r (r refers to a 100 mg ritonavir tablet) were explored. Similar to intravenous docetaxel, neutropenia and fatigue were seen as dose-limiting toxicities (DLTs), but the most frequently observed DLTs were gastrointestinal toxicities, such as diarrhoea, vomiting, nausea, and anorexia.(10–12)

Pharmacokinetic (PK)-pharmacodynamic (PD) modelling and simulation has proved to be an useful tool to study the PK-toxicodynamic (TOX) relationships.(13) PK-TOX models quantify the relationship between drug exposure and toxicity and can be used to further evaluate the dose regimen and predict toxicity of alternative dose regimes by simulation studies.(14,15)

The aims of the current study were: 1) to establish a PK-TOX model for oral docetaxel co-administered with ritonavir based on the accumulated data from the two finished phase I clinical trials performed; 2) to optimise the dosing schedules of ModraDoc/r formulations and to support clinical drug development.

Methods

Clinical studies

Docetaxel as ModraDoc capsules or tablets was given weekly once-daily or twice-daily in two phase I studies in a classical 3+3 dose escalating schema.(10,11) DLTs were evaluated over a four-week treatment period. In total, 85 patients were evaluable for DLT assessment, among which 50 patients received a weekly once-daily dose and 35 patients received a weekly twice-daily dose. The studies were approved by institutional review boards and independent ethics committees, and were carried out in accordance with the ethical principles of the Declaration of Helsinki. Informed consent was obtained from all individual patients participating in the studies. In total, 18 (21.2%) patients developed a DLT within the first four weeks of treatment (DLT period), of which 11

patients showed a DLT by the second week. Detailed information on the number of patients and DLTs included in the current analysis is shown in Table 1.

Table 1. Overview of the information on the dose levels and dose-limiting toxicity included in the model development

	Once-daily dosing[a]		Twice-daily dosing[b]	
	ModraDoc001 capsule	**ModraDoc006 tablet**	**ModraDoc001 capsule**	**ModraDoc006 tablet**
ModraDoc dose levels (mg/day)	40, 60, 80	60, 80	40, 60, 80	40, 50, 60
Ritonavir dose levels (mg/day)	100	100	200	100, 200
Number of patients				
Total	37	13	17	18
Dose-limiting toxicity	9		9	
Dose-limiting toxicity at week 1	1		1	
Dose-limiting toxicity at week 2	5		4	
Dose-limiting toxicity at week 3	2		2	
Dose-limiting toxicity at week 4	1		2	

[a] (11) [b] (10)

Model development

Sequential modelling of PK and TOX was used to establish the full PK-TOX model.(16) Firstly, an integrated PK model of oral docetaxel and ritonavir was used in this analysis. (17) The individual parameter estimates of docetaxel and ritonavir were generated from the PK model and used as input in the subsequent PK-TOX modelling.

The probability of the occurrence of DLTs was estimated by logistic regression. Several measures for drug exposure, such as dose, area under plasma concentration-time curve (AUC) and cumulative AUC in both the central and gastrointestinal compartment originating from the population PK model, were considered in the logistic regression model. An effect compartment model relating drug exposure to the probability of DLT was also considered.

Model evaluation

The models were required to reach successful minimisation with plausible and precise parameter estimates. For hierarchical models, the significant level in the difference of objective function values (dOFV) was defined as $p < 0.01$ (degree of freedom = 1, dOFV = -6.6).

Simulations

In the simulation study the following outcome measures were studied: 1) the simulated probability of DLT was compared to the observed incidence; 2) the time course of the

probability of DLT was investigated for both once-daily and twice-daily regimens; 3) the differences in the probability of DLT were shown between once-daily and twice-daily regimens.

Simulations of the probability of DLT were performed based on the PK-TOX model in 1,000 patients at each dose regimen for four weeks. For all simulations the ModraDoc006 tablet was used as the formulation, since this formulation will be used in further clinical trials. The simulated doses included: weekly once-daily 60 mg and 80 mg; weekly twice-daily 20 mg (20/20 mg), 30 mg followed by 20 mg (30/20 mg), and 30 mg (30/30 mg). A 100 mg ritonavir tablet was co-administered at each drug intake. The commonly defined MTD in rule-based designs of dose-escalation studies is the dose at which the probability of DLT is < 33%. Therefore, this value was used as a cut-off value in the simulations as comparison with the observed incidences of DLT. In addition, in model-based designs of dose-escalation studies, a pre-defined target toxicity rate was mostly set between 10–33%.(18) Accordingly, a target probability for a DLT was chosen as the probability of DLT incidence of 25% when further evaluating the recommended phase II dose.

Software
Model estimations and simulations were performed using NONMEM (version 7.3.0, ICON Development Solutions, Ellicott City, MD, USA) together with a gfortran compiler with Piraña used as graphical interface.(19,20) The model estimation used second-order conditional (Laplacian) estimation method. R (version 3.0.3) was used for pre-processing of the data, plotting and calculating the significance of DLT predictor.(21)

Results

Model development

In total, 16 DLTs were observed, of which most were gastro-intestinal related DLTs (nausea, diarrhoea, vomiting and mucositis). The final PK-TOX model that described the occurrence of DLTs in patients treated with ModraDoc/r is shown in Figure 1. The parameter estimates are listed in Table 2.

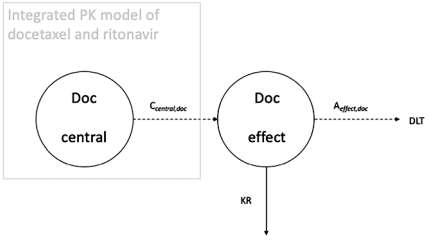

Figure 1. Schematic representation of the pharmacokinetic-toxicodynamic model for oral docetaxel.

Table 2. Parameter estimates of pharmacokinetic-toxicodynamic model of oral docetaxel co-administered with ritonavir

	Units	Estimate	RSE (%)
Recovery rate constant (KR)	day^{-1}	0.21	39
Intercept (B_0)	-	-15.8	23
Slope (B_1)	-	2.42	22

Abbreviations: RSE, relative standard error.

The cumulative AUC of docetaxel was not a significant predictor of the probability of DLT. It overpredicted the probability of DLT in weeks 3 and 4 of the DLT period. Therefore, an effect compartment representing harmful effect was introduced. The input of the effect compartment was the concentration of docetaxel in the central compartment, the output was modelled as a first order recovery rate. Subsequently, the log-transformed docetaxel amount in the effect compartment ($A_{effect,doc}$) was related to the probability of DLT. $A_{effect,doc}$ was a significant predictor of the probability of DLT ($p < 0.01$). Compared to the model using the cumulative AUC as a predictor for DLT, the final model showed a strongly improved fit (dOFV of -10.6 points). Introduction of inter-individual variability (IIV) did not improve model fit and was thus not included in the model. The differential equation of the effect compartment and the logistic regression function are shown in Eq. 1–3.

$$\frac{dA_{effect,doc}}{dt} = C_{central,doc} - KR \cdot A_{effect,doc} \quad \text{(Eq. 1)}$$

$$t = B_0 + B_1 \cdot \log(A_{effect,doc}) \quad \text{(Eq. 2)}$$

$$\Pr = \frac{\exp(t)}{1+\exp(t)} \quad \text{(Eq. 3)}$$

Where $A_{effect,doc}$ represents the amount of the docetaxel in the effect compartment, $C_{central,doc}$ represents the concentration of docetaxel in the central compartment, *KR* represents the recovery rate of the effect compartment, *t* is a linear function of log-transformed $A_{effect,doc,}$ with B_0 and B_1 as intercept and slope, respectively, Pr is the logistic function representing the probability of DLT.

The *KR* was estimated as 0.21 day^{-1} (RSE 39%), translating into a recovery half-life of 3.3 days. Based on the estimated B_0 and B_1 (Table 2), the $A_{effect,doc}$ when Pr is 50%, 33% and 25%, respectively, was calculated as 685 µg·h/L, 511 µg·h/L and 435 µg·h/L. Figure 2 shows the predicted Pr curve with corresponding $A_{effect,doc}$. It can be seen that 98% of patients without DLT, and 81% patients with DLT in four weeks have a Pr < 33%; 96% of patients without DLT, and 69% patients with DLT have a Pr < 25%. The final model was successfully minimised. The parameter estimates of the final PK-TOX model showed acceptable precision (RSE < 40%, Table 2).

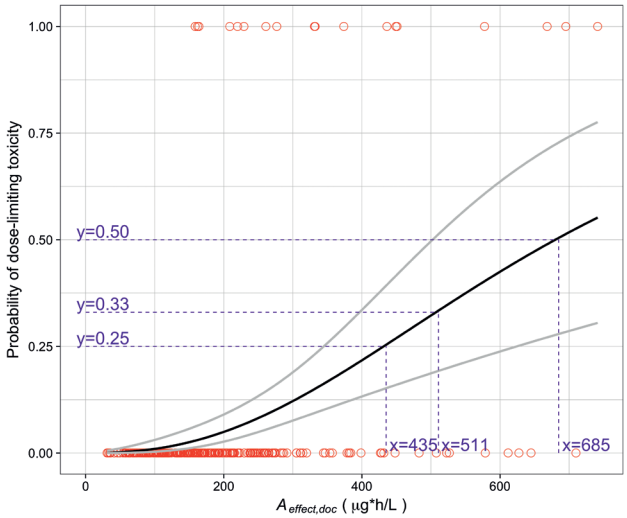

Figure 2. Probability of dose-limiting toxicity predicted by the amount in the effect compartment of docetaxel. $A_{effect,doc}$, amount in the effect compartment of docetaxel. The solid black curve represents the probability of dose-limiting toxicity (DLT) predicted by $A_{effect,doc}$; the solid grey lines represent the 95% confidence interval; the empty circles present the observed DLT events corresponding to $A_{effect,doc}$; the dashed lines show the $A_{effect,doc}$ when the probability is predicted at 0.25, 0.33, and 0.5, respectively.

Simulations

Figure 3 shows the model simulated Pr with a cut-off of 33% versus the observed DLT incidence in patients treated with the ModraDoc006 tablet. At weekly once-daily 60 mg of docetaxel, 10% of patients in the simulation showed Pr > 33%, and one DLT was observed in 11 patients (1/11); at once-daily 80 mg, 19% in the simulation had a Pr > 33% while two DLTs out of four patients (2/4) were observed. For 20/20 mg weekly twice-daily, 18% of patients had a Pr > 33% while zero out of three (0/3) was observed; for 30/20 mg, the Pr increased to 27%, with one out of nine patients (1/9) developed DLT; for 30/30 mg, Pr further increased to 37%, and two out of six patients (2/6) showed a DLT.

In order to visualise the change of the $A_{effect,doc}$ over time, Figure 4 shows the median and 10%–90% percentile of simulated $A_{effect,doc}$ for weekly once-daily 60 mg and weekly twice-daily 30/20 mg doses for a period of four weeks. In both dose regimens, the $A_{effect,doc}$ increased within the first two weeks, afterwards steady-state was almost reached (further accumulation in $A_{effect,doc}$ was 3% and 5% for once-daily dose and twice-daily dose, respectively). By week 4, the median of $A_{effect,doc}$ for twice-daily dose was 53% higher than for once-daily dose, which translated into a higher Pr for this regimen. In the twice-daily dosing regimen, ritonavir was also dosed twice-daily instead of once-daily. This resulted in higher docetaxel plasma concentrations, and higher $A_{effect,doc}$ despite the slightly lower total daily dose.

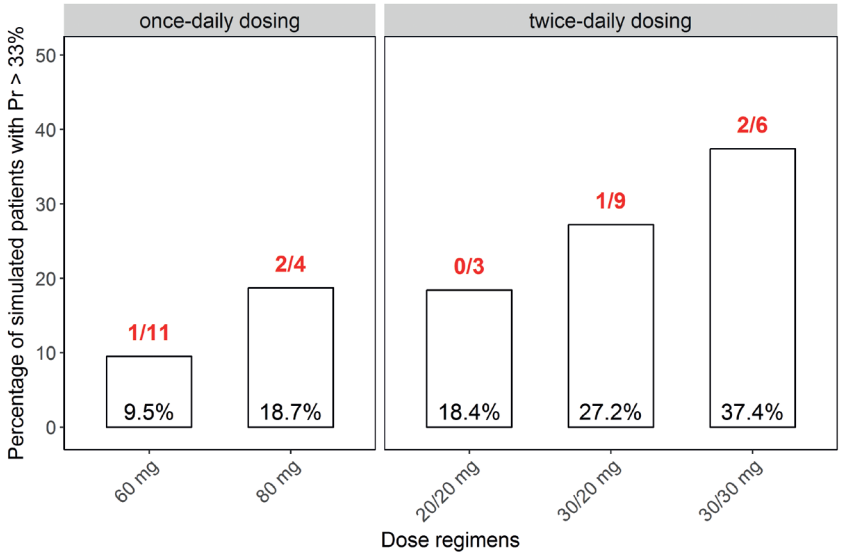

Figure 3. Percentage of simulated patients with > 33% of probability of dose-limiting toxicity at different ModraDoc006/r (100 mg ritonavir with every ModraDoc006 administration) dose regimens and the observed incidence of dose-limiting toxicity. Pr, probability of dose-limiting toxicity. The bars and the numbers inside the bars show the percentage of simulated patients with Pr > 33% at different dose regimens; the numbers above the bars indicate the observed number of patients with dose-limiting toxicity out of the total evaluable patients treated at that dose.

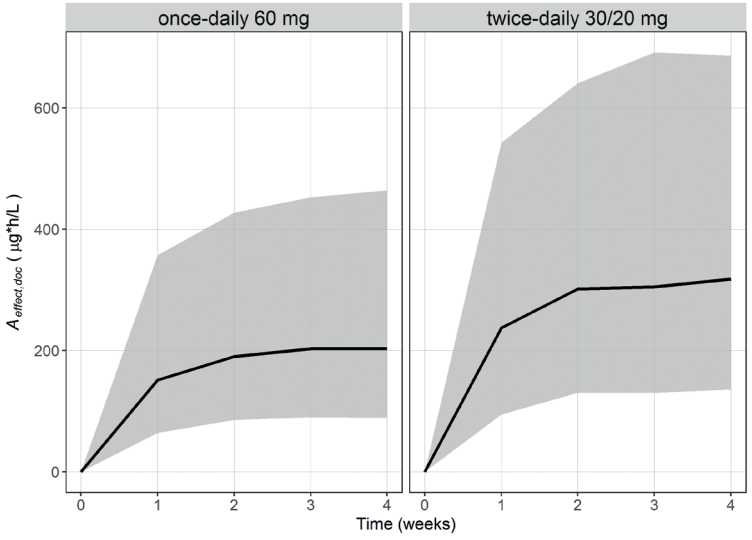

Figure 4. Simulated amount in the effect compartment of docetaxel over four weeks at weekly once-daily and weekly twice-daily dose regimens (n = 1,000). $A_{effect,doc}$, amount in the effect compartment of docetaxel. The solid curve represents the simulated median of $A_{effect,doc}$ over time; the grey areas show the simulated $A_{effect,doc}$ between 10% and 90% percentiles.

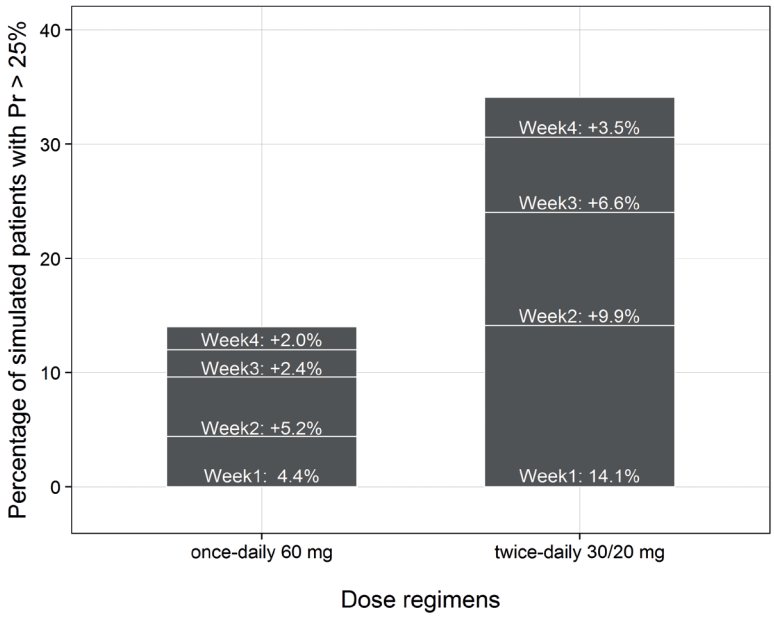

Figure 5. Cumulative percentage of simulated patients with > 25% of probability of dose-limiting toxicity at each treatment week with once-daily and twice-daily dose regimens (n = 1,000). Pr, probability of dose-limiting toxicity. This figure shows the cumulative percentage of patients with Pr > 25%. The increment of patients at each week was indicated. In total, 14% of patients receiving once-daily 60 mg, and 34.1% of patients receiving twice-daily 30/20 mg of docetaxel with Pr > 25%.

Quantitatively, Figure 5 shows the cumulative percentage of patients with the target of Pr of 25% at each week for once-daily 60 mg and twice-daily 30/20 mg doses. The newly occurred incidence of DLTs lowered gradually over treatment time. The majority of DLTs, 67% for 60 mg and 73% for 30/20 mg, developed within the first two weeks. This was supported by the dynamic change in $A_{effect,doc}$ over the treatment period.

Discussion

A PK-TOX model relating the docetaxel exposure to the probability of DLT was developed. This model was developed on data from two dose-escalation trials in which at each dose level only a few patients were evaluated. Furthermore, docetaxel PK shows wide inter-patient variability.(17) These two issues challenge dose finding of oral docetaxel. The currently developed model enables the *in silico* evaluation of the different dose levels tested. Furthermore, alternative dosing regimens can be evaluated and toxicity predicted, albeit that extrapolations outside the conditions on which the model was developed should be performed with caution.

The $A_{effect,doc}$ proved to predict the probability of DLT better than cumulative AUC in plasma, cumulative dose and local exposure in the gastrointestinal tract. In Figure 4, it can be seen that the amount in the effect compartment, representing hypothetical harmful effect, reached steady-state at approximately week 2 after start of treatment and accordingly the probability of DLT reached steady-state at the same time. This is in agreement with the clinical observation that 70% of DLTs occurred within the first two weeks. The recovery half-life of DLT was estimated at 3.3 days, with relative good precision given the limited dataset.

The simulations with the PK-TOX model supported the MTDs found in dose-escalation trials. Among the evaluated dose regimens, the MTDs of interest of ModraDoc006/r for the weekly once-daily dose is 60 mg, and for the twice-daily dose is 30/20 mg (both regimens in combination with 100 mg ritonavir). For once-daily dose regimens, the model simulation agreed with the percentage of DLTs that have occurred at 60 mg (9.5% vs. 1/11) but suggested much lower incidences of DLTs at 80 mg (19% vs. 2/4), which is lower than the model predicted Pr at the 30/20 mg twice daily regimen. For twice-daily dose regimens, the simulation supported the findings in 20/20 mg (18% vs. 0/3) and 30/30 mg (37% vs. 2/6), while indicated a slightly higher incidence of DLTs at 30/20 mg (27% vs. 1/9). However, this comparison should be interpreted with caution due to the low number of patients on the different dose levels.

Conclusion

A PK-TOX model was built for the prediction of the probability of DLT in oral docetaxel co-administered with ritonavir. The simulation of the PK-TOX model suggested that the model adequately predicts the DLTs that were observed in the phase I trials. Therefore, this model is suitable to be used to predict the toxicity of dosing regimens for future phase II trials.

References

1. Jibodh RA, Lagas JS, Nuijen B, Beijnen JH, Schellens JHM. Taxanes: Old drugs, new oral formulations. Eur J Pharmacol. 2013;717:40–6.

2. Moes JJ, Stuurman FE, Hendrikx JJMA, Marchetti S, Huitema ADR, Beijnen JH, et al. Pharmacokinetic evaluation of three oral formulations of docetaxel boosted with ritonavir: Two single-drug formulations vs. a fixed-dose combination tablet. Drug Deliv Transl Res. 2013;3:243–51.

3. Moes JJ, Koolen SLW, Huitema ADR, Schellens JHM, Beijnen JH, Nuijen B. Pharmaceutical development and preliminary clinical testing of an oral solid dispersion formulation of docetaxel (ModraDoc001). Int J Pharm. 2011;420:244–50.

4. Sawicki E, Beijnen JH, Schellens JHM, Nuijen B. Pharmaceutical development of an oral tablet formulation containing a spray dried amorphous solid dispersion of docetaxel or paclitaxel. Int J Pharm. 2016;511:765–73.

5. Koolen SLW, Beijnen JH, Schellens JHM. Intravenous-to-oral switch in anticancer chemotherapy: a focus on docetaxel and paclitaxel. Clin Pharmacol Ther. 2010;87:126–9.

6. Schellens JH, Malingré MM, Kruijtzer CM, Bardelmeijer HA, van Tellingen O, Schinkel AH, et al. Modulation of oral bioavailability of anticancer drugs: from mouse to man. Eur J Pharm Sci. 2000;12:103–10.

7. TAXOTERE 20 mg/0.5 ml concentrate and solvent for solution for infusion. Summary of product characteristics.

8. Oostendorp RL, Huitema A, Rosing H, Jansen RS, Heine R Ter, Keessen M, et al. Coadministration of ritonavir strongly enhances the apparent oral bioavailability of docetaxel in patients with solid tumors. Clin Cancer Res. 2009;15:4228–33.

9. Bardelmeijer HA, Ouwehand M, Buckle T, Huisman MT, Schellens JHM, Beijnen JH, et al. Low systemic exposure of oral docetaxel in mice resulting from extensive first-pass metabolism is boosted by ritonavir. Cancer Res. 2002;62:6158–64.

10. de Weger VA, Stuurman FE, Hendrikx JJMA, Moes JJ, Sawicki E, Huitema ADR, et al. A dose-escalation study of bi-daily once weekly oral docetaxel either as ModraDoc001 or ModraDoc006 combined with ritonavir. Eur J Cancer. 2017;86:217–25.

11. de Weger VA, Stuurman FE, Koolen SL, Moes JJ, Hendrikx JJMA, Sawicki E, et al. A phase I dose escalation study of once weekly oral administration of docetaxel as ModraDoc001 capsule or ModraDoc006 tablet in combination with ritonavir. Clin Cancer Res. 2019;25:5466-5474.

12. Ho M, Mackey J. Presentation and management of docetaxel-related adverse effects in patients with breast cancer. Cancer Manag Res. 2014;6:253.

13. de Vries Schultink AHM, Suleiman AA, Schellens JHM, Beijnen JH, Huitema ADR. Pharmacodynamic modeling of adverse effects of anti-cancer drug treatment. Eur J Clin Pharmacol. 2016;72:645–53.

14. van Hasselt JGC, Gupta A, Hussein Z, Beijnen JH, Schellens JHM, Huitema ADR. Population pharmacokinetic-pharmacodynamic analysis for eribulin mesilate-associated neutropenia. Br J Clin Pharmacol. 2013;76:412–24.

15. Zandvliet AS, Schellens JHM, Beijnen JH, Huitema ADR. Population pharmacokinetics and pharmacodynamics for treatment optimization in clinical oncology. Clin Pharmacokinet. 2008;47:487–513.

16. Zhang L, Beal SL, Sheiner LB. Simultaneous vs. sequential analysis for population PK/PD data I: best-case performance. J Pharmacokinet Pharmacodyn. 2003 Dec;30:387–404.

17. Yu H, Janssen JM, Sawicki E, Hasselt JGC, Weger VA, Nuijen B, et al. A Population Pharmacokinetic Model of Oral Docetaxel Coadministered With Ritonavir to Support Early Clinical Development. J Clin Pharmacol. 2019; Epub ahead of print.

18. van Brummelen EMJ, Huitema ADR, van Werkhoven E, Beijnen JH, Schellens JHM. The performance of model-based versus rule-based phase I clinical trials in oncology: A quantitative comparison of the performance of model-based versus rule-based phase I trials with molecularly targeted anticancer drugs over the last 2 years. J Pharmacokinet Pharmacodyn. 2016;43:1–8.

19. Keizer RJ, van Benten M, Beijnen JH, Schellens JHM, Huitema ADR. Pirana and PCluster: A modeling environment and cluster infrastructure for NONMEM. Comput Methods Programs Biomed. 2011;101:72–9.

20. Beal SL, Boeckman AJ, Sheiner LB. NONMEM user guides. San Francisco, CA; 1988.

21. Development Core Team R. R: A Language and Environment for Statistical Computing. Vienna, Austria: R Foundation for Statistical Computing; 2008.



Chapter 3.3

Longitudinal nonlinear mixed effects modelling of EGFR mutations in circulating tumour DNA as predictor of disease progression in treatment of EGFR-mutant non-small cell lung cancer

Manuscript in preparation

J.M. Janssen
R.B. Verheijen
T.T. van Duijl
M.M. van den Heuvel
J.H. Beijnen
N. Steeghs
D. van den Broek
A.D.R. Huitema
T.P.C. Dorlo

Abstract

Introduction

In 5-20% of patients with non-small cell lung cancer (NSCLC) mutations in the epidermal growth factor receptor (EGFR) gene are present, such as the L858R point mutation on exon 21 (L858R) and deletions on exon 19 (exon19del). The resistance point mutation on exon 20 (T790M) additionally occurs in approximately 50% of patients treated with anti-EGFR therapy. Correlations between increasing concentrations of circulating tumour DNA containing these mutations (ctDNA) in human plasma and progression of disease have been shown, suggesting that longitudinally collected ctDNA can be used to guide treatment decision making. However, the analysis of heterogeneous longitudinally collected data is challenging. A non-linear mixed effects model to describe the dynamics of EGFR ctDNA data in combination with a parametric survival model was developed to evaluate the ability of these modelling techniques to describe ctDNA data.

Methods

Repeated ctDNA measurements on L858R, exon19del and T790M mutants were available from 54 patients with EGFR mutated NSCLC treated with erlotinib or gefitinib. Different dynamic models were tested to describe the longitudinal ctDNA concentrations of the driver and resistance mutations. Subsequently, a parametric time-to-event model for progression free survival was developed. Predicted L858R, exon19del and T790M concentrations were used to evaluate their value as predictor for progression of disease.

Results

The ctDNA dynamics were best described by a model consisting of a zero-order increase and first-order elimination (19.7 /day (95% confidence interval (CI)14.9 – 23.6 /day)) of ctDNA concentrations. In addition, time-dependent development of resistance ($5.0x10^{-4}$ (95%CI $2.0x10^{-4}$ - $7.0x10^{-4}$ /day) was included in the final model. Relative change in L858R and exon19del concentrations from baseline was identified as most significant predictor of disease progression ($p = 0.001$.

Conclusion

The dynamic model for L858R, exon19del and T790M concentrations in ctDNA and time-to-event model adequately described the observed concentrations and progression-free-survival data in our clinical cohort. In addition, it was shown that nonlinear mixed effects modelling is a valuable method for the analysis of longitudinal and heterogeneous biomarker datasets obtained from clinical practice and provides a framework for prediction of progression based on observed ctDNA concentrations.

Introduction

Over the past two decades, new targeted therapies have been introduced in the treatment of several types of cancer. The pharmacology of these drugs is characterized by targeting specific biological processes that have been related to tumour development. As a result, new approaches to identify and to quantify the response to these drugs are needed. The identification of drug-specific biomarkers can provide guidance in monitoring the response to treatment and can enable individualization of therapy, both based on the change in biomarker levels. To this end, mutation analysis in liquid biopsies has gained interest. These patient friendly methods are being used to determine the genotype of tumours in human blood or plasma. These methods allow for a less invasive way of taking repeated measurements compared to the traditional method in which a biopsy from the tumour is obtained. This may facilitate the determination of the quantitative change in biomarker response.(1,2) During treatment, selected drug-specific genes can be quantified and monitored to predict either response or progression of the tumour.

It has been shown that 5-20% of patients with non-small cell lung cancer (NSCLC) present with activating mutations in the epidermal growth factor receptor (EGFR) gene.(3,4) Of these mutations, the L858R point mutation on exon 21 (L858R) and deletions on exon 19 (exon19del) of the EGFR gene are the most common.(5,6) Erlotinib and gefitinib are orally available tyrosine kinase inhibitors (TKI) targeting these EGFR mutations. Both TKIs are ATP competitors at the ATP-binding pocket in the intracellular kinase domain of EGFR and it has been shown that mutant kinases are more sensitive to inhibition by erlotinib and gefitinib. Significant improvements in progression free survival (PFS) and overall survival (OS) have been shown in patients that were treated with either erlotinib or gefitinib. However, after an initial response, the tumour is likely to acquire resistance mechanisms, resulting in relapse of the disease.(7,8) Resistance to EGFR inhibitors in NSCLC has been related to the development of a point mutation on exon 20 (T790M) in approximately 50% of patients.(9–11) Several studies have shown correlations between increasing concentrations of EGFR mutants (L858R, exon19del and T790M) that were measured by droplet digital polymer chain reaction (ddPCR) and progression of disease during treatment with erlotinib or gefitinib.(2,12–14) Also, low concentrations of these mutants have been observed during response to treatment.(1,15) In addition, we previously reported on the dynamics of the L858R, exon19del and T790 mutations in a NSCLC cohort and showed that an increase in EGFR driver mutations may predict clinical progression.(16) However, a significant relationship between the increase in EGFR driver mutation and time to progression could not be identified in this cohort.

The analysis of heterogenous longitudinal data collected in clinical practice is highly challenging. Conventional statistical techniques are impractical since most of these

require homogenous sampling. Therefore, more sophisticated techniques are required. The use of nonlinear mixed-effects modelling enables the analysis of longitudinal and heterogeneous datasets as has extensively been described in the field of pharmacokinetics and pharmacodynamics.(17) In this study, the application of these modelling techniques to ctDNA biomarker and survival data was explored.

Methods

Patients, study design and data

Data was available from an observational study that was performed in the outpatient clinic of the Netherlands Cancer Institute, Amsterdam, The Netherlands. In this study, ctDNA from patients with NSCLC who received erlotinib or gefitinib as first-line therapy was analysed in surplus plasma samples. Plasma samples were collected at random time points during treatment during routine hospital visits into EDTA tubes and stored at (at least) -20°C until DNA isolation. In addition, erlotinib and/or gefitinib dosing information, plasma sampling time and date and PFS details were collected retrospectively from medical records. The period from first dosage of erlotinib or gefitinib to the date of disease progression, based on CT, was defined as PFS. For this retrospective observational study no informed consent was required in accordance with code of conduct for responsible use of human tissue and medical research.(18)
Cell-free DNA was isolated from 1 mL plasma for mutation analysis. The EGFR mutations L858R, exon19del and T790M were a priori selected and hence quantified in purified DNA using ddPCR assays.(19) Quantification of the ddPCR results was based on the quantity of positive droplets for mutation and wildtype, double positive droplets and total accepted droplets in the assay. Allele concentrations were calculated by using the initial plasma sample volume from which the ctDNA was obtained and presented as copies per mL plasma.

ctDNA model development

Different dynamic models, such as baseline, turnover and first-order growth models, were tested to describe the longitudinal data of ctDNA concentrations of L858R, exon19del and T790M.(20) Initially, models for the three mutations were developed separately. In order to explore correlations between the mutations, the final model was a joint model including the complete dataset. Treatment with erlotinib or gefitinib was tested as a binary covariate in the final ctDNA model. We also used previously developed population pharmacokinetic (PK) models to derive individual parameter estimates, as only dosing information was available for our patient population. These individual PK parameters were used to predict individual concentration-time profiles of erlotinib or gefitinib.(21,22) ctDNA concentrations were related to individual drug exposure, dose and cumulative dose, to explore exposure-response relationships. Linear, E_{max} and sigmoid E_{max} relationships were investigated.

Inter-individual variability (IIV) was evaluated for all parameters using an exponential error model (equation 1):

$$P_i = P_{pop} \cdot exp\,(\eta_i) \quad \text{(Eq. 1)}$$

where the typical population parameter estimate and the individual parameter estimate for individual i are represented by P_{pop} and P_i, respectively.

The IIV for subject individual i is represented by η_i, which was assumed to be normally distributed following N (0, ω^2). Residual unexplained variability was described by a proportional error (equation 2):

$$C_{obs,ij} = C_{pred,ij} \cdot (1 + \varepsilon_{p,ij}) \quad \text{(Eq. 2)}$$

where $C_{obs,ij}$ represents the observed concentration for individual i and observation j, $C_{pred,ij}$ represents the individual predicted concentration and $\varepsilon_{p,ij}$ represents the proportional error distributed following N (0, σ^2). Separate residual unexplained variability was estimated for exon19del concentrations and for L858R and T790M concentrations combined, in order to account for the different ddPCR methods that were used.

Survival model

To investigate the relationship between ctDNA concentrations and disease progression, a parametric time-to-event model was developed. First, the exponential, Gompertz and Weibull hazard functions were explored. From the final developed ctDNA model, individual ctDNA concentrations for the driver and T790M resistance mutations were predicted until the recorded time of progression/censoring. These predicted concentrations were then used to evaluate their value as predictors for disease progression. Absolute concentrations and relative change from baseline over time were tested for significance and biological plausibility. Harbouring the exon19del or L858R mutation and treatment with erlotinib or gefitinib were tested as covariates in the survival model.

Model evaluation

Discrimination between models was guided by physiological and scientific plausibility, general goodness-of-fit (GOF) plots, precision of parameter estimates and change in objective function value (dOFV). A drop of ≥3.84, corresponding to a $P < 0.05$ (χ^2-distribution with 1 degree of freedom (df)), was considered a significant improvement of the fit for hierarchical nested models. Kaplan-Meier plots were generated to evaluate the survival model. Prediction intervals were derived from 500 simulations and visually compared to the observed data. Parameter precision was assessed by the sampling importance resampling (SIR) procedure.(23)

Software

Nonlinear mixed-effects modelling was performed using NONMEM® (version 7.3, ICON Development Solutions, Ellicott City, MD, USA) and Perl-speaks-NONMEM (PsN, version 4.4.8) with First-Order Conditional Estimation with interaction (FOCE-I) as estimation method for the ctDNA model. For the survival model, the Laplacian estimation method was used. Pirana (version 2.9.7) was used to compare and interpret model output. (24–26) R (version 3.4.3) was used for data management and graphical diagnostics.(27)

Results

Patients and data

In total, 198 samples from 54 patients with NSCLC were available for this analysis. The L858R and exon19del driver mutations were detected in ctDNA of 19 (35.2%) and 35 (64.8%) patients, respectively. Observed T790M concentrations were lower compared to L858R and exon19del concentrations. In total, 32 (59.3%) patients were treated with erlotinib, 16 (29.6%) with gefitinib and 6 (11.1%) patients switched from erlotinib to gefitinib or vice versa.

ctDNA model

The observed L858R, exon19del and T790M concentrations were best described by a zero-order growth model. The data was best described when the L858R and exon19del concentrations were combined and thus described by shared parameters.(20,28) Equation 3 and 4 describe the model for the L858R and exon19del driver mutations:

$$\frac{dy}{dt} = k_{in} - k_{out} \cdot y(t) \cdot R(t) \quad \text{(Eq. 3)}$$

$$R(t) = e^{-\lambda \cdot t} \quad \text{(Eq. 4)}$$

where y(t) is the change in either L858R or exon19del over time. k_{in} represents the zero-order increase in ctDNA concentrations, k_{out} represents the drug-driven decrease in ctDNA concentrations and R(t) accounts for the time-dependent development of resistance where λ is the progression rate. The addition of this time-dependent resistance term resulted in a significant increase of the model fit (dOFV = -32.5) and was thus included in the model. T790M concentrations were also best described by a zero-order growth model, similar to equation 3. In contrast to the time-dependent resistance development of the driver mutations, the T790M concentrations were better described (dOFV = -21.4) by a model in which the resistance is depending on an increase in driver concentrations (y(t)) (equation 5):

$$R(t) = e^{-\lambda \cdot y(t)} \quad \text{(Eq. 5)}$$

Table 1. Population estimates for the final ctDNA model

		L858R & exon19del		T790M	
	Units	**Estimate (95% CI[a])**	**IIV[b] (95% CI[a])**	**Estimate (95% CI[a])**	**IIV[b] (95% CI[a])**
Population parameter					
Baseline	copies/mL	12.5 (7.73–18.6)	451% (279%-887%)	7.96 (5.76 – 10.8)	185% (139% -290%)
k_{in}	copies/mL/ day	101 (76.7–121)	-	88.5 (70.2 – 109)	-
k_{out}	/day	19.7 (14.9–23.6)		16.3 (12.9 – 20.0)	
Progression rate (λ)	/day	$5.0x10^{-4}$ ($2.0x10^{-4}$–$7.0x10^{-4}$)	782% (320%-986%)	$1.6x10^{-3}$ ($7.0x10^{-4}$ – $2.2x10^{-3}$)	1245% (324% - 1542%)
Residual variability					
Proportional residual error	CV%	30.9% (27.6% - 34.9%)	-	80.5% (69.0% - 94.5%)	-

Abbreviations: CI, confidence interval; CV%, coefficient of variation; IIV, inter-individual variability. [a] 95% CI values were obtained from SIR. [b] IIV expressed as CV%, calculated as sqrt(exp(variance)-1)

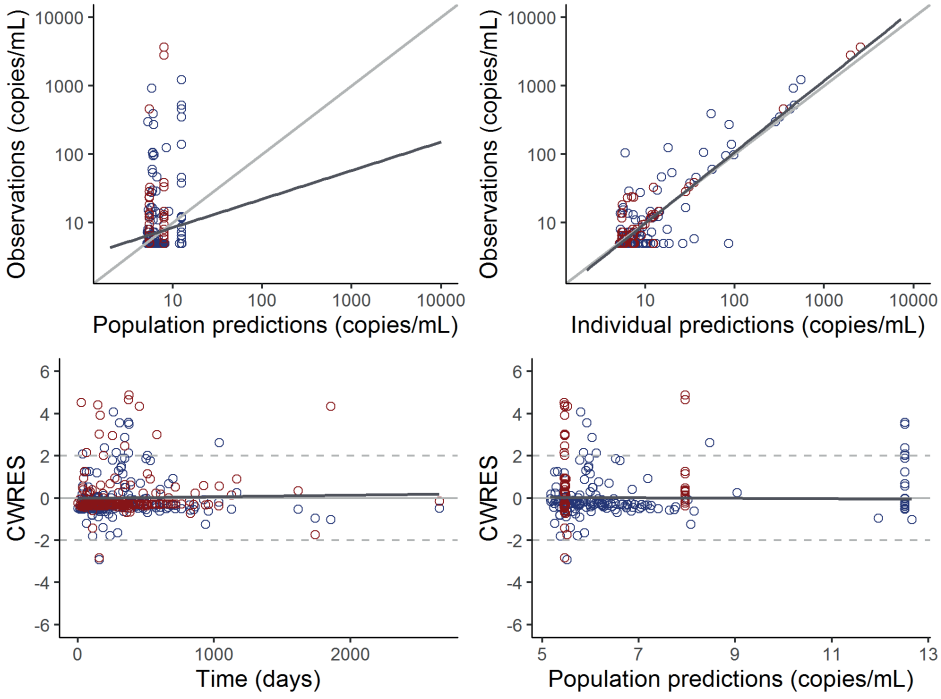

Figure 1. Goodness-of-fit plots of the final ctDNA model for the driver (blue dots) and T790M (red dots) concentrations. Including individual (IPRED) and population predictions (PRED) vs. observed values and conditional weighted residuals (CWRES) vs. time after dose and PRED. Blue dots represent the driver concentrations and red dots are the T790M concentrations.

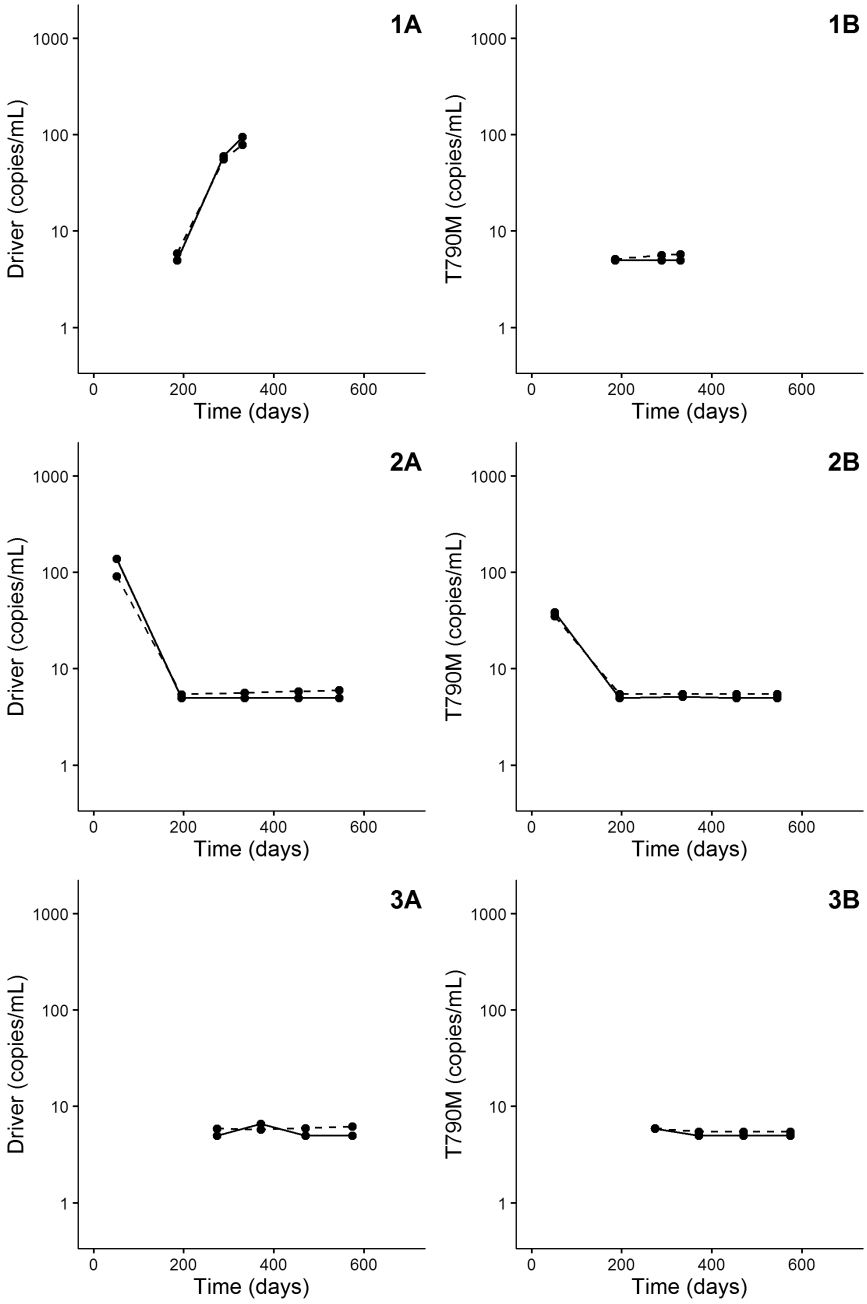

Figure 2. Individual plots for observed (solid line) and individual predicted (dashed line) driver (A) and T790M (B) concentrations over time for three representative patients (1, 2 and 3). **1** patient with an increase in driver concentrations and stable T790M concentrations after approximately 1 year of treatment. **2** patient with an initial decrease in both driver and T790M concentrations. **3** patients with stable driver and T790M concentrations during approximately 1.5 years of treatment.

Plasma samples were collected after start of treatment with erlotinib or gefitinib and as a consequence the baseline before start of treatment was unavailable. An additional parameter was estimated in the final model to account for the baseline concentrations. Parameter estimates are depicted in table 1. High IIV was observed for all parameters for which IIV could be estimated (451%, 782%, 185% and 1245% for driver baseline, driver progression factor, T790M baseline and T790M progression factor, respectively). Mixture models and models incorporating eta-transformations were tested in order to explore this high variability but were unable to improve the model.(29) The GOF (Figure 1) and a selection of individual plots for three representative patients (Figure 2) show an adequate description of the L858R, exon19del and T790M concentrations over time.

Table 2. Population estimates for the final survival model for progression-free-survival

	Units	Estimate (95% CI[a])
Population parameter		
Hazard coefficient (λ)	/day	0.0013 (0.0011 – 0.0017)
Shape (α)	-	1.3338 (1.0494 – 1.6130)
Covariate effect (β)	-	0.0387 (0.0229 – 0.0503)

[a] 95% CI values were obtained from SIR.

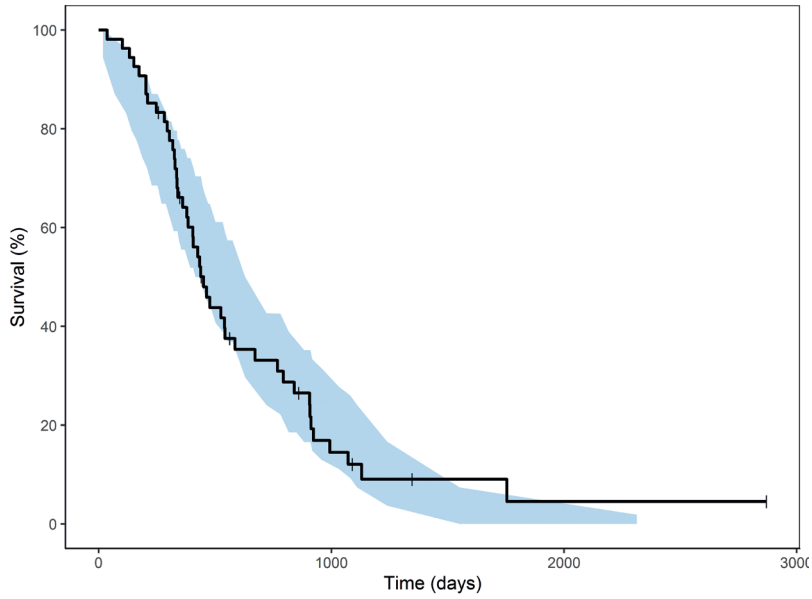

Figure 3. Kaplan-Meier plot of progression-free-survival data. Blue line is the observed Kaplan-Meier curve and the shaded area represents the 95% prediction intervals (n = 500 simulations).

An effect of erlotinib or gefitinib dosing on the dynamics of the ctDNA concentrations could not be identified, most likely explained by the fact that all data was collected during treatment. In addition, no difference in parameters was identified for patients that were treated with gefitinib compared to patients that were treated with erlotinib.

Survival model

Exponential, Gompertz and Weibull hazard functions were explored in order to describe the disease progression data. The Weibull distribution with increasing hazard over time best described the baseline hazard for disease progression (dOFV = + 5.55 and dOFV = + 5.37 for the exponential and Gompertz model, respectively) (Table 2). The VPC of the survival model showed a good predictive performance of the model (Figure 3).

Relative change in driver concentration from estimated baseline was a statistically significant predictor of disease progression as shown by the diagnostic stratified Kaplan-Meier curve (Figure 4) and was therefore included in the model (dOFV = -10.9, p = 0.001). Absolute driver and T790M concentrations did not show an improvement of the model fit compared to the relative change in driver concentrations, as well as the relative change in T790M concentrations. The final Weibull model is described by equation 6:

$$h(t) = \lambda \cdot t^{a-1} \cdot e^{\beta \cdot Driver_{REL}} \qquad \text{(Eq. 6)}$$

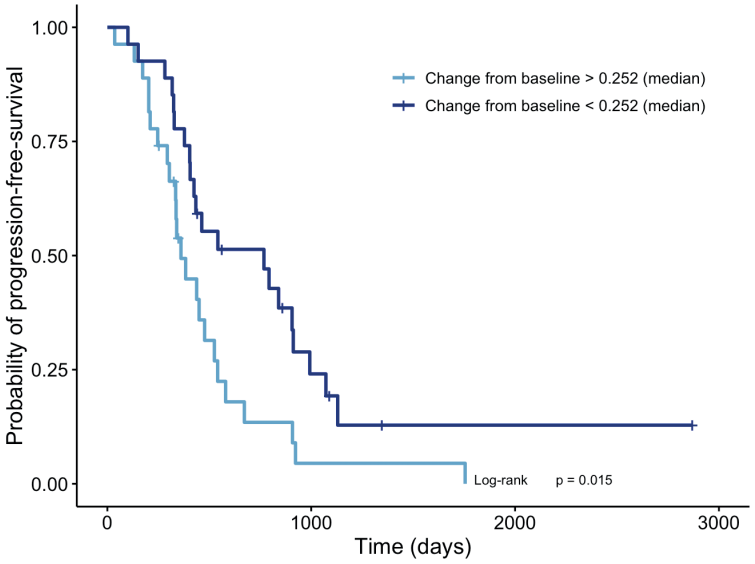

Figure 4. Kaplan-Meier plot of observed progression-free-survival data stratified by median relative change in driver concentration from baseline at time of progression (p = 0.005, Log-rank).

where λ is the hazard coefficient and α is the shape parameter. $Driver_{REL}$ is the relative change in driver concentrations from baseline, the covariate effect is represented by β. The final estimate for β was 0.0387 (95% confidence interval (95% CI 0.0229 – 0.0503). No differences in PFS were observed for patients with the exon19del compared to the L858R mutation and for patients treated with erlotinib or gefitinib.

Discussion

We successfully developed a nonlinear mixed effects model that describes the dynamics of L858R, exon19del and T790M concentrations in plasma of NSCLC patients who were treated with erlotinib or gefitinib. In addition, by using a parametric time-to-event model, the relative change in L858R and exon19del concentrations was identified as significant predictors of disease progression in this patient population. To the best of our knowledge, we are the first in presenting a non-linear mixed effects biomarker model that describes ctDNA concentrations that were longitudinally collected from NSCLC cancer patients. To this end we used a similar model as has been used previously to describe tumour size dynamics following anti-cancer treatment.(20)
It has previously been shown that the trend of ctDNA concentrations measured in the plasma of patients correlated with the mutations detected in patient tumour tissue and the change in tumour volume as measured by CT scan. In this study, patients with ctDNA concentrations below the detection limit (i.e. 0 copies/mL) showed longer PFS and OS compared to patients with detectable ctDNA concentrations. Furthermore, both the EGFR driver and resistance mutation concentrations in plasma showed a progressive increase during disease progression. Measurements of ctDNA allowed earlier detection of NSCLC relapse compared to standard CT scan diagnostics with a median interval of 70 days (range 10-346 days).(2,13) In addition to an earlier detection of progression, measuring ctDNA concentrations in plasma samples is much less invasive for patients compared to conventional diagnostics such as taking tumour tissue biopsies or making CT scans. This permits repeated determinations of ctDNA concentrations, thereby allowing for the monitoring of the change in these levels over time during treatment with EGFR inhibitors. Our survival model was significantly improved by the addition of the relative change in EGFR driver concentrations from baseline as a predictor for disease progression. This finding further confirms that a relationship exists between EGFR driver concentrations in ctDNA and progression of NSCLC in patients treated with the EGFR inhibitors erlotinib and gefitinib.

Nonlinear mixed effects modelling supports the longitudinal and mechanism-based prediction of the full time course of biomarker concentrations in response to anti-cancer treatment. By coupling dynamic biomarker models to time-to-event models, the relationship between time-varying biomarker concentrations and survival can be assessed. Also, the effects of drug administration and thus development of resistance

under drug treatment can be explored. This model can also be used for the analysis of ctDNA concentrations obtained from future clinical trials with targeted anticancer drugs.

Previous work has been focussing on fixed time points descriptors of drug exposure, biomarker concentrations or tumour size as predictor for disease progression or overall survival. Modelling of continuous biomarker concentrations uses all available data and allows for simulations of the response to future treatment regimens.(30) This has also been shown by a PK/PD model that describes the tumour size dynamics in patients with gastrointestinal stromal tumours (GIST). This model describes overall survival and tumour size dynamics as a function of the relative change in stem cell factor receptor, daily sunitinib exposure and relative change in the soluble vascular endothelial growth factor receptor 3.(31)

Our study does, however, harbour some limitations. As this was a retrospective analysis of data that was collected in a cohort study from routine clinical care patients, only limited data was available. The dynamics of the ctDNA concentrations, in particular the time-dependent development of resistance during treatment, could be captured by our model but was driven by a limited number of patients in our dataset. As a result, very high IIV was estimated for the progression factors. Mixture models and eta-transformations were tested but could not improve the eta-distributions. In addition, patient samples were collected as part of routine care. The number of samples collected directly after start of treatment was therefore limited. As a result, the final model estimates for k_{in} and k_{out} were overestimated, complicating simulations based on this model early after initiation of treatment. Also, repeated tumour size and PK measurements were unavailable. Therefore, we could not relate the model for ctDNA to tumour dynamics or assess the effects of PK on the ctDNA dynamics. It has, however, been shown that ctDNA concentrations in plasma correlated with tumour size measurements in patients with NSCLC.(2) Therefore, our model probably provides a good approximation of the tumour size dynamics in this patient population. We used previously developed PK models for erlotinib and gefitinib and individual dosing records to incorporate the effect of PK on the ctDNA dynamics but this did not improve the model. Most likely as a result of the very small dosing range and patients being on steady-state.

We analysed the combined concentrations of patients harbouring the exon19del or L858R mutations. Separate modelling showed similar parameter estimates for both mutations, but with poor parameter precision. In order to improve the power of this analysis, we decided to describe both driver concentrations by the same dynamics and parameters. It has previously been suggested that patients with the exon19del mutation have a higher response rate and longer median OS compared to patients with the L858R mutation.(32) We performed a covariate analysis to explore this relationship,

but could not identify a difference between these groups in our data. In addition, no differences were found in either the ctDNA model or the survival model for patients who were treated with erlotinib or gefitinib. These results are in line with previous studies that compared erlotinib with gefitinib for differences in PFS, OS and biomarker tumour size dynamics.(32–34)

Conclusion

In conclusion, we successfully developed a model that describes the longitudinal dynamics in ctDNA in a clinical cohort and identified the relative change in EGFR driver mutations from baseline as a predictor for disease progression following erlotinib or gefitinib treatment. In addition, this model shows that nonlinear mixed effects modelling is a valuable method for the analysis of longitudinal and heterogeneous biomarker datasets obtained from clinical practice and provides a framework for prediction of disease progression based on observed ctDNA concentrations.

References

1. Oxnard GR, Paweletz CP, Kuang Y, Mach SL, O'Connell A, Messineo MM, et al. Noninvasive detection of response and resistance in egfrmutant lung cancer using quantitative next-generation genotyping of cell-free plasma DNA. Clin Cancer Res. 2014;20:1698–705.

2. Lee JY, Qing X, Xiumin W, Yali B, Chi S, Bak SH, et al. Longitudinal monitoring of EGFR mutations in plasma predicts outcomes of NSCLC patients treated with EGFR TKIs: Korean Lung Cancer Consortium (KLCC-12-02). Oncotarget. 2016;7:6984–93.

3. Dearden S, Stevens J, Wu Y-L, Blowers D. Mutation incidence and coincidence in non small-cell lung cancer: meta-analyses by ethnicity and histology (mutMap). Ann Oncol Off J Eur Soc Med Oncol. 2013;24:2371–6.

4. Boch C, Kollmeier J, Roth A, Stephan-Falkenau S, Misch D, Grüning W, et al. The frequency of EGFR and KRAS mutations in non-small cell lung cancer (NSCLC): routine screening data for central Europe from a cohort study. BMJ Open. 2013;3:e002560.

5. Arcila ME, Nafa K, Chaft JE, Rekhtman N, Lau C, Reva BA, et al. EGFR Exon 20 Insertion Mutations in Lung Adenocarcinomas: Prevalence, Molecular Heterogeneity, and Clinicopathologic Characteristics. Mol Cancer Ther. 2013;12:220–9.

6. Murray S, Dahabreh IJ, Linardou H, Manoloukos M, Bafaloukos D, Kosmidis P. Somatic Mutations of the Tyrosine Kinase Domain of Epidermal Growth Factor Receptor and Tyrosine Kinase Inhibitor Response to TKIs in Non-small Cell Lung Cancer: An Analytical Database. J Thorac Oncol. 2008;3:832–9.

7. Zhao H, Fan Y, Ma S, Song X, Han B, Cheng Y, et al. Final Overall Survival Results from a Phase III, Randomized, Placebo-Controlled, Parallel-Group Study of Gefitinib Versus Placebo as Maintenance Therapy in Patients with Locally Advanced or Metastatic Non–Small-Cell Lung Cancer (INFORM; C-TONG 0804). J Thorac Oncol. 2015;10:655–64.

8. Greenhalgh J, Dwan K, Boland A, Bates V, Vecchio F, Dundar Y, et al. First-line treatment of advanced epidermal growth factor receptor (EGFR) mutation positive non-squamous non-small cell lung cancer. Cochrane Database Syst Rev. 2016;(5):CD010383.

9. Sequist L V, Waltman B a, Dias-Santagata D, Digumarthy S, Turke AB, Fidias P, et al. Genotypic and histological evolution of lung cancers acquiring resistance to EGFR inhibitors. Sci Transl Med. 2011;3:75ra26.

10. Yu HA, Arcila ME, Hellmann MD, Kris MG, Ladanyi M, Riely GJ. Poor response to erlotinib in patients with tumors containing baseline EGFR T790M mutations found by routine clinical molecular testing. Ann Oncol. 2014;25:423–8.

11. Wang Z, Chen R, Wang S, Zhong J, Wu M, Zhao J, et al. Quantification and dynamic monitoring of EGFR T790M in plasma cell-free DNA by digital PCR for prognosis of EGFR-TKI treatment in advanced NSCLC. PLoS One. 2014;9:1–7.

12. Sorensen BS, Wu L, Wei W, Tsai J, Weber B, Nexo E, et al. Monitoring of epidermal growth factor receptor tyrosine kinase inhibitor-sensitizing and resistance mutations in the plasma DNA of patients with advanced non-small cell lung cancer during treatment with erlotinib. Cancer. 2014;120:3896–901.

13. Huang C, Liu S, Tong X, Fan H. Extracellular vesicles and ctDNA in lung cancer: biomarker sources and therapeutic applications. Cancer Chemother Pharmacol. 2018;82:171–83.

14. Mok T, Wu YL, Lee JS, Yu CJ, Sriuranpong V, Sandoval-Tan J, et al. Detection and dynamic changes of EGFR mutations from circulating tumor DNA as a predictor of survival outcomes in NSCLC Patients treated with first-line intercalated erlotinib and chemotherapy. Clin Cancer Res. 2015;21:3196–203.

15. Riediger AL, Dietz S, Schirmer U, Meister M, Heinzmann-Groth I, Schneider M, et al. Mutation analysis of circulating plasma DNA to determine response to EGFR tyrosine kinase inhibitor therapy of lung

adenocarcinoma patients. Sci Rep [Internet]. 2016 Dec 19 [cited 2019 Jun 20];6(1):33505. Available from: http://www.nature.com/articles/srep33505

16. Verheijen RB, van Duijl TT, van den Heuvel MM, Beijnen JH, Schellens JHM, van den Broek D, et al. Monitoring of circulating tumor DNA in non-small cell lung cancer patients treated with EGFR-inhibitors. J Clin Oncol. 2017;35(15_suppl):11535–11535.

17. Upton RN, Mould DR. Basic concepts in population modeling, simulation, and model-based drug development: part 3-introduction to pharmacodynamic modeling methods. CPT pharmacometrics Syst Pharmacol. 2014;3:e88.

18. Federation of Dutch Medical Scientific Societies. Human Tissue and Medical Research: Code of conduct for responsible use (2011). 2011. http://www.federa.org/sites/default/files/digital_version_first_part_code_of_conduct_in_uk_2011_12092012.pdf.

19. Yung TKF, Chan KCA, Mok TSK, Tong J, To K-F, Lo YMD. Single-Molecule Detection of Epidermal Growth Factor Receptor Mutations in Plasma by Microfluidics Digital PCR in Non-Small Cell Lung Cancer Patients. Clin Cancer Res. 2009;15:2076–84.

20. Ribba B, Holford NH, Magni P, Trocóniz I, Gueorguieva I, Girard P, et al. A Review of Mixed-Effects Models of Tumor Growth and Effects of Anticancer Drug Treatment Used in Population Analysis. CPT Pharmacometrics Syst Pharmacol. 2014;3:e113.

21. White-Koning M, Civade E, Geoerger B, Thomas F, Deley MC Le, Hennebelle I, et al. Population analysis of erlotinib in adults and children reveals pharmacokinetic characteristics as the main factor explaining tolerance particularities in children. Clin Cancer Res. 2011;17:4862–71.

22. FDA. Clinical Pharmacology Review Gefitinib. 2014;

23. Dosne A-G, Bergstrand M, Karlsson MO. An automated sampling importance resampling procedure for estimating parameter uncertainty. J Pharmacokinet Pharmacodyn. 2017;44:509–20.

24. Lindbom L, Ribbing J, Jonsson EN. Perl-speaks-NONMEM (PsN)—a Perl module for NONMEM related programming. Comput Methods Programs Biomed. 2004;75:85–94.

25. Bauer RJ. NONMEM USERS GUIDE INTRODUCTION TO NONMEM 7.3.0. ICON Development Solutions, 2014.

26. Keizer RJ, van Benten M, Beijnen JH, Schellens JHM, Huitema ADR. Pirana and PCluster: A modeling environment and cluster infrastructure for NONMEM. Comput Methods Programs Biomed. 2011;101:72–9.

27. Development Core Team R. R: A Language and Environment for Statistical Computing. Vienna, Austria: R Foundation for Statistical Computing; 2008.

28. Claret L, Girard P, Hoff PM, Van Cutsem E, Zuideveld KP, Jorga K, et al. Model-Based Prediction of Phase III Overall Survival in Colorectal Cancer on the Basis of Phase II Tumor Dynamics. J Clin Oncol. 2009;27:4103–8.

29. Petersson KJF, Hanze E, Savic RM, Karlsson MO. Semiparametric distributions with estimated shape parameters. Pharm Res. 2009;26:2174–85.

30. Bender BC, Schindler E, Friberg LE. Population pharmacokinetic-pharmacodynamic modelling in oncology: a tool for predicting clinical response. Br J Clin Pharmacol. 2015;79:56–71.

31. Hansson EK, Amantea MA, Westwood P, Milligan PA, Houk BE, French J, et al. PKPD Modeling of VEGF, sVEGFR-2, sVEGFR-3, and sKIT as Predictors of Tumor Dynamics and Overall Survival Following Sunitinib Treatment in GIST. CPT Pharmacometrics Syst Pharmacol. 2013;2:e84.

32. Yang JJ, Zhou Q, Yan HH, Zhang XC, Chen HJ, Tu HY, et al. A phase III randomised controlled trial of erlotinib vs gefitinib in advanced non-small cell lung cancer with EGFR mutations. Br J Cancer. 2017;116:568–74.

33. Eigenmann MJ, Frances N, Hoffmann G, Lavé T, Walz A-C. Combining Nonclinical Experiments with Translational PKPD Modeling to Differentiate Erlotinib and Gefitinib. Mol Cancer Ther. 2016;15:3110-3119.

34. Bronte G, Rolfo C, Giovannetti E, Cicero G, Pauwels P, Passiglia F, et al. Are erlotinib and gefitinib interchangeable, opposite or complementary for non-small cell lung cancer treatment? Biological, pharmacological and clinical aspects. Crit Rev Oncol Hematol. 2014;89:300–13.

CHAPTER 4

Therapeutic drug monitoring



Chapter 4.1

Development and validation of a liquid chromatography-tandem mass spectrometry assay for nine oral anticancer drugs in human plasma

J Pharm Biomed Anal. 2019; 174: 561-566

J.M. Janssen
N. de Vries
N. Venekamp
H. Rosing
A.D.R. Huitema
J.H. Beijnen

Abstract

A liquid chromatography-tandem mass spectrometry assay was developed and validated for the nine oral anticancer agents alectinib, cobimetinib, lenvatinib, nintedanib, osimertinib, palbociclib, ribociclib, vismodegib and vorinostat in order to support therapeutic drug monitoring (TDM). The assay was based on reversed-phase chromatography coupled with tandem mass spectrometry operating in the positive ion mode. The assay was validated based on the guidelines on bioanalytical methods by the US Food and Drug Administration and European Medicines Agency. The method was validated over a linear range of 10-200 ng/mL for alectinib, lenvatinib, nintedanib and vismodegib; 50-1000 ng/mL for cobimetinib and palbociclib; 100-2000 ng/mL for osimertinib; 5.00-100 ng/mL for ribociclib; 25-500 ng/mL for vorinostat. Intra-assay and inter-assay bias was within ±20% for all analytes at the lower limit of quantification and within ±15% at remaining concentrations. Stability experiments showed that osimertinib is unstable in the biomatrix and should be shipped on dry-ice and stored at -20 ˚C until analysis. All other compounds were stable in the biomatrix. The described TDM method was successfully validated and applied for TDM in patients treated with these KIs.

Introduction

The number of oral anticancer agents approved for the treatment of various malignancies is rapidly expanding. These anticancer drugs are designed to interact with a specific target expressed by malignant cells. For many of these kinase inhibitors (KIs), exposure-response and exposure-toxicity relationships have already been examined during the development phase, mainly in phase II and III clinical trials. During these clinical trials, only fixed doses are explored, resulting in fixed dose treatment strategies when the drug is registered and used in clinical practice. It has however been shown that drug exposure may considerable vary between patients. Patients with a high exposure may develop excessive toxicity while patients with low exposures may be at risk of treatment failure.(1)

By using Therapeutic Drug Monitoring (TDM), treatment outcomes can be optimized. Based on the quantification of individual plasma concentrations and interpretation of these concentrations with respect to proposed target concentrations, dose individualizations can be applied.(2)

A TDM assay was developed and validated for the concurrent quantification of the new KIs alectinib, cobimetinib, lenvatinib, nintedanib, osimertinib, palbociclib, ribociclib, vismodegib and vorinostat. These drugs are registered or under investigation for various oncological indications. Several bioanalytical methods using liquid chromatography coupled to mass spectrometry have been described for the quantification of alectinib, cobimetinib, lenvatinib, nintedanib, osimertinib, vismodegib and vorinostat in human plasma, either alone or in combination assays.(3–8)For TDM purposes, a rapid, robust and efficient quantification is preferable, which we describe here. Most importantly, our assay enables simultaneous quantification of the plasma concentrations of patients receiving one of these KIs. In addition, we demonstrate that the assay is applicable in clinical routine care.

Material and methods

Chemicals

Alectinib, $^{2}H_{8}$-alectinib, lenvatinib, $^{2}H_{5}$-lenvatinib, nintedanib, $^{13}C,^{2}H_{3}$-nintedanib, osimertinib, $^{13}C,^{2}H_{3}$-osimertinib, palbociclib, $^{2}H_{8}$-palbociclib, ribociclib, $^{2}H_{6}$-ribociclib, vismodegib, $^{13}C_{7}$-vismodegib, $^{13}C_{6}$-vorinostat and $^{13}C_{6}$-cobimetinib were purchased from Alsachim (Illkirch Graffenstaden, France). Vorinostat and ammonium bicarbonate were bought at Sigma Aldrich (Zwijndrecht, the Netherlands) and cobimetinib was bought at Selleckchem (Houston, USA). Acetonitrile, methanol and water (all Supra-Gradient grade) were from Biosolve Ltd (Valkenswaard, The Netherlands). K_{2}EDTA plasma was obtained from Bioreclamation LLC (Hicksville, USA). The chemical structures of the analytes are depicted in figure 1.

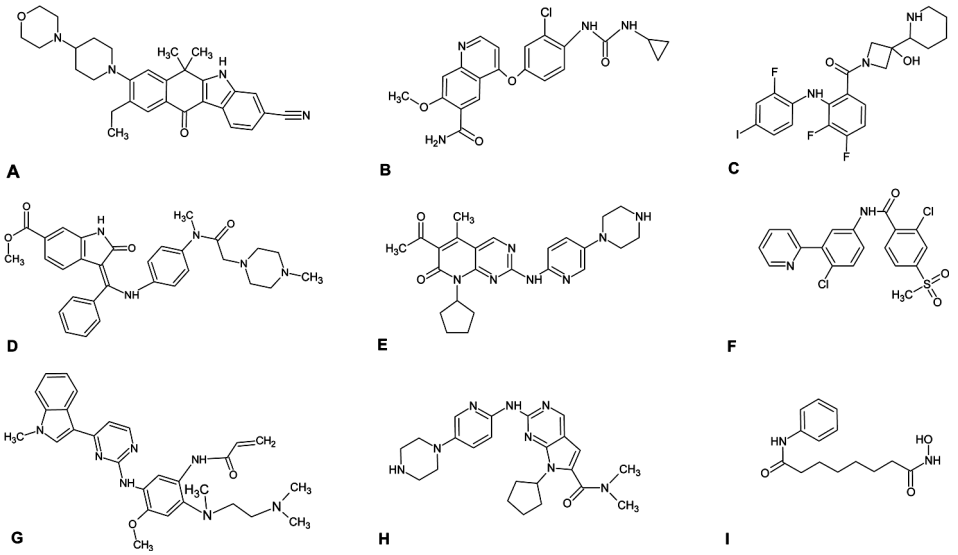

Figure 1. Molecular structure of alectinib (A), lenvatinib (B), cobimetinib (C), nintedanib (D), palbociclib (E), vismodegib (F), osimertinib (G), ribociclib (H) and vorinostat (I).

Stock solutions and working solutions

Stock solutions were prepared at a concentration of 1 mg/mL in DMSO for cobimetinib, lenvatinib, nintedanib, osimertinib, ribociclib, vismodegib and vorinostat. The stock solution containing alectinib was prepared at a concentration of 0.5 mg/mL in DMSO. Since palbociclib is only soluble in acetic aqueous solutions, 0.1% formic acid in water was used as a solvent for the palbociclib stock solution. The stock solutions were diluted with methanol to obtain working solutions. For alectinib, lenvatinib, nintedanib and vismodegib working solutions were prepared at concentrations of 200, 500, 2,000, 4,000 and 20,000 ng/mL, at concentrations of 1,000, 2,500, 10,000 and 20,000 ng/mL for cobimetinib and palbociclib, at concentrations of 100, 250, 1,000, 2,000 and 10,000 ng/mL for ribociclib, at concentrations of 500, 1,250, 5,000 and 10,000 ng/mL for vorinostat and at concentrations of 2,000, 5,000, 20,000 and 40,000 ng/mL for osimertinib. Two independent stock solutions and working solutions were prepared for the preparation of calibration standards and quality control (QC) samples. Stock solutions for all internal standards (IS) were prepared at a concentration of 1 mg/mL in DMSO, except for $^{2}H_{8}$-palbociclib which was prepared in 0.1% formic acid in water and stored in amber-coloured 2.0-mL tubes. Subsequently, a mixture of the internal stock solutions was prepared and diluted with methanol at concentrations of 2,500 and 25,000 ng/mL for $^{2}H_{8}$-alectinib, $^{13}C_{6}$-cobimetinib, $^{2}H_{5}$-lenvatinib, $^{13}C,^{2}H_{3}$-osimertinib, $^{2}H_{8}$-palbociclib and $^{13}C_{7}$-vismodegib and at concentrations of 250, 2,500 and 25,000 for $^{13}C,^{2}H_{3}$-nintedanib and $^{2}H_{6}$-ribociclib. All stock- and working solutions were stored at -20˚C.

Calibration standards, quality control samples

1900 µL blank human K_2EDTA plasma was spiked by 100 µL of the calibration standard working solution. The QC samples were prepared by spiking 100 µL of the separately prepared working solution to 1900 µL blank human K_2EDTA plasma to obtain the final QC low, QC mid and QC high concentrations. Both calibrators and QC samples were subsequently stored in aliquots of 50 µL and stored at -70˚C. Back-calculated concentrations of the calibrators were used for the determinations of the linearity of the calibration model, using the reciprocal of the squared concentrations ($1/x^2$) as the weighting factor. For all analytes, linearity was concluded for the previously described validation concentration ranges. All other requirements were also in accordance with the guidelines, for all nine analytes (≥ 75% of the calibrators within ±15% (±20% for the LLOQ) of the nominal concentrations and analyte response at LLOQ level was ≥ 5 times the response compared to the blank response).

Sample preparation

Samples were collected by venipuncture in the clinic. Directly after withdrawal, samples were centrifuged for 10 minutes at 2,000 g at 4˚C. After centrifugation, plasma was isolated and stored at -20˚C. Prior to processing, each sample was thawed and 50 µL was aliquoted in 1.5 mL amber-coloured tubes. Samples were spiked with 20 µL of IS working solution and 150 µL acetonitrile was added. Afterwards, samples were vortex-mixed for 10 seconds and centrifuged for 10 minutes at 15,000 rpm. 100 µL supernatant was added to an amber-coloured autosampler vial with insert that contained 100 µL 10 mM ammonium bicarbonate in water. The final extract was vortex-mixed for 10 seconds and stored at 2-8˚C until analysis.

Chromatographic equipment and conditions

A Waters Acquity I class UPLC system with binary pump, integrated degasser, column oven and I class autosampler were used (Waters, Milford, MS, USA). The temperature of the autosampler and column were kept at 8˚C and 40 ˚C, respectively. The highest selectivity was obtained by a basic eluent. Mobile phase A consisted of 10 mM ammonium bicarbonate (pH 10.5) in water and mobile phase B consisted of 10 mM ammonium bicarbonate (pH 10.5) in methanol-water (1:9, v/v). Gradient elution was applied at a flow of 0.25 mL/min through a Gemini C_{18} column (50 x 2.0 mm ID, 5.0 µm) with an additional Gemini C18 guard column (4 x 2.0 mm ID, 5.0 µm) (both Phenomenex, Torrance, CA, USA). The applied gradient program was based on a previously reported TDM-assay (40% B at 250 µL/min (0-0.1 min); 40 to 100% B at 250 µL/min (0.1-1 min); 100% B at 250 µL/min (1.0 – 3.0); 40% B at 500 µL/min (3.01 – 3.50 min); 40% B at 250 µL/min (3.51 – 4.0 min)).(9)

MS equipment and conditions

A QTRAP5500 triple quadrupole mass spectrometer (MS) equipped with a turbo ion spray interface, operating in positive ion mode was used (AB Sciex, Framingham, MA,

USA). Multiple reaction monitoring (MRM) chromatograms were acquired and processed using Analyst™ software (AB Sciex, version 1.6.2). The MS operating parameters are summarized in Table 1 and supplementary Figure S1 shows chromatograms of QC lower limit of quantification (LLOQ) level and double blank samples.

Table 1. Mass spectrometric settings for the analytes and their internal standards

Parameter	
Run duration	4.00 min
Ion spray voltage	4000 V
Nebulizer gas	30 au
Collision gas	9 au
Curtain gas	30 au
Turbo gas	40 au
Temperature	500 °C
Dwell time	20 ms

Specific parameters Analyte	**MRM (Da)**	**Collision energy (V)**	**Collision exit potential (V)**	**Declustering potential (V)**	**Retention time (min)**
Alectinib	483.1 → 396.1	41	54	71	1.62
$^{2}H_{8}$-alectinib	491.1 → 396.1	41	54	71	1.61
Cobimetinib	532.1 → 249.0	45	22	171	1.54
$^{13}C_{6}$-cobimetinib	538.1 → 255.0	45	22	171	1.54
Lenvatinib	428.1 → 371.0	43	52	61	1.22
$^{2}H_{5}$-lenvatinib	433.1 → 371.0	43	52	61	1.21
Nintedanib	540.3 → 113.1	33	14	136	1.42
$^{13}C,^{2}H_{3}$-nintedanib	544.3 → 117.1	33	14	136	1.41
Osimertinib	500.2 → 72.1	47	20	120	1.69
$^{13}C,^{2}H_{3}$-osimertinib	504.2 → 72.1	47	20	120	1.69
Palbociclib	448.2 → 380.1	43	48	51	1.36
$^{2}H_{8}$-palbociclib	456.2 → 388.1	43	48	51	1.35
Ribociclib	435.2 → 322.1	49	30	181	1.34
$^{2}H_{6}$-ribociclib	441.2 → 322.1	49	30	181	1.23
Vismodegib	420.9 → 342.2	51	26	186	1.27
$^{13}C_{7}$-vismodegib	430.9 → 349.7	51	26	186	1.26
Vorinostat	265.2 → 232.0	15	30	51	1.07
$^{13}C_{6}$-vorinostat	270.2 → 237.0	15	30	51	1.07

Validation procedures

The assay was validated based on the FDA and EMA guidelines on bioanalytical method validation.(10,11)

Results and Discussion

Accuracy and Precision

In order to assess intra- and inter-assay accuracies and imprecisions, five replicated QC samples were analyzed in three consecutive runs at the LLOQ, midrange and high concentrations. The accuracy (bias) was determined in percentage difference between the mean measured concentration (per run for intra-assay bias and overall for inter-assay bias) and the nominal concentration and coefficient of variation (CV%) were used to assess the intra-run precision. Analysis of Variance (ANOVA) was used to assess inter-run precision. The inter- and intra-assay accuracy and imprecision were ≤ 20% for the LLOQ and ≤ 15% for midrange and high concentrations and thus within the acceptance criteria for all analytes. Details on the assay performance data are listed in Table 2.

Dilution integrity

High and variable concentrations in patient samples were expected for vismodegib and alectinib based on previously published pharmacokinetic studies.(12,13) To investigate the dilution integrity for these analytes, five replicates of both vismodegib (100-fold dilution) and alectinib (10-fold dilution) were prepared in blank human plasma. Bias was within ± 15% and the CV% was ≤ 15% for both vismodegib and alectinib.

Carry-over

Two double blank samples were injected after an ULOQ sample, in order to determine carry-over. Interferences in the double blank sample should be ≤ 20% of the analyte peak area of the LLOQ sample and ≤ 5% of the peak area of the IS. For cobimetinib, osimertinib, palbociclib and vorinostat, eluting peaks with areas exceeding 20% of the LLOQ were observed in blank samples injected after ULOQ samples. Carry-over into the second double blank samples was around 20% of the LLOQ for osimertinib, ribociclib and vorinostat. Two blank samples were injected after ULOQ and QC high samples during the validation to control the carry-over. Clinical samples containing these drugs should not be grouped during analysis to circumvent impact of carry-over.

Specificity and selectivity

The selectivity of the method was determined by the analysis of LLOQ samples prepared in six different batches of blank human plasma. For at least 5 out of 6 batches, the mean measured concentrations at LLOQ level were within ± 20% of the nominal

Table 2. Assay performance data for the analysis of alectinib, cobimetinib, lenvatinib, nintedanib, osimertinib, palbociclib, ribociclib, vismodegib and vorinostat

Analyte		Intra-assay		Inter-assay	
	Nominal concentration (ng/mL)	Bias (%)	CV%	Bias (%)	CV%
Alectinib	10	-0.1 – 6.4	7.5 – 15.9	3.7	-[a]
	100	-3.3 – 13.6	2.5 – 6.3	3.2	8.5
	200	5.0 – 10.3	1.6 – 12.2	7.4	-[a]
Cobimetinib	50	-13.4 – 8.8	4.6 – 10.2	-3.9	11.5
	500	-0.1 – 10.5	3.4 – 7.2	3.5	5.2
	1000	11.0 – 12.8	1.2 – 8.7	11.6	-[a]
Lenvatinib	10	1.7 – 8.8	10.1 – 16.1	5.8	-[a]
	100	-3.0 – 7.8	4.4 – 5.5	2.2	4.8
	200	8.7 – 13.7	4.4 – 11.9	11.0	-[a]
Nintedanib	10	-4.4 – 15.8	9.0 – 16.9	3.3	8.9
	100	-1.2 – 5.2	3.9 – 11.6	2.3	-[a]
	200	7.3 – 14.7	4.5 – 11.7	10.2	-[a]
Osimertinib	99.9	-15.3 – 9.2	3.7 – 4.3	0.2	13.3
	999	-13.5 – 5.0	1.6 – 4.4	-1.4	10.5
	2000	-8.8 – 7.8	1.3 – 2.4	2.2	9.3
Palbociclib	50.2	-3.2 – 10.5	2.9 – 9.6	5.2	6.2
	502	-5.1 – 9.8	2.0 – 10.2	2.4	6.8
	1000	3.5 – 14.4	3.5 – 14.4	8.6	3.5
Ribociclib	4.99	-8.8 – 2.2	3.7 – 8.3	-2.3	5.1
	49.9	0.3 – 13.9	2.4 – 8.6	9.1	6.5
	99.8	-1.2 – 8.8	4.3 – 5.6	3.4	4.4
Vismodegib	10	-2.1 – 12.5	4.0 – 10.6	7.3	6.9
	100	-1.8 – 14.0	8.2 – 11.1	5.2	6.3
	200	2.5 – 11.8	2.0 – 8.8	6.8	3.1
Vorinostat	25	-2.2 – 4.2	6.9 – 15.1	1.4	-[a]
	250	-12.7 - -2.4	5.1 – 10.5	-6.7	4.5
	501	-4.3 – 7.2	3.5 – 12.7	1.5	4.0

[a] Inter-run precision could not be calculated because there is no significant additional variation owing to the performance of the assay in different runs.

concentrations for all analytes and interferences were ≤ 20% (≤ 5% for the IS) of the LLOQ areas in at least 5 of the 6 double blanks. The cross analyte/IS interferences were determined by separately spiking the analytes and IS to blank human plasma at their ULOQ. Cross-analyte interference was found for lenvatinib on the cobimetinib LLOQ signal (30%), cobimetinib on the nintedanib LLOQ signal (33%), nintedanib IS on the nintedanib LLOQ signal (22%) and for ribociclib IS on the ribociclib LLOQ signal (24%). Cross-analyte interference has no impact on the quantification of patient samples since

lenvatinib, cobimetinib and nintedanib are not used concomitantly by patients and thus samples contain only one analyte. The calibration standards and QC samples do not contain LLOQ and ULOQ levels in the same sample and therefore the cross-analyte interferences from lenvatinib and cobimetinib are negligible. Furthermore, the concentrations of the nintedanib and ribociclib IS were lowered in order to minimize cross-interfering on patient samples. Cross-analyte interferences of co-eluting peaks were accepted for all other IS and concentrations at LLOQ level.

Matrix effect

Six batches of individual blank human plasma at low and high concentrations in singular were prepared to determine the matrix effect. For both the analyte and IS, the matrix factor (MF) was calculated for each matrix lot by calculating the ratio of the peak area in the presence of matrix to the peak area in absence of matrix (working solution of the analyte). Furthermore, the IS normalized MF was calculated by dividing the MF of the analyte by the MF of the IS. At both tested QC concentration levels the CV of the IS-normalized matrix factor from the 6 batches ranged from 0.83 to 0.98 and CV% were ≤ 15% for all analytes and were thus considered acceptable.

Stability

The analytes were considered stable in the matrix when 80-120% of the initial measured concentration was found for the LLOQ level and when 85-115% of the nominal concentration was found for the other concentration levels. For stock and working solutions acceptance criteria of 95%-105% were applied. Plasma samples were stable for at least up to 48 hours at 20-25˚C when protected from light, 5 weeks at -20˚C, 18 weeks at -70˚C and after three freeze (-20˚C) -thaw (20-25˚C) cycles. The processed samples were stable for at least 48 hours at 2-8˚C except for osimertinib. Additional stability experiments have been performed to assess the stability of osimertinib. These experiments showed that osimertinib is stable for 4 hours at 20-25˚C, 6.5 hours at 2-8˚C and 5 weeks at -20˚C. Similar results were observed during the validation of a previously reported LC-MS/MS assay for osimertinib.(14) Therefore, clinical samples containing osimertinib should be sent on dry-ice to the laboratory and stored at -20˚C until analysis. In addition, sample preparation and analysis time should be limited to 4 hours. The stock and working solutions were stable at -20˚C for at least 8 and 5 months, respectively. Long-term stability at -70˚C is still ongoing.

Clinical application

As part of routine clinical care, K_2EDTA whole blood samples were collected from patients who were treated at our institute. Representative chromatograms and corresponding concentrations are depicted in Figure 2. Mean measured concentrations and corresponding ranges are listed in table 3. These results demonstrate the applicability of this assay for alectinib, cobimetinib, lenvatinib, nintedanib, osimertinib or palbociclib. The collection of sufficient samples for ribociclib, vismodegib and vorinostat is still ongoing.

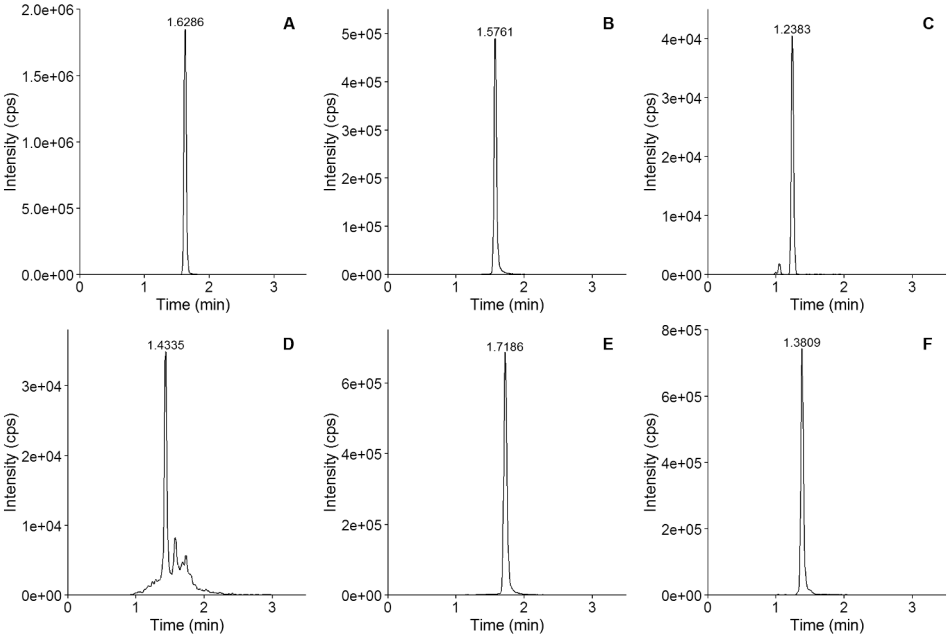

Figure 2. Chromatograms of analyzed plasma samples collected from patients treated with alectinib (A, 793 ng/mL), cobimetinib (B, 253 ng/mL), lenvatinib (C, 91.1 ng/mL), nintedanib (D, 5.05 ng/mL), osimertinib (E, 331 ng/mL) and palbociclib (F, 75.3 ng/mL).

Table 3. Plasma concentrations and calibration range of alectinib, cobimetinib, lenvatinib, nintedanib, osimertinib, palbociclib, ribociclib, vismodegib and vorinostat of patients treated with these drugs (n=10)

Analyte	Mean plasma concentration (ng/mL)	Range (ng/mL)	Calibration range (ng/mL)
Alectinib[a]	793	262 – 2520	10 – 200
Cobimetinib	253	69.7 – 649	50 – 1000
Lenvatinib	91.1	20.4 – 267	10 – 200
Nintedanib[b]	24.5	13.0 – 36.0	10 – 200
Osimertinib	331	123 – 798	100 – 2000
Palbociclib	90.3	54.2 – 186	50 – 1000
Ribociclib[c]	-	-	5 – 100
Vismodegib[c]	-	-	10 – 200
Vorinostat[c]	-	-	25 - 500

[a] Alectinib samples are diluted 10-fold prior to analysis. [b] Only three clinical samples have been collected for nintedanib. [c] No clinical samples have been collected yet for ribociclib, vismodegib and vorinostat

Conclusion

We successfully developed a sensitive LC-MS/MS assay for the simultaneous quantification of alectinib, cobimetinib, lenvatinib, nintedanib, osimertinib, palbociclib, ribociclib, vismodegib and vorinostat in human plasma. The validated linear assay ranges are 10-200 ng/mL for alectinib, lenvatinib, nintedanib and vismodegib, 50-1000 ng/mL for cobimetinib and palbociclib, 25-500 ng/mL for vorinostat, 100-2000 for osimetinib and 5-100 for ribociclib. Stability showed that, with the exception of osimertinib, all analytes were stable in human K_2EDTA plasma at room temperature for longer than 4 hours. This assay is considered suitable to facilitate TDM.

References

1. Gao B, Yeap S, Clements A, Balakrishnar B, Wong M, Gurney H. Evidence for therapeutic drug monitoring of targeted anticancer therapies. J Clin Oncol. 2012;30:4017–25.

2. Verheijen RB, Beijnen JH, Schellens JHM, Huitema ADR, Steeghs N. Clinical Pharmacokinetics and Pharmacodynamics of Pazopanib: Towards Optimized Dosing. Clin Pharmacokinet. 2017;56:987-997.

3. Heinig K, Miya K, Kamei T, Guerini E, Fraier D, Yu L, et al. Bioanalysis of alectinib and metabolite M4 in human plasma, cross-validation and impact on PK assessment. Bioanalysis. 2016;8:1465–79.

4. Cardoso E, Mercier T, Dorothea A, Homicsko K, Michielin O, Ellefsen-lavoie K, et al. Quantification of the next-generation oral anti-tumor drugs dabrafenib, trametinib, vemurafenib, cobimetinib, pazopanib, regorafenib and two metabolites in human plasma by liquid chromatography-tandem mass spectrometry. J Chromatogr B. 2018;1083:124–36.

5. Dubbelman AC, Rosing H, Thijssen B, Gebretensae A, Lucas L, Chen H, et al. Development and validation of LC – MS / MS assays for the quantification of E7080 and metabolites in various human biological matrices. J Chromatogr B. 2012;887–888:25–34.

6. Reis R, Labat L, Allard M, Boudou-rouquette P, Chapron J, Bellesoeur A, et al. Journal of Pharmaceutical and Biomedical Analysis Liquid chromatography-tandem mass spectrometric assay for therapeutic drug monitoring of the EGFR inhibitors afatinib , erlotinib and osimertinib , the ALK inhibitor crizotinib and the VEGFR inhibitor nint. J Pharm Biomed Anal. 2018;158:174–83.

7. Deng Y, Wong H, Graham RA, Liu W, Shen H, Shi Y, et al. Determination of unbound vismodegib (GDC-0449) concentration in human plasma using rapid equilibrium dialysis followed by solid phase extraction and high-performance liquid chromatography coupled to mass spectrometry. J Chromatogr B. 2011;879:2119–26.

8. Suresh P, Devaraj V, Srinivas N, Mullangi R. Review of bioanalytical assays for the quantitation of various HDAC inhibitors such as vorinostat, belinostat, panobinostat, romidepsin and chidamine. Biomed Chromatogr. 2017;31:e3807-e3821.

9. Herbrink M, de Vries N, Rosing H, Huitema ADR, Nuijen B, Schellens JHM, et al. Development and validation of a liquid chromatography-tandem mass spectrometry analytical method for the therapeutic drug monitoring of eight novel anticancer drugs. Biomed Chromatogr. 2017;32:e4147-e4156.

10. US Food Drug Administration (FDA), FDA Guidance for Industry: Bioanalytical Method Validation (2001).

11. European Medicines Agency (EMA), Guideline on Bioanalytical Method Validation. Committee for Medicinal Products for Human Use and European Medicines Agency, 2011, London.

12. Morcos PN, Yu L, Bogman K, Sato M, Katsuki H, Kawashima K, et al. Absorption, distribution, metabolism and excretion (ADME) of the ALK inhibitor alectinib: results from an absolute bioavailability and mass balance study in healthy subjects. Xenobiotica. 2017;47:217–29.

13. Abou-Alfa GK, Lewis LD, LoRusso P, Maitland M, Chandra P, Cheeti S, et al. Pharmacokinetics and safety of vismodegib in patients with advanced solid malignancies and hepatic impairment. Cancer Chemother Pharmacol. 2017;80:29–36.

14. Rood JJM, Bussel MTJ Van, Schellens JHM, Beijnen JH, Sparidans RW. Liquid chromatography – tandem mass spectrometric assay for the T790M mutant EGFR inhibitor osimertinib (AZD9291) in human plasma. J Chromatogr B. 2016;1031:80–5.

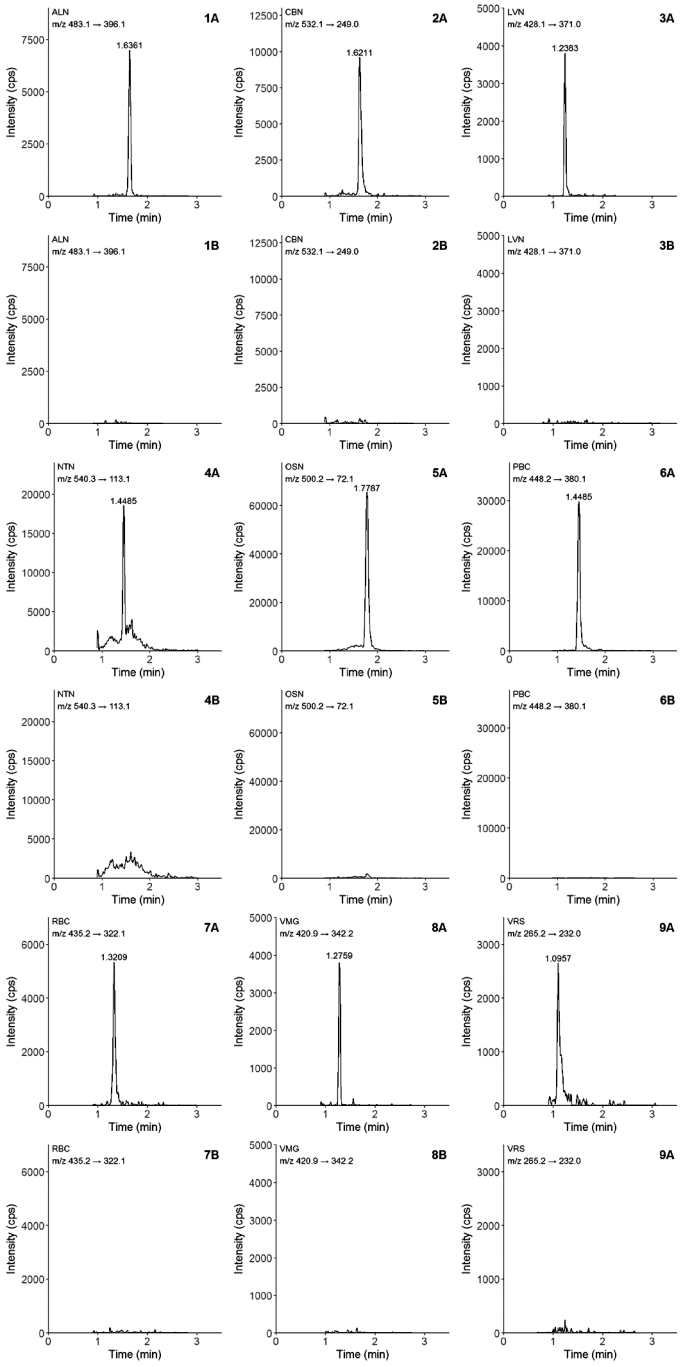

Figure S1. Representative LC-MS/MS chromatograms of processed LLOQ samples (A) and their respective double blank samples (B), for alectinib (1, ALN), cobimetinib (2, CBN), lenvatinib (3, LVN), nintedanib (4, NTN), osimertinib (5, OSN), palbociclib (6, PBC), ribociclib (7, RBC), vismodegib (8, VMG) and vorinostat (9, VRS).



Chapter 4.2

Evaluation of extrapolation methods to predict trough concentrations to guide therapeutic drug monitoring of oral anticancer drugs

Submitted

J.M. Janssen
T.P.C. Dorlo
J.H. Beijnen
A.D.R. Huitema

Abstract

Introduction

For kinase inhibitors used in oncology, the trough concentration (C_{min}) is usually used as target for therapeutic drug monitoring (TDM). In clinical practice, collecting trough samples is highly challenging in outpatients, with typically large variability in time after dose of the collected sample. In order to estimate C_{min} from the concentration in the randomly collected sample, various methods are used in clinical practice. This simulation study aims to evaluate the predictive performance of three different methods to estimate the C_{min} in individual patients, exemplified by four oral anticancer drugs for which TDM is regularly performed.

Methods

Published population PK models for abiraterone, dabrafenib, imatinib and pazopanib were used to simulate a single plasma concentration at a random time ($C_{t,sim}$) and at the end of the dosing interval ($C_{min,sim}$) for 1000 patients. These simulated predicted concentrations were converted into simulated observed concentrations ($C_{t,sim,obs}$ and $C_{min,sim.obs}$, respectively) by adding residual error. From the simulated plasma concentration at random time points ($C_{t,sim,obs}$) values for C_{min} ($C_{min,pred}$) were predicted using Bayesian estimation (1), by taking the ratio of the $C_{t,sim,obs}$ and typical population concentration and multiplying this ratio with the typical population value of $C_{min,sim}$ (2), and log-linear extrapolation (3). Bias and precision were assessed by comparing $C_{min,pred}$ to $C_{min.sim}$. As best case scenario $C_{min,sim,obs}$ was compared to $C_{min,sim}$. Target attainment was assessed by comparing $C_{min,pred}$ to proposed PK targets related to efficacy and calculating the positive and negative predictive value (PPV and NPV, respectively).

Results

Bayesian estimation and the concentration ratio showed similar performance and out-performed log-linear extrapolation. Sampling of the $C_{min,sim,obs}$ was also associated with some degree of imprecision due to residual error. In addition, target attainment in terms of PPV was adequately predicted by all three methods (92.1%, 92.5% and 93.1% for method I, II and II, respectively for abiraterone, 87.3% (I), 86.9% (II) and 99.1% (III) for dabrafenib, 79.3% (I), 79.3% (II) and 75.9% (III) for imatinib and 72.5% (I), 73.5% (II) and 67.6% (III) for pazopanib), meaning that dose adjustments would be correctly predicted.

Conclusion

Both Bayesian estimation and the concentration ratio provide accurate and precise individual $C_{min,pred}$ values. The concentration ratio extrapolation method is easier to implement compared to Bayesian estimation to guide individual dose adjustments in TDM programs.

Introduction

In recent years new targeted small molecule kinase inhibitors (KI) have become available for the treatment of patients with several types of cancer. These KIs are targeted against specific molecular defects that are expressed by malignant cells. Exposure-efficacy relationships can be expected for these anticancer drugs. It has been shown that exposure may show considerable variability between patients for many of these orally administered drugs due to both patient specific factors, such as genetics, concomitant intake of food, as well as the fixed dosing strategy and co-administration of other drugs.(1–3) This may result in treatment failure as a result of underdosing.(2)

Therapeutic drug monitoring (TDM) is based on the quantification of individual exposure and interpretation of this exposure with respect to proposed target exposures for any type of treatment response. Subsequently, dose individualizations may be applied in order to improve target attainment.(4–6) TDM has proven its benefits in treatment optimization in terms of minimal target attainment related to clinical efficacy of many oral anticancer drugs and indications.(7–10) Target exposure in oncology is most commonly defined by exposure-efficacy analyses using the trough concentration (C_{min}) as pharmacokinetic (PK) parameter for minimal target attainment.

Oral KIs are mostly used by outpatients, patient blood samples are therefore typically collected at any time point within a dosing interval when patients are in the hospital for regular visits. As this is not the exact C_{min}, extrapolation to the C_{min} is required. Several methods for extrapolation of a single individual plasma concentration at a variable time point after dose to C_{min} have been proposed. Model-based methods using population PK models have been suggested.(11–13) These methods should provide good predictive performance and enable the use of an individual plasma concentration sampled at variable times after dose. A method in which the individual C_{min} is derived based on the ratio of the individual plasma concentration at variable time point after dose versus a population mean concentration at that same time point could also be considered. In addition, a log-linear extrapolation approach that uses the typical value of the elimination rate constant has been reported by Wang et al.(14)

The aim of the here presented simulation study is to explore the predictive performance of different extrapolation methods for the determination of the C_{min} in individual patients in terms of target attainment, bias and precision. To this end we applied these extrapolation methods for TDM to the four widely used oral anticancer drugs abiraterone, dabrafenib, imatinib en pazopanib.

Methods

Extrapolation methods

Population PK models for abiraterone, dabrafenib, imatinib and pazopanib were obtained from literature (Table 1).(15–18) A densely sampled steady-state concentration-time curve was simulated for 1000 individual patients using these models at the approved dose (1000 mg once-daily (OD), 150 mg twice-daily (BID), 400 mg OD and 800 mg OD for abiraterone, dabrafenib, imatinib and pazopanib, respectively). Any covariate effects, if reported in the model, were fixed to their reference value. From the individual concentration-time curves, a random time point during a dosing interval and corresponding concentration were randomly sampled ($C_{t,sim}$). These simulation results were used in the following three extrapolation methods.

- Method 1. Deriving the empirical Bayes PK parameter estimates using NONMEM with MAXEVAL=0 in order to obtain the individual predicted C_{min} ($C_{min,pred}$) based on the randomly sampled $C_{t,sim}$.

- Method 2. Approximation of $C_{min,pred}$ by taking the ratio of C_{obs} versus the population concentration based on a population PK model and multiply this ratio with the simulated population $C_{min,sim}$.

- Method 3. Log-linear extrapolation using the algorithm as previously proposed (14):

$$C_{min,pred} = C_{t,sim} \times 0.5^{\left(\frac{\tau - TAD}{t_{1/2}}\right)} \quad \text{(Eq.1)}$$

where is the dosing interval (24 hours for abiraterone, imatinib and pazopanib and 12 hours for dabrafenib), TAD is the time of $C_{t,sim}$ after last administered dose and $t_{1/2}$ is the reported elimination half-life (16 hours for abiraterone, 10 hours for dabrafenib, 18 hours for imatinib and 31 hours for pazopanib).(15,18–20)

All three extrapolation methods were explored for two scenarios:

A. Timing of $C_{t,sim}$ randomly sampled between T_{max} (2 hours for abiraterone, 2 hours for dabrafenib, 2.5 hours for imatinib and 4 hours for pazopanib) and the end of the dosing interval (12 hrs for dabrafenib and 24 hrs for abiraterone, imatinib and pazopanib).(21–24)
B. Random sampling from 0.5 hours after intake until the end of the dosing interval.

In addition, the true $C_{min,sim,obs}$ at the end of the dosing interval was simulated. The concentration in this sample is also expected to be associated with random residual error, so also this concentration should be regarded as a prediction of the true Cmin.

Evaluation of predictive performance

Predictive performance was assessed in terms of bias relative prediction error (RPE) and mean relative prediction error (MPE)) and precision (root mean squared relative prediction error (RMSE))(25):

$$RPE = \frac{(C_{min,pred} - C_{min,sim})}{C_{min,sim}} \quad \text{(Eq.2)}$$

$$RMSE\ (\%) = \sqrt{\frac{\sum_{i=0}^{n}(\frac{C_{min,pred} - C_{min,sim}}{C_{min,sim}})}{n}} \times 100\% \quad \text{(Eq.3)}$$

In order to determine these measures, the $C_{min,sim}$ was used as the true trough concentration. In addition, the positive predictive value (PPV) was used to evaluate how often the $C_{min,pred}$ is truly above the PK efficacy target. The negative predictive value (NPV) was calculated to evaluate whether $C_{min,pred}$ is truly below the PK efficacy target. The following previously proposed minimal PK targets that were related to improved efficacy of treatment were used: C_{min} > 8.4 ng/mL for abiraterone, C_{min} > 46.6 ng/mL for dabrafenib, C_{min} > 1100 ng/mL for imatinib and C_{min} > 20 mg/L for pazopanib.(5)

Software

Simulation and estimation was performed using NONMEM® (version 7.3, ICON Development Solutions, Ellicott City, MD, USA) and Perl-speaks-NONMEM (PsN, version 4.4.8) with First-Order Conditional Estimation with interaction (FOCE-I) as estimation method.(26) R (version 3.4.3) was used for data processing, calculations and graphical diagnostics.(27)

Results

Abiraterone

The population PK model for abiraterone that was used for the simulations was a two-compartment model with absorption through transit compartments and sequential zero- and first-order absorption processes. Inter-individual variability was included for apparent clearance (CL/F), bioavailability (F), the first-order absorption rate (k_a) and the duration of zero-order absorption (D1) (Table 1).(15)

The goodness-of-fit (GOF) plots for abiraterone show that the log-linear extrapolation method resulted in a structural overprediction of $C_{min,pred}$ for both sampling intervals. For the Bayesian estimation and concentration ratio, an overprediction was present for the lower true $C_{min,sim}$ values (figures 1-4). This overprediction appears worsened when the single samples were collected at a variable time point during the entire dosing interval (figure 4 and 6). In addition, plots of the RPE show a trend towards positive outliers as depicted in figure 2 and 3. These plots particularly show the overprediction by log-linear extrapolation.

Table 1. Summary of identified population PK models and parameter estimates used in the simulations for the evaluation of the four extrapolation methods

	Base model structure	Parameter estimates	Inter-individual variability (CV%)	Covariate relationships	Refe-rences
Abiraterone	Two-compartment, transit compartments, sequential zero- and first-order absorption	K_a = 1.91 h^{-1} D1 = 0.267 h F = 1.24[a] V_c = 5620 L Q = 1360 L/h V_p = 17400 L CL = 1550 L/h	K_a = 58.0% D1 = 144% F = 61.1% CL = 28.2%	mCRPC/healthy subjects, food effect	(15)
Dabrafenib	Two-compartment, first-order absorption, lag-time, dose-dependent clearance	K_a = 1.8 h^{-1} T_{lag} = 0.482 h V_c/F = 69.1 L Q/F = 3.44 L/h V_p/F = 149 L CL/F = 98.8 L/h	K_a = 160% V_c/F = 54.1% Q/F = 102% CL/F = 60.8%	Weight, sex, drug formulation, last administered dose	(18)
Imatinib	One-compartment, zero-order absorption, linear elimination	D1 = 1.7 h V_c/F = 284 L CL/F = 10.2 L/h	V_c/F = 35.8% CL/F = 34.6%	Albumin, WBC	(16)
Pazopanib	Two-compartment, fast and slow first-order absorption, dose-dependent bioavailability	$K_{a,fast}$ = 0.40 h^{-1} $K_{a,slow}$ = 0.12 h^{-1} $T_{lag,slow}$ = 0.98 h V_c = 2.43 L Q = 0.99 L/h V_p/F = 25.1 L CL/F = 0.27 L/h	K_a = 140% F = 35.6% V_p/F = 98.2% CL/F =30.9%	Dose	(17)

Abbreviations: K_a, first-order absorption rate constant; D1, zero-order absorption duration; F, bioavailability; CL, apparent clearance; V_c, central volume of distribution; Q, inter-compartmental clearance; V_p, peripheral volume of distribution; T_{lag}, lag-time; mCRPC, metastatic castration resistant prostate cancer; WBC, white blood cell count.
[a] F for modified fasted conditions (i.e. fasting 2 hours before to 1 hour after dosing).

Measures of the predictive performance of the three extrapolation methods are presented for sampling scenarios A and B, in Table 2 and 3, respectively. Comparison of the three methods showed that Bayesian estimation had similar performance compared with the concentration ratio in terms of both bias (MPE) and precision (RMSE), regardless of the sampling interval. These methods performed slightly worse compared to sampling at C_{min} but clearly out-performed the log-linear extrapolation. These differences in bias and precision in $C_{min,pred}$ did not result in marked differences in the PPV between Bayesian estimation, the concentration ratio and log-linear extrapolation. In addition, sampling at C_{min} results in a slightly higher PPV compared to the three extrapolation methods. The NPV did however show differences between these three methods. Meaning that the $C_{min,pred}$ is truly above the PK target to the same extent but the log-linear extrapolation performs worse in predicting a $C_{min,pred}$ that is truly below the PK target.

Table 2. Predictive performance of the three different extrapolation methods for a sample collected after T_{max} compared to sampling at the end of the dosing interval (scenario A)

Parameter	Bayesian estimation (1)	Concentration ratio (2)	Log-linear extrapolation (3)	Sampling
Abiraterone				
MPE (ng/mL)	7.52	7.89	25.4	5.74
RMSE (%)	37.4	37.3	72.0	28.3
PPV (%)	92.1	92.5	93.1	94.6
NPV (%)	78.5	78.8	71.5	84.8
Dabrafenib				
MPE (ng/mL)	1.05	2.08	177	2.43
RMSE (%)	67.2	61.3	443	27.8
PPV (%)	87.3	86.9	99.1	93.8
NPV (%)	68.1	68.5	33.1	88.5
Imatinib				
MPE (ng/mL)	3.82	3.89	0.976	2.93
RMSE (%)	27.1	27.2	26.1	26.9
PPV (%)	79.3	79.3	75.9	81.5
NPV (%)	80.0	80.0	82.4	82.7
Pazopanib				
MPE (mg/L)	4.73	3.93	-1.05	3.39
RMSE (%)	30.8	30.6	28.8	26.4
PPV (%)	72.5	73.5	67.6	73.5
NPV (%)	95.5	95.7	97.0	93.7

Abbreviations: MPE, mean prediction error; RMSE, relative root mean squared error; PPV, positive predictive value; NPV, negative predictive value.

Dabrafenib

For dabrafenib, a two-compartment model with first-order absorption following a lag time, dose-dependent clearance and inter-individual variability on CL_0/F, apparent central volume of distribution (V_c/F), apparent inter-compartmental clearance (Q/F) and k_a was used (Table 1).(18)

Figures 1-6 show a wide spread in RPE and large overpredictions of the lower $C_{min,sim}$ for dabrafenib for all three extrapolation methods. MPE and RMSE were high for Bayesian estimation, the concentration ratio and in particular for the log-linear extrapolation. These results improve only slightly when samples are collected after T_{max} compared to sample collection during the entire dosing interval. Still, Bayesian estimation showed a higher RMSE compared to the concentration-ratio and sampling at the end of the dosing interval. Additional simulations with shorter sampling intervals

Table 3. Predictive performance of the three different extrapolation methods for a sample collected during the complete dosing interval compared to sampling at the end of the dosing interval (scenario B)

Parameter	Bayesian estimation (1)	Concentration ratio (2)	Log-linear extrapolation (3)	Sampling
Abiraterone				
MPE (ng/mL)	5.76	6.17	45.1	5.74
RMSE (%)	40.2	44.0	125	28.3
PPV (%)	91.2	90.1	90.3	94.6
NPV (%)	78.5	78.5	65.2	84.8
Dabrafenib				
MPE (ng/mL)	4.02	2.83	243	2.43
RMSE (%)	83.0	76.6	615	27.8
PPV (%)	87.7	81.8	97.4	93.8
NPV (%)	62.7	69.2	35.0	88.5
Imatinib				
MPE (ng/mL)	3.73	3.82	-0.945	2.93
RMSE (%)	27.1	27.2	26.9	26.9
PPV (%)	78.4	78.4	72.7	81.5
NPV (%)	79.7	79.5	82.6	82.7
Pazopanib				
MPE (mg/L)	6.27	5.47	4.73	3.39
RMSE (%)	35.5	35.5	38.0	26.4
PPV (%)	72.5	73.5	71.6	73.5
NPV (%)	95.3	95.1	94.9	93.7

Abbreviations: MPE, mean prediction error; RMSE, relative root mean squared error; PPV, positive predictive value; NPV, negative predictive value.

were performed. When samples were collected from 6 hours and 9 hours after dabrafenib intake until the next intake, predictive performance improved considerably (detailed results in supplementary material). Nevertheless, the log-linear extrapolation still performed worse compared to the other two extrapolation methods and compared to sampling at the end of the dosing interval, while Bayesian estimation and the concentration ratio showed similar performance. When the sampling interval is reduced to sampling between 9 and 12 hours after intake, similar results for predictive performance were observed for all four methods. The differences in MPE and RMSE did not result in large differences in target attainment between the three extrapolation methods. Log-linear extrapolation results in the highest PPV and lowest NPV. When samples are collected between 6 and 12 hours after intake, all four methods showed similar results with regard to the PPV.

Imatinib

The population PK model for imatinib that was used was a one-compartment model with linear elimination from the central compartment. Inter-individual variability was included on the parameters for V_c/F and CL/F (Table 1).(16)

For imatinib, both the GOF plots (figure 3-6) and the RPE (figure 1-2) show an adequate prediction of the $C_{min,sim}$ by all three extrapolation methods. The three extrapolation methods resulted in similar predictive performance as shown by the MPE and RMSE in Tables 2 and 3. Similar performance was observed for the three extrapolation methods compared to sampling at the end of the dosing interval. In addition, no noteworthy differences in PPV and NPV were observed between the methods. Sampling at the end of the dosing interval showed the highest PPV and NPV, followed by Bayesian estimation and the concentration ratio. The extrapolation interval did not seem to affect the predictive performance of any of the methods, which demonstrates that the three methods provide good predictions when a sample is collected at various time points during the entire dosing interval.

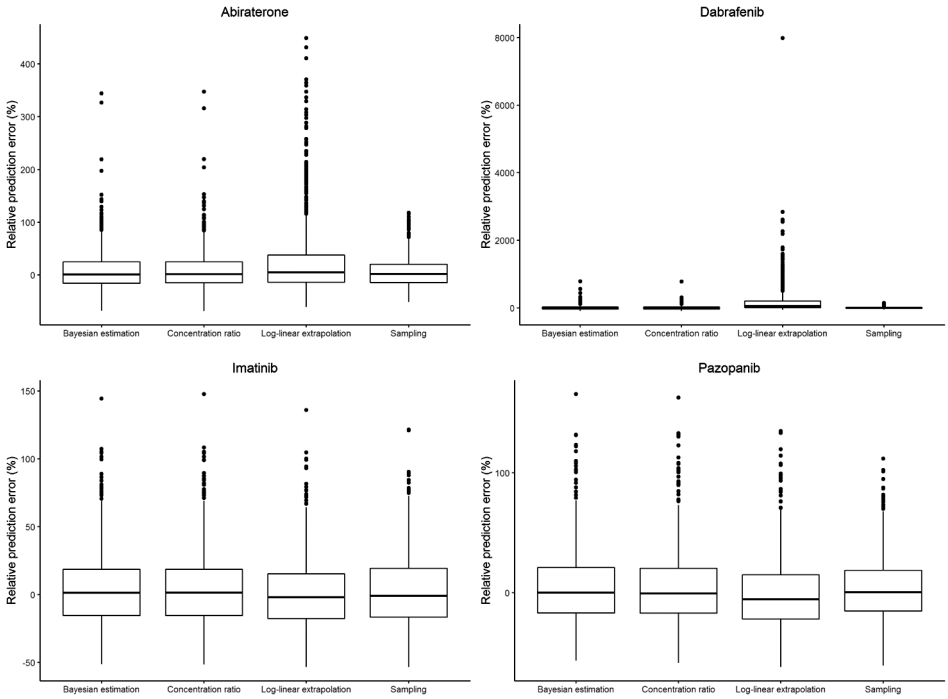

Figure 1. Relative prediction error of $C_{min,pred}$ for the three extrapolation methods for abiraterone, dabrafenib, imatinib and pazopanib for a sample collected after T_{max} compared to sampling at the end of the dosing interval (scenario A)

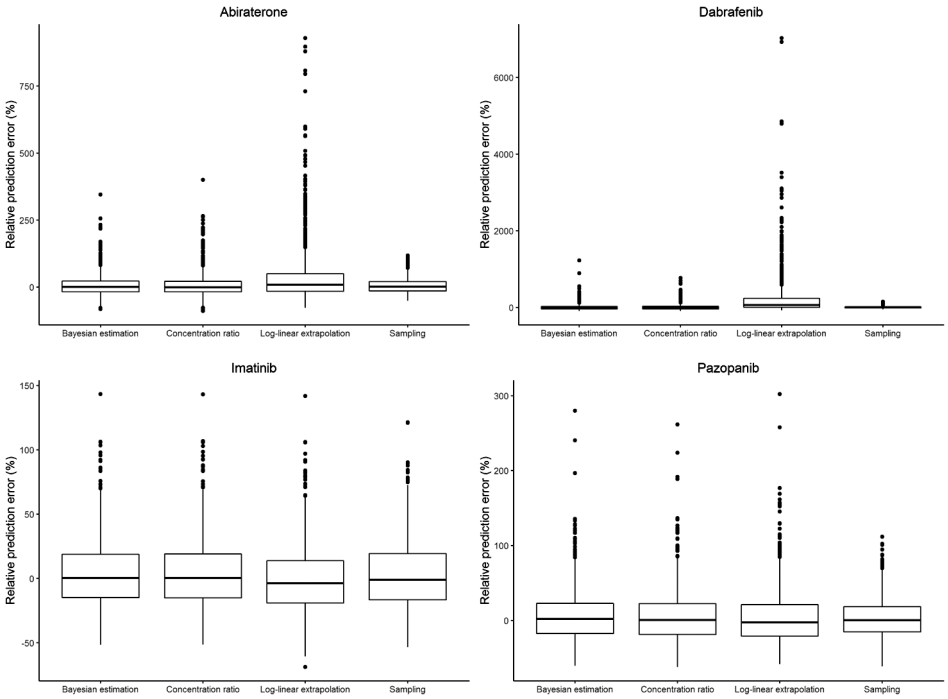

Figure 2. Relative prediction error of $C_{min,pred}$ for the three extrapolation methods for abiraterone, dabrafenib, imatinib and pazopanib for a sample collected during the complete dosing interval compared to sampling at the end of the dosing interval (scenario B).

Pazopanib

A two-compartment model with fast and slow first-order absorption processes, dose-dependent bioavailability and inter-individual variability for K_a, CL/F, peripheral volume of distribution (V_p/F) and F was previously published and used for the simulations (Table 1).(17)

The simulation results for pazopanib showed a slight overprediction of the lower $C_{min,sim}$ values for the Bayesian estimation, concentration ratio and log-linear extrapolation (figure 3-6). This overprediction was reduced when samples were only collected after T_{max}. Bias (MPE) and precision (RMSE) were comparable and adequate for all three extrapolation methods (Table 2 and 3). Nevertheless, large variability in RPE was observed (figure 1-2). The adequate bias and precision resulted in an adequate NPV for all four methods, therefore dose adjustments will be recommended when needed. The PPV showed, however, that the log-linear extrapolation method would result in more $C_{min,pred}$ values falsely classified as above the PK target for efficacy, which would result in a continuation of the dose while a dose increase should have been advised. In additional simulations the sampling interval was shortened to the last 6 and 3 hours

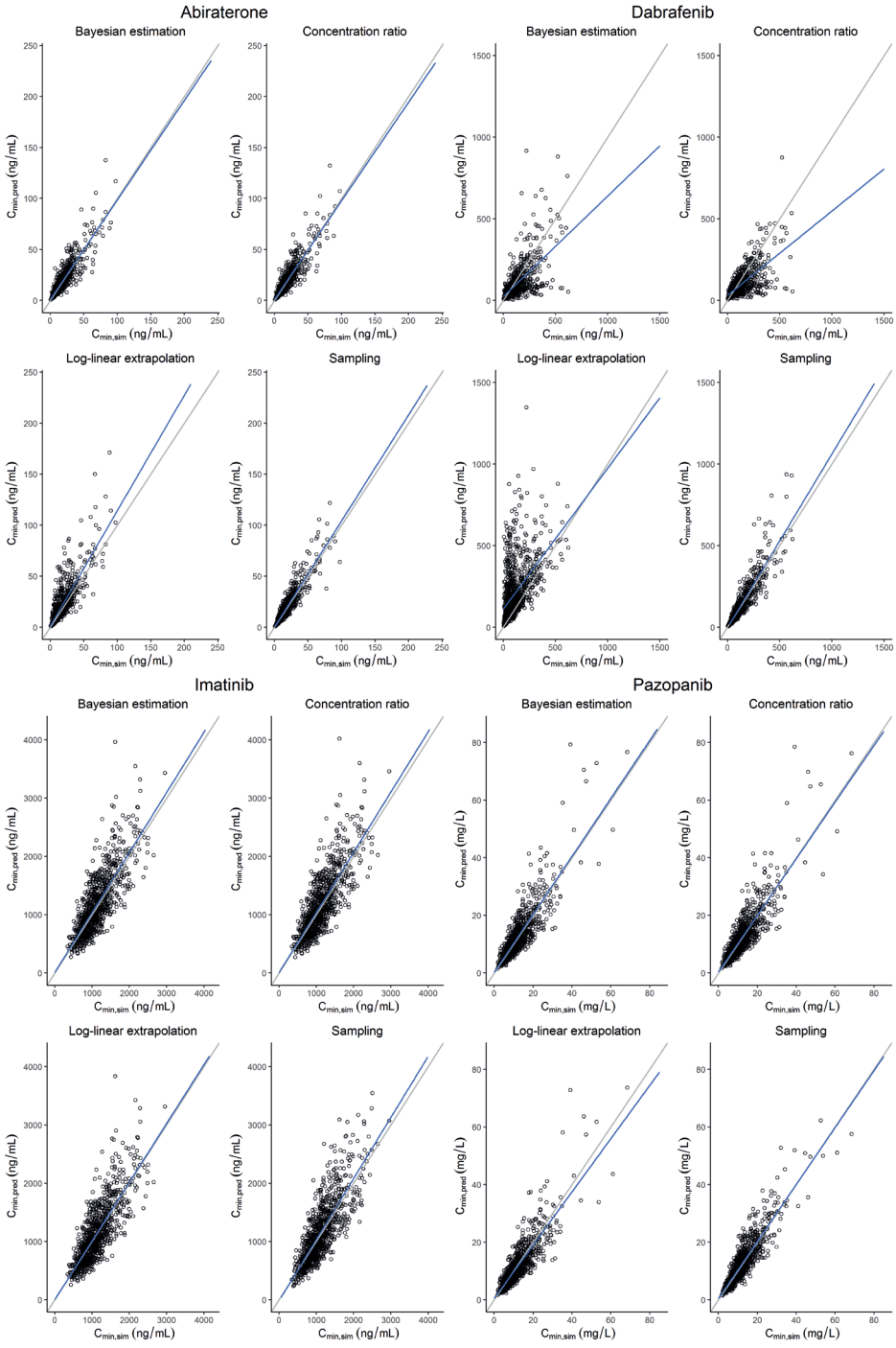

Figure 3. Goodness-of-fit plots of $C_{min,pred}$ versus $C_{min,sim}$ for the three extrapolation methods for abiraterone, dabrafenib, imatinib and pazopanib for a sample collected after T_{max} (scenario A) compared to sampling at the end of the dosing interval

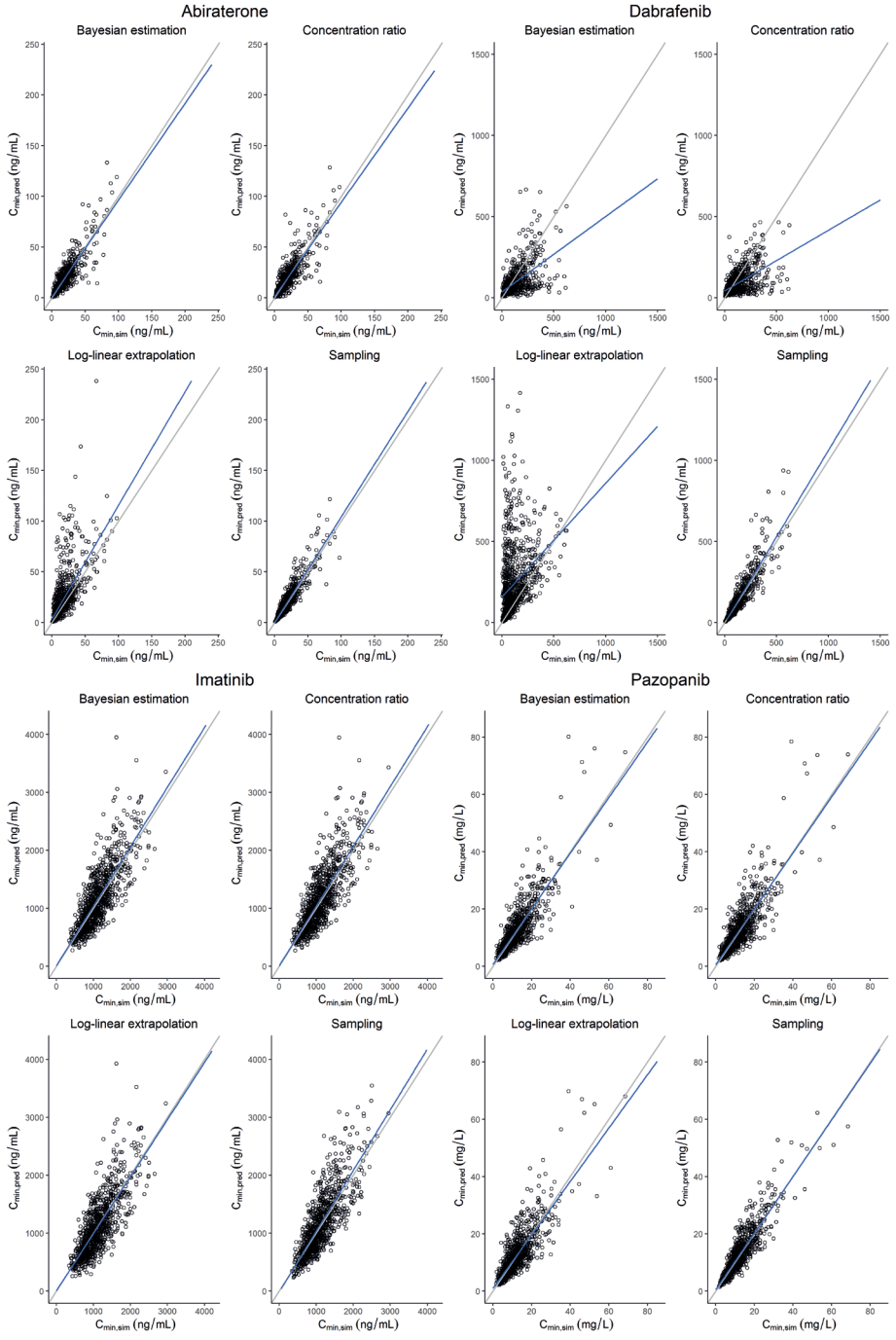

Figure 4. Goodness-of-fit plots of of $C_{min,pred}$ versus $C_{min,sim}$ for the four extrapolation methods for abiraterone, dabrafenib, imatinib and pazopanib for a sample collected during the complete dosing interval (scenario B).

before the next pazopanib intake. These simulations showed a further decrease in over-prediction and improved bias, precision, PPV and NPV (detailed results in supplementary material). In addition, all three extrapolation methods showed similar performance compared to each other and when compared to sampling at the end of the dosing interval.

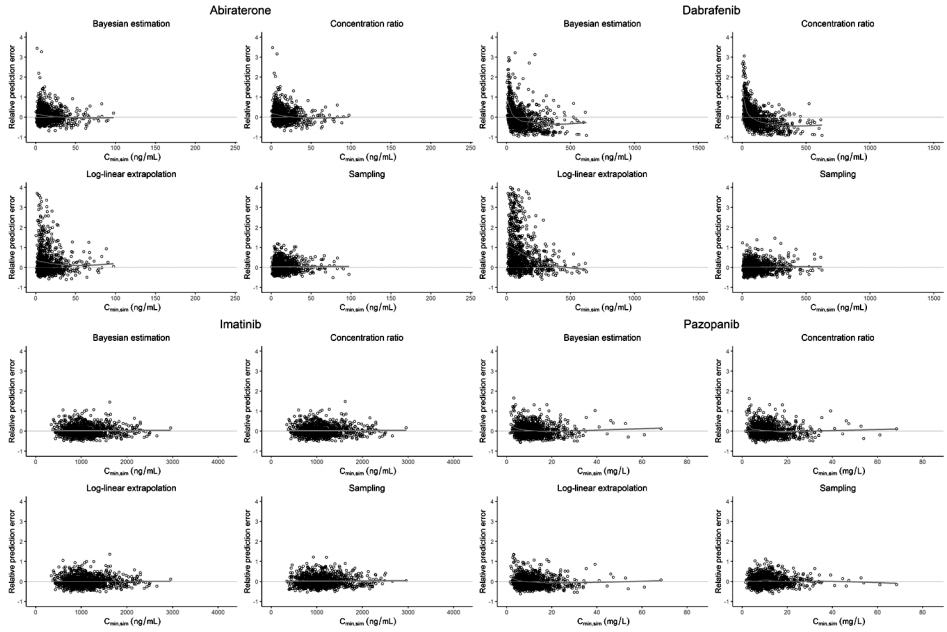

Figure 5. Relative prediction error of $C_{min,pred}$ versus $C_{min,sim}$ for the four extrapolation methods for abiraterone, dabrafenib, imatinib and pazopanib for a sample collected after T_{max} (scenario A).

Discussion

With this work we have evaluated three extrapolation methods for the determination of the $C_{min,pred}$ based on a single measured concentration, sampled with different scenario's. This was compared to the best case scenario in which a sample at the end of the dosing interval was collected. As this sample is also associated with random residual error, this still results in an imperfect estimate of the true $C_{min,sim,obs}$.

Bayesian estimation of the individual $C_{min,pred}$ should have several advantages over other simpler extrapolation approaches. It allows handling of deviations from the planned or registered sampling times. In addition, model-informed TDM enables the prediction of expected exposure after a dose adjustment has been implemented.(12,13) Our results show that Bayesian estimation does not result in superior performance

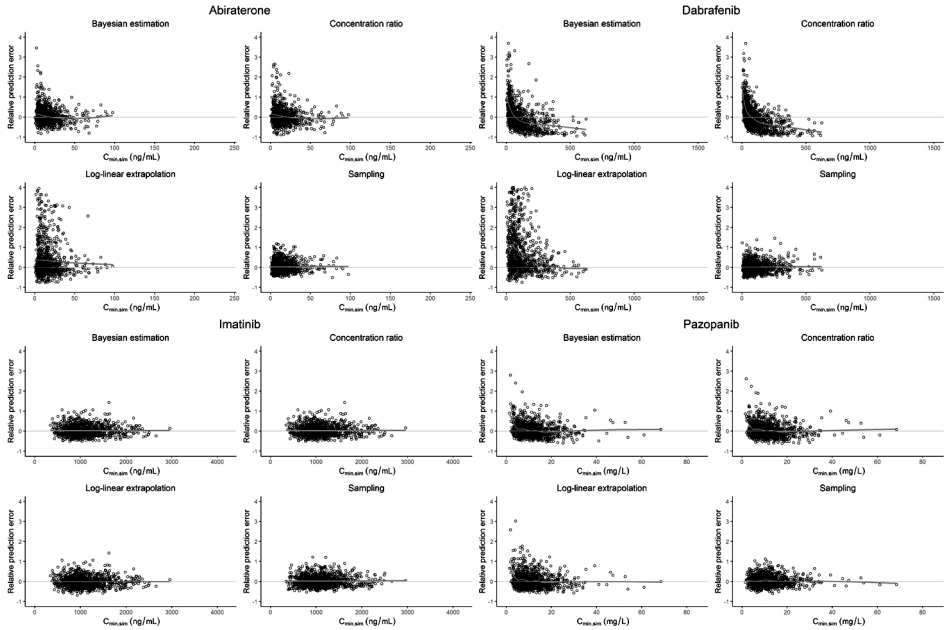

Figure 6. Relative prediction error of $C_{min,pred}$ versus $C_{min,sim}$ for the four extrapolation methods for abiraterone, dabrafenib, imatinib and pazopanib for a sample collected during the complete dosing interval (scenario B).

compared to using the concentration ratio in terms of bias, precision and target attainment. This method does, however, show a better performance compared to the log-linear extrapolation. Even when samples are collected over the entire dosing interval, Bayesian estimation shows similar performance compared to the concentration ratio.

The imatinib PK was characterized by a one-compartment PK model. All three extrapolation methods showed similar bias, precision and target attainment, including log-linear extrapolation. Nevertheless, the log-linear extrapolation method performed worse in terms of bias and precision (MPE and RMSE) for abiraterone, dabrafenib and pazopanib for which the PK was described by more complex two-compartment models. More specific, lower $C_{min,sim}$ values were typically overpredicted by the log-linear extrapolation method. The MPE and RMSE were higher for this method, but this did not result in a marked difference in target attainment. The PPV reflects the percentage of $C_{min,pred}$ truly being above the pre-specified PK target. A higher PPV thus indicates less false positives for which a dose adjustment is not advised while this would have been indicated. In clinical practice, this is the most important measure for an adequate extrapolation method.

Bias, precision and target attainment were similar for all three drugs when comparing Bayesian estimation with the concentration ratio. Bayesian estimation did, however, result in an overprediction of low $C_{min,sim}$ values for abiraterone, dabrafenib and pazopanib. In these PK models, high inter-individual variability is present, therefore, individual predictions will shrink towards the typical value as a result of the extremely sparse sampling. As the lower $C_{min,sim}$ values are extreme values, their Bayesian estimates will be weighted towards the typical concentration. The effect of this shrinkage was shown to decrease when samples are taken closer towards the time of C_{min}. The concentration-ratio uses the ratio between the measured patient concentration and the population concentration at the same time point and multiplies this ratio with the population $C_{min,sim}$. Hence, this method does not require estimation by nonlinear mixed-effects software, therefore, be easier to implement this method in clinical practice. In addition, this extrapolation method resulted in similar performance for all four drugs investigated in our study.

A previous report on the development of a Bayesian approach for imatinib TDM showed a wide range in RPE when log-linear extrapolation was used and concluded that Bayesian estimation is a suitable method for the prediction of individual imatinib trough concentrations. This research focused on imatinib alone and did not explore the concentration-ratio as an extrapolation method. Our results show that all three methods provided suitable predictions for imatinib. Taken all our results together it should be noted that the population PK model for imatinib is characterized by moderate inter-individual variability and might therefore not reflect the majority of oral anti-cancer drugs that are currently being used in clinical practice.

Conclusion

In conclusion, our study shows that using the concentration ratio of a concentration at a variable time point within the dosing interval versus the population median concentration and multiplying this with the population $C_{min,sim}$ (method 2) provides accurate and precise individual predictions as well as Bayesian estimation (method 1) for the here presented four KIs. The concentration ratio extrapolation method is easier to implement. When a drugs PK parameters are characterized by large inter-individual variabilities it is additionally advised to narrow the sampling window to 3-6 hours before the next drug intake until the end of the dosing interval.

References

1. Terada T, Noda S, Inui K. Management of dose variability and side effects for individualized cancer pharmacotherapy with tyrosine kinase inhibitors. Pharmacol Ther. 2015;152:125–34.

2. Gao B, Yeap S, Clements A, Balakrishnar B, Wong M, Gurney H. Evidence for therapeutic drug monitoring of targeted anticancer therapies. J Clin Oncol. 2012;30(32):4017–25.

3. Widmer N, Bardin C, Chatelut E, Paci A, Beijnen J, Levêque D, et al. Review of therapeutic drug monitoring of anticancer drugs part two--targeted therapies. Eur J Cancer. 2014;50:2020–36.

4. Yu H, Steeghs N, Nijenhuis CM, Schellens JHM, Beijnen JH, Huitema ADR. Practical guidelines for therapeutic drug monitoring of anticancer tyrosine kinase inhibitors: Focus on the pharmacokinetic targets. Clin Pharmacokinet. 2014;53:305–25.

5. Verheijen RB, Yu H, Schellens JHM, Beijnen JH, Steeghs N, Huitema ADR. Practical Recommendations for Therapeutic Drug Monitoring of Kinase Inhibitors in Oncology. Clin Pharmacol Ther. 2017;102:765-776.

6. Groenland SL, van Nuland M, Verheijen RB, Schellens JHM, Beijnen JH, Huitema ADR, et al. Therapeutic Drug Monitoring of Oral Anti-Hormonal Drugs in Oncology. Clin Pharmacokinet. 2018;58:299-308.

7. De Wit D, Guchelaar HJ, Den Hartigh J, Gelderblom H, Van Erp NP. Individualized dosing of tyrosine kinase inhibitors: Are we there yet? Drug Discov Today. 2015;20:18–36.

8. Verheijen RB, Bins S, Mathijssen RHJ, Lolkema M, van Doorn L, Schellens JHM, et al. Individualized pazopanib dosing: a prospective feasibility study in cancer patients. Clin Cancer Res. 2016;22:5738-5746.

9. Lankheet NAG, Kloth JSL, Gadellaa-van Hooijdonk CGM, Cirkel GA, Mathijssen RHJ, Lolkema MPJK, et al. Pharmacokinetically guided sunitinib dosing: a feasibility study in patients with advanced solid tumours. Br J Cancer. 2014;110:2441–9.

10. Zuidema S, Desar IME, van Erp NP, Kievit W. Optimizing the dose in patients treated with imatinib as first line treatment for gastrointestinal stromal tumours: A cost-effectiveness study. Br J Clin Pharmacol. 2019;85:1994–2001.

11. Rousseau A, Marquet P, Debord J, Sabot C, Lachâtre G. Adaptive control methods for the dose individualisation of anticancer agents. 2000;38:315-53.

12. Rousseau A, Marquet P. Application of pharmacokinetic modelling to the routine therapeutic drug monitoring of anticancer drugs. Fundam Clin Pharmacol. 2002;16:253–62.

13. Darwich AS, Ogungbenro K, Vinks AA, Powell JR, Reny J-L, Marsousi N, et al. Why has model-informed precision dosing not yet become common clinical reality? lessons from the past and a roadmap for the future. Clin Pharmacol Ther. 2017;101:646–56.

14. Wang Y, Chia YL, Nedelman J, Schran H, Mahon F-X, Molimard M. A therapeutic drug monitoring algorithm for refining the imatinib trough level obtained at different sampling times. Ther Drug Monit. 2009;31:579–84.

15. Stuyckens K, Saad F, Steven X, Charles X, Smith MR, Griffin TW, et al. Population Pharmacokinetic Analysis of Abiraterone ¨ ve and Docetaxel-Treated Patients in Chemotherapy-Naı with Metastatic Castration-Resistant Prostate Cancer. Clin Pharmacokinet. 2014;53:1149–60.

16. Demetri GD, Wang Y, Wehrle E, Racine A, Nikolova Z, Blanke CD, et al. Imatinib plasma levels are correlated with clinical benefit in patients with unresectable/metastatic gastrointestinal stromal tumors. J Clin Oncol. 2009;27:3141–7.

17. Yu H, van Erp N, Bins S, Mathijssen RHJ, Schellens JHM, Beijnen JH, et al. Development of a Pharmacokinetic Model to Describe the Complex Pharmacokinetics of Pazopanib in Cancer Patients. Clin Pharmacokinet. 2016;17:1–11.

18. Ouellet D, Gibiansky E, Leonowens C, O'Hagan A, Haney P, Switzky J, et al. Population pharmacokinetics of dabrafenib, a BRAF inhibitor: Effect of dose, time, covariates, and relationship with its metabolites. J Clin Pharmacol. 2014;54:696–706.

19. Gotta V, Widmer N, Montemurro M, Leyvraz S, Haouala A, Decosterd LA, et al. Therapeutic drug monitoring of imatinib: Bayesian and alternative methods to predict trough levels. Clin Pharmacokinet. 2012;51:187–201.

20. Hurwitz HI, Dowlati A, Saini S, Savage S, Suttle AB, Gibson DM, et al. Phase I trial of pazopanib in patients with advanced cancer. Clin Cancer Res. 2009;15:4220–7.

21. Xtandi (INN-enzalutamide) product information [Summary of Product Characteristics]. Leiden, The Netherlands: Astellas Pharma Europe B.V.; 2013.

22. Tafinlar (INN-dabrafenib) product information [Summary of Product Characteristics]. Camberley, United Kingdom: Novartis Europharm Ltd, 2013.

23. CHMP. Glivec, INN-imatinib.

24. Votrient (INN-pazopanib) product information [Summary of Product Characteristcs]. Camberley, United Kingdom: Novartis Europharm Limited; 2010.

25. Sheiner LB, Beal SL. Some suggestions for measuring predictive performance. J Pharmacokinet Biopharm. 1981;9:503–12.

26. Beal S, Boeckmann A, Sheiner L (1988). NONMEM user guides. University of California, San Francisco.

27. Development Core Team R. R: A Language and Environment for Statistical Computing. Vienna, Austria: R Foundation for Statistical Computing; 2008.

Table S1. Predictive performance of the three different extrapolation methods compared to sampling at the end of the dosing interval for adjusted sampling intervals for dabrafenib.

Parameter	Bayesian estimation	Concentration ratio	Log-linear extrapolation	Sampling
Sampling from 6 hours after dose				
MPE (ng/mL)	4.54	9.73	51.0	2.43
RMSE (%)	46.1	49.2	105	27.8
PPV (%)	93.1	94.2	98.4	93.8
NPV (%)	73.1	70.8	48.1	88.5
Sampling from 9 hours after dose				
MPE (ng/mL)	6.87	8.10	16.0	2.43
RMSE (%)	34.8	34.0	40.2	27.8
PPV (%)	93.9	94.9	97.2	93.8
NPV (%)	81.9	79.2	73.8	88.5

Table S2. Predictive performance of the three different extrapolation methods compared to sampling at the end of the dosing interval for adjusted sampling intervals for pazopanib.

Parameter	Bayesian estimation	Concentration ratio	Log-linear extrapolation	Sampling
Sampling from 6 hours after dose				
MPE (ng/mL)	5.14	5.26	0.915	3.39
RMSE (%)	28.4	28.2	26.6	26.4
PPV (%)	76.5	76.5	74.5	73.5
NPV (%)	94.8	94.8	95.5	93.7
Sampling from 9 hours after dose				
MPE (ng/mL)	4.61	4.71	2.41	3.39
RMSE (%)	27.8	27.7	26.8	26.4
PPV (%)	76.5	76.5	75.5	73.5
NPV (%)	94.7	94.8	95.4	93.7

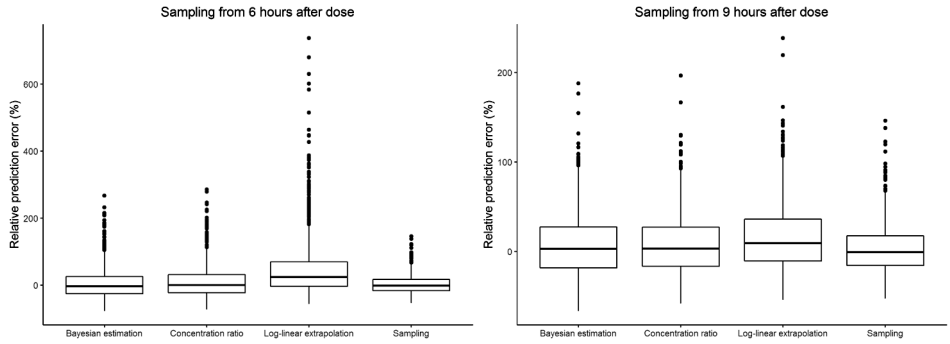

Figure S1. Relative prediction error of $C_{min,pred}$ for the three extrapolation methods for adjusted sampling intervals for dabrafenib.

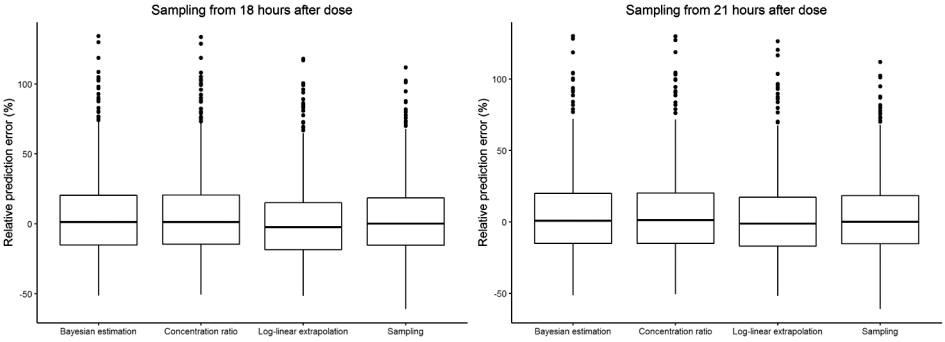

Figure S2. Relative prediction error of $C_{min,pred}$ for the three extrapolation methods for adjusted sampling intervals for pazopanib.

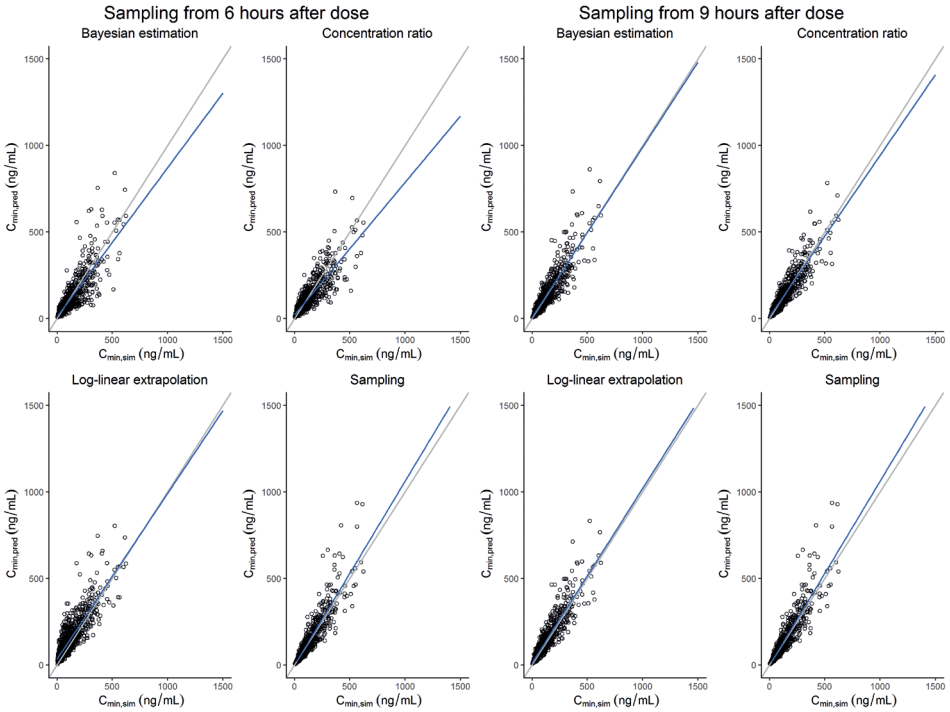

Figure S3. Goodness-of-fit plots of $C_{min,pred}$ versus $C_{min,sim}$ for the four extrapolation methods for adjusted sampling intervals for dabrafenib.

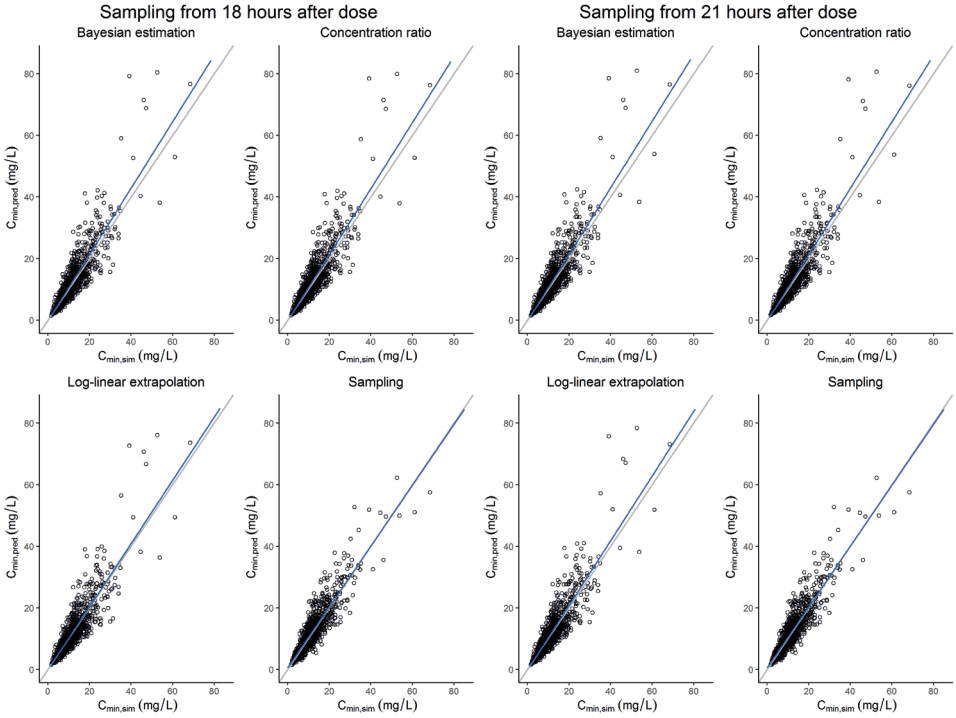

Figure S4. Goodness-of-fit plots of $C_{min,pred}$ versus $C_{min,sim}$ for the four extrapolation methods for adjusted sampling intervals for pazopanib.

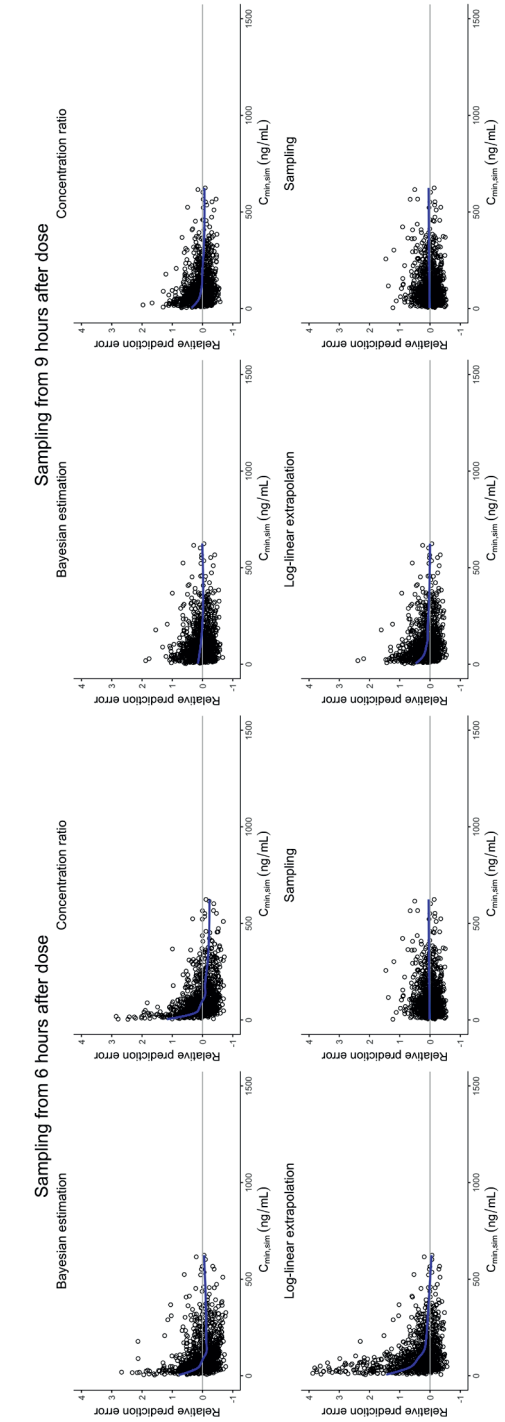

Figure S5. Relative prediction error of $C_{min,pred}$ versus $C_{min,sim}$ for the four extrapolation methods for adjusted sampling intervals for dabrafenib.

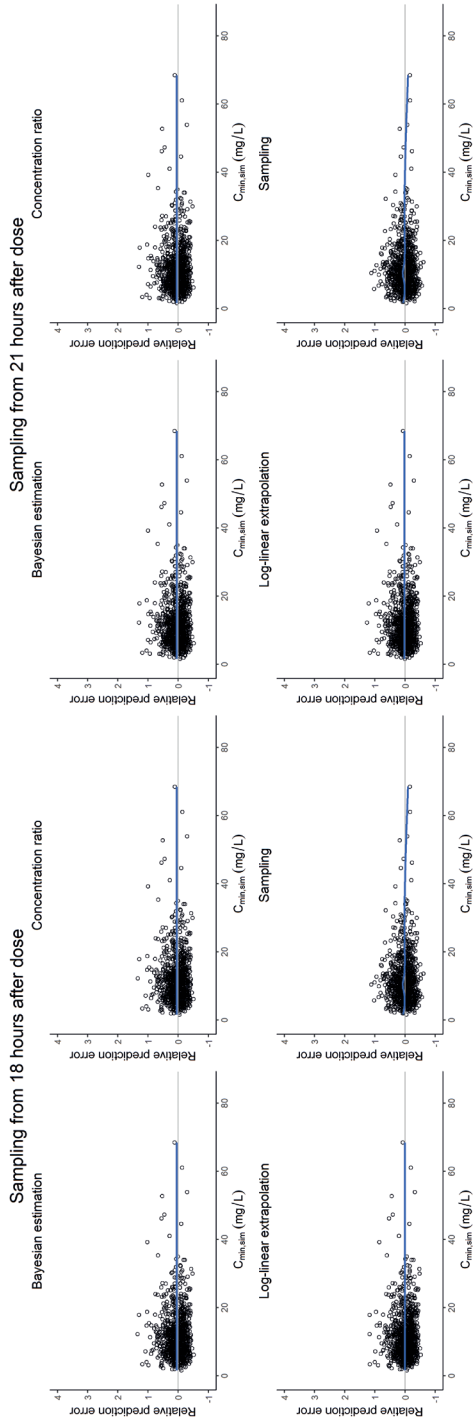

Figure S6. Relative prediction error of $C_{min,pred}$ versus $C_{min,sim}$ for the four extrapolation methods for adjusted sampling intervals for pazopanib.



Chapter 4.3

Tyrosine kinase inhibitor levels matter in treating chronic GVHD

Bone Marrow Transplant. 2019; 54: 1141-1144

L. van der Wagen
J.M. Janssen
R. Raijmakers
E. Petersen
M. de Witte
N. de Jong
M. Bellido
E. Meijer
B. Bär
J.J. Boelens
A.D.R. Huitema
J. Kuball

Key points

- *We observed a possible concentration effect relationship for nilotinib on resolution of chronic Graft versus Host Disease (cGVHD).*
- *These data suggest therapeutic drug monitoring might be useful for patients receiving tyrosine kinase inhibitors for cGVHD.*

Tyrosine kinase inhibitor levels matter in treating chronic GVHD

Graft versus Host Disease (GVHD) remains the major complication of allogeneic stem cell transplantation (allo-SCT) thereby limiting its widespread use despite many recent advances in transplantation techniques and management.(1) In particular, chronic GVHD (cGVHD) results in substantial mortality and reduced quality of life. Tyrosine kinase inhibition (TKI) using imatinib has shown clinical efficacy in cGVHD.(2–6) Other TKI's such as nilotinib as monotherapy or in combination with rituximab have been investigated.(7,8) Observed overall response rates of 25% (partial response after six months monotherapy nilotinib) and 71% (complete and partial response after sequential treatment of rituximab and nilotinib) were found.(7,8) Many kinase inhibitors show both exposure-response and exposure-toxicity relationships and consequently therapeutic drug monitoring is widely accepted and already applied in Chronic Myeloid Leukemia (CML) treatment.(9) Here we performed a retrospective analysis of samples obtained from our prospective clinical trial to study this relationship.(8)

In our prospective phase II clinical trial in patients with steroid refractory (SR) sclerotic cGVHD, patients were sequentially treated with 4 cycles of rituximab followed by six months of nilotinib 300 mg b.i.d. treatment.(8) A dose reduction to 200 mg b.i.d. was allowed when patients experienced side effects. The study was conducted in accordance with the Declaration of Helsinki and the protocol was reviewed by the local ethics committee. All patients provided written informed consent. This trial was registered at the Dutch clinical trial registry as NTR1222. During the study blood sampling at regular intervals was performed. Plasma samples were stored at -80˚C. Response was assessed after 13 months of follow-up. Nilotinib concentrations in plasma were determined using a validated high-performance liquid chromatography tandem mass spectrometry assay.(10) Trough levels were calculated using the algorithm proposed and validated by Wang *et al*.(11):

$$C_{min} = C_{measured} \times 0.5^{(\frac{\tau - TAD}{t_{1/2}})} \quad \text{(Eq.1)}$$

where is the dosing interval (i.e. 12 hours for nilotinib), TAD is the time since last dose and t1/2 is the nilotinib half-life (i.e. 17 hours). Samples drawn before the time point at which the maximal concentration is reached (i.e. 3 hours) or samples drawn more than 12 hours after the last dose were excluded from the analysis. Number of samples ranged from 1-4 per patient and were obtained at sampling times 2, 3, 5 or 7 months. For statistical analysis, for each patient the mean of the available trough levels were used. Twenty-nine patients were included in the clinical trial of which 24 were eligible

for response evaluation (Supplementary Table S1). In total, 17 patients (71%) showed a response (15 patients achieving a partial response and two patients a complete response). The remaining 7 patients were termed non-responders (6 patients had stable disease and 1 patient had progressive disease). The reference therapeutic range for nilotinib was 829-1500 µg/L, as used as reference in CML.

Nilotinib trough concentrations were available for 18 patients of 24 that completed the study (11 responders and 7 non-responders). Samples from remaining patients were unavailable due to practical reasons, 1 patient forgot to withhold his medication at time of sampling and from 1 patient the wrong tubes were sampled. Four remaining missing patients all used nilotinib less than one month due to side effects as described earlier and were therefor not sampled for trough concentrations.(8) Patients of whom trough concentrations were available all used nilotinib for a duration of 4,5-6 months (median 6 months). Nilotinib concentration in one patient was not measurable which indicated non-compliance. This patient was omitted from further analysis as he was already during the trial suspected of non-compliance due to erroneous medication administration. The number of samples did not differ between responders (median 2,5 and mean 2,5) and non-responders (median 2 and mean 2,14). Nilotinib trough concentrations in responders were significantly higher than in non-responders (mean nilotinib trough level 1071 µg/L versus 782 µg/L, p=0.03, figure 1A). Interestingly, no significant difference in trough concentration was observed between patients treated with 300 mg b.i.d. and 200 mg b.i.d. (1067 µg/L vs 974 µg/L, p=0.66, figure 1B). We could not relate this to drug interactions e.g. by use of azoles. Remarkably, no significant difference in nilotinib trough concentration was found between patients with and without reported drug toxicity (Figure 1C). Nilotinib 300 mg b.i.d. was tolerated by 10 patients whereas the remaining patients needed a dose reduction to 200 mg b.i.d.. Duration of nilotinib use did not impact trough concentrations (data not shown). Most frequently observed side effects were fatigue, myalgia, nausea, respiratory tract infections and prolonged QT interval as described before.(8) In the 4 patients with nilotinib trough concentrations available before and after dose reduction from 300 to 200 mg b.i.d. we observed a decrease in mean trough concentrations from 1163 µg/L to 928 µg/L (p 0.33, Figure 1D). Prednisolone doses did not differ between responding and non-responding patients at any timepoint throughout the study period (data not shown) however due to the limited sample size these date are purely descriptive and should be interpreted with caution.

In our prospective cohort of cGVHD patients we showed that trough concentrations of nilotinib correlate with clinical outcome and the optimal concentration range seems to overlap with the recommended concentration range in CML. As these are results of a posthoc analysis from a phase 2 study not primarily set up to study this relationship results are exploratory. We conclude that dose monitoring of nilotinib should be considered for patients treated for cGVHD, especially in non-responding patients. Intriguingly our study might also explain the lower response rates of only 25% reported

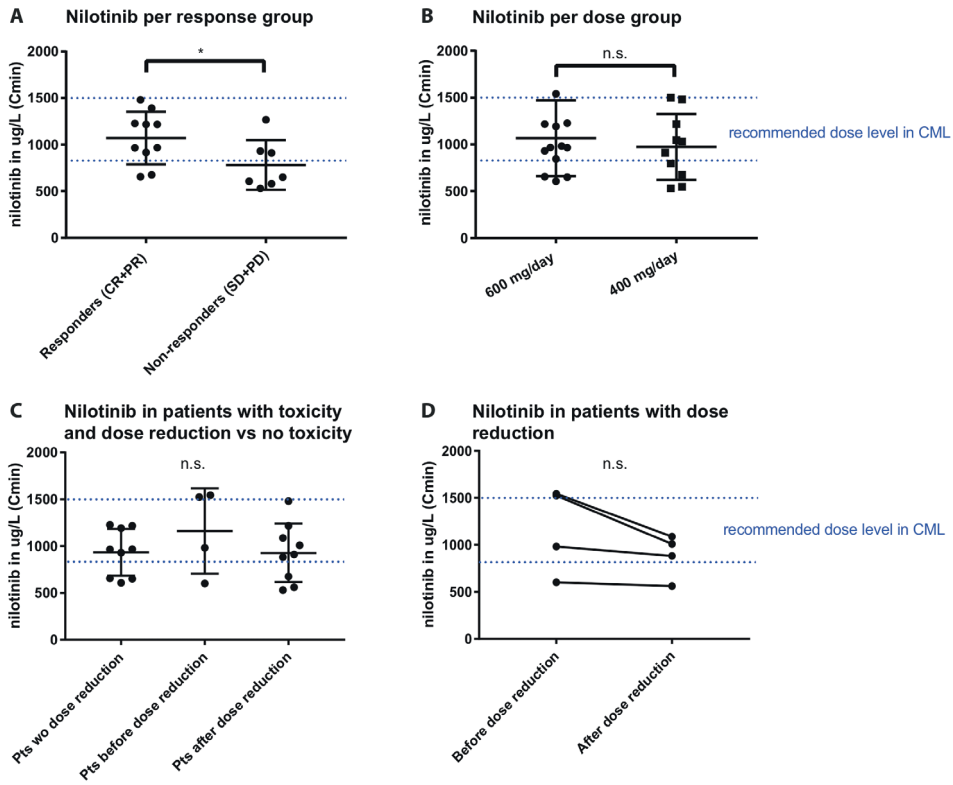

Figure 1. Nilotinib trough levels. a) Responding patients (1 CR and 10 PR) show significantly higher mean nilotinib trough concentrations compared to nonresponders (1071 vs. 782 µg/L, p = 0.03). b) Mean nilotinib trough concentrations did not differ between the different dose groups of 300 vs. 200 mg b.i.d. (1067 vs. 974 µg/L, p = 0.66). c) Mean trough concentrations did not differ between patients not experiencing toxicity (935 µg/L) vs. patients that experienced toxicity on nilotinib 300 mg b.i.d. (928 µg/L). d) Nilotinib trough concentrations before and after dose reduction in 4 patients show a non-significant (1163 vs. 885 µg/L, p = 0.125) decrease.

by Chen *et al*, as median trough serum nilotinib concentration reached in this study were only 407 µg/L which is more than 50% lower than the observed trough levels in our study.(7)

We could not clearly link trough levels of nilotinib with observed toxicity. This might be due to the fact that the initial doses administered in our study are lower as compared to dosing in CML patients. Alternatively the lack of correlation is a consequence of the small sample size, therefor we cannot make strong conclusions regarding toxicity.

In conclusion, a possible concentration-effect relationship for nilotinib on response of cGVHD was observed, indicating that therapeutic drug monitoring of nilotinib might improve response rates for patients receiving TKI and rituximab for the treatment of cGVHD.

References

1. Chabannon C, Kuball J, Bondanza A, Dazzi F, Pedrazzoli P, Toubert A, et al. Hematopoietic stem cell transplantation in its 60s: A platform for cellular therapies. Sci Transl Med. 2018;10:eaap9630.

2. Magro L, Mohty M, Catteau B, Coiteux V, Chevallier P, Terriou L, et al. Imatinib mesylate as salvage therapy for refractory sclerotic chronic graft-versus-host disease. Blood. 2009;114:719–22.

3. Magro L, Catteau B, Coiteux V, Bruno B, Jouet J-P, Yakoub-Agha I. Efficacy of imatinib mesylate in the treatment of refractory sclerodermatous chronic GVHD. Bone Marrow Transplant. 2008;42:757–60.

4. Olivieri A, Locatelli F, Zecca M, Sanna A, Cimminiello M, Raimondi R, et al. Imatinib for refractory chronic graft-versus-host disease with fibrotic features. Blood. 2009;114:709–18.

5. de Masson A, Bouaziz J-D, de Latour RP, Wittnebel S, Ribaud P, Rubio M-T, et al. Limited efficacy and tolerance of imatinib mesylate in steroid-refractory sclerodermatous chronic GVHD. Blood. 2012;120:5089–90.

6. Arai S, Pidala J, Pusic I, Chai X, Jaglowski S, Khera N, et al. A Randomized Phase II Crossover Study of Imatinib or Rituximab for Cutaneous Sclerosis after Hematopoietic Cell Transplantation. Clin Cancer Res. 2016;22:319–27.

7. Chen GL, Carpenter PA, Broady R, Gregory TK, Johnston LJ, Storer BE, et al. Anti–Platelet-Derived Growth Factor Receptor Alpha Chain Antibodies Predict for Response to Nilotinib in Steroid-Refractory or -Dependent Chronic Graft-Versus-Host Disease. Biol Blood Marrow Transplant. 2018;24:373–80.

8. van der Wagen L, Te Boome L, Schiffler M, Nijhof I, Schoordijk M, van Dorp S, et al. Prospective evaluation of sequential treatment of sclerotic chronic graft versus host disease with rituximab and nilotinib. Bone Marrow Transplant. 2018;53:1255–62.

9. Verheijen RB, Yu H, Schellens JHM, Beijnen JH, Steeghs N, Huitema ADR. Practical Recommendations for Therapeutic Drug Monitoring of Kinase Inhibitors in Oncology. Clin Pharmacol Ther. 2017;10:765-776.

10. Herbrink M, de Vries N, Rosing H, Huitema ADR, Nuijen B, Schellens JHM, et al. Quantification of 11 therapeutic kinase inhibitors in human plasma for therapeutic drug monitoring using liquid chromatography coupled with tandem mass spectrometry. Ther Drug Monit. 2016;38:649-656.

11. Wang Y, Chia YL, Nedelman J, Schran H, Mahon F-X, Molimard M. A therapeutic drug monitoring algorithm for refining the imatinib trough level obtained at different sampling times. Ther Drug Monit. 2009;31:579–84.

Table S1. Baseline characteristics

	n	% of patients
Baseline characteristics		
Patients	17	100%
Male sex	15	88%
Age (years)	49.3[a]	22 – 68[b]
Responders	10	59%
cGVHD characteristics		
Organ involvement (%)		
Skin (scleroris)	17	100%
Joints-fascia	16	94%
Mouth	13	76%
Eyes	16	94%
GI	7	41%
Liver	7	41%
Lungs	12	71%
Genital	5	29%
Severe cGVHD (NIH criteria)	14	78%
Transplantation characteristics		
Donortype		
Sibling	9	50%
MUD	8	44%
Haploidentical	1	6%
Myeloablative conditioning regimen	3	17%
Days after allo SCT	1432[a]	538 – 3820[b]
Primary diagnosis		
AML	3	18%
Multiple myeloma	5	29%
ALL	2	12%
Lymphoma	1	6%
MDS	2	12%
CLL	1	6%
Myeloproliferative disorder	2	12%
Aplastic anemia	1	6%
Nilotinib characteristics		
Patients with mean nilotinib C_{min} within CML range	11	65%
Patients with mean nilotinib C_{min} below CML range		
in responding patients	2 out of 10	
in nonresponding patients	4 out of 7	

Abbreviations: cGVHD, chronic Graft versus Host Disease; MUD, Matched Unrelated Donor; AML, Acute Myeloid Leukemia; ALL: Acute Lymphoblastic Leukemia; MDS, Myelodysplatic Syndrome; CLL, Chronic Lymphocytic Leukemia; CML, Chronic Myeloid Leukemia.
[a] Mean. [b] Range.

CHAPTER 5

Conclusions and perspectives

This thesis focuses on precision dosing and treatment optimization in special patient populations with cancer. Various modelling, simulation and extrapolation methods were used to characterize and to predict the pharmacokinetics (PK), pharmacodynamics (PD), toxicity and efficacy of a variety of anticancer drugs. These models can be used to select the optimal dose for the individual patient and thereby optimize treatment. This thesis focused in particular on the following topics: advanced methodologies for special patient populations, utilization of prior knowledge to extrapolate to special patient populations, optimal utilization of longitudinal biomarker data and dose individualization in clinical practice, which will be further discussed and put in perspective in this chapter.

Advanced methodologies for special patient populations

When analysing data from special patient populations, the number of patients are typically low as a result of low incidence. In addition, both paediatric and pregnant cancer patients represent heterogeneous patient cohorts with a broad age and body weight range for paediatrics and broad gestational age range for pregnant women. It is preferred to use limited sampling strategies in order to prevent these vulnerable patients from unnecessary harm and thus sparse and heterogeneous data will be available. Nonlinear mixed effects modelling enables the analysis of these limited and heterogeneous datasets. The population PK model that was developed for bortezomib in paediatric patients (chapter 1.3) showed that allometric scaling results in an adequate description of the observed paediatric PK. In addition, this model provides a more in-depth description of the mechanisms behind the PK and PD of bortezomib, which were similar to previously reported results in adults. The PD was described by bortezomib concentrations directly inhibiting the 20S proteasome activity. This integrated PK/PD model can be used to simulate future dosing regimens that would result in sufficient inhibition of the 20S proteasome activity which could improve treatment efficacy.

The PK changes in pregnant women for docetaxel, paclitaxel, doxorubicin and epirubicin have been evaluated in chapter 2.1. By the addition of PK data from non-pregnant control patients and by using an empirical population PK approach a decreased exposure to these cytotoxic drugs in the pregnant population was identified. It has been shown that treatment of pregnant cancer patients with cytotoxic drugs during the second and third trimester is safe in the short and middle long term for both the mother and the child, when considering perinatal and childhood outcomes. This has resulted in an increased use of these cytotoxic drugs and an increase in livebirths and decrease in prematurity.(1) The developed empirical PK models can be used to guide dose adjustments in pregnant patients in order to match exposure as observed in the non-pregnant population. It should however be noted that dose adjustments are only warranted when the identified changes in PK result in decreased maternal efficacy or increased toxicity.

Utilization of prior knowledge to extrapolate to special patient populations

Despite the fact that the number of new drugs approved for the treatment of cancer is rapidly expanding, drug development for special patient populations such as paediatrics and pregnant women is lacking behind. Physiological changes such as an increase in total body water, increased glomerular filtration and changes in metabolizing enzyme activity might theoretically affect the PK of cytotoxic drugs.(2–4) The resulting over- or under exposure might in turn lead to a change in efficacy and toxicity. Efforts have been made by the regulatory agencies in order to accelerate drug development in special patient populations.(5–8) It is encouraged to use extrapolation methods and thereafter perform efficient clinical trials that fill the knowledge gaps. Existing information on changing physiology, pathophysiology of the disease, the pharmacology of the drug and the clinical efficacy or toxicity of the drug should be evaluated and translated to the population of interest. After establishment of exposure-response relationships, doses that achieve similar exposure, PD effect or clinical response should be predicted. As has been demonstrated before, mechanism based extrapolations show the best performance.

In chapter 1.2 a previously published population PK model for bosutinib that was developed based on adult PK data was used to optimize a paediatric phase I trial design. In this innovative paediatric clinical trial design, dose-finding was based on achieving similar exposure as observed in adults. By allometric scaling of the PK parameters, the exposure in the paediatric population was predicted and the power of the trial design was assessed. Evaluation of this simulation framework using a population PK model and paediatric PK data for sunitinib showed that body-weight based allometric scaling resulted in exposure that was similar to the observed exposure in paediatrics. This model-based approach can be used in future clinical trial designs to predict the starting dose that most likely results in similar exposure compared to adults. In addition, adequate sampling schedules and numbers of patients that are needed for an adequately powered trial can be predicted.

Information about drug exposure in adults can also be used to extrapolate to paediatrics in clinical practice when clinical study results in paediatric patients are not available yet. Kinase inhibitors (KIs) represent a novel group of anticancer drugs that are designed to act against specific molecular targets involved in cancer pathophysiology. Therefore, relationships between exposure to the drug and specific target inhibition or response are to be expected. As long as similarity between the cancer pathophysiology or pharmacological target between adults and paediatrics exists or can be expected, established adult exposure-response relationships can be used to guide individual dosing in paediatrics. To optimally treat children with cancer, empirical and practical PK targets are proposed for several targeted small molecule KIs based on extrapolation from adults in chapter 1.1. Thereby providing guidance to adjust individual dosing regimens and optimize treatment. These targets should, however,

be further evaluated in prospective clinical studies. In addition, caution should be given to potential differences in short-term and long-term toxicity between children and adults.

In pregnant women, precision dosing is also challenging. Empirical PK data in this population is only scarcely available. Model-based predictions based on non-pregnant PK data is the only reasonable option to guide dosing and to optimize the use of cytotoxic drugs in the pregnant population. In chapter 2.2, a novel method is presented in which existing empirical PK models developed from data in non-pregnant patients was enriched with quantitative models describing the changing physiology during pregnancy. This framework was successfully evaluated using the four cytotoxic drugs and observed PK data from pregnant patients that are described in chapter 2.1. This model allows for the prediction of the exposure to cytotoxic drugs during pregnancy and can be used to predict effective and safe dosing regimens in pregnant women for anticancer drugs for which the gestational changes in PK during pregnancy are unknown. Also, this model can be used to guide dose selection for future clinical trials where drugs are introduced in the pregnant population for the first time.

Optimal utilization of longitudinal biomarker data

Modelling and simulation of response to treatment is of importance to determine effective and safe dosing regimens. Additionally, PD modelling may be used to test or generate hypotheses for further research into a specific biomarker or drug specific mechanisms of action. Biomarkers might show a dynamic change in response to drug treatment which may be predictive of potential efficacy or toxicity. The results from the study presented in chapter 4.3 show such a positive relationship. Nilotinib trough concentrations (C_{min}) in patients with chronic Graft versus Host disease (cGVHD) were significantly higher in responders compared to non-responders. A significant relationship between C_{min} and toxicity could not be identified. In chapter 3.3, which describes the development of the first population PD model for circulating tumor DNA (ctDNA), a positive relationship between the relative change in ctDNA concentration and progression of disease was identified. Measuring ctDNA concentrations provides a less invasive way of taking repeated measurements compared to obtaining tumour biopsies or measuring tumour volume by CT scan and is therefore a promising biomarker.(9) The developed model provides a basis for further research into the dynamics and predictive role of ctDNA concentrations in patients with cancer. Future studies should focus on the ctDNA dynamics over the complete course of treatment and might identify thresholds that are predictive of response to treatment. Modelling of longitudinal data offers the possibility of efficient analysis of all collected data in contrast to classical methods in which data are summarized e.g. by cross-sectional analysis or by summary measures as change from baseline or nadir values. As a consequence, modelling is less sensitive to missing data and is able to handle heterogeneous datasets as exemplified here, using data from samples collected during routine clinical care.

As side effects are also a response to anti-cancer treatment, modelling and simulation can provide a mechanistic explanation and describe the development and time course of these unwanted effects. A model defining the relationship between PK of oral docetaxel and dose-limiting toxicities (DLTs) is presented in chapter 3.2. Where the treatment with intravenous docetaxel is well-known to cause side effects such as neutropenia and fatigue, treatment with oral docetaxel co-administered with ritonavir mainly results in gastrointestinal toxicities, such as diarrhea, nausea and anorexia. The model predicts the DLTs well and can thus be used to predict the toxicity of alternative dosing regimens for future clinical trials. For the oral anti-cancer drug capecitabine, the relationship between hand-and-foot syndrome (HFS) and exposure to capecitabine or metabolites was explored in chapter 3.1. The exact mechanism for the development of HFS is still unknown but it has been hypothesized that intracellular accumulation of capecitabine metabolites in the keratinocytes in the skin could play a key role. A PK model describing the intracellular 5-fluorouridine 5'-triphosphate (FUTP) concentrations in peripheral blood mononuclear cells (PBMCs) was developed and used to identify a predictor for the development of HFS. HFS grade 1, 2 and 3 developed after two weeks of capecitabine treatment, and intracellular FUTP was identified as the best predictor of increased HFS grades. This strengthens the hypothesis for accumulation of metabolites as the major cause of development of HFS in this patient population. In addition, this model can be used to predict alternative dosing regimens and to explore the effect of these doses on the development of HFS. Measurement and modelling of biomarkers or drug related toxicities provides guidance in monitoring of the response to treatment and can enable individualization of therapy. In addition, biomarkers can provide an early identification of an individual response or predict the development of toxicity in individual patients. Modelling and simulation can be used to identify specific thresholds or patient groups, associated with an increased risk of disease progression or major toxicities.

Dose individualization in clinical practice

Many orally administered anticancer drugs show large inter-individual variability in PK exposure. This may result in potential under- or overdosing and a fixed-dosing approach may thus not be appropriate for these drugs. To prevent for possible treatment failure, PK targets have been provided in chapter 1.1 to guide individual dosing in paediatric patients with cancer. Individualized dosing, or *therapeutic drug monitoring* (TDM), focuses on increasing target attainment and thereby improving treatment outcomes. In order to provide a reliable and well-established TDM platform, bioanalytical assays and PK guidance are pivotal.

In chapter 4.1, the development and validation of a LC-MS/MS method for simultaneous determination of concentrations of alectinib, cobimetinib, lenvatinib, nintedanib, osimertinib, palbociclib, ribociclib, vismodegib and vorinostat is presented. For TDM purposes, a single rapid, robust and efficient quantification of drug concentrations

obtained from clinical practice is preferable. A bioanalytical assay that enables simultaneous quantification of these nine drugs in a short run time per sample is presented. The validation of this assay indicated that osimertinib is unstable in human plasma at room temperature. Clinical samples containing osimertinib should therefore be transported and stored at -20°C. The presented assay was successfully validated based on guidelines on bioanalytical method validation provided by the FDA and EMA and thus considered adequate for the determination of patients' plasma samples. Most oral anticancer drugs are used by outpatients, samples for TDM purposes are therefore most often collected at a random time point within the dosing interval. To compare individual concentrations to the proposed efficacy PK targets, most often defined in terms of a minimal C_{min} to be attained, extrapolation of the observed value to the C_{min} value is needed. In chapter 4.2 different extrapolation methods are evaluated. It is shown that using the typical concentration-time curve as a reference provides the best predictive performance. This method enables a simple and unbiased prediction of the individual C_{min} and can thus be used in clinical practice. Furthermore, home sampling devices are under development which could provide an easy and accurate method of collecting a blood sample at the end of the dosing interval. Although dose individualization is scientifically reasonable, future clinical trials should focus on identification and confirmation of this treatment strategy. The development of population PK and PD models, such as the models presented in chapters 1.2, 1.3, 2.1, 3.1, 3.2 and 3.3, may facilitate the identification of exposure-efficacy and exposure-toxicity relationships. Thereafter, thresholds or risk factors can be determined and confirmed in prospective clinical trials.

In summary, modelling and simulation of PK and PD using a population approach may be of great value for special patient populations such as paediatrics and pregnant women with cancer as presented in this thesis. It allows the analysis of heterogeneous datasets with a limited number of patients and limited and infrequently collected samples. In addition, both a population of interest and control patients can be included in one analysis, which enables the identification of covariates that influence the PK of these patients. Subsequently, a developed model, either in adults or in children, can be used to simulate new dosing regimens or clinical trial designs. Furthermore, a developed PK model can be linked to the PD or response related to treatment with anticancer drugs and provide further guidance for dose individualization. By determination of predictors or covariates, patients that are more sensitive to develop toxicities or at risk of progression of disease can be identified and treatment can be optimized.

APPENDICES

Summary
Samenvatting
Author Affiliations
List of publications
Dankwoord
Curriculum Vitae

Summary

Special patient populations, such as children and pregnant women, are not regularly included in drug development programs. Changes in physiological processes in these patients affect the pharmacokinetics (PK) and pharmacodynamics (PD) of drugs. This may result in suboptimal efficacy or substantial toxicity caused by under- or overexposure to these drugs, which is especially problematic for drugs with a narrow therapeutic index such as anticancer agents. This thesis aims to apply modelling and simulation to optimize treatment and further develop precision dosing with anticancer drugs in these special patient populations. In addition, modelling and simulation techniques are used to identify exposure-efficacy and exposure-response relationships to, ultimately, contribute to the precision medicine paradigm in clinical oncology.

Special patient populations
Chapter 1 addresses the PK of anticancer drugs in paediatric patients with cancer. Therapeutic drug monitoring (TDM) aims to individualize a patient's dose by quantification of individual plasma concentrations and interpretations of these concentrations with respect to proposed target levels. Children with cancer might benefit disproportionally from the application of TDM, since particular dose-finding studies are often not performed in children. Chapter 1.1 reviews the available literature on exposure-response and exposure-toxicity relationships for targeted small molecule kinase inhibitors (KIs) in paediatric oncology. Based on these relationships and knowledge on the PK, mechanism of action, molecular driver and pathophysiology of the disease, empirical and practical targets to guide TDM for paediatric patients with cancer are proposed. As exposure-response and exposure-toxicity relationships are not yet reported for these drugs in the paediatric population, extrapolation based on data available from adults was performed to provide exploratory targets and guidance for dose adjustments in individual patients.

Extrapolation methods were also used in chapter 1.2 in which a simulation study is described aiming to investigate the performance of a paediatric phase I dose-finding clinical trial. When a paediatric clinical trial is designed, information on the clinical pharmacology of the drug is already available from adult patients. This information can then be extrapolated to the paediatric population in order to design efficient clinical trials. In this paediatric trial it is particularly important to avoid underexposure as much as possible and the sample size should be as small as possible, given the low incidence of paediatric cancers. In the clinical trial used in this simulation study, dose-finding was based on achieving equivalent systemic exposure in paediatrics compared to adult patients. By applying allometric scaling to a population PK model that was developed based on PK data from adults, the PK in children was predicted. Subsequently, the clinical trial design was simulated to determine the power of the proposed design. The proposed trial design however performed insufficient as a result of high variability in

exposure between individual patients with a target attainment of 67% only for the starting dose and proposed sampling schedule. Additional simulations showed that the power of the trial design could only be improved when more patients would be included (power of 79% to attain the target for n=10 patients). Other adaptations such as collection of more blood samples per patient did not result in increased power.

In chapter 1.3 the paediatric PK and PD of bortezomib is described by a semi-mechanistic population PK/PD model. Higher bortezomib plasma concentrations were observed in the second week of treatment, which can be ascribed to drug accumulation in red blood cells. To account for this, a Langmuir binding model was incorporated in the final PK model. Bortezomib caused a decrease in 20S proteasome activity, which was best described by a direct effect PD model with a sigmoidal inhibitory effect of the bortezomib plasma concentrations. The exposure and subsequently target inhibition resulting from future paediatric dosing regimens can be simulated with this PK/PD model, aiming for adequate 20S proteasome activity inhibition, which should lead to improved treatment efficacy.

Chapter 2 of this thesis focusses on modelling and simulation of the PK of cytotoxic drugs in pregnant cancer patients. The PK of cytotoxic drugs might be changed in pregnant patients compared to non-pregnant patients as a result of physiological changes such as increased body fluids, increased glomerular filtration rate and altered activity of metabolizing enzymes. In chapter 2.1 these changes are quantified for docetaxel, paclitaxel, doxorubicin and epirubicin. For this empirical analysis, PK data from pregnant (during the 2nd and 3rd trimester) and non-pregnant patients were combined and a fixed pregnancy effect was included as covariate in the respective PK models. This covariate effect could be identified for the central and peripheral volumes of all four drugs and for the clearance of docetaxel, doxorubicin and paclitaxel. These changes resulted in lower plasma concentrations for some of the drugs in pregnant patients compared to non-pregnant patients. The relative change in the typical area under the plasma concentration-time curve was -6.0%, -12%, -10% and -1% for docetaxel, paclitaxel, doxorubicin and epirubicin, respectively, in pregnant versus non-pregnant patients. The results of this analysis highlight the need to examine the efficacy of chemotherapy when administered during pregnancy.

By integration of the physiological changes that occur during pregnancy and available population PK models developed based on data from non-pregnant patients, a semi-physiological enriched PK model to predict the PK during pregnancy was developed which is presented in chapter 2.2. Drug exposure was predicted to be lower in pregnant women compared to non-pregnant patients, which is in line with the empirical PK results as presented in chapter 2.1. At an estimated gestational age of 28 weeks, clearance was increased with 18.1%, 19.8%, 15.8% and 14.2% for docetaxel, paclitaxel, doxorubicin and epirubicin. In addition, the peripheral volumes of distributions were

increased by 13.7% to 39.0% at that time. The predictions using this model framework provided a good reflection of the plasma concentrations of the four cytotoxic drugs in pregnant patients that were also presented in chapter 2.1. Therefore, this model can be used to explore dosing regimens in pregnant patients for anticancer drugs for which PK data during pregnancy are unavailable while treatment is indicated.

Exposure-response relationships

Modelling and simulation can be used to assess and to characterize the relationship between drug exposure and either wanted (i.e. efficacy) or unwanted (i.e. toxicity) effects. Biomarkers are very useful to describe these effects, as they are most often continuous, show a dynamic change in response to drug administration and may provide an early prediction of treatment failure or (severe) toxicity. Different relationships between exposure to anticancer drugs and efficacy or toxicity are investigated in chapter 3. For capecitabine, chapter 3.1 describes the relationship between exposure to the intracellular metabolite 5-fluorouridine 5'-triphosphate (FUTP) and the development and grade of hand-and-foot syndrome (HFS). A population PK model for the plasma concentrations of capecitabine and four metabolites was extended with an intracellular compartment describing FUTP concentrations within peripheral blood mononuclear cells. These intracellular FUTP concentrations showed the best predictive performance for the development and grade of HFS in the subsequently developed continuous-time Markov model. Simulations with different dose-levels showed a more than doubled percentage of patients experiencing grade 2 or grade 3 HFS with higher dose regimens. Plasma capecitabine and metabolite concentrations performed worse in predicting HFS, which strengthens the previously proposed hypothesis that HFS is a result of intracellular metabolite accumulation. This study indicates that monitoring FUTP concentrations may be a viable option to develop precision dosing strategies for capecitabine.

In chapter 3.2 the risk of developing dose-limiting toxicities (DLT) in patients treated with a new oral formulation of docetaxel was assessed. In addition to the classic toxicities such as neutropenia and fatigue, gastro-intestinal toxicities were observed in the patients who were treated with oral docetaxel in combination with the boosting agent ritonavir. The probability of developing a DLT was best described by an effect compartment representing the harmful effect caused by docetaxel, where the amount of docetaxel was a significant predictor for DLT. Simulations with the final model showed an adequate description of the observed data. This model can be used to further assess the recommended phase II dose. When additional data is collected during future drug development of this oral docetaxel formulation, the model can be updated to get more precise estimates of the exposure-toxicity relationship. Furthermore, the model can be extended with differentiation of the type of toxicity as the exposure-toxicity relationship is not necessarily the same for all types of severe toxicity.

In addition to exposure-toxicity relationships, exposure-efficacy analyses may provide a basis for treatment optimization in cancer patients. A dynamic model for circulating tumour DNA (ctDNA) and its relationship with tumour progression in patients with non-small cell lung cancer (NSCLC) is presented in chapter 3.3. Increasing ctDNA concentrations may serve as a biomarker for early detection of tumour progression in these patients. Nonlinear mixed effects modelling was used to characterize the ctDNA dynamics, including progressive time-dependent development of resistance to treatment. A parametric time-to-event model was developed and the relative change in driver mutation concentrations from baseline was identified as most significant predictor of disease progression. This may form a basis for future research into the ctDNA dynamics over the complete duration of treatment and the use of ctDNA concentrations in clinical decision making.

Therapeutic Drug Monitoring

Chapter 4 focusses on the clinical application of precision dosing, in particular by the implementation of TDM. In order to support TDM, validated bioanalytical methods are needed to quantify drug concentrations in plasma. Chapter 4.1 describes such a bioanalytical assay for the determination of human plasma concentrations of nine KIs used in cancer treatment. This assay enables a simultaneous and rapid quantification of the plasma concentrations of these nine drugs, thereby being useful for application in clinical routine care. The development and validation of these assays, taking into account the specific requirements for TDM, is a crucial part of implementing precision dosing in clinical practice.

In clinical care, patient samples for TDM are mostly collected at a random moment within the dosing interval. As target concentrations for efficacy are mostly determined at the end of the dosing interval (C_{min}), extrapolation methods are needed to determine the individual C_{min}, based on the measured concentration at random sampling time points. In chapter 3.2 three different methods of determination of the C_{min} are evaluated. It is shown that the typical concentration-time curve as a reference provides unbiased and precise prediction of the individual C_{min}. Bayesian estimation shows similar performance, but is more complicated to be used in clinical practice.

Chapter 3.3 describes the application of TDM of an anticancer KI outside oncology, demonstrating that the principles applied in this thesis also apply to other therapeutic areas. In this study nilotinib was used to treat chronic Graft versus Host Disease (GVHD) after an autologous hematopoietic cell transplantation. In this study, it is demonstrated that a relationship exists between nilotinib C_{min} and response after 13 months of treatment. The nilotinb C_{min} value was significantly higher in responders (1071 µg/L) compared to non-responders (782 µg/L). Dose adjustments are thus warranted in patients with low nilotinib exposure to further improve treatment outcome.
In conclusion, this thesis presents how modelling and simulation can be deployed to

optimize anticancer treatment of special patient populations. By identification of predictors or covariates that influence the clinical pharmacology of anticancer drugs, treatment may be further optimized by individualization of treatment. In addition, the developed models can be used to predict future dosing regimens, expected toxicities or outcomes and are particularly useful to extrapolate to special patient populations for which typically limited data is available.

Samenvatting

Bijzondere patiëntenpopulaties, zoals kinderen en zwangere vrouwen, worden normaal niet geïncludeerd in ontwikkelingsprogramma's van nieuwe antikankergeneesmiddelen. Verschillen in fysiologische processen in deze patiënten kunnen de farmacokinetiek (PK) en farmacodynamiek (PD) van geneesmiddelen beïnvloeden. Dit kan zowel een suboptimale geneesmiddelblootstelling als een te hoge blootstelling met ernstige toxiciteit tot gevolg hebben. Dit proefschrift beschrijft de toepassing van modellering en simulering om de behandeling van bijzondere patiëntenpopulaties met antikankergeneesmiddelen te optimaliseren. Daarnaast wordt de toepassing van modelmatige technieken beschreven om relaties tussen blootstelling en effectiviteit of toxiciteit van behandeling met deze geneesmiddelen te identificeren.

Bijzondere patiëntenpopulaties
Hoofdstuk 1 is gericht op de PK van antikankergeneesmiddelen in kinderen met kanker. *Therapeutic drug monitoring* (TDM) is een methode die in de klinische praktijk wordt gebruikt om de dosering van geneesmiddelen met een nauwe therapeutische breedte te optimaliseren. Op basis van het meten van geneesmiddelconcentraties in bloed, plasma of serum, kan de behandeling van een patiënt worden geïndividualiseerd. De gemeten geneesmiddelconcentraties worden hiervoor vergeleken met een gestelde streefwaarde waarna een dosisadvies wordt gegeven waarmee de streefwaarde bereikt kan worden. De pediatrische patiëntenpopulatie is uitermate geschikt voor de toepassing van TDM in de klinische praktijk. Voor deze kwetsbare groep patiënten is de behoefte aan efficiënte en veilige behandelingen groot.

Hoofdstuk 1.1 geeft een overzicht van de beschikbare literatuur over de relaties tussen geneesmiddelblootstelling en de effectiviteit van de behandeling van kinderen met kanker met doelgerichte kinase remmers. Op basis van deze relaties en beschikbare kennis over de PK, het werkingsmechanisme, het moleculaire aangrijpingspunt en de pathofysiologie van de maligniteit zijn empirische en praktische streefwaarden voor TDM bij kinderen met kanker voorgesteld. Voor de onderzochte geneesmiddelen zijn in de literatuur echter nog geen relaties tussen geneesmiddelblootstelling en effectiviteit of toxiciteit van de behandeling bij kinderen met kanker gerapporteerd. Desondanks is er behoefte aan handvatten waarmee de behandeling van deze patiëntenpopulatie kan worden verbeterd. Met behulp van extrapolatie van beschikbare informatie bij volwassen patiënten naar kinderen werden exploratieve streefwaarden aanbevolen op basis waarvan dosisaanpassingen in individuele patiënten kunnen worden gedaan.

In hoofdstuk 1.2 wordt een simulatiestudie beschreven waarin een fase I studie voor het vinden van de optimale dosis van bosutinib voor kinderen geoptimaliseerd werd door extrapolatie vanuit beschikbare kennis in volwassenen. Door middel van

simulaties werd de kans op succes van een klinische fase I studie binnen de kinderoncologie onderzocht. Er is altijd voorkennis over de farmacologie van een geneesmiddel beschikbaar alvorens dit bij kinderen met kanker wordt onderzocht. Een vertaling van deze voorkennis naar de pediatrische situatie kan de onderzoeksopzet verbeteren. In deze klinische studie is gekozen voor een strategie waarbij de juiste dosering bij kinderen werd bepaald door de systemische blootstelling met die bij volwassen patiënten te vergelijken. Door allometrische schaling toe te passen op de parameters van een model dat de populatie PK in volwassenen beschrijft, kan de PK in kinderen worden voorspeld. De resultaten van de simulaties lieten zien dat de slagingskans van deze studie, door grote variabiliteit tussen patiënten, erg laag is. In slechts 67% van de gesimuleerde studies waarbij de startdosering en het voorgestelde afname schema gehanteerd werden, was de blootstelling bij kinderen binnen het gestelde doel van blootstelling. De simulaties lieten daarnaast ook zien dat de kans van slagen verhoogd kan worden wanneer meer patiënten zouden worden geïncludeerd (79% succesvolle studies bij inclusie van 10 versus 6 patiënten). Andere aanpassingen, zoals het afnemen van meer bloedmonsters per patiënt, zorgden niet voor een verbetering van het percentage succesvolle studies.

De PK en PD van bortezomib in kinderen wordt in hoofdstuk 1.3 beschreven door middel van een semi-mechanistisch populatie PK/PD model. Als gevolg van accumulatie in rode bloedcellen werden in de tweede week van behandeling hogere bortezomib plasmaconcentraties geobserveerd. In het finale PK model werd deze accumulatie beschreven door de Langmuir vergelijking. Het effect van bortezomib kan gemeten worden door het bepalen van 20S proteasoom activiteit. De daling in activiteit na toediening van bortezomib kon het beste worden gekarakteriseerd door een model dat een direct effect van de bortezomib concentraties in plasma op de 20S proteasoom activiteit beschrijft. Dit model kan in de toekomst gebruikt worden om nieuwe doseerschema's te ontwikkelen. Deze doseringen kunnen dan gebaseerd worden op adequate inhibitie van de 20S proteasoom activiteit, waarmee de effectiviteit van de behandeling verbeterd kan worden.

Hoofdstuk 2 van dit proefschrift is gericht op het modelleren en simuleren van de PK van cytotoxische geneesmiddelen in zwangere vrouwen met kanker. Bij zwangere patiënten kan als gevolg van fysiologische veranderingen in de vochthuishouding, nierfunctie en activiteit van metaboliserende enzymen de PK van geneesmiddelen veranderen ten opzichte van niet zwangere patiënten. In hoofdstuk 2.1 zijn de gevolgen van deze fysiologische processen voor docetaxel, paclitaxel, doxorubicine en epirubicine gekwantificeerd. Voor deze empirische analyse werden PK data van zwangere en niet zwangere patiënten gecombineerd, waarna het effect van zwangerschap als covariaat kon worden geïdentificeerd. Zwangerschap was een significante covariaat voor het centrale en perifere verdelingsvolume van alle vier geneesmiddelen en voor de klaring van docetaxel, doxorubicine en paclitaxel. Het resultaat hiervan zijn lagere

geneesmiddelconcentraties in plasma bij zwangere patiënten in vergelijking tot niet zwangere patiënten. De relatieve afname in de oppervlakte onder de plasma concentratie-tijd curve (AUC) in zwangere versus niet zwangere patiënten was 6.0%, 12%, 10% en 1% voor respectievelijk docetaxel, paclitaxel, doxorubicine en epirubicine.

Hoofdstuk 2.2 beschrijft een semifysiologisch model dat de eerdergenoemde fysiologische veranderingen tijdens de zwangerschap combineert met gegevens over de PK van geneesmiddelen bij niet zwangere patiënten. Met dit semifysiologische model kunnen geneesmiddelconcentraties bij zwangere patiënten worden voorspeld waarna een dosisadvies kan worden gegeven. Voorspellingen met dit model lieten een goede voorspelling van de geobserveerde geneesmiddelconcentraties uit hoofdstuk 2.1 zien. Voor een zwangerschapsduur van 28 weken werd een toename in geneesmiddelklaring van 18.1%, 19.8%, 15.8% en 14.2% voorspeld voor respectievelijk docetaxel, paclitaxel, doxorubicine en epirubicine. Daarnaast werd een toename in de perifere verdelingsvolumina voorspeld van 13.7% tot 39.0%. De geneesmiddelconcentraties werden slechter voorspeld wanneer gebruik gemaakt werd van een model dat geen rekening houdt met de veranderende fysiologie tijdens de zwangerschap. Dit semifysiologische zwangerschapsmodel kan worden gebruikt om doseringen te voorspellen voor geneesmiddelen waarvan nog geen PK data in de zwangere populatie beschikbaar zijn. Deze resultaten onderschrijven daarnaast ook de behoefte aan meer onderzoek naar de effectiviteit van chemotherapie in de zwangere populatie.

Blootstelling-respons relaties

De ontwikkeling van kwantitatieve modellen die de relatie tussen blootstelling en respons beschrijven zijn van toegevoegde waarde in het beoordelen van de relatie tussen de PK en gewenste en ongewenste effecten van geneesmiddelen. Deze effecten zijn niet altijd direct meetbaar, zogenaamde *biomarkers* kunnen worden gemeten en toenemen of afnemen in reactie op de toediening van geneesmiddelen en kunnen dus worden gebruikt om deze effecten te beschrijven. Verschillende relaties tussen de blootstelling aan antikankergeneesmiddelen en de effectiviteit of toxiciteit van de behandeling worden beschreven in hoofdstuk 3. Voor capecitabine beschrijft hoofdstuk 3.1 de relatie tussen de blootstelling aan de intracellulaire metaboliet 5-fluorouridine 5'-trifosfaat (FUTP) en het ontwikkelen van hand-voetsyndroom. Een eerder gepubliceerd populatie PK model dat de plasmaconcentraties van capecitabine en vier metabolieten karakteriseert, werd uitgebreid met een intracellulair compartiment voor FUTP concentraties in mononucleaire cellen uit het perifere bloed. De resultaten van het continue Markov model lieten zien dat de intracellulaire FUTP concentraties een betere voorspeller voor het ontwikkelen van hand-voetsyndroom waren dan capecitabine en andere plasma metabolieten. Deze resultaten versterken de hypothese dat hand-voetsyndroom een gevolg is van intracellulaire accumulatie van capecitabine metabolieten. Simulaties met dit model lieten zien dat het aantal patiënten met graad 2 of graad 3 hand-voetsyndroom verdubbelt bij tweemaal daagse dosering van

950/1600 mg/m^2 vergeleken met 375/625 mg/m^2.

In hoofdstuk 3.2 wordt het risico op het ontwikkelen van een dosislimiterende toxiciteit (DLT) bij behandeling met een nieuwe orale formulering van docetaxel onderzocht. Naast de klassieke toxiciteiten, zoals neutropenie en vermoeidheid, ontwikkelden patiënten die behandeld werden met oraal docetaxel in combinatie met ritonavir gastro-intestinale bijwerkingen. De kans op het ontwikkelen van een DLT werd gerelateerd aan de cumulatieve bloostelling aan docetaxel. Dit model kan daarom worden gebruikt om de te verwachten toxiciteit in toekomstige klinische studies te voorspellen.

Ook analyses naar de relatie tussen geneesmiddelblootstelling en effectiviteit kan een basis vormen voor optimalisatie van de behandeling met antikankergeneesmiddelen. Een longitudinaal model voor circulerend tumor DNA (ctDNA) en de relatie met tumorprogressie bij patiënten met niet kleincellig longcarcinoom (NSCLC) is beschreven in hoofdstuk 3.3. Een toename in ctDNA-concentraties in bloed kan dienen als *biomarker* voor een vroege detectie van tumorprogressie in deze patiëntengroep. Door middel van *nonlinear mixed effects* modellering kon de dynamische verandering en ontwikkeling van progressie in ctDNA concentraties beschreven worden. Ter aanvulling op dit PD model wordt in hoofdstuk 3.3 een parametrisch *time-to-event* model beschreven. Dit model laat zien dat de relatieve verandering in ctDNA concentraties van significante voorspellende waarde is voor NSCLC progressie.

Therapeutic Drug Monitoring

Hoofdstuk 4 gaat in op de klinische toepassing van het individualiseren van de behandeling van patiënten met kanker, in het bijzonder door de implementatie van TDM. Ter ondersteuning van TDM zijn gevalideerde bio-analytische methodes, waarmee geneesmiddelconcentraties kunnen worden gemeten, onmisbaar. In hoofdstuk 4.1 wordt een bio-analytische methode voor de bepaling van de concentraties van negen nieuwe kinase remmers in humaan plasma beschreven. Met deze methode kunnen de plasmaconcentraties van deze geneesmiddelen gelijktijdig en in korte tijd worden bepaald. Hierdoor is deze methode bijzonder geschikt om in de klinische praktijk toe te passen.

Streefwaarden voor TDM van antikankergeneesmiddelen worden doorgaans als de concentratie aan het einde van het doseerinterval gedefinieerd. Dit wordt ook wel de minimale concentratie (C_{min}) genoemd. Binnen de klinische patiëntenzorg worden echter op een willekeurig moment binnen een doseerinterval bloedmonsters afgenomen. Hierdoor zijn methodes nodig om de bijbehorende C_{min} te bepalen. In hoofdstuk 3.2 worden drie verschillende methodes voor het bepalen van deze C_{min} waarden geëvalueerd. Wanneer de typische concentratie-tijd curve als referentie wordt gebruikt, wordt de individuele C_{min} met de beste precisie voorspeld. Het advies is

daarom om deze methode voor het berekenen van de $C_{min,}$ voor de toepassing van TDM, in de klinische praktijk te gebruiken.

De toepassing van TDM kan ook van toegevoegde waarde zijn voor de behandeling van patiënten met chronische *graft-versus-host* ziekte (GVHD), die met nilotinib behandeld worden. Hoofdstuk 3.3 laat de correlatie tussen de nilotinib C_{min} en respons na 13 maanden zien. De nilotinib C_{min} was significant hoger in patiënten met ziekterespons in vergelijking met patiënten zonder ziekterespons. Aanpassingen in de nilotinib dosering zouden daarom een behandelvoordeel voor patiënten met een lage nilotinib C_{min} kunnen opleveren.

In conclusie beschrijft dit proefschrift hoe modellering en simulering ingezet kunnen worden om de behandeling van bijzondere patiëntenpopulaties te optimaliseren. De klinische farmacologie van antikankergeneesmiddelen kan door covariaten beïnvloed worden. Door identificatie van deze factoren kan de behandeling verder worden geïndividualiseerd en geoptimaliseerd. Daarnaast kunnen PK en PD modellen worden gebruikt voor het bepalen van doseerstrategieën of het voorspellen van toxiciteiten en klinische uitkomsten. Dit proefschrift illustreert dat zulke modellen bij uitstek van waarde kunnen zijn voor het extrapoleren naar bijzondere patiëntenpopulaties waarvoor doorgaans beperkte gegevens beschikbaar zijn.

Author affiliations

Frédéric C.H. Amant	Department of Oncology, Catholic University of Leuven, Leuven, Belgium; Centre for Gynaecological Oncology Amsterdam (CGOA), The Netherlands Cancer Institute, Amsterdam, The Netherlands
Andishe Attarbaschi	Department of Pediatric Hematology and Oncology, St. Anna Children's Hospital, Vienna, Austria; Department of Pediatrics and Adolescent Medicine, Medical University Vienna, Austria
Brigitte Bär	Department of Hematology, Radboud university medical center, Nijmegen, The Netherlands
André Baruchel	Department of Pediatric Hematology, Hospital Saint Louis, Paris, France
Jos H. Beijnen	Department of Pharmacy & Pharmacology and Division of Pharmacology, The Netherlands Cancer Institute, Amsterdam, The Netherlands; Division of Pharmacoepidemiology and Clinical Pharmacology, Utrecht Institute for Pharmaceutical Sciences, Utrecht University, Utrecht, The Netherlands
Ruud L.M. Bekkers	Department of Obstetrics and Gynaecology, Catharina Hospital, Eindhoven, The Netherlands
Mar D.M. Bellido	Department of Hematology, University Medical Center Groningen, Groningen, The Netherlands
Jaap J. Boelens	Laboratory of Translational Immunology, University Medical Center Utrecht, Utrecht University, Utrecht, The Netherlands; Department of Pediatrics, Stem cell transplant and cellular therapies program, Memorial Sloan Kettering Cancer Center, New York, United States of America

Ingrid A. Boere	Department of Medical Oncology, Erasmus MC Cancer Institute, Erasmus University Medical Center, Rotterdam, The Netherlands
Daan van den Broek	Department of Laboratory Medicine, The Netherlands Cancer Institute, Amsterdam, The Netherlands
Kristel Van Calsteren	Department of Development and Regeneration, Obstetrics & Gynaecology, KU Leuven, Leuven, Belgium
Ellen J.B. Derissen	Department of Pharmacy & Pharmacology, The Netherlands Cancer Institute, Amsterdam, The Netherlands
Thomas P.C. Dorlo	Department of Pharmacy & Pharmacology and Division of Pharmacology, The Netherlands Cancer Institute, Amsterdam, The Netherlands
Vít Drochýtek	Department of Obstetrics and Gynaecology, University Hospital Kralovske Vinohrady, 3rd Medical Faculty, Charles University, Prague, Czech Republic
Tirsa T. van Duijl	Department of Pharmacy & Pharmacology, The Netherlands Cancer Institute, Amsterdam, The Netherlands
Natasha K.A. van Eijkelenburg	Princess Máxima Center for Pediatric Oncology, Utrecht, The Netherlands
Franca Fagioli	Università degli Studi di Torino, Turin, Italy
Robert Fruscio	Clinic of Obstetrics and Gynecology, Department of Medicine and Surgery, University of Milan-Bicocca, San Gerardo Hospital, Monza, Italy
Michael J. Halaška	Department of Obstetrics and Gynaecology, University Hospital Kralovske Vinohrady, 3rd Medical Faculty, Charles University, Prague, Czech Republic
Lidwien M. Hanff	Princess Máxima Center for Pediatric Oncology, Utrecht, The Netherlands

J.G. Coen van Hasselt	Division of Systems Biomedicine and Pharmacology, Leiden Academic Center for Drug Research, Leiden University, Leiden, The Netherlands
Michel M. van den Heuvel	Department of Respiratory Disease, Radboud university medical centre, Nijmegen, The Netherlands; Department of Thoracic Oncology, The Netherlands Cancer Institute, Amsterdam, The Netherlands
Alwin D.R. Huitema	Department of Pharmacy & Pharmacology and Division of Pharmacology, The Netherlands Cancer Institute, Amsterdam, The Netherlands; Department of Clinical Pharmacy, University Medical Center Utrecht, Utrecht University, Utrecht, The Netherlands
Bart A.W. Jacobs	Department of Pharmacy & Pharmacology, The Netherlands Cancer Institute, Amsterdam, The Netherlands
C. Niels de Jong	Department of Hematology, Erasmus University Medical Center, Rotterdam, The Netherlands
Gertjan L. Kaspers	Department of Pediatric Oncology/Hematology, VU University Medical Center, Amsterdam, The Netherlands; Princess Máxima Center for Pediatric Oncology, Utrecht, The Netherlands
Thomas E. Klingebiel	Department of Pediatrics, University Hospital Frankfurt, Frankfurt am Main, Germany
Jürgen H.E. Kuball	Department of Hematology, University Medical Center Utrecht, Utrecht, The Netherlands; Laboratory of Translational Immunology, University Medical Center Utrecht, Utrecht University, Utrecht, The Netherlands
Jasper van der Lugt	Princess Máxima Center for Pediatric Oncology, Utrecht, The Netherlands

Serena Marchetti	Division of Medical Oncology, Department of Clinical Pharmacology, The Netherlands Cancer Institute, Amsterdam, The Netherlands
Ellen Meijer	Department of Hematology, Amsterdam University Medical Center, Amsterdam, The Netherlands
Barbara De Moerloose	Department of Pediatrics, Ghent University Hospital, Ghent, Belgium
Denise Niewerth	Department of Pediatric Oncology/Hematology, VU University Medical Center, Amsterdam, The Netherlands
Bastiaan Nuijen	Department of Pharmacy & Pharmacology, The Netherlands Cancer Institute, Amsterdam, The Netherlands
Rebecca C. Painter	Department of Gynaecology and Obstetrics, Amsterdam University Medical Centers, University of Amsterdam, Amsterdam, The Netherlands
Giuseppe Palumbo	Ospedale Pediatrico Bambino Gesù, Rome, Italy
Eefke J. Petersen	Department of Hematology, University Medical Center Utrecht, Utrecht, The Netherlands
Reinier A.P. Raijmakers	Department of Hematology, University Medical Center Utrecht, Utrecht, The Netherlands
Hilde Rosing	Department of Pharmacy & Pharmacology, The Netherlands Cancer Institute, Amsterdam, The Netherlands
Jeroen Roosendaal	Department of Pharmacy & Pharmacology, The Netherlands Cancer Institute, Amsterdam, The Netherlands

Jan H.M. Schellens	Division of Pharmacology and Division of Medical Oncology, Department of Clinical Pharmacology, The Netherlands Cancer Institute, Amsterdam, The Netherlands; Division of Pharmacoepidemiology and Clinical Pharmacology, Utrecht Institute for Pharmaceutical Sciences, Utrecht University, Utrecht, The Netherlands
Arend von Stackelberg	Department of Pediatric Oncology/Hematology, Charité Universitätsmedizin, Berlin, Germany
Neeltje Steeghs	Division of Medical Oncology, Department of Clinical Pharmacology, The Netherlands Cancer Institute, Amsterdam, The Netherlands
Rik E. Stuurman	Department of Pharmacy & Pharmacology, The Netherlands Cancer Institute, Amsterdam, The Netherlands
Nikkie Venekamp	Department of Pharmacy & Pharmacology, The Netherlands Cancer Institute, Amsterdam, The Netherlands
Remy B. Verheijen	Department of Pharmacy & Pharmacology, The Netherlands Cancer Institute, Amsterdam, The Netherlands
Niels de Vries	Department of Pharmacy & Pharmacology, The Netherlands Cancer Institute, Amsterdam, The Netherlands
Lotte E. van der Wagen	Department of Hematology, University Medical Center Utrecht, Utrecht, The Netherlands; Laboratory of Translational Immunology, University Medical Center Utrecht, Utrecht University, Utrecht, The Netherlands
Vincent A. de Weger	Division of Pharmacology and Division of Medical Oncology, Department of Clinical Pharmacology, The Netherlands Cancer Institute, Amsterdam, The Netherlands

Bram J. Wilhelm	Clinical Pharmacology & Pharmacy, VU University Medical Center, Amsterdam, The Netherlands
Moniek A. de Witte	Department of Hematology, University Medical Center Utrecht, Utrecht, The Netherlands
Petronella O. Witteveen	Department of Medical Oncology, University Medical Center Utrecht, Utrecht, The Netherlands
C. Michel Zwaan	Princess Máxima Center for Pediatric Oncology, Utrecht, The Netherlands

List of publications

Janssen JM, Dorlo TPC, Steeghs N, Beijnen JH, Hanff LM, van Eijkelenburg NKA, van der Lugt J, Zwaan, CM, Huitema ADR. Pharmacokinetic Targets for Therapeutic Drug Monitoring of Small Molecule Kinase Inhibitors in Pediatric Oncology. Clin Pharmacol Ther. 2020;Epub ahead of print.

Yu H, **Janssen JM**, Sawicki E, van Hasselt JGC, de Weger VA, Nuijen B, Schellens JHM, Beijnen JH, Huitema ADR. A Population Pharmacokinetic Model of Oral Docetaxel Coadministered With Ritonavir to Support Early Clinical Development. J Clin Pharmacol. 2019;Epub ahead of print.

Janssen JM, Dorlo TPC, Niewerth D, Wilhelm AJ, Zwaan CM, Beijnen JH, Attarbaschi A, Baruchel A, Fagioli F, Klingebiel T, De Moerloose B, Palumbo G, von Stackelberg A, Kaspers GJL, Huitema ADR. A Semi-Mechanistic Population Pharmacokinetic/Pharmacodynamic Model of Bortezomib in Pediatric Patients with Relapsed/Refractory Acute Lymphoblastic Leukemia. Clin Pharmacokinet. 2019;59:207-216.

Janssen JM, de Vries N, Venekamp N, Rosing H, Huitema ADR, Beijnen JH. Development and validation of a liquid chromatography-tandem mass spectrometry assay for nine oral anticancer drugs in human plasma. J Pharm Biomed Anal. 2019;174:561-566.

van der Wagen L, **Janssen JM**, Raijmakers R, Petersen E, de Witte M, de Jong N, Bellido M, Meijer E, Bär B, Boelens JJ, Huitema ADR, Kuball J. Tyrosine kinase inhibitor levels matter in treating chronic GVHD. Bone Marrow Transplant. 2019;54:1141-1144.

van Nuland M, **Janssen JM**, van Hoek B, Rosing H, Beijnen JH, Bergman AH. Efficacy, tolerance, and plasma levels of abiraterone and its main metabolites in a patient with metastatic castration-resistant prostate cancer with a hepatic transplant. Clin Genitourin Cancer. 2019;17:e893-e896.

Crombag MBS, van Doremalen JGC, **Janssen JM**, Rosing H, Schellens JHM, Beijnen JH, Steeghs N, Huitema ADR. Therapeutic drug monitoring of small molecule kinase inhibitors in oncology in a real-world cohort study: does age matter? Br J Clin Pharmacol. 2018;84:2770-2778.

Janssen JM, Zwaan CM, Schellens JHM, Beijnen JH, Huitema ADR. Clinical trial simulations in paeditric oncology: A feasibility study from the Innovative Therapies for Children with Cancer Consortium. Eur J Cancer. 2017;85:78–85**.**

Dankwoord

De afgelopen vier jaar heb ik met heel veel plezier gewerkt aan dit promotieonderzoek. Omdat ik dit nooit alleen had kunnen doen zijn er veel mensen die ik wil bedanken voor hun bijdrage aan dit proefschrift.

Ten eerste wil ik alle patiënten en hun ouders bedanken voor hun deelname aan de onderzoeken waarvan ik de data heb mogen gebruiken. Zonder hun inzet was dit proefschrift er niet geweest.

Ten tweede wil ik mijn promotoren Alwin Huitema en Jos Beijnen en copromotor Thomas Dorlo bedanken. Alwin, ik heb ontzettend veel bewondering voor jouw analytische blik. Je had altijd ontzettend snel door waar het probleem in mijn projecten zat waarna ik weer vol goede moed aan de slag ging. Maar ook weet je je begeleiding individueel aan te passen, hierdoor heb ik de kans gekregen om mijzelf en mijn eigen manier van werken te ontwikkelen. Heel veel dank daarvoor. Jos, bedankt dat ik mijn promotieonderzoek binnen jouw onderzoeksgroep mocht doen. Ook veel dank voor je grondige feedback op al mijn presentaties en manuscripten. Thomas, heel veel dank voor je begeleiding en de fijne samenwerking. Jouw gedrevenheid en passie voor de farmacometrie en die toepassing daarvan op klinische problemen zijn een inspiratie.

Collega's, we begonnen in de keet, zaten een tijdje in het O-gebouw en uiteindelijk zijn we neergestreken op H3. Vier jaar promoveren was nóg leuker met jullie als collega's. In het bijzonder (al) mijn kamergenoten die de revue gepasseerd zijn: Huixin, Aurelia, Remy, Rose, Steffie, Willeke, Kimberley, Marit, Linda, Lotte, Jeroen, Merel, Maaike, Jonathan, Karen, Paniz en David. Heel veel dank voor de gezelligheid, het luisteren en alle kritische discussies.

Everyone from the pharmacometrics group, thank you all for the fun and the useful Tuesday meetings. I am very happy that the group is still growing and I hope to see you all soon at PAGE or at other meetings!

Alle collega's van het laboratorium van de apotheek, hartelijk dank voor jullie ondersteuning. Jullie werk en inbreng is van onschatbare waarde en ik kon me geen beter team wensen voor het meten en rapporteren van alle studie én TDM samples.

Ook alle onderzoekers en clinici uit het Antoni van Leeuwenhoek en andere centra wil ik bedanken voor de goede en leuke samenwerkingen. In het bijzonder, Bart, Coen, Frederic, Kristel, Jan, Michel, Neeltje en Serena.

Bedankt lieve teamgenoten voor alle afleiding en ontspanning de afgelopen vier jaar. De gezellige trainingen, borrels op zondag, teamweekenden en vooral het tolereren

van mijn afwezigheid de afgelopen maanden hebben me er doorheen gesleept. Vanaf nu ben ik er gewoon weer elke zondag bij en zal er weer ouderwets geloot moeten worden.

Maartje en Laura, bedankt voor jullie interesse in mijn onderzoek. Ik ben ontzettend blij dat we elkaar na al die jaren nog zo vaak zien en kijk uit naar alle etentjes die nog gaan komen.

Mama en Papa, de meeste dank gaat natuurlijk uit naar jullie. Mijn hele leven lang hebben jullie mij gesteund en gestimuleerd om het beste uit mezelf te halen. Ik denk nog wel eens aan de situatie met het rekenboek op de basisschool. Wie had gedacht dat ik nu een proefschrift vol formules zou afleveren? Berend en Sebastiaan, ik hoop dat jullie nu echt geloven dat ik de afgelopen vier jaar mijn tijd nuttig besteed heb en niet alleen maar op vakantie ben geweest. Alvast bedankt dat jullie mij als paranimfen willen bijstaan tijdens mijn verdediging.

Lieve Cedric, je zegt altijd dat je niks bijgedragen hebt aan dit proefschrift en dat ik je hier dus niet hoef te noemen. Voor wat betreft de inhoud is dat misschien ook wel zo, maar toch zijn de laatste woorden van dit dankwoord voor jou. Jouw onvoorwaardelijke vertrouwen, humor en ongelimiteerde energie hebben mij écht wel geholpen, heel veel dank voor alles.

Curriculum Vitae

Julie Janssen was born on February 3rd 1991 in Eindhoven and grew up in Beuningen. After graduating from high school at the Dominicus College in Nijmegen, she started studying Pharmacy at Utrecht University in 2009. As part of her master's program, she did a six month research project at the hospital pharmacy of the Academic Medical Center, Amsterdam. Here she developed a population pharmacokinetic model for gentamicin and investigated the inter-occasion variability in peak levels of this antibiotic drug. After graduating in 2016, Julie started her PhD research at the Netherlands Cancer Institute/Antoni van Leeuwenhoek hospital, under supervision of prof. dr. A.D.R. Huitema, prof. dr. J.H. Beijnen and dr. T.P.C. Dorlo. During her PhD she started the clinical pharmacology training of the Dutch Society of Clinical Pharmacology & Biopharmacy. Furthermore, she joined the Board of Directors of her field hockey club "Phoenix Hockey Zeist" in 2018 where she is responsible for the daily management and activities of all adult teams. Her PhD research resulted in this thesis, which she will defend at Utrecht University on April 23rd 2020.